STUDIES OF SOLIDS FLOWING DOWNWARDS FROM A HOPPER THROUGH VERTICAL PIPES

A Thesis submitted for the Degree of Doctor of Philosophy in the University of Leeds

by

R.J.F. PULLEN, B.Sc.

These investigations were carried out under the supervision of

I.R. McDougall, B.Sc., C.Eng., F.I.Chem.E.

Department of Chemical Engineering,
Houldsworth School of Applied Science,
The University of Leeds,
Leeds, LS2,
England.

March, 1974

Studies of solids flowing downwards from a hopper through vertical pipes.

R.J.F. Pullen

Ph.D. Thesis, 1974 Department of Chemical Engineering

ERRATA

Page no.	Line no.	
(i)	7	'Haselden' not 'Haseldon'
(viii)	19	' m/s^2 ' not ' m/S^2 '
(ix)	23	'error of estimate' not 'Error of Estimate'
(x)	12	insert ' ϕ '
	13	insert ' ψ '
7	25	'judicious' not 'judicial'
8	2	'valve' not 'value'
12	4	eq. 2.6, 3rd group, ' $\frac{l_B}{D_o}$ ' not ' $\frac{D_B}{D_o}$ '
14	11	'function' not 'factor'
15	16	'Bernoulli' not 'Berroulli'
	20	' ρ_a ' not ' ρ_f '
	25	under eq. 2.12, insert ' C_3 = correction factor for cone angle '
18	16	eq. 2.22: insert ' β ' to read ' $\sin^{2.5}\beta$ '
20	11	replace by: $-\frac{dP_a}{dR} = \frac{(U_s - U_a)}{k'}$
22	18	'Shinohara' not 'Shinhara'
23	5	delete comma after 'author'
31	22	' $0.85 \times (5d_p)^2 \times 1.4$ ' not ' $0.85\ (5d_p)^2\ 1.4$ ' ' $6.15\ d_p$ ' not ' $5.45\ d_p$ '
37	20	'percolating' not 'precolating'
39	5,6,19	eq. 3.13 and 3.14, and line 6: ' C_g ' not ' Cg '
39 - 41	-	eq. 3.15, 3.16, 3.17, 3.19, 3.20, 3.21, 3.22: ' C_p ' not ' Cp '
43	8	delete ' 's ' from ' Massimilla's '
	27	substitute 'flowing through' for 'frowing'
44	-	eq. 3.27, after ') ', replace ' - ' by ' = '
46	18	delete ' . ' and add 'since ϕ is a function of voidage, equation 3.27.'
50	12	'velocities' not 'valocities'
51	1	'indefinitely' not 'indefinately'
53	2	'inertial' not 'initial'
69	8	' $1\frac{1}{2}$" ' not ' $\frac{1}{2}$" '
71	20	' 750 ' not ' 1500 '
74	14	'first' not 'just'
77	5	'position' not 'posisition'
87	7	' 22.5 ' not ' 22.2 '
87 ff.	-	figs. 5.3 to 5.10 inclusive: add to each, 'for notation see p.87'
92	24	delete 'and'
93	2	transpose 'diameter ratios for' to 'for diameter ratios'
106	5	eq. 6.4a, ' $S(1 - e_B)\rho_s$ ' not ' $S(1 - e_B)$ '
	15	'unity' not 'unit'
	21	' Q_{ap} ' not ' Q_{qp} '
110	18	eq. 6.11, after 2nd ' = ', ' $\frac{M_s}{\rho_B}$ ' not ' $\frac{M_s}{\rho_s}$ ' and also in eq. 6.10
113	15	after 'for' insert 'each'
125	13	eq. 6.29, ' $(D - kd_p)^{2.0}$ ' not ' $(D - kd_p)^{2.1}$ '

(cont.

ERRATA (cont.)

Page no.	Line no.	
143	5 from bottom	'pneumatically' not 'penumatically'
154	22	eq. 3.47, ' f_s ' not ' f '
	27	eq. 3.49, ' e_x ' not ' e_o '
156	11	'value' not 'valve'
170	17	'contrast' not 'constrast'
175	3	after 'indicating' insert 'the'
176	14	delete 'it was much less marked for the larger orifices'
188	19	after 'relate the' insert 'percolating'
208	ref. 55	'Pyle' not 'Pule'

Acknowledgements

The author wishes to express his sincere thanks to Mr. I.R. McDougall for the invaluable guidance and helpful advice given freely throughout the study and the preparation of this thesis.

The author is indebted to the Science Research Council for the financial support which enabled him to perform this research, and to his wife, Jenni, and to his parents for their encouragement. He is grateful to Professor G.G. Haselden and to all the members of the Department of Chemical Engineering who either indirectly or directly assisted him and, in particular, to Mr. C. Howden of the technical staff.

Abstract

This work confirmed that the addition of a standpipe to a hopper/orifice system increased the rate of discharge of particular solids through an orifice by reducing the fluid pressure below this orifice; however, the standpipe dimensions could not be simply related to the solids mass flow rate. The experimental programme highlighted the existence of a 'core' flow of solids within the standpipe, while the theoretical analysis confirmed this by indicating that the effective single particle drag coefficients (C_D') in the standpipe were substantially lower than the equivalent free field coefficients (C_D), and that the former could be satisfactorily related to the position along the standpipe ($\frac{x}{L_t}$) by the equation:

$$C_D' = C_D(1 - e^{-w\frac{x}{L_t}})$$

where w was a parameter indicating the degree of expansion and expansion profile of the solids core.

In addition, the rate of discharge of solids (M_s) through an orifice of a given diameter (D_t) under the influence of a co-current air stream was related to the fluid pressure drop across the orifice (ΔP_o) by the semi-empirical equation:

$$M_s = C \frac{\pi}{4} (2g\rho_B)^{0.5} (D_o - kd_p)^{2.0} (\Delta P_o + \Delta P_C)^{0.5}$$

where ΔP_C was a 'pseudo pressure' to account for the gravity flow contribution.

Subsidiary investigations determined the bulk density of a flowing particulate solids bed, the air flow through such a bed, and also the voidage of the flowing solids stream at the hopper orifice, using the main apparatus, while a secondary apparatus enabled a study of the effects on the solids mass flow rate of interposing an 'expansion chamber' between the hopper outlet and the standpipe entrance.

Table of Contents

List of Illustrations

Nomenclature

A_B Cross-sectional area of constant depth solids bed (m^2).

A_o Cross-sectional area of orifice (m^2).

A_t Cross-sectional area of standpipe (m^2).

C Constant in equations, different for each equation.

C_D Single particle free-field drag coefficient.

C'_D Effective particle drag coefficient in standpipe.

d_p Particle diameter (m).

D_B Constant depth bed diameter (m).

D_o Orifice diameter (m).

D_t Standpipe diameter (m).

e_B Solids bed bulk voidage.

e_o Voidage at the orifice.

$\bar{e}_p$ Average standpipe voidage.

e_x Voidage at distance x down the standpipe.

f_a Air Fanning friction factor.

f_s Solids Fanning friction factor.

F Cohesion between particles (N).

g Gravitational acceleration (m/S^2).

H_B Solids bed height (m).

k Constant for orifice annulus.

k_1 Constant (equation 3.29).

k_2 Constant (equation 3.29).

k_3 Constant (equation 3.33).

k_B Constant (equation 3.6).

k_D Particle drag coefficient at the orifice.

k_{fb} Constant (equation 6.3) (m^3/kg).

k'' Kozeny constant.

l Length (m).

l_B Depth of constant depth solids bed (m).

l_c Length of chamber - from orifice to standpipe entrance (m).

L_t Standpipe length (m).

m_p Mass of solids isolated in standpipe (kg).

M_a Mass flow rate of air (kg/s).

M_s Mass flow rate of solids (kg/s).

P Pressure (mm H_2O, N/m^2).

ΔP_B Constant depth solids bed pressure drop (mm H_2O).

ΔP_o Orifice pressure drop (mm H_2O).

ΔP_c 'Pseudo-pressure' at the orifice (mm H_2O).

Q Volume flow rate (m^3/s).

Q_{ai} Interstitial solids bed air flow rate (m^3/s).

Q_{ap} Percolating air flow rate (m^3/s).

Q_{at} Total air flow rate (m^3/s).

Q_a Air flow rate (non specific) (m^3/s).

Q_{fb} Air flow rate into feed hopper (m^3/s).

Q_s Solids volume flow rate (m^3/s).

r Radial distance from centre of orifice (m).

r_o Orifice radius (m).

R Constant radial distance from orifice (m).

Re' Particle Reynolds' number (free-field).

Re'_1 Particle Reynolds' number (solids bed).

S Particle specific surface (m^{-1}).

S_L Logarithmic standard Error of Estimate.

t Time (s).

U_a Air velocity (m/s).

U'_a Superficial air velocity (m/s).

U_{ac} Air velocity in the chamber (m/s).

U_{ao} Air velocity at the orifice (m/s).

U_r Particle-air relative velocity (m/s).

U_s Solids velocity (m/s).

U'_s Superficial solids velocity (m/s).

U_{so} Solids velocity at the orifice (m/s).

U_{st} Limiting solids velocity (m/s).

x Distance (m).

Z Particle shape factor.

β Included $\frac{1}{2}$ angle of flow channel.

φ_a Air density (kg/m^3).

φ_B Solids bed bulk density (kg/m^3).

φ_s Solids density (kg/m^3).

φ_o Orifice solids bulk density (kg/m^3).

μ Air viscosity (Ns/m^2).

μ_1 Tan , coefficient of friction.

μ_2 Tan ; coefficient of friction.

ϕ Angle of internal friction.

ϕ_s Sphericity.

ψ Drained angle of repose.

θ Full internal hopper cone angle.

Prefatory Note on Dimensions

Throughout this thesis, pressures have been expressed in the old-fashioned weight per unit area units rather than the correct force per unit area units. This has resulted in the production of equations which may appear to be dimensionally inconsistent, and this is regretted.

The reason for this is that the entire literature of this subject used this type of pressure unit, and it seemed to the author that it would cause less confusion to adhere to this obsolete convention than to present every equation in both forms.

CHAPTER I

Introduction

1.1 Development of the Topic

One of the main features of present day industrial development is the increasing scale of operations in the chemical industry and the rapidly increasing volume rates of flow used for process materials. This has created problems in the storage and handling of all materials, and none more so than in the handling of bulk or particulate solids (85). In the past, the problems associated with the flow of granular solids were often overcome by handling and storage in some form of small container such as a bag or drum, but as the scale of operations increased, bulk handling, and with it an understanding of the fundamental factors governing its operation, became increasingly necessary.

The elements of powder mechanics have been known for a long time - Hagon's experiments on the flow of sand in 1852 (3) and Reynolds' observations of dilatancy in 1885 (27) - but unlike fluid mechanics, the mechanics of flow of granular materials has largely been neglected until recently, due to the apparent complexity of such systems and the large number of possible variables. As a result, the experimental information on the subject that did exist was fragmented and generally uncо-ordinated, with engineers turning to soil mechanics or to fluid systems for analysis and attempting to overcome the difficulties empirically and piecemeal. Only recently has the interstitial fluid been recognised as important and included in the theoretical developments of solids flow models. Further, it would seem that it is only now being realised that some aspects from most of the various approaches to solids flow have to be combined for a full theoretical determination of the subject (46, 80).

Fundamental Approaches

The fundamental equations of powder mechanics are the same as those

of soil mechanics, based on the early work of Coulomb (1776) and Rankine (1857) on the frictional behaviour of a mass of sand (27). Both knew of the existence of cohesion, but neither introduced it into their analyses; it was considered a safety factor which would increase the strength of a soil but reduce the pressure exerted by it. Further confusion also existed about the angle of internal friction, no doubt due to a statement by Coulomb that the terms angle of internal friction and angle of repose were synonymous. The link between early soil mechanics studies and the design of storage bunkers was the theory of retaining walls, and the fallacies regarding cohesion and angle of repose unfortunately accompanied this theory.

A different approach was developed by Janssen (21) based on the concept of a semi-fluid first proposed by Wicsback (98). The need to classify bulk materials led to dry sand, wheat and other materials being regarded as an intermediate position between fluids and solids and called 'semi-fluids', the solids mass being regarded without cohesion, with particles held in place only by friction. The most important property of these systems was considered to be the internal angle of friction or angle of repose as it was frequently called.

As the early classical retaining wall theories based solely on angle of repose failed when applied to cohesive, clayey materials, so the semi-fluid theory of bunker design failed when applied to cohesive materials such as wet coal, iron ore and limestone. It was likely that these failures prompted the predominantly practical approach to bunker design which reigned for many years until increased interest in the handling of solids, due in part to the development of the catalytic cracking processes in the petroleum industry (62), promoted experimental programmes to investigate the problems.

1.2 Approaches to Particulate Solids Systems

Fluid Analogy

It would not be expected that blind application of the laws of fluid mechanics or soil mechanics would adequately describe the flow of powders, but it is worth looking at the differences between fluids, massive solids and granular solids to find a logical explanation.

At first sight, since particulate solids could be made to flow under gravity through a hopper and orifice, and down a chute or pipe, it appeared natural to look for similarities to liquid flow: but it rapidly proved that virtually the only resemblance between the two was the fact that flow could occur. These two classes of matter could be differentiated most readily by their behaviour under static conditions. Liquids sought a constant horizontal level in a container whereas, although particulate solids also showed a free surface, the material did not seek its own level; and the solids achieved equilibrium with the free surface at an angle to the horizontal - the angle of repose. Associated with this was the fact that solids could also transmit shearing forces when stressed under static conditions, whereas liquids could not. The flow of liquids through orifices set in the base of a container depended on the height or head of the liquid above the orifice, whereas for particulate solids the concept of head had little value: for it had only a slight effect on the rate of outflow. There was no unique definition of pressure within a solids bed, since unlike liquids, pressure was not transmitted equally in all directions in a solids bed, and was neither constant at a given distance from the free surface nor proportional to the distance from that surface. Also, solids were able to possess cohesive strength enabling them to form stable arches over outlets, whereas liquids did not show this property.

Soil Mechanics Analogy

The other main analogy used in tackling the problems of particulate

solids was that of soil mechanics. The flowing material was regarded as a particle bed subject to shear due to the gravitational forces acting upon it. The main attention was focussed on the frictional and cohesive forces - shearing and compressive/tensile stresses - within the bed of solids. The model was based on analogies with massive solids, and Jenike in his analysis of the stress distribution within a body of flowing material made four main simplifying assumptions:

1. that a dynamic or equilibrium system could be analysed as if it were a static problem,
2. that the bulk materials could be regarded as continuous and not as discrete particles,
3. that the solid was considered to be isotropic,
4. the boundaries of the system were considered to be fixed in space, i.e. the top surface remained at a constant level.

Thus this approach, by contrast with the fluid analogy, really represented a static rather than a dynamic system, and the model was based on a continuous solid subject to plastic and elastic deformation. The approach could be criticised on both these accounts. To overcome the difficulties of solution for static beds, the particulate solids were considered to be at the point of incipient failure where the frictional forces were fully mobilised and the powder was then said to be in a state of plastic equilibrium. Nevertheless, these criticisms were relatively unimportant and, in general, this approach has proved very successful in the formulation of design methods for hoppers, silos and bunkers.

Fluid/Particle Interaction

A powder could be regarded essentially as the result of a congregation of large numbers of solids particles, no two of which were likely to be identical in shape or size. The process of bringing

these particles together may be assumed to bring them into contact with one another and to leave voids in between them which in general were filled with a fluid, usually air. The presence of the interstitial air in the voids meant that there was a continuous phase fluid through which the particles must move or, alternatively, which must move with the particles. As soon as this was recognised it became apparent that any interactions between the solids and the ambient fluid should have been included in attempts to determine the nature of particle flow. Further, since the particles were in contact with each other, some consideration of inter-particle friction and cohesive forces (if any) should also have been included. This has been demonstrated only recently by an extended experimental and theoretical programme at Warren Spring (72, 45, 46, 47). A force balance taken over an element of the particle bed included these considerations, but owing to lack of data they were not included in the final analysis. However, simplification of the theoretical equation reduced it to Brown's equation (41) for the flow of particulate solids which had neglected fluid drag and particle-particle friction and cohesive forces.

From their own investigations and from the application of the information in the literature, Brown and Richards (27) noted three main principles of powder mechanics:

1. Principle of Dilatancy: A tightly packed mass of granules enclosed within an envelope invariably increases in volume when the envelope is deformed: if the envelope is inextensible but not inflexible, no deformation is possible until the applied forces rupture the bag or fracture the particles (Reynolds, 1885).
2. Principle of Mobilisation of Friction: Considered as rigid bodies, the particles will be subject to frictional forces at the points where they are in contact. The frictional

force at any contact point can take any value between zero and a limiting value, this maximum value being reached when the granules are just about to move relatively to each other whilst remaining in contact: the limiting value depends on the normal force between the granules. When the powder is at rest the frictional forces are less than the maximum value and the stress distribution in the particles is intermediate. Equally, due to the variable frictional forces in a granular bed, there exist a variety of possible equilibrium states for the powder mass, and hence the observations of a range of bulk densities and angles of repose.

Further, if over a number of more or less co-planar contact points the shearing forces exceed the maximum frictional forces, a surface of sliding can be initiated. At first sight this appears incompatible with the dilatancy principle which permits a surface of sliding to occur only when there are slack contacts between the particles, i.e. when the tangential and normal stresses are zero. As such, these two principles cannot co-exist, but it is possible to consider the process as transient or consecutive phenomena. If the shearing force exceeds the frictional resistance then movement may commence, but for movement to occur at all there must be expansion, and this must be the first result, followed then by movement. This particle movement being likely to cause completely new inter-particle contacts may result in the shearing force no longer exceeding that of friction: but the slack contacts also produced by the initial movement will still allow further sliding.

3. Principle of Minimum Energy of Flowing Granules (41): implies

that the total energy of particles flowing towards an aperture under gravity decreases as the aperture is approached. Reasonable though this appears in principle, it has not been confirmed experimentally.

Effect of Fluid Flow on Solids Discharge

The effect of an imposed counter-current air flow or solids discharge from a hopper through an orifice was known before the effect of the interstitial air on gravity discharge of solids was fully realised (8, 34). The pressure drop across the solids hopper was considered as the sum of two separate pressure drops, one over the solids orifice and one over the moving bed. It was found that the pressure drop over the orifice greatly exceeded that over the solids bed and that the head of solids above the orifice had little effect on the solids flow rate, showing that a relatively small flow of air was sufficient to cause cessation of solids flow (34).

It was found that solids discharge from a hopper through an orifice increased with an imposed co-current air flow and that it could be correlated with the air pressure difference across the solids bed and orifice (49), or more precisely across the orifice alone (52). Under both these conditions the effect of the air flow on the particulate solids was attributed to fluid drag (34, 51) although apparently this was not considered to be relevant to the intermediate situation, i.e. gravity flow with a 'static' ambient fluid. However, as a consequence of the observations on the effects of imposed air flows, it was realised that the solids flow rates could be controlled by judicial variation of the air pressure drop across the solids flow orifice (80).

1.3 Problems to be Investigated and Aims of Research

One method of inducing a co-current air flow through a solids orifice and facilitating control of the air pressure drop across the orifice was by attaching a standpipe to the outlet of a hopper:

preferably by means of an intermediate chamber of diameter larger than that of the standpipe (36, 99) to allow the solids control valve to be retained in the base of the hopper above both the chamber and the standpipe. There was a considerable volume of empirical information on the flow of solids through an orifice together with some theoretical justifications, but very little had been published on the flow through a standpipe or the influence of a standpipe, connected below a hopper, on the solids flow rate through an orifice. There had been some progress in the investigation of the gravity flow of catalyst between the cracking unit and regenerating unit in the catalytic cracking processes (65, 66), but since the catalyst in these containers was usually fluidised, and since the solids flow through the connecting pipes could be either fluidised bed flow or packed bed flow or, indeed, a combination of the two, the conditions could not be regarded as analogous with those in a standpipe attached beneath a bulk solids storage hopper. For this latter type of system, there was virtually no information regarding flow through the standpipe (alternatively referred to as an extended orifice or efflux tube) other than a general agreement that the addition of a long tube to the orifice of a hopper increased the solids flow rate, and that the solids flow rate depended to some degree on the length of the tube. There have been no theoretical analyses of this system except for general qualitative descriptions of the effect of the tube.

The aims of this project were: to investigate the influence of different standpipes on the flow of loose particulate solids through a range of orifices set in the base of a hopper; that is, to determine the effect of the standpipe dimensions on the solids flow rate: to determine the factors effecting the flow through the orifice and standpipe: and to study the fluid pressure throughout the hoppers and standpipes, with their effect on the solids flows and air flows

throughout the system.

An attempt was made to clarify the understanding of the equations for air-induced solids flow through the orifice and for this, extensive use was made of the literature. A mathematical model was developed to describe the conditions within the standpipe, and to relate the pressures to the air and solids flow rates. For this purpose, it was necessary to modify the free field, single particle drag coefficients and to impose an expansion profile on the solids stream in the standpipe.

CHAPTER 2

Literature Review

2.1 Gravity Flow of Solids from Hoppers

The majority of the work in the field of gravity flow of granular solids has been directed at determining the rate of discharge of the solids through an orifice set in the base of a hopper. The explanation of the flow of solids from hoppers through such restrictions also led to further investigations of the many considerations involved in such systems. Although interest has been shown in this subject for over 100 years, the initial investigations were few and far between, with the result that many of the fundamental questions were not recognised, let alone investigated or codified. Research into the subject has gained momentum since the mid-1940's and some of these fundamental questions are being clarified although, as many authors recognise, there is still much to be understood (1, 2).

The earliest available correlation for the rate of discharge of granular material through an orifice in the base of a vessel was Hagen's formula (3):

$$M_s = C(D_o - 2.0d_p)^{2.5} l_B^{0.5} \qquad (2.1)$$

indicating that the solids mass flow rate was dependent on the solids bed height. The absence of any such a dependence was pointed out by later authors (4, 5) and has been amply confirmed by subsequent investigations (6, 7). Only in one later case was any mention of the existence of the influence of bed depth made by Newton et al (8), who suggested:

$$M_s = 8.5 D_o^{2.96} l_B^{0.04} \qquad (2.2)$$

the very small value of the index of the depth term l_B, however, indicating virtually no effect of bed depth (6).

Because of difficulties involved in theoretical analysis of the discharge of granular solids through orifices, the majority of correlations have been empirical. In an early study with conical hoppers, Dahming et al (9) proposed an equation of the form:

$$M_s = \frac{100 D_o^{2.5} \varphi_B}{\mu_2 [34.6 + (67.4 + 444 \sin \frac{\theta}{2})] [(\frac{d_p}{D_o}) + 0.130 - 0.161 \mu_2]} \text{ g/min} \quad (2.3)$$

This work, together with a later publication (10) represented a complete study of all the parameters investigated up to that time, together with a new one, the cone angle of the hopper. It was suggested that the comparative rate of flow of solids could be determined if the angles of repose, the bulk densities and the average particle diameter were known in that order of importance (10).

Simpler relationships of the form:

$$M_s = C D_o^n \quad (2.4)$$

were suggested by many authors, various values of n being used; Ketchum (4) suggested n = 3 for wheat, whereas Hinchley (7) found that n = 2.7 for sand. Other values were n = 2.84 for pellet catalyst (11), n = 2.5 for the flow of powders from pipes (12), and n = 2.5 for discharge of solids into liquid (13).

Takahashi (14) in 1933 carried out a large number of runs with different materials and correlated them by an equation of the form:

$$M_s = \frac{C_1 (g \varphi_B)^{0.5} D_o^{2.5}}{[f_n(\mu_2) + C_2 (\frac{d_p}{D_o})]} \quad (2.5)$$

although he did not appear to have claimed any specific accuracy for this equation, and did not show how he derived it. In contrast to other fields of study, there have been many varied analytical approaches to general equations for the discharge rate of solids through an orifice.

Dimensional Analysis

As a starting point, dimensional analysis has been used to suggest

groupings of variables by several authors (9, 19). The most complete analysis of this type was by Rose et al (6), who produced an equation of the form:

$$M_s = f_n\left(\frac{D_o}{d_p}, \frac{D_B}{D_o}, \frac{D_B}{D_o}, \frac{F}{D_o^3 \varphi g}, \mu_2, Z, \theta\right) \qquad (2.6)$$

for various solids, leading to:

$$\frac{M_s}{\varphi_B g^{0.5} D_o^{2.5}} = 0.16\left(\frac{D_o}{d_p}\right)^{0.3} f_n(\theta)(Z-5)^{-0.5} \qquad (2.7)$$

for $\left(\frac{D_o}{d_p}\right) > 12$, where $f_n(\theta) = (\tan \frac{\theta}{2})^{-0.35}$ for $\frac{\theta}{2} < (90-\psi)$

$f_n(\theta) = (\tan (90-\psi))^{-0.35}$ for $\frac{\theta}{2} \geq (90-\psi)$

which was similar to an earlier equation put forward by Tanaka (17, 16). Fowler et al (18), using similar methods, correlated their results to:

$$\frac{M_s}{\varphi_B (2g)^{0.5} D_o^{2.5}} = C\left(\frac{D_o}{\phi_s a_p}\right)^{0.185} \qquad (2.8)$$

for various solids using a flat-bottomed hopper. Other authors have also used this technique, suggesting (15):

$$\frac{M_s}{\varphi_B g^{0.5} D_o^{2.5}} = 2.82 \qquad (2.9)$$

and (20),

$$\frac{M_s}{\varphi_B g^{0.5} D_o^{2.5}} = f_n(\mu_2) \qquad (2.10)$$

Soil Mechanics Analogy

A different and fundamental approach to the problem of solids flow and storage in hoppers and bins was by the soil mechanics analogy and the concept of semi-fluids.

An initial definition of a semi-fluid was by Janssen (21), who asserted that granular solids occupied an intermediate position between fluids and solids because, although dry particulate masses were without cohesion, they exhibited some internal friction in that they formed heaps with the surface at some angle to the horizontal. The initial interest

in this line of investigation was the determination of horizontal and vertical pressures in static beds of granular materials: for dry materials without significant cohesion a method of calculation had already been provided by the well established earth pressure theories of Rankine and Coulomb (22). Early experiments (23, 24) did much to establish the properties of semi-fluids, and several workers (21, 25, 26) developed equations to determine the pressures on the walls of hoppers by considering the particles en masse. The assumptions implicit in these equations were: that the bulk density was independent of depth, that the ratio of horizontal pressure to vertical pressure was constant and independent of depth, that the surfaces of equal solids pressure were horizontal planes, that the wall friction was fully mobilised, and that the powder was on the point of slip in the container (27). These assumptions and the resulting equations appeared to be quite reasonable (27) although they became less valid when the particle mass was in motion (1). Jenike (28) stated, "A solid in a bin is partly in a Rankine state of plastic equilibrium and partly in an elastic state. Neither the Modulus of Elasticity nor the Poisson's Ratio of the material are constant. The problem does, therefore, not yield to mathematical analysis." These initial assumptions and equations were also found to be inapplicable to granular masses exhibiting cohesion, i.e. where the particles could not be considered as individual units (29).

The above investigations were mainly concerned with the stresses and pressures associated with static granular masses in bins. Delaplaine (33) was one of the first to analyse the forces acting on dry, non-cohesive particles in a flowing system of solids; he considered the stresses on an element of bed under conditions of uniform flow and concluded that, among other things, for bed depth greater than five times the bed diameter, the stresses were independent of depth and that at any given bed depth horizontal stresses were equal in all directions.

The inadequacies of the semi-fluid theory due to the omission of cohesive forces and the misconception in regarding the angle of repose as synonymous with the angle of internal friction were recognised by Jenike who, in a way similar to that used by Delaplaine (33), analysed very thoroughly the stress distribution in flowing beds of solids. In a long series of investigations (28, 30, 31, 32) many major advances were made in the understanding of the nature of solids flow in bins, notably by the inclusion of cohesion into the analysis, and in the explanation of rat-holing effects and the ability of bulk solids to form a stable arch across a bunker outlet. Perhaps the major contribution was the concept of a 'solids flow factor', measured from the yield locus of the materials strength/cohesive curve.

It is true to say that many of the advances that have been made in powder mechanics stemmed from the analogy between powder and soil: but as Brown and Richards pointed out (27) this analogy must not be followed blindly. Soil mechanics as a science was rather differently orientated from powder mechanics. Almost invariably in soil mechanics, although incipient failure conditions had to be calculated, this was to ensure that such conditions were never obtained in practice: this was, of course, in complete contrast to the situation for powders, where movement was required and consequently it was desired to calculate the continuous failure condition represented by the mass movement of the powder bed. There appeared to be no a priori reason to assume that these conditions would be the same, or even necessarily analogous.

Soil mechanics is essentially the study of frictional and cohesive forces - shearing and compressive/tensile stresses - in static beds of divided solids: and finds its main application in the design of bunkers for powder storage; one of the great advantages of this stress analysis technique is its ability to deal satisfactorily with cohesive materials. In soil mechanics, however, although stress analysis led to meaningful

pressure calculations for retaining walls, etc., difficulties arising in the interpretation of plastic equilibrium and the fact of two different types of failure, active and passive, make the solution of the differential equations difficult in the case of flowing powders. Jenike and Johanson (32) have offered a theoretical solution based on such reasoning, but most authors have used a simpler approach based on Janssen's model (21).

The concept of a solids pressure acting at the base of a hopper in conjunction with the observation that fine solids flowing through large orifices seemed to behave like real fluids (34, 36) led to the fluid analogy approach to the determination of solids flow rate from hoppers.

Fluid Analogy

Rausch (34) developed the equation originally determined to describe the pressures at the base of a static bed by Janssen (21) and combined it with a modified Berroulli equation for fluid flow to give a theoretical relationship for the flow of dry, non-cohesive particulate solids through orifices. This, when simplified, was of the form:

$$M_s = C_1 \frac{\pi}{4} \varphi_B D_o^{2.5} \left(\frac{g}{C_2 \tan\psi}\right)^{\frac{1}{2}} \qquad (2.11)$$

for $l_B > 5D_o$, $D_o \ll D_B$, $\varphi_s \gg \varphi_f$, $C_1 = \frac{\varphi_o}{\varphi_B}$, $C_2 = \frac{\text{lateral pressure}}{\text{vertical pressure}}$

It did not fit the experimental data exactly, and a modified form was produced to take into account the particle diameter:

$$M_s = C_4 C_3 \varphi_B \frac{\pi}{4} D_o^{2.5} \left(\frac{g}{2 \tan\psi}\right)^{0.5} \left(\frac{D_o}{d_p}\right)^n \qquad (2.12)$$

where $n = 0.43$ for $\frac{D_o}{d_p} < 25$; $n = 0.30$ for $\frac{D_o}{d_p} > 25$

$C_4 = 0.193$ " $C_4 = 0.294$ "

A similar theoretical equation developed along the same lines, but coupled with a less comprehensive experimental investigation was published by

Shirai (35):

$$M_s = C \cdot \frac{\pi}{4} \rho_B D_o^{2.5} \left(\frac{f}{2 \tan \psi}\right)^{0.5} \qquad (2.13)$$

where C was considered to be a discharge coefficient analogous to that for a pure fluid discharging through an orifice.

Evans (36) approached the subject by considering the solids bed to be in an 'active' state, i.e. a bed of solids which was on the point of movement as distinct from 'passive', compacted or at rest. He analysed the forces in the bed in a similar manner to Delaplaine (33) to find the solids pressure at the base of the hopper and combined the results with a modified Berroulli equation. The pressure drop across the orifice was taken as the solids pressure above the orifice minus the fluid pressure below the orifice. Thus:

$$M_s = \frac{\pi}{4} D_o^2 (2g \rho_B)^{0.5} (P_1 - P_2)^{0.5} \qquad (2.14)$$

where P_1 = solids pressure above the orifice = $\frac{\rho_B D_o}{4 \mu_1} (1 + 3 \mu_1)^2$

P_2 = fluid pressure below the orifice

For simple orifice flow $P_2 = 0$, so:

$$M_s = \frac{\pi}{4} \rho_B D_o^{2.5} \left(\frac{g (1 + 3 \mu_1^2)}{2 \mu_1}\right)^{0.5} \qquad (2.15)$$

The pure fluid analogy approach has largely been discredited due to the major differences between true fluids and particulate solids, as mentioned previously. This was in fact recognised by Evans (36) who stated, "It is postulated .... that the Euler equations can be applied to the flow of solid particles, although the results must be considered with some reservations, since the forces acting between solids particles are completely different from the inter-molecular forces in a fluid, and because there is no longer a non-viscous continuous medium."

A novel method of describing the solids discharge from a hopper was used by Zenz (37) - the weir analogy. Recognising that the solids flow

was essentially independent of the head of solids except for low values, he likened the situation to fluid flow over a weir by introducing the angle of repose to account for the decrease in effect of the solids head. Thus:

$$h_w = C_1 \left({}^{Q}/_{l_w} \right)^{\frac{2}{3}} \quad \text{(Francis weir equation)} \qquad (2.16)$$

where h_w = height of liquid crest over weir, l_w = length of weir was developed to give, for solids flow:

$$M_s = C_2 \frac{\pi}{4} \varphi_B D_o^{2.5} \qquad (2.17)$$

Energy Balance and Number Profiles

A completely different approach was made by Brown and Richards. Initially (38), they correlated their flow data in terms of dimensionless groups, including a term first proposed by Wieghardt (39) to account for blocking orifice diameters.

$$\frac{M_s}{\varphi_s A_o (g d_p)^{0.5}} = C_1 \left(\frac{D_o}{D'_o} \right)^{0.5} \exp. \left(-C_2 \frac{D'_o}{D_o} \right) \qquad (2.18)$$

$D'_o = 4\ d_p$ for circular orifices, blocking orifice diameter.

In a subsequent study, a statistical approach was taken (40). The work stemmed from Hagen's (3) early observations of a 'vena contracta' in the discharge of granular solids through an orifice. Brown and Richards postulated a 'statistically empty annulus' at the perimeter of the orifice, of width $\frac{k}{2}$, thus reducing the effective orifice diameter for solids flow to $(D_o - k)$. If $n(x)dA$ was the number of particles passing an elementary area dA distance x from the edge of the aperture, then Brown and Richards showed that $n(x)$, the 'number profile', did not depend on the size or shape of the aperture, and this profile was given by:

$$n(x) = \frac{C \varphi_s}{\pi_p} g^{0.5} (x - \tfrac{k}{2})^{0.5} \qquad (2.19)$$

where C was a dimensionless parameter for the square root relationship. The range of materials used was not sufficient to establish the factors

governing C and k, which thus remained empirical. They showed that twice the width of the empty annulus corresponded to the width of a blocked slit, and this in turn was almost half that of a blocked circle.

In later studies, Brown (41) postulated that the energy per unit volume in a powder flowing towards the aperture decreased in the direction of flow. By assuming the flow to be radial, the bulk density of the bed to be constant and the total energy to be a minimum at the surface $R = \frac{D_o - k}{2 \sin\beta}$ the velocity (U_p) distribution at the orifice was obtained from:

$$2U_p^2(\alpha) = \frac{g(D_o - k)\cos\alpha}{2\sin\beta} \qquad (2.20)$$

for circular orifices and α , the angular co-ordinate of stream measured from the vertical. The solids mass flow rate was given by:

$$M_s = \varphi_B\, 2\,\frac{\pi}{4}\,\frac{(D_o - k)^2}{\sin^2\beta}\int_o^\beta U_p(\alpha)\sin\alpha\, d\alpha \qquad (2.21)$$

which, on combination with equation 2.20, revealed the more familiar form:

$$M_s = \varphi_B\,\frac{\pi}{4}\,g^{0.5}(D_o - k)^{2.5}\int_o^\beta \frac{\cos^{0.5}\alpha\,\sin\alpha\, d\alpha}{\sin^{2.5}} \qquad (2.22)$$

Using average values of U_s at the orifice and the average height of the arc at the orifice, equation 2.21 gave:

$$M_s = \varphi_B\,\frac{\pi}{4}\,g^{0.5}(D_o - k)^{2.5}\left(\frac{(1 - \cos\beta)}{2^{0.5}\sin^{2.5}\beta}\right)^{0.5} \qquad (2.23)$$

A similar approach was also employed by Harmens (42), who included the effect of the physical properties of the solids by a term based on the angle of repose. Shinohara et al (44) determined the position of the free fall arch by calculating the velocities of the particles below the orifice using simple dynamic equations.

This form of theoretical study of the solids discharge from a hopper seems to be the most satisfactory yet devised. The postulates are clearly reasonable, since the initial potential energy is partly converted into kinetic energy and partly expended as frictional work in the inter-particle

contacts. The assumptions of radial flow and the statistically empty space were partly substantiated by observation. Implicit in this theory is that the solids fall from a 'free-fall arch' above the orifice and, although the existence of such an arch has been observed by several authors, it had not yet been shown conclusively that the theoretical and observed positions of such arches inevitably coincide. Nevertheless, although the system used was regarded as ideal, the particles showing no cohesion, this type of analysis has been the basis for much subsequent investigation - notably the postulate of the statistically empty space.

This concept has been used by several authors to reduce the index of the orifice diameter term to the hypothetical value of 2.5 (19, 37). Beverloo et al (19), investigating the flow of various agricultural seeds and sands, found:

$$W_s \propto D_o^n \qquad (2.24)$$

where n ranged from 2.85 to 3.05 for seeds and 2.77 for sand.
They considered the empty space to be proportional to the particle size and took the effective orifice diameter available for solids flow as $(D_o - kd_p)$ where k = 1.5 for seeds and 2.9 for sand, giving:

$$W_s = 0.58\ \varphi_B\ g^{0.5}(D_o - kd_p)^{2.5} \qquad (2.25)$$

A remarkable feature shown in this wide survey was the variety of hypotheses suggested for the correlation of solids flow rate with orifice diameter. The agreement with the experimental determination was generally regarded as good. Evans (36) noted that the average values of the index of orifice diameter was 2.7 for some of the more notable experimental correlations (43), and the agreement was further improved when the empty annulus concept was introduced (19, 37, 38, 40, 41).

Ambient Fluid Effects

In general, the above investigations ignored the presence of ambient fluid (usually air) and its effects on the solids discharge rate. A series

of papers by various authors at Warren Spring (45, 46, 47, 72) described an experimental and theoretical programme dealing with such effects. A generalised force balance was carried out on an elemental volume in the solids mass (46), including the effects of the interstitial fluid drag. The resulting theoretical equation proved impossible to solve, but on simplification it reduced to the same expression obtained by Brown (equation 2.20). Examination of the complete expression and the simplifications showed why Brown's equations only applied to the discharge of coarse granules. The fluid pressure gradient in the solids was related to the relative velocity by Darcy's Law

$$-\frac{dP_f}{dR} = \frac{(U_p - U_f)}{k'}$$

If the granules were large, then the permeability of the solids mixture (k') would be correspondingly high. Thus $\frac{dP_f}{dR}$ approached zero for large diameter particles. This term, together with a stress tensor term dealing with inter-granule frictional effects, and the effects of porosity change as the orifice was approached were not included in Brown's analysis, and might well explain the inability of his resulting equation to deal with fine particles (46). The experimental programme (45, 72) showed that the bed voidage increased as the solids approached the orifice, and that with flows of fine particles reduced pressures were produced in the solids bed due to fluid/particle drag effects. This was also shown by Wlodarsky (48) in an independent investigation. The definitive equations developed by the Warren Springs authors (46, 47) required a knowledge of porosity changes within the hopper, and thus were not readily solved. Carlton (102) developed a less rigorous practical equation for the solids mass flow rate including fluid drag effects which did not contain porosity terms, and which could be calculated relatively easily with the aid of a nomogram.

Air Induced Solids Flow from Hoppers

The effect of the ambient fluid on solids-fluid systems was further

investigated under co-current air/solids flow conditions. Kuwai (49) investigated the effect of air pressure above the solids bed on the mass flow rate of various materials and concluded that:

$$M_s = C \frac{\pi}{4} D_o^2 [2g \varphi_B (P + P_c)(D_o/l_B)]^{0.5} \qquad (2.26)$$

where $c = (D_o/d_p)^{0.25} \exp. [-5.0(D_o/D_B)]$

The pressure P was the pressure above the particle bed and P_c was a hypothetical pressure corresponding to the solids mass flow rate due to gravity. Kuwai noted the need for a constant level bed in this type of investigation since, clearly, if the air pressure above the bed were constant, the air flow rate through it would increase if the bed depth were decreased. Little subsequent work has been reported from this area of study. Bulsara et al (50) performed a similar investigation. They fitted their data to a modified orifice equation for fluid flow originally published by Zenz (37):

$$M_s = C(g \varphi_B)^{0.5}(P_2 - P_1)^{0.5}(D_o - kd_p)^{2.0} \qquad (2.27)$$

where $P_2 - P_1$ was the orifice pressure drop.

Bulsara et al also investigated the associated air flow, and concluded that the pressures above the orifice could be calculated by considering the flow of air through fixed beds, although they did not specify any particular method. It should be noted also, that equation 2.27 did not include any term for gravity flow of solids, i.e. when $P_2 - P_1$ was zero. Resnick et al (51) modified the theories of Harmens (42) by adding a pressure term into the energy balance. They conducted tests for several bed heights and showed that the pressure above the orifice could be calculated by assuming that the pressure drop across the bed was a function of bed depth only for any constant gas flow rate. They also showed that the solids efflux rate at a given gas flow rate was independent of bed depth. Their correlation, however, depended on particle and apparatus properties which were difficult to obtain.

Knowles (52) carried out an experimental study of the flow rate of solids under the influence of co-current air flow through the orifice. He performed direct measurements of the pressures above and below the orifice and concluded that:

$$M_s = C(\Delta P_o + \Delta P_c)^{0.48} D_o^{2.54} \qquad (2.28)$$

The term ΔP_o was taken as the air pressure drop needed across the orifice to stop the flow of solids. This was a practical analogy to the term used by Kuwai (49) to account for the gravity contribution to the total solids flow. Also associated with this topic, the work of Engh (53) led to:

$$M_s = C \frac{\pi}{4} D_o^2 (2g \Delta P_o \varphi_B)^{0.5} \qquad (2.29)$$

while Yunan et al (74) suggested:

$$M_s = C \varphi_B^{0.5} (P_o - P_1)^{0.5} (D_o - kd_p)^2 \qquad (2.30)$$

where P_1 was the pressure below the orifice, P_o atmospheric pressure. Papazoglou (55) related the flow rate of solids directly to the flow rate of co-current air. Makishima et al (56) adapted Shirai's (35) fluid analogy for solids pressure and by adding to it a term to account for the interstitial fluid pressure calculated from the Ergun equation (103) for fluid flow through packed beds. De Jong (57) based an empirical correlation for the solids flow rate on a mechanical energy balance. Shinbara (54) recently published an account of an investigation on the effect of the ambient fluid and a co-current air stream on the flow of cohesive solids through an orifice.

Solids Flow through Orifices Set in the Sides of Fluidised Beds

Another topic which seemed relevant was the flow of solids through orifices set in the walls of fluidised bed containers. Massimilla et al (58, 59) assumed that the fluid pressure drop in passing through the orifice was mainly due to frictional losses incurred in percolating past the flowing solids, since at the orifice the fluid was travelling faster than the particles. This fluid pressure drop was related to the air flow by a Kozeny-Carman equation for the turbulent region by employing a radial flow

model for the conditions just upstream from the orifice. Attempts were made to check the result by a force balance on the particles at the orifice, although these suffered from a lack of data regarding suitable drag coefficients. The correlations presented were not regarded as suitable by the present author, for calculating solids mass flow rates, but the method of analysis did prove useful in the determination of voidage values at the orifice (Chapter 3).

Zenz (37) drew the analogy between the efflux of fluidised solids through an orifice and the efflux of a true fluid by modifying the fluid orifice equations:

$$M_f = C\,\varphi_f A_o (2gH_o)^{0.5} \qquad (2.31)$$

where C = orifice coefficient, H_e = height of liquid

to give:

$$M_s = C\,\frac{\pi}{4}\,\varphi_B (D_o - kd_p)^2 (2gH_B)^{0.5} \qquad (2.32)$$

Stemerding (60) noted a similar result in that data for a wide range of particle sizes discharged from fluidised beds through square and circular orifices fitted the equation:

$$M_s = C A_o \varphi_B (2gH_B)^{0.5} \qquad (2.33)$$

where φ_B was the bulk density at incipient fluidisation,

H_B was the height of the bed,

C = 0.5, discharge coefficient.

Jones and Davidson (61) noted a remarkable similarity between this result and the orifice equation for true fluids and showed that the data from their extensive experimental programme, as well as that of Massimilla et al (59), could be correlated by:

$$M_s = C A_o \varphi_B (2gH_B)^{0.5} \qquad (2.34)$$

where C was a discharge coefficient ranging from 0.28 - 0.50, depending on orifice diameter. Further, the pressure drop across the orifice could be related to the height of the bed above the orifice at incipient fluidisation

by $\Delta P_o = \varphi_B H_B$ for ΔP_o in mm H_2O. Thus, equations (2.32, 2.33 and 2.34) became identical to:

$$M_s = C A_o (2g \varphi_B \Delta P_o)^{0.5} \qquad (2.35)$$

with the appropriate value of C in each case.

The analogy between true fluid flow and air-induced solids flow seemed to have far more justification than the analogy with gravity solids flow, since the inertia forces to accelerate the particles could be provided by drag forces due to the flow of fluid through the orifice with the particles.

2.2 Solids Flow in Standpipes and the Effect of Standpipes on the Discharge of Solids from a Hopper

Much of the early interest in the down-flow of solids in standpipes started around 1940 with the problems of moving solids between the various stages of catalytic cracking processes in the petroleum industry (62). The down-flow of solids in such standpipes was associated with the movement of the interstitial fluid medium, i.e. either in counter-current flow (upwards) or co-current flow (downwards). Usually, the solids movement could be considered as packed bed flow, but if the solids moved downwards rapidly enough to produce effective counter-current fluid flow through the interstices, then the particles could become fluidised, and would flow at considerably higher rates than predicted by correlations referring to the systems of true fixed bed density (e.g. orifice flow correlations) (62).

Shanahan and Schwarz (63) studied the down-flow of uniform sized beads in a 1-inch internal diameter standpipe with a superimposed air flow in either direction, the solids flow rate being controlled by an orifice at the base of the standpipe. They were interested in the conditions for fluidisation to take place in any part of the standpipe, and deduced from their results that fluidisation could occur over any section of the standpipe when the pressure drop per unit length was equivalent to the weight of solids in that particular section, even though the pressure at the point of fluidisation was less than the equivalent weight of the column above it. Kojabashian (64), in a subsequent work, investigated the down-flow of

fluidised solids through a standpipe from a feed hopper in which the solids were already fluidised. He was concerned with the conditions at which defluidisation in the standpipe took place and demonstrated that this was caused both by wall friction and reductions in air velocity. The present author did not consider that this type of flow was completely analogous to the situation in a standpipe connected to the outlet of a bulk storage hopper. In the latter case, the air flow was always co-current, and the air and solids flow rates in the standpipe were interdependent and not independently controlled; however, it was worth noting that this type of investigation proved important in the determination of the factors influencing the flow between the various stages of fluidised catalytic cracking processes, and that work in this field was still progressing (65, 66).

The first investigation of the effect on solids flow of standpipes attached to the outlet of a hopper was made by Bingham and Wikoff (67). They studied the flow of dry sand through capillary tubes, but clearly their work was on a very small scale for the field of solids handling, the 'hopper' being a 30 mm diameter funnel to which they attached capillaries of three different diameters (max. 3.5 mm) and eight different lengths (max. 202 mm). Nevertheless, their work was interesting as a first account, and their main conclusions worth noting:

(i) The solids mass flow rate was virtually independent of head.

(ii) The rate of efflux increased as the length of capillary was increased.

(iii) The solids mass flow rate was proportional to $D_t^{2.65}$, where D_t was the radius of the capillary.

Evans (36) reported the work of two student projects on this subject: Shipley (68) investigated the flow of powder under gravity through tubes of varying length and diameters under different degrees of vacuum. He found that the flow rate of sand through the tubes decreased as the total pressure

in the apparatus decreased. He explained this by saying that when the sand fell down the tube it created a drag on the air, causing it to flow co-currently and creating a pressure difference between the top and bottom of the tube. The pressure at the top of the tube was thus lower than the pressure surrounding the apparatus, so that there was a pressure drop acting across the solids bed in the hopper and the flow rate was increased. When the apparatus was evacuated, there was less air available and hence the drag effect of the sand in the standpipe was not so pronounced. The other student, Whiteway (69), supplementing this work, found an increased flow with increase in length of standpipe attached to a hopper orifice. He noted that a small increase in pressure was sufficient to stop the flow completely. He thus concluded, qualitatively, that the flow rate through a hopper orifice was highly dependent on the fluid pressure below the orifice.

Trees (70) carried out experimental work in tonnage quantities (up to 74 tons/h) to determine the rate of flow of particulate iron oxide through open-ended, sloping pipes and through sloping pipes connecting fluidised beds. Using four pipe diameters (1", 2", 3" and 4" nominal), three pipe lengths (3', 6' and 9') and three angles of inclination (45°, 60° and 75°) to the horizontal (θ_1) he found that the flow rates through open-ended pipes were correlated by:

$$M_s = C D_t^{2.5} \theta_1^{2.5} \qquad (2.36)$$

His range of pipe lengths was rather small so that the effect of length could not be determined accurately, although his results did suggest that for large diameter pipes, solids flow rate decreased with increase in length, and that for small diameter pipes the solids flow rate increased with increase in length, this effect being more pronounced at the steeper angles of inclination of the pipe. No explanation of these phenomena was attempted by Trees.

Evans (36) reported that the presence of a standpipe increased the rate of discharge of solids through an orifice and reduced the pressure below the

orifice. He attached the standpipe (12' x 1") to the hopper orifice by means of a chamber interposed between the hopper orifice and the standpipe entrance, thus allowing independent control of the orifice diameter (max. 4"). His main interest was pressurised flow of solids through the orifice and he used the standpipe together with a supply of air to the chamber as a convenient means of controlling the pressure below the orifice. Nevertheless, he showed that in some circumstances the hopper outflow could be increased by up to 400% by an air pressure difference across the orifice, and incidently demonstrated some interesting facts about the solids carrying capacity of vertical pipes. In one case, the solids flow through a 4" orifice was entirely carried by a 1" diameter standpipe (using silica gel catalyst). In addition, he performed an empirical study of the fluid pressure distribution along the standpipe which showed similar profile shapes to those presented in the present investigation. He did not, however, pursue the effect of the standpipe on the solids flow rate in depth, and gave only a qualitative account of the suction effect of the standpipe.

A further small-scale investigation on the flow of solids through vertical and inclined tubes was performed by Manchanda et al (71), making extensive use of specially constructed funnels. They determined the solids flow rate under constant and varying head conditions, varying discharge openings (with constant inclination of the funnel leg), and varying the inclination of the leg (from vertical to 60° from the vertical), keeping the discharge opening constant. The results for vertical funnels with varying discharge openings correlated to:

$$M_s = C D_t^{2.53} \qquad (2.37)$$

and they concluded that the flow rate was independent of head. The effect of inclination of the funnel leg for constant discharge opening was to increase the solids flow rate. It must be noted, however, that the leg of the funnel was integral with the main body and that moving bed flow was present throughout the apparatus, so that the results seemed more applicable

to inclined hoppers than to standpipe flow.

Bulsara (50) noted that attaching a tube to a hopper orifice induced very cohesive materials such as fly-ash to flow freely. The runs were started with the tube full and the fly-ash was seen to extrude from the bottom like toothpaste, thus moving bed conditions were present in the standpipe. Miles et al (72) studied the effects on solids flow of varying hopper cone angles and tubular extensions to the orifice. They noted that, in general, extending the hopper outlet by means of a tube increased the flow rate of sand (60 μm) in the non-mass flow hoppers but had an insignificant effect on the flow from the mass flow hoppers. There was no effect with gravel (3 mm).

Richards (85) showed that for fine sands, the solids mass flow rate increased greatly as the standpipe length increased to 2 or 3 diameters, but that the rate of increase was less for longer standpipes. At 50 diameters the solids flow rate could be 50% or more over that through orifices of the same diameter for fine sands, but only 15% for coarser sands.

McDougall (73) developed a model to account for the results of Evans (36). From a force balance performed on the particles in the standpipe and an energy balance over a section of the standpipe, he was able to calculate the pressure profile along the standpipe. However, owing to the necessarily large number of basic assumptions and the paucity of experimental data, the agreement between the theoretical and experimental pressure values was not good, although the forms of the theoretical profiles were very similar to the experimental profiles. The model threw little light on the problem of predicting solids flow rates but it did illustrate how many variables might be involved in the description of this type of flow. He emphasised that the lack of data was one of the main problems, and that further work, both experimental and theoretical, was needed.

A more detailed investigation of the standpipe effect was carried out by Yusa et al (74). They studied the flow of glass beds through standpipes

attached directly to an orifice in the base of a hopper, using five tube diameters (max. 9 mm) and five tube lengths (max. 1.5 m). They demonstrated that the flow rate of solids increased with increased standpipe length and that it tended towards a limiting value; increases in flow rate of up to 600% could be obtained compared with that obtained without the tubes. They showed that the particle diameter affected both the fluid pressure below the orifice and the solids mass flow rate, the flow rate and reduction of orifice pressure increasing with decrease in particle diameter. They correlated the solids flow rate with the absolute pressure below the orifice (P_1) (presumably measured just below the entrance to the standpipe, although this is not clear). Neglecting the pressure above the orifice and basing their equation on that used by Bulsara (50), they found that:

$$M_s = C \varphi_B^{0.5} (P_o - P_1)^{0.5} (D_o - kd_p)^{2.0} \qquad (2.30)$$

where P_o was atmospheric pressure

which did not account for the flow due to gravitational forces. Further tests conducted while externally controlling the air pressures below the orifices showed that this equation was suitable for describing the pressurised solids flow, although the authors did not seem to recognise that a term to account for gravity flow might be necessary as well.

The pressures in the 1.5 m tube were measured at four points, showing a 'hooked' shape at the entrance to the tube with a linear progression to the exit. A pressure gradient per unit length, based on a linear approximation, was assumed to be roughly proportional to the solids flow rate, particle diameter and standpipe diameter, given by:

$$(P_o - P_1) = C_1 \left(M_s L_t / d_p D_t^2 \right)^Y \qquad (2.38)$$

where $Y = 0.7$ and $C_1 = 1.26 \times 10^{-3}$

Combining this with equation 2.30 and a term for gravity flow, derived also from equation 2.30, they concluded that:

$$\frac{(M_s^2 - M_{so}^2)}{M_s} = C_1 C^2 \varphi_B (D_o - kd_p)^4 (L_t / d_p D_o^2)^\gamma \qquad (2.39)$$

The left-hand side of equation 2.39 was plotted against the right-hand side divided by C_1. At very low solids flow rates there was some agreement but over most of the range, and especially at the higher flow rates, there was considerable divergence. It was not shown how equation 2.38 was arrived at and the present author concluded that this sketchy relation was the main source of error in the work. Although the simple empirical relationship presented did not seem at all satisfactory, nevertheless, the descriptions of the phenomena associated with this type of system were most valuable.

2.3 The Gravity Flow of Particulate Solids

Many factors are known to affect the flow of particulate solids through hoppers, pipes and orifices - not all of which have been satisfactorily included in the general correlations so far published for solids flow rate. In addition, a main difficulty with equipment handling granular solids is the interruption of flow by arching or stick-slip movement of the solids particles. Sets of empirical equations and conditions have been presented for which arching is less likely to occur, and which aim at overcoming the difficulties in the handling of dry particulate solids. Some general rules regarding the avoidance of blockage, together with the effect on the solids mass flow rate of some of the particle and apparatus variables, are given below, viz:

(i) The internal diameter of the solids bed container should exceed 5-7 times the diameter of the largest particle (12), and above this ratio there should be no effect on solids flow rate (18); in addition, Rose et al stated that container diameter to orifice diameter ratios exceeding 2.6 have no effect on the solids mass flow rate (6).

(ii) Materials of narrow size range flow better than those with a wider size range (12).

(iii) Smaller particle size tends to increase the solids mass flow rate (34, 33, 45): experimental work (45) indicated that this was due to dilation of the solids bed about the orifice. However, Gregory (12) noted that fine materials of particle size less than 75 μm have a pronounced tendency to stick, which agrees with the generally accepted view that powders containing a substantial proportion of particles 100 μm or smaller in diameter differ considerably in flow behaviour from larger particles (80). At small orifice diameter to particle diameter ratios, blockage at the orifice is liable to occur. It has been noted that as D_o/d_p approaches 6.0, the flow becomes irregular (18) or stops (8) while others say the orifice is likely to block at $D_o/d_p \leq 4.0$ (38) or $D_o/d_p < 3.0$ (6, 75). Harmens (42) conducted experiments with $D_o/d_p \geq 5.0$ and Beverloo (19) stated that for $D_o/d_p > 20.0$ the effect of this diameter ratio was negligible. Rose et al (75) related blocking aperture diameter to particle diameter and shape factors and also, quoting Tanaka, stated that the flow of non-cohesive materials from hoppers ceased when:

$$\frac{d_p(v/s)}{D_o(c)} = 0.17 \text{ to } 0.23 \qquad (2.40)$$

where d_p (v/s) = diameter of a sphere having the same specific surface as the particle, and $D_o(c)$ = the critical or blocking orifice diameter. Furman (1), quoting Kvapil, stated that the critical area of a circular orifice was $0.85\ (5d_p)^2 1.4$, or critical diameter was $5.45\ d_p$.

(iv) Mild steel containers give rise to slip-stick flow more readily than stainless steel or glass (12).

(v) The solids head above the orifice has no effect on the flow rate except at very low heads (6, 16, 18, 19, 34, 38).

(vi) The solids flow rate is independent of initial voidage (16, 38) and that during flow the solids bed forms its own characteristic voidage (33, 83).

(vii) Deming (9) and Rausch (34) found that the solids flow rate

increased with increase in hopper cone angle. Miles (72) showed that for gravel, the solids mass flow rate was constant for hopper angles less than the internal angle of friction of the solids, and that the solids flow increased with hopper cone angles above that value, although this was not so pronounced for sand. Others have confirmed this type of situation (16) and Harmens (42) states that for the hopper cone angle less than the solids internal flow angle, the mass flow rate is the same as that with a flat-bottomed hopper.

(viii) Surface moisture should be kept below 1% - 2% (12, 77).

(ix) Any abrupt change in direction should be accompanied by an increase in cross-sectional area of the conduit (77).

Flow Patterns

A flowing powder often has the characteristic that there is a rapid change of voidage within a small region of the powder and, as a first approximation, this region can be treated as a surface -- the surface of sliding. As a result of such surfaces, the behaviour of the solids in the bed can be described in terms of flow patterns which highlight regions of different modes of solids flow. The general method of observing these flow patterns is by using a hopper with a transparent wall containing alternate layers of coloured and uncoloured powder, and to photograph the pattern at intermediate periods during the flow (76, 80). For a three-dimensional system, in which the flow patterns are different from the two-dimensional system (27), the solids flow can be 'frozen' in wax or resin and then cut into sections for examination (81, 82).

Brown and Richards (83) have noted that an appreciable time can elapse between initiation of flow through a hopper orifice and observation of movement at the top surface of the solids bed. They attributed this to the Reynolds' Principle of Dilatancy (Chapter 1) and to the likelihood of a dilation wave passing through the bed. This has been observed and described by several authors (36, 40, 80, 82).

For fully developed flow, Brown and Richards (38) postulated several well-defined regions of movement; Kvapil (76) took a different view and conceived only two basic regions:

(i) a mode of 'primary' movement, in which all the particles move in a vertical direction, and

(ii) a mode of 'secondary' movement, in which particles also have transverse and rotational velocities.

He considered that these regions took the form of ellipsoids. Other workers have postulated different regions of flow for both the initial period of flow (82) and fully developed flow (84).

2.4 Related Fields of Study

Investigation into the literature of subjects that were, at the outset, considered to be related to the flow of solids, especially in connection with the flow through the standpipe, e.g. pneumatic conveying of solids, fluidisation, sedimentation, and theoretical fluid dynamics, showed that these fields of study were, in general, of little relevance to the present investigation. Thus, it was proposed not to present a detailed survey in this text, and only to reference those papers mentioned in the main body of the work. Nevertheless, it should be noted that books by Zenz and Othmer (62), Soo (86), Boothroyd (87) and Davidson and Harrison (88) were considered to give very good coverage to some, or all, of those subjects and to cite between them almost all of the important literature in those fields of study.

CHAPTER 3

Theory

An early study of the results in conjunction with the nature of the apparatus showed that far more could be studied than just the flow of particulate solids through vertical standpipes and the effect of these standpipes on the solids mass flow rate from the hopper. Full use of the various sections of the apparatus was made, allowing subsidiary investigations into the bulk density of a moving bed, the air flow through a moving bed, the voidage at the hopper orifice and the effect of air flow on the solids discharge through the orifice. This chapter is divided into sections corresponding to the different units and regions apparent in the apparatus.

3.1 The Feed Hopper - the Moving Solids Bed Bulk Density and Voidage

Consider a solids bed in a hopper where the solids discharging from an opening at the base of the hopper induced a metered flow of air into the hopper through another opening above the surface of the bed: such was the case in the solids feed hopper (Figure 4.1). It was assumed that any air pressure differences across the feed bed were small and had no effect on the air flow due to the comparatively large resistance of the feed bed compared with the gas meters. It was also assumed that the flow of solids was slow enough not to induce any slip between the phases in the feed bed and that the interstitial air was carried co-currently with the solids: thus the air flow rate Q_{fb} through the meter 1 was a measure of the total volume flow rate of the bed. If it could also be assumed that the air flow rate Q_{fb} was dependent only on the solids mass flow rate, and that the feed bed voidage did not vary with solids mass flow rate, then:

$$Q_{fb} \propto M_s$$

The proportionality constant turned out to be the inverse of the bulk

density for the flowing solids bed, thus:

$$\rho_{fb} = \frac{1}{\varphi_B} M_s \qquad (3.1)$$

The voidage of the moving solids bed was related to the particle and air densities by:

$$\varphi_B = e_B \varphi_a + (1 - e_B) \varphi_s$$

$$\text{or } e_B = \frac{\varphi_s - \varphi_B}{\varphi_s - \varphi_a}$$

In the present system where $\varphi_s \gg \varphi_a$ the equation could be simplified to:

$$e_B = 1 - \frac{\varphi_B}{\varphi_s} \qquad (3.2)$$

Clearly, this was the same as the voidage relationship for a static bed due, of course, to the assumptions made previously.

3.2 The Constant Depth Bed - Air Flow through a Moving Solids Bed

Consider a solids bed enclosed in a cylindrical, flat-bottomed hopper where, as the solids discharged through an orifice at the base of the bed, further solids flowed into the hopper keeping the upper surface of the bed at a constant level: such was the case in the lower section of the hopper system in the present apparatus (Figure 4.1). A pressure drop existed across this bed due to a reduced pressure below the orifice caused by the flow of solids through the standpipe below. The resultant air flow into the system above the surface of the bed was recorded by meter 2.

It was assumed that the constant depth bed had the same bulk density as that in the feed hopper and that the same values of moving bed bulk density and voidage applied. The total air flow through this bed was considered as the sum of the flow rate of the interstitial air introduced with the solids from the feed bed and the flow rate of the air entering above the bed induced by the pressure drop $P_2 - P_3$ (Figure 4.1), that is the percolating air Q_{ap} measured by meter 2.

For the flow through a fixed bed it is usual to relate the air flow

with the pressure drop across the bed by means of equations of the Kozeny-Carman type.

For streamline flow conditions the Kozeny-Carman (96) equation has the form (for Re', < 2.0):

$$Q_a = U'_a A_B = \frac{1}{k''} \frac{e^3_B}{(1 - e_B)^2} \frac{A_B}{S^2} \frac{\Delta P_B}{\mu l_B} \qquad (3.3)$$

where:

$$Re'_1 = \frac{U'_a}{e_B} \frac{e_B}{S(1 - e_B)} \frac{\varphi_a}{\mu} = \frac{U_a e_B \varphi_a}{S(1 - e_B)\mu} \qquad (3.3a)$$

and:

$$U'_a = e_B U_a \qquad (3.3b)$$

If the bed was moving as a whole, i.e. the particles were in motion relative to the container wall, and if it could be assumed that:

1. the average particle velocity was constant at any part of the bed, and
2. the particles remained essentially in contact with each other during their passage through the bed (i.e. the voidage remained constant over the whole bed),

then it could reasonably be expected that the above form of expression could be used to describe the flow of air through a moving bed of particles.

The simple Kozeny-Carman equations, however, balance the forces relating the flow of air past stationary particles. As the particles were moving, it was thus necessary to include also the relative velocity between the air and the particles.

Hence the appropriate expression for streamline flow was:

$$e_B A_B (U_a - U_s) = \frac{1}{k''} \frac{e^3_B}{(1 - e_B)^2} \frac{A_B}{S^2} \frac{\Delta P_B}{\mu l_B} \qquad (3.4)$$

This equation gave Q_{ap}, the flow rate of the air percolating through

the constant depth bed. The total air flow rate through the bed was, of course, still given by the same relation used for a fixed bed.

$$Q_{at} = A_B U'_a = e_B A_B U_a \tag{3.5}$$

For a particle bed of constant depth, equation 3.4 could be expressed as:

$$Q_{ap} = e_B A_B (U_a - U_s) = k_B \Delta P_B \tag{3.6}$$

since:

$$k_B = \frac{1}{k''} \frac{e^3_B}{(1 - e_B)^2} \frac{A_B}{S^2 \mu l_B}$$

which would remain constant.

A superficial solids velocity could be defined in the same way as that for the superficial air velocity (equation 3.3b):

$$(1 - e_B) A_B U_s = A_B U'_s = Q_s$$

$$\text{or } U'_s = (1 - e_B) U_s \tag{3.7}$$

Substitution of equations 3.3b and 3.7 into equation 3.6 gave:

$$A_B U'_a - \frac{A_B e_B U'_s}{(1 - e_B)} = k_B \Delta P_B$$

$$\text{or} \quad Q_{at} - \frac{Q_s e_B}{(1 - e_B)} = k_B \Delta P_B \tag{3.8}$$

As $Q_s = \frac{M_s}{\varphi_s}$

then:

$$Q_{at} = \frac{e_B}{(1 - e_B)} \frac{M_s}{\varphi_s} + \frac{1}{k''} \frac{e^3_B}{(1 - e_B)^2} \frac{A_B}{S^2} \frac{\Delta P_B}{\mu l_B} \tag{3.9}$$

Thus, as already stated, the total air flow rate (Q_{at}) could be treated as the sum of the interstitial air flow rate (Q_{ai}) and the percolating air flow rate (Q_{ap}).

Equation 3.3 was developed for spherical particles. For those cases where the particles could not be considered completely spherical, a shape factor is usually incorporated. One shape factor for uniform sized particles used in the Kozeny-Carman equation was that reported by Morse (102),

the sphericity, ϕ_s, defined as the surface area of a sphere of the same volume as the particle divided by the actual surface area of the particle. The definition of specific surface (5) for non-spherical particles involved this concept:

$$S = \frac{6}{d_p \phi_s} \quad \text{for non-spherical particles.} \qquad (3.10)$$

With this proviso, it was clear that both equation 3.9 and the definition of Re' could be broadened to cover moving beds of non-spherical particles.

3.3 Solids Discharge through an Orifice

As noted in the literature survey, one of the most remarkable features of the investigations into the flow of particulate solids through an orifice was the variety of hypotheses suggested for the correlation of solids flow rate with orifice diameter. Nevertheless, it was not the main aim of this project to study in detail such flow, and consequently the apparatus had not been designed for such a study. However, there did seem to be some confusion in the literature about the relationship of solids flow rate with orifice diameter when the solids flow was aided with a co-current stream of air through the orifice: moreover, confusion also seemed apparent over the inclusion of the solids flow due to gravitational forces in the equations for air-induced flow. It was concluded that some classification of these equations would be useful not only for the correlation of the present experimental data but also for future workers.

Initial investigations (4, 7, 11, 12) into flow of particulate solids through an orifice were only concerned with gravity flow, that is the solids fall through a horizontal orifice under the influence of gravitational force only. Experimental observations showed that the solids mass flow rate was a function of orifice diameter:

$$W_s = k D_o^n \quad \text{where } n = 2.5 \text{ to } 3.0 \qquad (3.11)$$

Various theoretical determinations (9, 34, 37, 38) using widely differing

lines of approach consistently indicated a relationship of the form:

$$M_s = kD_o^{2.5} \qquad (3.12)$$

These expressions generally included other variables and could be summarised by the equation:

$$M_s = C_g \frac{\pi}{4} \varphi_B (2g)^{0.5} D_o^{2.5} \qquad (3.13)$$

where C_g was a correction factor often described as an orifice discharge coefficient. The theoretical investigations related this factor to various solids variables, including the angle of repose, angle of internal friction, and particle size, and might be regarded as attempts to reconcile the differences between the fluid analogy and the soil mechanics analogy for granular solids flow.

Another semi-empirical correction factor had been introduced to reconcile the observed variability of the index of orifice diameter. This was based on the concept of the 'statistically empty annulus' at the edge of the orifice (38). This space, related to the particle diameter, changed the orifice diameter term to $(D_o - kd_p)$, and had the effect of reducing the experimental values of the index to 2.5, so that:

$$M_s = C_g \frac{\pi}{4} \varphi_B (2g)^{0.5} (D_o - kd_p)^{2.5} \qquad (3.14)$$

Further investigations into solids flow through orifices included the effects of air flowing co-currently or counter-currently to the solids stream. Initial attempts at describing this situation produced relationships of the form[50]:

$$M_s = C_p (2g \varphi_B)^{0.5} D_o^{2.0} \Delta P_o^{0.5} \qquad (3.15)$$

Such a relationship clearly did not account for the flow through the orifice when the air pressure difference across the orifice was zero, i.e. in the case of gravity flow; further suggestions produced equations of the form [49, 52, 51]:

$$M_s = \frac{\pi}{4} C_p (2g \varphi_B)^{0.5} D_o^{2.5} (\Delta P_o + \Delta P_c)^{0.5} \qquad (3.16)$$

where ΔP_c was a 'pseudo-pressure drop' introduced to account for the

gravity flow. Kuwai (49) proposed finding the value of ΔP_c by projecting the graph of M_s vs ΔP_o back to the abscissa ($M_s = 0$), whereas Knowles (52) suggested continuing the measurement of the solids mass flow rate with counter-current air (i.e. negative values of ΔP_o) to find the value of ΔP_o which caused the solids flow to cease, so that $\Delta P_o = \Delta P_c$.

Investigation of air-induced solids flow alone was not possible in conventional solids hopper systems, but it has been studied in connection with the flow of solids streams through vertical orifices set in the walls of fluidised bed containers (57, 60, 61). It was found that there was a remarkable similarity between the equation for solids mass flow rate through such orifices and the well known equation for the flow of inviscid fluid through an orifice, giving:

$$M_s = Cp \frac{\pi}{4} D_o^2 (2g \varphi_B \Delta P_o)^{0.5} \qquad (3.17)$$

for the flow of solids.

An attempt at explaining this similarity was made by considering the forces between the air flow and the solids particles (61). The inertial forces needed to accelerate the particles were provided by drag forces due to the co-current flow of air through the orifice with the particles (61), and so it was expected that this equation would describe the flow rate of small particles more accurately than that of larger particles, due to the lower inertia of small particles (72).

If it could be assumed that the air-induced flow of solids through a horizontal orifice at the base of a hopper was caused by the sum of two pressure components, one due to gravity flow and the other due to pressure flow, then equations 3.12 and 3.17, suitably combined, might describe the consequent solids mass flow rate.

Thus, equation 3.17 showed that for pure pressure flow, the solids flow rate (M_{sp}) was caused by the pressure difference ΔP_o:

$$\Delta P_o = \frac{M_{sp}^2}{(Cp \frac{\pi}{4} (2g\varphi_B)^{0.5})^2 D_o^4} \qquad (3.18)$$

while for gravity flow the pseudo-pressure ΔP_C caused the flow (M_{sg}) so that if:

$$\Delta P_C = \frac{C^2 g}{C^2 p} \varphi_B D_o \qquad (3.19)$$

an equation analogous to 3.18 could be produced for gravity flow, i.e.

$$\Delta P_C = \frac{M^2_{sg}}{(Cp \frac{\pi}{4}(2g \varphi_B)^{0.5})^2 D^4_o} \qquad (3.20)$$

which was nevertheless consistent with equation 3.17.

Then the total flow due to both pressures, M_s, would be given by:

$$(\Delta P_o + \Delta P_C) = \frac{M^2_s}{(Cp \frac{\pi}{4}(2g \varphi_B)^{0.5})^2 D^4_c} \qquad (3.21)$$

Comparison between equations 3.16 and 3.21 showed a different index value for the orifice diameter term; 2.5 in equation 3.16 and 2.0 in equation 3.21. Use of equation 3.16 required the orifice discharge coefficient to have a dimension $L^{-\frac{1}{2}}$, whereas the orifice discharge coefficient in equation 3.21 was dimensionless, as was the case for fluid flow. If it could be assumed that the two orifice coefficients in equation 3.19 were identical (19, 61), then equation 3.19 became:

$$\Delta P_C = \varphi_B D_o \qquad (3.19a)$$

As in the case of gravity flow, the concept of the statistically empty space could be introduced, without any conflict, into the present equations to describe the air-induced flow of solids. Thus modifying equations 3.19a and 3.21 to:

$$M_s = Cp \frac{\pi}{4} (D_o - kd_p)^2 (2g \varphi_B)^{0.5} (\Delta P_o + \Delta P_C)^{0.5} \qquad (3.22)$$

where

$$\Delta P_C = \varphi_B (D_o - kd_p) \qquad (3.23)$$

and where the value of k had to be found from experiment or the literature.

3.4 Particle Velocities and Voidage in the Region of the Orifice

In order to calculate the velocities of the particle stream in the transition chamber and the standpipe (Figure 4.1), it was necessary to

have a knowledge of the particle velocities at the orifice. In the case of gravity flow, Brown (41) developed a model for determining the particle velocity profile across the orifice, integration of which then gave the solids mass flow rate. This model was used with some success for large particles where there was little influence of the interstitial air (46). In the case of smaller particles, or air-induced flows, this model was less useful (46) due to the significant effect of air drag on the particles. Recently, other investigators (45, 46, 47) have extended Brown's model to cover the effect of interstitial air flow and have concluded that the values of the voidage around the orifice must be determined before an accurate prediction of the solids flow rate can be made.

Previously, the usual method of estimating solids velocities at the orifice was to use a value of the voidage for the solids bed and to use this value in a continuity equation assuming a flat velocity profile across the orifice to obtain an average value of particle velocity. This value of voidage, recommended by Delaplaine (33) and subsequently used by Evans (36), was the maximum static bed voidage or, if possible, a moving bed voidage value.

Recent work has shown good evidence to suggest that the voidage of the moving bed increased as the solids moved towards the orifice (45) and that actually at the orifice itself there was a substantial increase as the solids passed through the free fall arch and moved into the particle cloud flow condition.

Little has been published about the effect of air flow on the particle velocities and voidage at the orifice of a hopper. There has, however, been some investigation into the flow of a solids stream through a vertical orifice in the walls of a fluidised bed container (58, 59, 61). This orifice was set between the air distributor and the surface of the fluidised bed: Jones et al (61) measured particle velocities and tailored their equations specifically to predict the flow of solids for various

fluidised bed heights. Massimilla et al (58), on the other hand, investigated the fluid pressure drop across the orifice and while the present author considered that their equations were not suitable for solids flow rate determination, their method of approach was more applicable to the present situation in that it had been used to estimate the voidage at the orifice.

The method used in the present investigation was essentially that of Massimilla's, although extensive modifications were made in applying it. It was necessary to make certain assumptions in using this method of analysis of the orifice region: 1) the voidage in the region above the orifice was assumed constant; and the solids and air velocities were assumed to depend only on distance from the orifice, that is the flows obeyed a continuity relationship of the form:

$$U_s = \frac{Q_s}{\pi r^2 (1 - e)} \quad , \quad U_a = \frac{Q_{at}}{\pi r^2 e} \qquad (3.24)$$

which was equivalent to assuming a spherical symmetry restrained to a conical approach to the orifice: 2) the percolation of the air through the moving solids was governed by equations for fixed beds, e.g. Kozery-Carman or Ergun equations as discussed in Section 3.2: 3) the solids/air stream moved as an inviscid fluid and that the inter-particle friction forces were negligible; the motion of the particle stream would be governed by fluid flow and the relevant pressure at any point would be the air pressure: 4) the particle and air velocity profiles were flat, although the average particle and air velocities would not, in general, be equal. Further, Massimilla et al stated that the pressure drop across the orifice was due almost entirely to frictional losses caused by the air percolating past the solids frowing the orifice, and that the energy losses due to the passage of air and solids through the orifice were negligible in comparison.

With these assumptions in mind it was possible to relate the air

pressure drop over the orifice to the flow of air and solids by using the same type of equations as those for fixed or moving beds. Massimilla et al (58) used a modified Kozeny-Carman equation for the turbulent region, while Jones et al (61) used a simple Darcy's Law model, which nevertheless amounted to the same thing. The values of particle Reynolds' numbers determined the type of equation used. The values in the present investigation extended from the streamline to the turbulent region. It was decided to employ the Ergun equation (103) in the present context, since this was a combined form of the Kozeny-Carman equation and the Blake equation and best described the present range of conditions. Thus, for fixed beds:

$$\frac{dP}{dl} = \frac{150\mu U_a}{d_p^2 g \phi_s^2} \frac{(1-e)^2}{e^2} + \frac{1.75 \rho_a U_a^2}{d_p g \phi_s} \frac{(1-e)}{e} \qquad (3.25)$$

For the moving bed situation the slip velocity must be incorporated:

$$U_r = U_a - U_s \qquad (3.26)$$

substituting from equation 3.24:

$$U_r = \frac{1}{\pi r^2}\left(\frac{Q_{at}}{e} - \frac{Q_s}{(1-e)}\right) \frac{Q}{\pi r^2} \qquad (3.27)$$

The distance from the orifice was measured in terms of r, a radius from the centre of the orifice, so substituting for l and U_r in equation 3.25 gave:

$$\frac{dP}{dr} = \frac{150\mu}{d_p^2 g \phi_s^2} \frac{(1-e)^2}{e^2} \frac{1}{\pi r^2}\left(\frac{Q_{at}}{e} - \frac{Q_s}{(1-e)}\right) + \frac{1.75\rho_a}{d_p g \phi_s} \frac{(1-e)}{e} \left(\frac{1}{\pi r^2}\right)^2 \left(\frac{Q_{at}}{e} - \frac{Q_s}{(1-e)}\right)^2 \qquad (3.28)$$

which was shortened to:

$$\frac{dP}{dr} = k_1 \frac{Q}{\pi r^2} + k_2 \frac{Q^2}{\pi^2 r^4} \qquad (3.29)$$

Equation 3.28 thus related the variation of pressure with distance r from the orifice for constant air and solids flow rates. The part of the system under consideration was that adjacent to the orifice. It was normally assumed that there was a free fall arch above the orifice from which the

particles fall and, further, this analysis implied that this arch was centred on the orifice with a radius r_o. It was noted that this did not tie up exactly with Brown's definition (38) of the shape of the arch, which he defined with the angle of sliding or hopper cone angle. In the present situation of pressure flow it had not been shown that the angle of sliding was the same as that for gravity flow: indeed, the angle was not known. Therefore, as a first assumption, it was felt that the restrained spherical symmetry adequately described the situation adjacent to the orifice.

As was assumed above, the use of a constant voidage in the region of the orifice meant that equation 3.28 could be integrated without difficulty. The assumptions of radial flow as described by equation 3.24 did not apply at a radial distance less than r_c (the orifice radius) from the orifice. It was, therefore, proposed that this distance r_o should be taken as the lower limit of integration. The validity of the position of the pressure tapping above the orifice, and the readings obtained from it, were not necessarily applicable in this context, since it was not considered wise to put the pressure tapping directly in the solids stream so near to the orifice where it might interfere with the solids flow. Consequently, some arbitrary position for the upper limit of integration was chosen, at a radial distance R.

The integration of equation 3.28 or 3.29

$$\frac{dP}{dr} = k_1 \frac{Q}{\pi r^2} + k_2 \frac{Q^2}{\pi^2 r^4} \quad \text{over the range } r_o \rightarrow R$$

gave:

$$\Delta P_o = \frac{k_1 Q}{\pi}\left(\frac{1}{r_o} - \frac{1}{R_o}\right) + \frac{k_2 Q^2}{\pi^2 3}\left(\frac{1}{r_o^3}\right) \qquad (3.30)$$

where R_o was considered to be sufficiently greater than r_o to render:

$$\left(\frac{1}{r_o^3} - \frac{1}{R^3}\right) \simeq \frac{1}{r_o^3}$$

Equation 3.30 was seen to be dependent on the value of R. Clearly a solution of equation 3.30 was possible by, for instance, a Newton-Raphson iteration procedure to give estimates of the voidage at the orifice region (e_o) for any value of R. The equation was tested by using different values of R in multiples of r_o with the results from several experimental runs. The resultant values of e_o converged very slowly with increase of R, the values of e_o obtained with $R = \infty$ were not significantly different from those where $R = 4r_o$, and thus it was concluded that the streamline term in equation 3.30 was of less importance than the other term. The position of the pressure tapping was generally within this region and consequently it was felt that the value of R could be taken as infinity without significantly affecting the resultant values of orifice voidage e_o. Thus, equation 3.30 reduced to:

$$\Delta P_o = \frac{k_1 Q}{\pi r_o} + \frac{k_2 Q^2}{3 \pi^2 r_o^3} \qquad (3.31)$$

Equation 3.31 thus gave the relationship between the fluid pressure drop across the orifice and the voidage at the orifice if all other factors were known.

The Air and Solids Velocities at the Orifice

With the values of orifice voidage known, it was possible to calculate the air and solids velocities at the orifice. It was assumed that the values of voidage calculated from equation 3.31 could be applied to the plane of the orifice itself, that the air and solids velocities could be described by an average velocity, and that the velocity profiles were flat at the plane of the orifice. Thus, from a continuity equation:

$$U_{so} = \frac{M_s}{A_o \rho_s (1 - e_o)} \quad , \quad U_{ao} = \frac{Q_{at}}{A_o \theta_o} \qquad (3.32)$$

Check on Voidage Values at the Orifice

Mansimilla et al (58) used an alternative method to check the orifice voidages based on a force balance between the fluid and particles adjacent

to the orifice. Although it was felt that the application of this method to the present system, to check the voidage values, was less justified since it had neglected gravitational forces, it did seem possible that it would elucidate to some extent the magnitude of the particle drag coefficients at the orifice.

Massimilla et al (58) produced from their force balance an equation of the form:

$$-U_s \frac{dU_s}{dr} = \frac{k_3}{\pi^2 r^4} (U_a - U_s)^2 \qquad \text{where } k_3 = \frac{3}{4} \frac{\varphi_a k_D}{\varphi_s d_p \Phi_s} \qquad (3.33)$$

and $k_D = f_n (Re')$ particle drag coefficient.

Integration between the same limits as before, assuming $R \gg r_o$, and substituting equation 3.24 gave:

$$\frac{G_{st}}{Q_s} = \frac{e_o}{1 - e_o} \left(1 + \left(\frac{3}{2k_3 r_o} \right)^{0.5} \right) \qquad (3.34)$$

There seemed no conflict between the two approaches, and so it was thought legitimate to use the values of voidage obtained from equation 3.31 for substitution into equation 3.34 to find values of the particle drag coefficient. Thus, if the reasoning were correct, the values of drag coefficient so obtained would be those for particles in the solids stream at the orifice, and they should correlate well against particle Reynolds' number.

3.5 The Flow of Solids through the Chamber

Situated directly between the hopper orifice and the entrance to the standpipe was the glass chamber (Figure 4.1). This chamber was considerably larger in diameter than any of the orifices or standpipes and it was considered that, due to its presence, the solids flow from the hopper orifice could be thought analogous to the flow into an infinite volume, such as normally would have been the case for solids discharge from a hopper.

It was thought that at the orifice the co-current air moved faster

than the solids (a necessary condition for increased solids flow rate) and that all the solids and air that entered the chamber by way of the orifice left it through the standpipe, i.e. there was no solids build-up in the chamber during steady flow conditions. In general, it was considered that after the air and solids stream had discharged through the orifice some of the air expanded out of the solids stream and flowed through the 'body' of the chamber, being re-entrained into the solids stream as it approached the standpipe entrance. Also, it was recognised that only the solids were subject to further significant acceleration due to gravitational forces, although the air may have been subject to fluid/particle drag forces from the solids within the chamber. At the orifice it was felt that solids were being accelerated by the air flow, whereas at the standpipe the solids stream could have been accelerated or retarded depending on the air flow rate and the orifice and standpipe diameters. Thus, a precise analysis of the solids and air flows in the chamber was not regarded as practicable due to major uncertainties concerning the nature of the expansion of the air from the solids stream below the orifice and its re-entrainment towards the entrance to the standpipe.

To calculate the solids velocities throughout the chamber, it was necessary to make certain assumptions regarding the flow mechanism in the chamber. There seemed to be two major possibilities:

1. A possible minimum value to the solids velocities in the chamber was given from the following assumptions:

   (a) Immediately the stream emerged from the orifice the air 'expanded' to fill the whole cross-section of the chamber, and its considerably reduced velocity was based on the chamber area and was assumed constant throughout the length of the chamber.

   (b) The particles fell under gravitational and fluid drag

influences as individuals without mutual interaction or interference, the relevant solids/fluid drag coefficient being the free field, single particle value based on the relative velocity between the particles and surrounding fluid.

(c) The air flow was immediately re-entrained into the solids stream at the standpipe entrance, and there were no energy losses in the fluid at the orifice or the standpipe entrance.

2. A possible maximum value for the solids velocities was given by assuming that:

(a) the behaviour of the air was as above, and

(b) the solids accelerated solely due to gravitational forces and there was no drag at all with the surrounding air in the chamber, or any particle-particle interference or interaction.

This last assumption was the usual one made when describing a solids stream discharging from a hopper orifice into free surroundings (87), and had been used in an attempt to locate the position of the free fall arch at the orifice (44). As noted above, the situation in the chamber was felt to be analogous to such conditions. In passing, it was worth noting that the sum of the exit effects at the orifice (i.e. solids acceleration due to faster flowing air) was, in the majority of cases, thought likely to be substantially cancelled out by the entrance effects at the standpipe (i.e. solids retardation due to slower moving air).

In accordance with assumptions 1. a force balance on the particles led to the equation:

$$\frac{dU_s}{dz} = \frac{b - a(U_s - U_{ao})^2}{U_s} \qquad (3.35)$$

where $b = g\left(1 - \frac{\varphi_a}{\varphi_s}\right)$, $a = \frac{3}{4} \frac{C_D \varphi_a}{d_p \varphi_s}$

The drag coefficient C_D was found from the usual single particle drag

coefficient relationships with particle Reynolds' number (96), showing that the flow was in the Intermediate region. Hence, the equation 3.35 was not easily solved analytically. Using such relationships as the Schiller-Naumann (96) equation to relate particle drag coefficients and Reynolds' numbers it was necessary to solve the equation numerically, using a Runge-Kutta-Merson method with the values of solids velocity at the orifice as initial values.

Adopting assumption 2. it was possible to use simple dynamic equations to describe the solids velocities. At the standpipe entrance the solids velocity would be given by:

$$U_s^2 = U_{so}^2 + 2gl_c \qquad (3.36)$$

In both cases, the corresponding air velocities and voidages at the standpipe entrance were found by substituting the solids velocity at that point into the continuity equations

$$M_s = (1 - e)\,\rho_s U_s A_t \qquad (3.37)$$

$$Q_{at} = eU_a A_t \qquad (3.38)$$

assuming constant volumetric flow rate of air.

3.6 Solids Flow and Air Pressure Gradient through the Standpipe

Qualitatively the model for the co-current flow of air and solids through a vertical standpipe appeared at first sight to be fairly obvious. Particles entering the top of the standpipe accelerated under gravitational forces and, due to fluid drag forces, the surrounding air was caused to move in the same direction, thus creating a flow of air away from the top of the standpipe and the chamber and reducing the static pressure. Further consideration, however, showed that the situation in the standpipe was more complex. The movement of the air co-currently with the solids served to reduce the particle/air relative velocity with a consequent reduction in mutual drag, thus allowing the particles to accelerate with less restriction. It could be seen that if there were no other forces

acting, then the mutual acceleration could carry on indefinately given a long enough standpipe. However, particle-particle, particle-wall, and air-wall frictional forces would oppose this notion, and at some point balance the accelerating forces, so that the solids and air velocities would reach some limiting values beyond which they could not increase. The nature of this balance of forces was not completely clear since there appeared to be three possible relative velocities to consider - particle-wall velocity, air-wall velocity and particle-air velocity - while it was not known how these would combine and affect each other as any one or any combination approached limiting values. A further consideration which seemed to be inherent in this type of standpipe flow was that the air was forced to flow from a low pressure region in the chamber to a high pressure zone at the exit from the standpipe, solely by the passage of solids.

In an attempt to model the behaviour of the solids and air in the standpipe, it was necessary to make several simplifying assumptions, viz:

1. Steady state flow conditions were assumed for both solids and air: the pressure profiles were, in fact, observed to be fairly constant during the runs, with only a little oscillation around a constant mean. Evans (36) had noted that in a given run the flow of solids could increase gradually to a constant maximum after the run was initiated. To allow for this, all readings were taken some time after the run was started - see experimental procedure in Chapter 4.

2. At any particular level in the standpipe all particles were assumed to have the same velocity and the particle concentration was uniform across the cross-section, i.e. the voidage at any level was assumed to be constant over the whole cross-section. The air velocity was considered constant over any particular cross-section. Although homogenous flow was not, in fact, observed throughout the standpipe, the precise nature of the flow was regarded as too complex to model at the present

stage of knowledge - see Chapter 6.8.

3. The compressibility of the air was not taken into account, constant volumetric flow rate of air through the standpipe being assumed. In this context the pressures generated in the apparatus were very small so that any error so introduced was negligible.

4. It was assumed that the drag between the particles and the air could be described by some form of drag coefficient.

5. The air-wall friction was assumed to be described by the usual Fanning equation, the presence of the particles being assumed to have no effect on this relationship. Although this was not generally thought to be the case in pneumatic conveying studies (86, 87), where the present assumption 2. was generally more applicable, the observations made of the flow in the standpipe showed that this assumption could be more justified in the present case (Chapter 6.8).

6. It was assumed that particle-particle friction and particle-wall friction could be treated together, and described by an equation analogous to the Fanning friction equation for fluids. This was found to be a usual assumption in the study of pneumatic conveying, and although the author did not think it was completely justified, such investigations as had been done in this context (86, 87) were not found to be relevant to the large scale operations which were possible with the present apparatus.

7. Finally, it was assumed that no significant amount of energy was lost as heat.

Development of the Model

A description of the flow in the standpipe could be obtained by a force balance over an elementary slice in the standpipe. Integration of the resulting equations along the length of the standpipe gave the variation of air pressure and other variables with position in the standpipe, producing in effect pressure and velocity profiles.

In descriptive terms, the force balance for an elementary volume of

unit cross sectional area, dx thick, could be expressed in the form:

initial force (up) = gravity force (down) - pressure force (up)

- frictional forces (up)

In vectorial form this was, for both phases:

$$e\,\varphi_a \frac{D\bar{U}_a}{Dt} + (1-e)\,\varphi_s \frac{D\bar{U}_a}{Dt} = (1-e)\bar{g}\,\varphi_s + e\,\varphi_a\bar{g} - \nabla P - eF_a - (1-e)F_s \quad (3.39)$$

where F_a and F_s represented the frictional terms.

Adopting the assumptions, the various terms in equation 3.39 were simplified:

(a) Inertia forces

With the assumptions of steady undimensional flow:

$$\frac{D\bar{U}}{Dt} = \frac{\partial U}{\partial t} + \frac{U\partial U}{\partial x}$$

$\frac{\partial U}{\partial t}$ was zero because the flow was also considered steady at any point with respect to time, so:

$$\frac{D\bar{U}}{Dt} = \frac{U\partial U}{\partial x}$$

(b) Pressure forces

$\nabla P = \frac{dP}{dx}$ for one dimension. For air there was a measurable pressure gradient throughout the tube. In the case of the solids the equivalent pressure force was not relevant or meaningful since the particles were not constantly in contact with each other and there could be no transmission of pressure through the particles, i.e. the weight of the particles was not borne by those below (46). In addition, the particles in question were large enough for the velocity component of each to be extremely low, due to its own thermal state, and thus the particulate phase did not contribute to the static pressure of the system (86).

(c) Gravitational forces

For one dimension $\bar{g} = g$.

(d) Frictional forces

The air-wall frictional force was assumed to be described by a

Fanning type equation:

$$F_a = \frac{dP_f}{dx} = \frac{2f_a \varphi_a U_a^2}{D_t}$$

A constant value of the friction factor f_a was proposed through the standpipe since the air velocities were not considered to vary substantially over the length.

There have been several attempts to describe the solids friction in pipe flow, using an analogy with fluid flow equations (86, 87). Separation of the various solids friction terms, however, has not generally been applied to the bulk flow situation and they have usually been amalgamated into a single solids friction term (86, 87). Since the present apparatus was not designed specifically to investigate the various solids friction components, it was necessary to follow this procedure, and to describe the solids friction as a whole by a single term of the Fanning friction equation form, i.e.:

$$F_s = \frac{dP_f}{dx} = \frac{2f_s \varphi_s U_s^2}{D_t}$$

Combining these simplifications with equation 3.39 and some re-arrangement, gave:

$$\frac{dP}{dx} = (1-e)\varphi_s g + e\varphi_a g - (1-e)\varphi_s U_s \frac{dU_s}{dx} - e\varphi_a U_a \frac{dU_a}{dx}$$

$$- (1-e)\frac{2\varphi_s f_s U_s^2}{D_t} - \frac{e2\varphi_a f_a U_a^2}{D_t} \qquad (3.40)$$

Integration of this equation from the top of the standpipe to any position down the standpipe gave the pressure at that point relative to pressure at the top of the standpipe. Thus, integrating from $0 \rightarrow x$:

$$\int_0^x dP = g\varphi_s \int_0^x (1-e)dx + g\varphi_a \int_0^x e dx - \varphi_s \int_0^x (1-e)U_s dU_s - \varphi_a \int_0^x eU_a dU_a$$

$$- \frac{2\varphi_s f_s}{D_t} \int_0^x (1-e)U_s^2 dx - \frac{2\varphi_a f_a}{D_t} \int_0^x eU_s^2 dx \qquad (3.41)$$

It was seen that values of the velocities and voidage at any point were needed before equation 3.41 could be integrated either analytically or

or numerically, but use of the continuity equations enabled some simplification, i.e.:

$$M_s = (1 - e)U_s \varphi_s A_t$$

$$Q_a = eU_s \varphi_a A_t \qquad (3.42)$$

Incorporating these equations into equation 3.41 gave:

$$\int_o^x dP = g \varphi_s \int_o^x (1-e)dx + g \varphi_a \int_o^x e dx - \frac{M_s}{A_t}\int_o^x dU_s - \frac{Q_a \varphi_a}{A_t}\int_o^x dU_a$$

$$- \frac{2f_s \varphi_s}{D_t}\int_o^x (1-e)U_s^2 dx - \frac{2f_a \varphi_a}{D_t}\int_o^x eU_s^2 dx \qquad (3.43)$$

To determine the particle and air velocities a further relationship was developed relating the motion of the air and particles in the standpipe.

Momentum Exchange Equations

As mentioned above, it was supposed that the drag forces resulting from particle motion caused the air motion, but if the air was moving faster than the particles, then this movement would aid the particle motion and the drag forces would assist gravitational forces to accelerate them. The solids velocity at the orifice was lower than the air velocity and, although the solids could accelerate while passing through the chamber whereas the air velocity was taken as constant, it was still regarded as possible that the air could be travelling faster than the solids at the standpipe entrance and in the upper regions of the standpipe. At some lower point the relative velocity would be reduced to zero due to particle acceleration, and below that point the particles would be travelling faster than the air.

To model the air and particle velocities, a force or momentum change balance was performed over a single particle. With the assumption of homogeneous flow and constant particle and air velocities at any level in the standpipe, it was considered that a single particle could be taken as representative of the particles as a whole. It was assumed that a drag

coefficient C_D' was applicable and that particles were accelerated by the sum of the gravitational forces, fluid drag forces and frictional forces. For a single particle,

(a) where $U_a > U_s$:

$$\frac{\pi d_p^3}{6}\varphi_s \frac{dU_s}{dt} = \frac{\pi d_p^2}{4}\frac{C_D'\varphi_a}{2}(U_a - U_s)^2 + \frac{\pi d_p^3}{6}\varphi_s g\left(1 - \frac{\varphi_a}{\varphi_s}\right)$$

inertia forces — fluid drag forces — gravitational forces

$$- \frac{\pi d_p^3}{6}\varphi_s \frac{f_s U_s^2}{D_t} \qquad (3.44)$$

frictional forces

so that:

$$\frac{dU_s}{dt} = g\left(1 - \frac{\varphi_a}{\varphi_s}\right) + (U_a - U_s)^2 \frac{3}{4}\frac{C_D'\varphi_a}{\varphi_s d_p} - \frac{f_s U_s^2}{D_t} \qquad (3.45)$$

Now

$$\frac{dU_s}{dt} = U_s \frac{dU_s}{dx}$$

so

$$\frac{dU_s}{dx} = \frac{b + a(U_a - U_s)^2}{U_s} - \frac{f_s U_s}{D_t} \qquad (3.46)$$

where $b = g\left(1 - \frac{\varphi_a}{\varphi_s}\right)$, $a = \frac{3}{4}\frac{C_D'\varphi_a}{\varphi_s d_p}$

(b) For $U_s > U_a$ the direction of the fluid drag force and the relative velocity was reversed, giving:

$$\frac{dU_s}{dx} = \frac{b - a(U_s - U_a)^2}{U_s} - \frac{f_s U_s}{D_t} \qquad (3.47)$$

(c) For the situation where the particle velocity did not show any further change with distance down the standpipe, i.e.:

$$\frac{dU_s}{dx} = 0$$

then

$$b - a(U_s - U_a)^2 - \frac{f_s U_s^2}{D_t} = 0 \qquad (3.48)$$

The three equations 3.46, 3.47 and 3.48 were used to define the variation of the particle velocity with distance (x) down the standpipe. In association with these, it was necessary to use the continuity equations to find the voidage and air velocities and the corresponding positions.

$$M_s = A_t (1 - e) \varphi_s U_s \qquad (3.49)$$

$$Q_a = A_t k \varphi_a \qquad (3.49a)$$

The solution of these equations was dependent on the physical properties of the solids and the drag coefficient C_D'. Integration of these equations was necessarily numerical due to the dependence of the term 'a' on the drag coefficient C_D' which, in turn, was dependent on the air and particle velocities. As the particle velocities were considered to approach exponentially the limiting value defined by equation 3.48, it was necessary to approximate this value by restraining the approach, which was taken as 0.99 U_{st} where U_{st} was the limiting value of particle velocity, satisfying equation 3.48.

The Particle-Fluid Drag Coefficient

It was noted from the literature that when particles fell in a close - packed system the single particle drag coefficient was unlikely to apply, due to the close proximity of other particles (44, 86, 87, 104). This proximity caused interference between the particles in the form of a shielding effect, reducing the drag coefficient for each particle below the single particle value (86, 104). For the single particle in an infinite fluid medium, on the other hand, the general effect of particle motion through the fluid was to produce turbulent wakes and eddies behind the particle which dissipated into the fluid without increasing its kinetic energy of mass motion, i.e. without causing bulk movement of the fluid in any direction. Also, of course, in this case the normal free field, single particle fluid drag coefficients apply (96).

In the case of a lean suspension, the particles were not considered to come into contact with each other, nor were they considered to be close

enough to interfere in this way with the wakes behind the particle. The energy gained by the fluid due to the passage of a particle through it was dissipated by the particle wake, and there was thus no increase in kinetic energy of the mass motion of the gas. In such a case there was justification for using the unmodified single particle drag coefficient to describe the interaction between each particle and the fluid (86).

For dense streams, the inter-particle distance was considerably reduced, with a consequent increase in particle interaction. The close presence of following particles interfered with the dissipation of the fluid turbulence in the wake of preceding particles. Thus, some of the energy gained by the fluid was not dissipated but stayed in the bulk fluid so that the total kinetic energy of the mass motion of the fluid increased. Suspensions of higher density would have allowed still less room for energy dissipation in the wakes and consequently increased still further the fluid bulk kinetic energy (86). Conversely, it was likely that where there was movement of the fluid caused by movement of the particles, the particles would be moving in a dense suspension.

Similar reasoning could be applied to the dependence of the reduction in particle drag coefficient on the solids concentration for a dense-phase particle stream. In such a stream each particle is followed by another close enough to effect the dissipation of its following wake: the first particle has its wake affected by the second particle, whereas the second has its incident fluid affected by the presence of the wakes from the first, in this way reducing drag on both particles (104). This 'lee' effect would carry on throughout the length of the particle stream in continuous flow, resulting in a general reduction of drag coefficient between particles and fluid compared with the lean-phase suspension, or single particle motion (104).

The effective drag coefficient for a particle in a dense solids stream flowing through a fluid medium would thus be expected to depend on:

1. the individual particle and velocity, and
2. the solids concentration or inter-particle distance in the dense solids stream (86).

For sufficiently dilute streams, the particle drag coefficient depended only on the relative velocities of air and particles and, consequently, the free field, single particle drag coefficient was regarded as the maximum value for dense-phase conditions. It was thought that for very dense streams, the drag coefficient approached zero: this situation has been assumed for the particle cloud flow immediately after discharge from a hopper (44, 87) and, in the present work, for the solids stream in the chamber. Subsequent expansion of such particle streams must increase the value of the drag coefficient asymptotically to the normal free field, single particle value as the stream attained infinite dilution.

Expansion of the stream also necessarily implied decrease in the solids concentration. The solids streams under investigation were observed to expand as they progressed down the standpipe (Chapter 6.8), so there was likely to have been a corresponding decrease in the solids volume fraction in the solids stream down the standpipe. Thus, it was reasonable to assume that the effective particle drag coefficient would increase as the particles progressed down the standpipe.

It was assumed that the solids stream expanded smoothly with position down the standpipe and the degree of expansion was related to the position down the standpipe. As a consequence of the assumption of zero drag coefficient for the particle stream in the chamber, the effective particle drag coefficient at the entrance to the standpipe was also assumed to be zero.

It was seen, therefore, that the effective particle drag coefficient C_D' was dependent on both the single particle drag coefficient C_D and the position down the standpipe, conveniently represented by the dimensionless

position ratio $\frac{x}{L_t}$, and that the ratio $\frac{C_D'}{C_D}$ approached unity as the stream approached infinite dilution.

Thus:

1. the greater the expansion of the stream, the greater the value of $\frac{C_D'}{C_D}$, and
2. the greater the expansion, the greater the value of $\frac{x}{L_t}$.

The boundary conditions were expressed as:

1. at the standpipe entrance, $\frac{x}{L_t} = 0$, $C_D' = 0$.
2. at the standpipe exit, $\frac{x}{L_t} = 1$, $0 < \frac{C_D'}{C_D} < 1$.
3. at infinite dilution, $C_D' = C_D$.

The simplest model equation which conformed to all the above equations was:

$$\frac{C_D'}{C_D} = (1 - e^{-\frac{x}{L_t}}) \qquad (3.50)$$

This model assumed that at the exit to any standpipe ($\frac{x}{L_t} = 1$) the drag coefficient ratio was always the same. Since this was thought quite unlikely, equation 3.50 was modified by the inclusion of a constant to give:

$$\frac{C_D'}{C_D} = (1 - e^{-w\frac{x}{L_t}}) \qquad (3.51)$$

thus allowing for different properties in different systems. The value of w was expected to depend in some way on both solids stream voidage and standpipe length. The adoption of the equation 3.51 effectively related the expansion of the solids stream to the distance down the standpipe.

With this relationship for the particle drag coefficient in the solids stream, it was possible to integrate the equations 3.45 and 3.46 to find the particle velocity at any point by using the free field, single particle drag coefficient calculated from the normal equations, relating it to the particle Reynolds' number (96). Use of the continuity equations 3.49 allowed values of air velocity and voidage corresponding to the solids velocity to be found at the same position. With the knowledge of these

values of velocity and voidage, it was then possible to numerically integrate equation 3.43 to find the corresponding fluid pressure values and to build up a pressure profile throughout the standpipe.

3.7 Summary of the Theory and Application of the Assumptions to the Present Work

The main assumptions underlying the various sections of the theory outlined above were seen to be those in common use in this field of work and thus were reasonable for the present system. The principal postulates are summarised below, with notes in each case on the application to the present work.

1. A Kozeny-Carman type relationship has been postulated to describe the flow of air through a moving solids bed, using the concept of relative velocity between the particles and air. The relationship in its simplest form (i.e. $Q_B = k_B \Delta P_B$), relating the air flow rate through a bed to the pressure drop across it, inferred a constant value for the bed density for all conditions of solids and air flow rates, i.e. if the value of k_B was to be constant for a particular granular material. Investigations of the air and solids flow rates through the top storage hopper has shown this to be the case and the extension of this behaviour to the constant depth bed was thought to be valid.

2. The total solids flow rate through the orifice has been treated as the sum of two constituents: (a) that due to gravitational influence, and (b) that induced by drag caused by movement of an air stream through the orifice. The two parts of the total solids flow rate through the orifice have been expressed as pressure functions: (a) the gravitational constituent of the solids flow rate has been related to a graphically determined 'pseudo-pressure' equivalent to that air back-pressure drop across the orifice needed to stop solids flow, and (b) the air drag constituent of the solids flow rate has been expressed as a function of the air pressure drop over the orifice. The total solids flow rate through

this orifice was then expressed as a function of the sum of two pressure terms, in this way combining two main approaches to the subject (i.e. the fluid flow and soil mechanics analogies) to describe the system.

3. The method of determining the voidage and the particle and air velocities at the orifice was adapted from the work of Massimilla (58) on the flow of fluidised particulate streams through vertical orifices. The assumption of radial continuity was believed to be consistent with the physical considerations, notably the presence of the dynamic arch formation generally agreed to exist in the regions above the orifice.

4. The difficulty of finding suitable friction factors and drag coefficients for the particle stream in the standpipe has necessitated the use of fairly gross assumptions to describe the situation. The proposed equations compared well with a large amount of experimental evidence and, while it was not possible to establish the assumptions with certainty in the present investigation, the method of calculation and the form of equations used, predicted the pressure profile in the standpipe to a fairly high degree of accuracy.

The necessity of investigating effective drag coefficients and friction factors in the standpipe was not seen at the outset of this project, but their calculation and the development of the equations have assisted greatly in increasing the understanding of the flow of a dense particle core through a vertical standpipe.

CHAPTER 4

Apparatus and Experimental Procedure

Initial Concepts

The aim of this research was to investigate the discharge of particulate solids from a hopper and down a standpipe, and to elucidate the effect of such standpipes on solids flow. As indicated in the literature review, very little information about this type of system had been published except for a general acknowledgement that a standpipe attached to an orifice increased the particulate flow rate over that for the unmodified orifice. For this reason, an apparatus was designed and built to study the effect of standpipe dimensions on the flow of particulate solids through an orifice from a hopper. Due to the paucity of quantitative information on the system as a whole, the project was essentially a general investigation into the topic, becoming more specific and detailed as it developed.

The apparatus built allowed solids to flow vertically down through the standpipe under the influence of gravity. Arrangements were made to meter all air entering and leaving the apparatus and to measure the air pressures at various points over the system.

4.1 Development and Description of the Apparatus

Since the project was considered as a survey of the flow of particulate solids through a hopper and down a standpipe, the apparatus was designed to cover as many aspects of the operation as could be envisaged initially.

It was decided to build the apparatus as large as possible, to simulate industrial conditions and to obviate problems of scale-up. There existed, in fact, a superficially suitable large scale hopper system available for modification in the Department (52). The size of

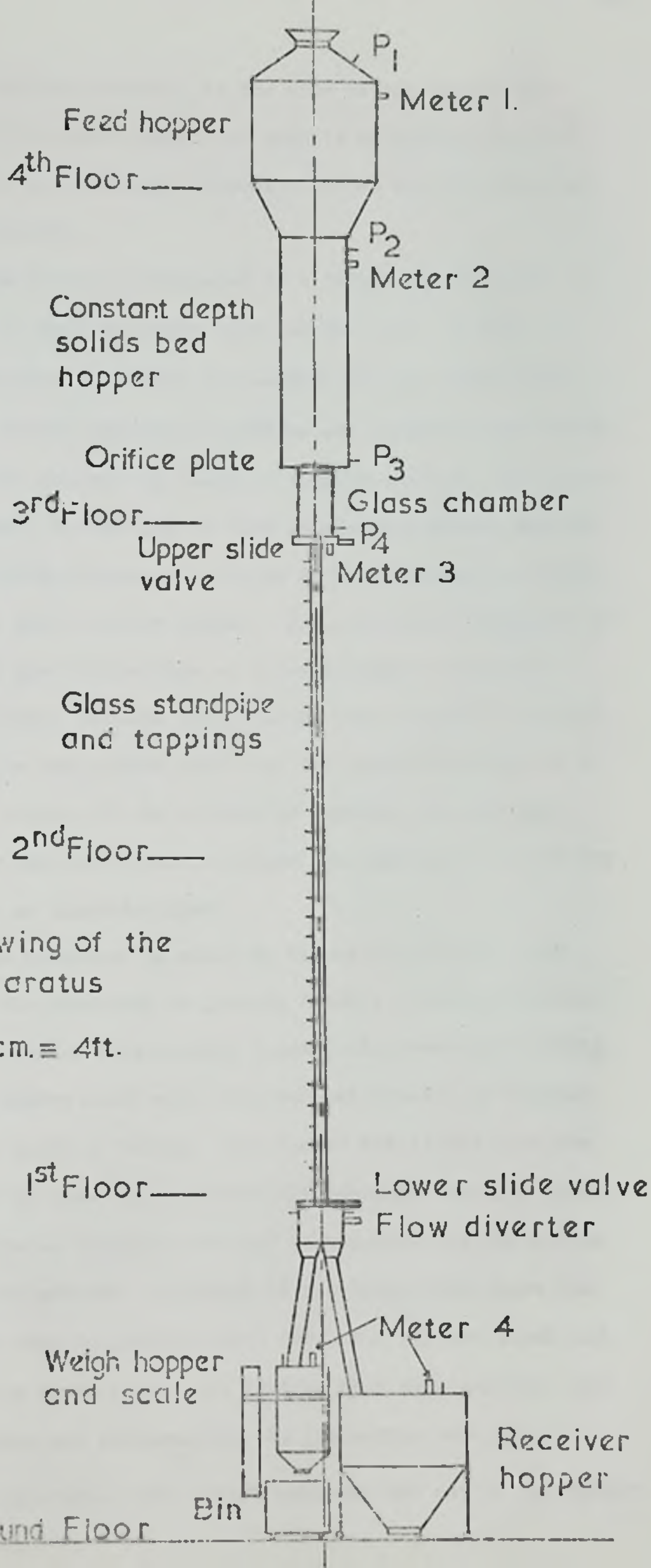

Fig. 4.1
Line drawing of the main apparatus

Scale 3cm. ≡ 4ft.

the operation was limited, however, by the size of the laboratory: an apparatus of 10.95 m total height and capable of holding 0.95 m^3 of granular material was achieved, producing solids flow rates up to 3.7 kg/sec or 13 tonnes/h.

Essentially the apparatus consisted of a double top storage hopper constructed so that the upper part fed the lower section to maintain a constant depth bed above the orifice for all solids flow rates. Connection between the hopper orifice and solids control valve and the standpipe was effected by means of a glass chamber. The glass standpipe was attached to the base of this chamber projecting down to dip into a flow divertor allowing the solids to be deflected to either a weigh hopper or a lower storage hopper. From previous experience in the Department with the difficulties of incorporating a pneumatic transport return system, and more importantly, with regard to present considerations of the space above and below the apparatus required to accommodate such a system, it was decided to recharge the top feed hopper by detaching the lower storage hopper and raising it to the top of the apparatus by an electric hoist.

A sketch of the apparatus is shown in Figure 4.1, Plate 1 and Figure 4.2 showing the apparatus in greater detail. The upper solids storage system comprised a twin section hopper, the lower part acting as a flat-bottomed bunker 0.487 m in diameter and capable of holding solids to a maximum depth of 0.9 m. This bunker was filled from the larger hopper above by means of a central leg insert so that the depth of solids in this bunker remained constant irrespective of the solids flow rate through the orifice. Although it was known that where the solids flow was due only to gravitational influence the bed depth had no effect on the flow rate, it was not certain that this was the case in the present system, and consequently the precaution was taken to keep the bed depth constant. The bunker aperture was set in the centre

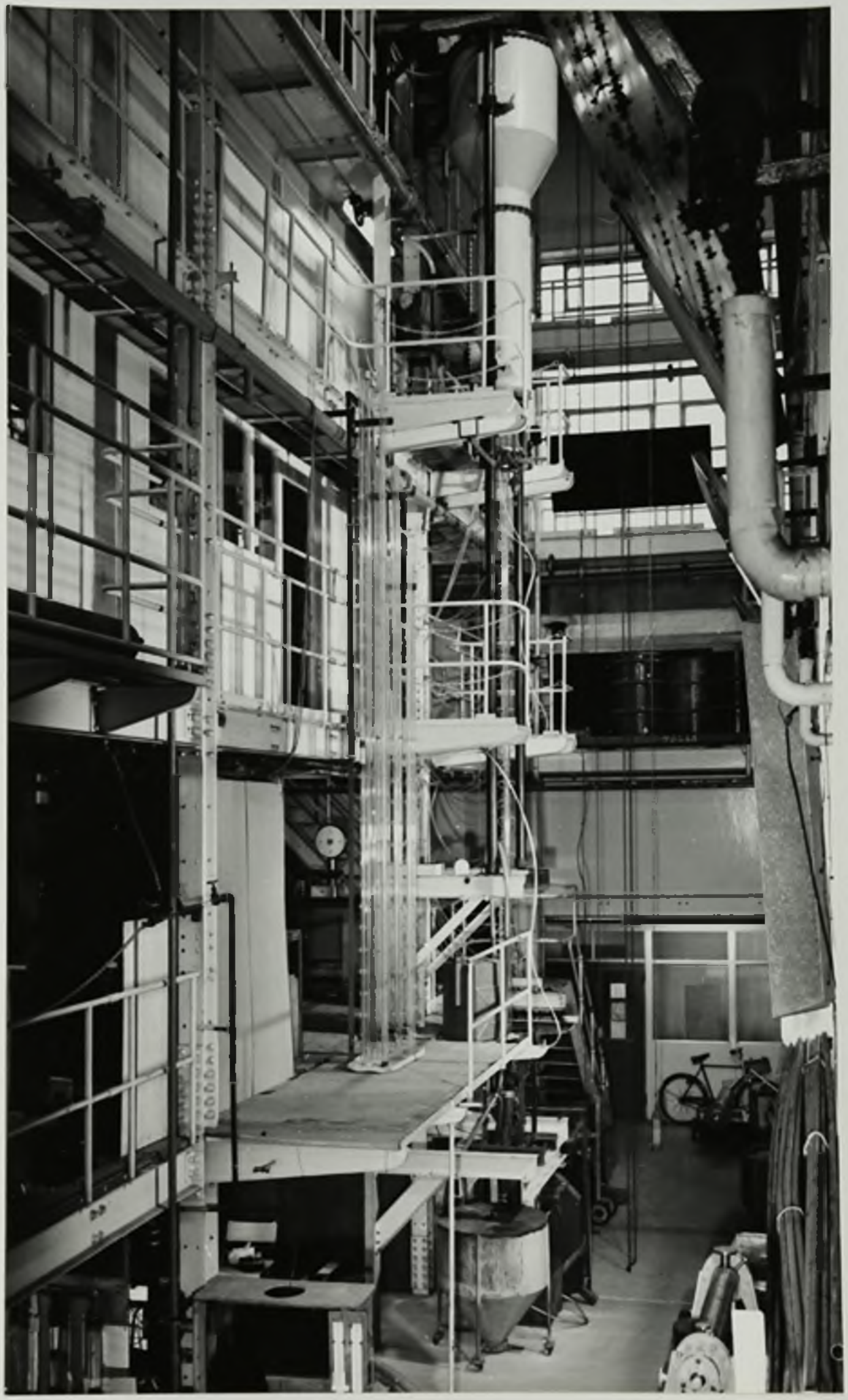

Plate I. Main apparatus

of the base and was designed to use interchangeable orifice plate inserts - the test orifices.

The orifice plates which were 'inherited' with the double hopper system had been manufactured to BS 1042 (1964). There seemed to be no special justification for this except that it gave a reproducible standard and fulfilled the requirement that orifices should have negligible thickness. It was therefore decided to continue with their use (Appendix 1).

Various pressure tappings and air flow metering positions were incorporated into the system; these are described below in a separate section for the whole apparatus.

The solids storage system was charged through a 'Mucon' valve (Appendix 2) set at the top of the upper hopper. This valve was closed after charging and proved to be an adequate seal against air leakage at the small pressures encountered in the top hopper during a run. A further 'Mucon' valve was employed below the orifice plate to act as the solids stop valve. This was used simply as an on-off device, and was controlled from the operating level on the first floor by cords passing over pulley wheels and hanging down the length of the apparatus.

The use of a glass chamber connecting the orifice to the standpipe entrance was based upon the results of qualitative work previously performed in the Department (36) and upon the recommendations of Wolf and von Hohenleiten (77) discussed in the literature review. It had been found that the use of such a chamber (36) was necessary to enable orifices of larger diameters than the standpipe to be used.

The effects of the chamber dimensions were unknown initially, especially the length since this determines the distance between the orifice and the standpipe entrance, and so a subsidiary experimental programme was carried out to investigate this dimension (see Chapter 5). Incorporated into the chamber (Figure 4.3), (Plate 2) were a pressure

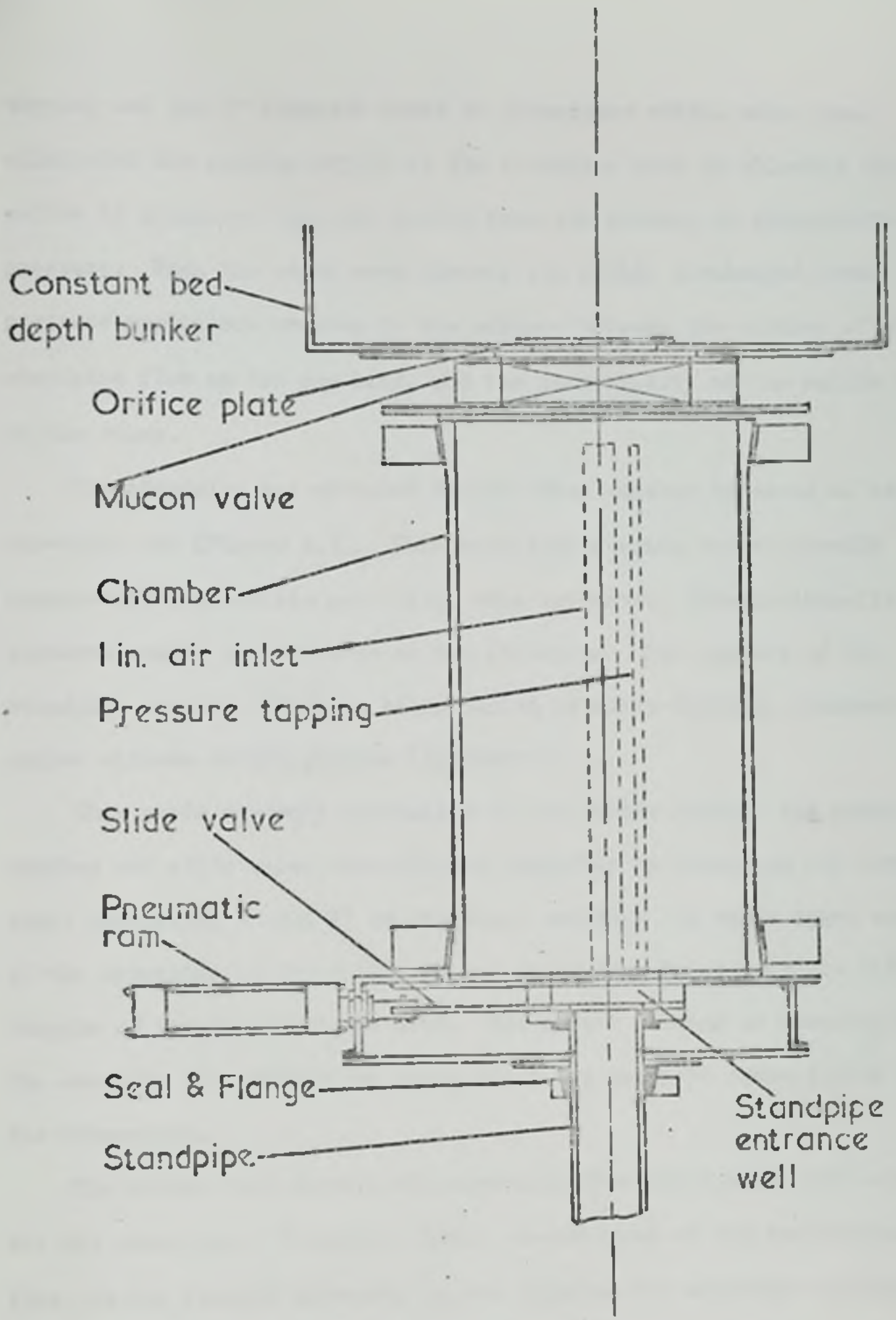

Fig.4.3 Detail of chamber and slide valve assembly Scale 1cm: 2ins

tapping and two 1" diameter vents to atmosphere which, when open, eliminated the suction effect of the standpipe flow by allowing the solids to discharge from the bunker into the chamber at atmospheric pressure. When the vents were closed, the solids discharged into pressure conditions created by the balance between the suction of the standpipe flow on the one hand, and the permeability of the solids bed on the other.

The standpipe was attached to the glass chamber by means of an air-tight box (Figure 4.3). This contained a slide valve assembly operated by a pneumatic ram which, when activated, closed virtually instantaneously the entrance to the standpipe. The top end of the standpipe entered this box, being sealed by close-fitting, doughnut-shaped silicon rubber gaskets (Appendix 2).

This whole assembly consisting of the double hopper, the glass chamber and slide valve assembly was supported by clamps on two vertical steel supporting tubes, 4" in diameter, enabling the whole upper section of the apparatus to be readily raised or lowered to accommodate different lengths of standpipe (Figure 4.2). The actual raising or lowering of the assembly was effected by using the 5 ton overhead crane fitted in the laboratory.

The solids flow through the apparatus from the chamber was continued via the standpipe. To enable visual observations of the particle/air flow, it was thought necessary to use glass as the standpipe material - perspex having proved unsatisfactory in earlier work (36) due to difficulties with electrostatic effects and distortion when in place. The use of glass also gave a smooth, joint-free pipe. Accordingly, glass tubes were supplied by James Jobling, ranging from 1.500 m to 4.875 m in six lengths and from 25.4 mm to 50.8 mm in three diameters (Appendix 1). The use of glass tubing of such lengths and comparatively small diameters had certain disadvantages due to its fragile nature - chiefly drilling

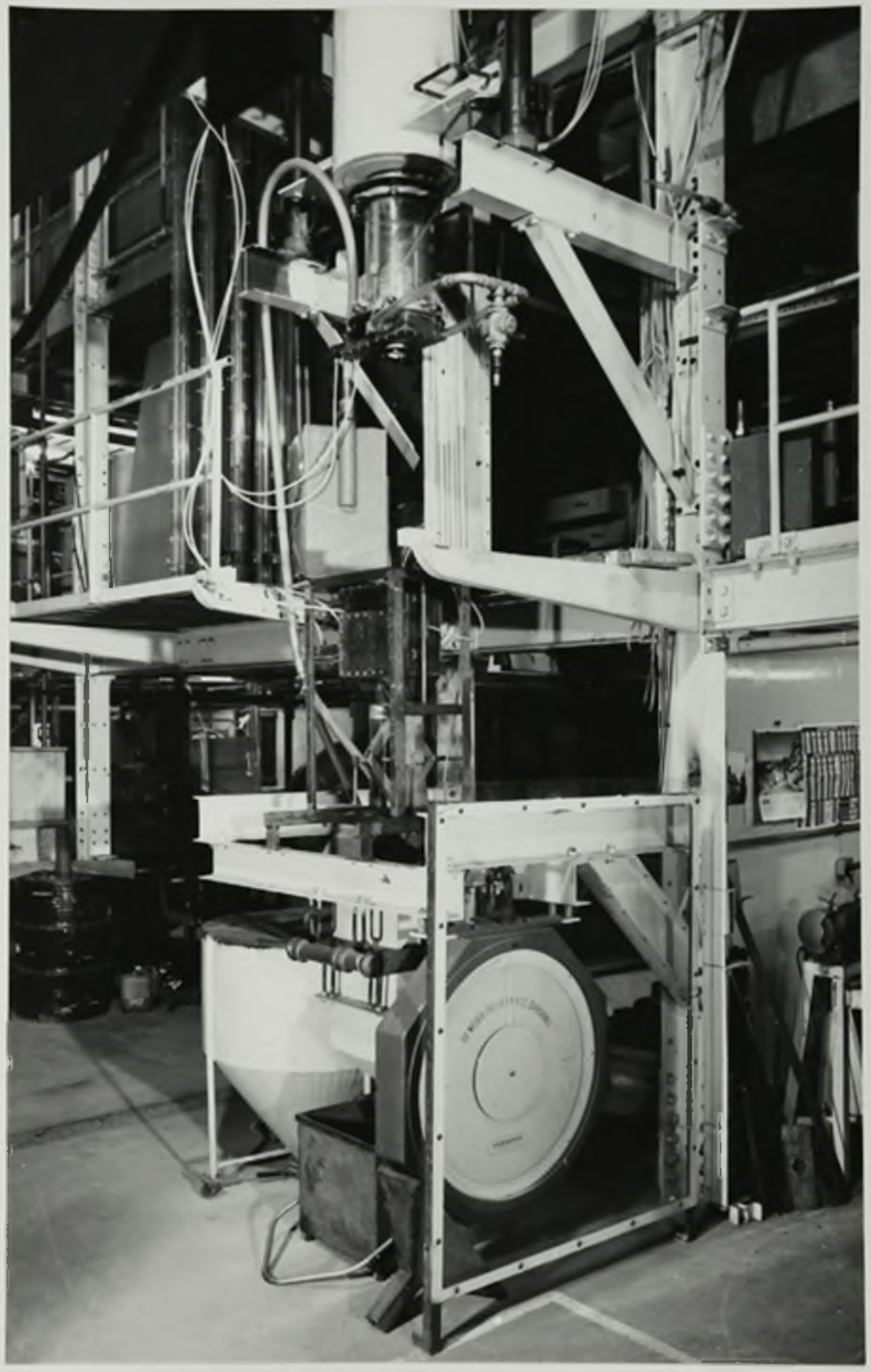

Plate 2. Main apparatus – detail

pressure tapping holes and the attachment of manometer tubes to these holes. The glass standpipes were sufficiently straight and rigid when held vertically but did need careful handling when being fitted into the apparatus.

The holes for the pressure tappings in the glass standpipes were drilled in the Department of Ceramics using a hollow, cylindrical diamond drill, 1/8 inch diameter. The drilling created considerable problems due to the fragility of the tubing when held horizontally, and due to the clear space needed each side of the drilling machine (up to 5 m on one side and 2.5 m on the other). The glass tubes were held on several supports during the drilling operation, the pairs of holes being drilled at 150 mm intervals with each second pair being drilled in a plane at 45° to its neighbours to try to reduce the likelihood of a fracture plane along the line of tapping holes. The method of attachment of the manometer tubing was simple but thought to be novel. Perspex tubes of similar internal diameter to the standpipe's external diameter were cut into 25 mm lengths; these were then cut into segments approximately 25 mm wide, forming a curved flange (Figure 4.4). The segments were then drilled and fitted with 30 mm lengths of ¼ inch diameter perspex tube. The completed flanges were positioned over the drilled holes in the standpipe and attached with epoxy resin adhesive. Pairs of tappings were provided on opposite sides of the standpipe at each position. These were joined together and to a manometer by means of a Y-piece and lengths of P.V.C. tubing. The lower end of the standpipe was fixed into an air-tight box containing a fast-acting pneumatic slide valve similar to that at the other end (Figure 4.5). The slide valves were arranged to be operated very rapidly and simultaneously by pneumatic rams operating at a pressure of 120 p.s.i.

Below the slide valve assembly and integral with it was the flow-diverting apparatus (Figure 4.5), (Plate 2). This consisted of an

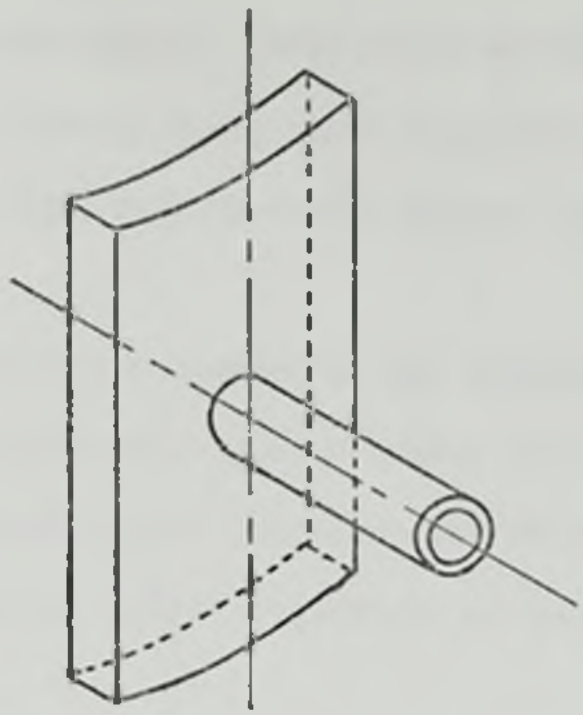

Fig.4.4 Detail of a standpipe pressure tapping

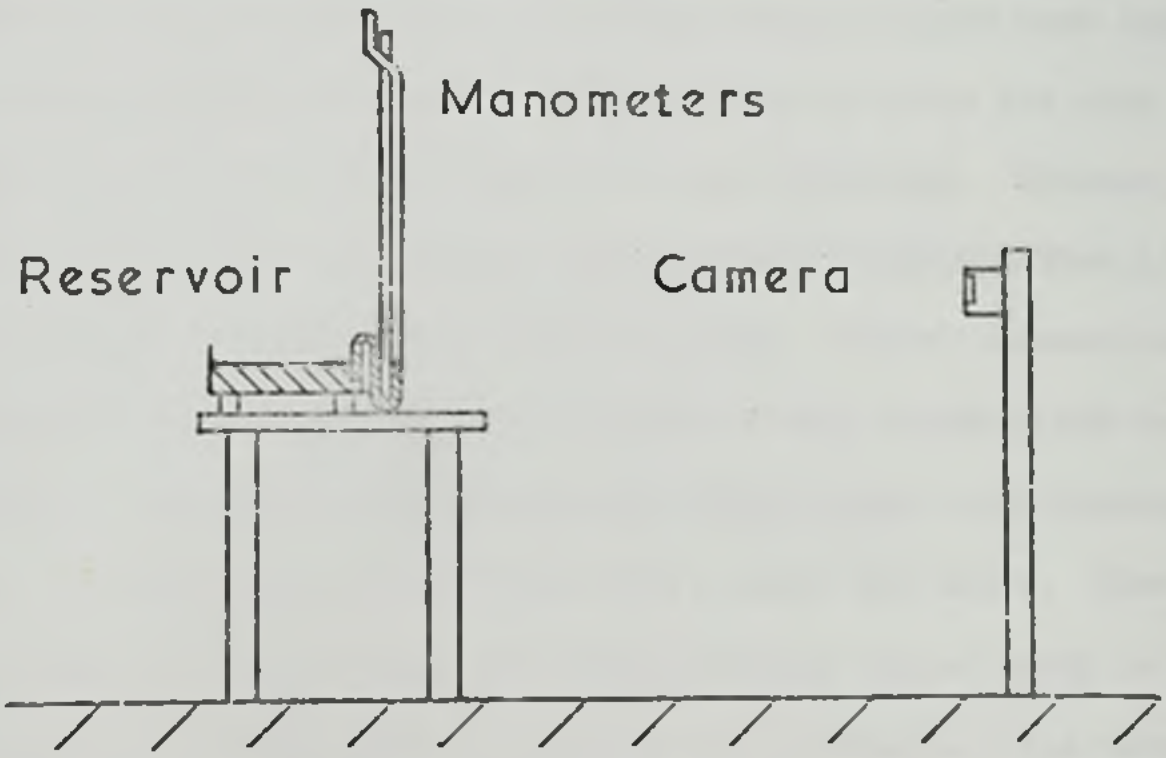

Fig.4.6 Layout of camera and manometer board

air-tight sheet steel box containing a pneumatically operated swinging flap to divert the solids/air stream to either the weigh hopper or the bottom storage hopper. Activation of this pneumatic ram simultaneously controlled an electric timer clock (Appendix 2) starting when the solids stream was diverted into the weigh hopper, and stopping on reversing the flap.

This assembly was mounted on two vertical guides in an angle iron frame with a simple screw-jack to raise or lower the flow diverter. This facility enabled the flow diverter to be adjusted in height by up to 0.4 m, so giving a fine adjustment of height for installing or removing a standpipe.

The weigh hopper could contain up to 0.3 m^3 of material and was suspended from a self-indicating weighing machine with a capacity of 150 lb (68 kg) indicated on a 30" diameter scale marked off in 4 oz divisions (Appendix 2). The hopper was fitted with two perspex windows on opposite sides, with suitable illumination to enable the level of solids to be easily seen.

Both the weigh hopper and the bottom storage hopper were connected to the flow diverter by flexible rubber tubing to allow for easy detachment and to enable the flow diverter to move unimpeded. However, this was removed from the weigh hopper during sample weighing since it was found to affect the readings if left in place. Outlet connections (to the meters) were provided in both hoppers to vent incoming air to atmosphere. The solids collected in the weigh hopper were discharged through a 'Mucon' valve in its base into a small bin below. When full, this in turn was emptied into the bottom storage hopper ready to be lifted by the electric hoist to recharge the apparatus. The bottom storage hopper was similarly fitted with a 'Mucon' valve at its base.

Details of commercial instruments used are given in Appendix 2.

Fig.4.5 Detail of flow

Scale: 1cm : 2ins

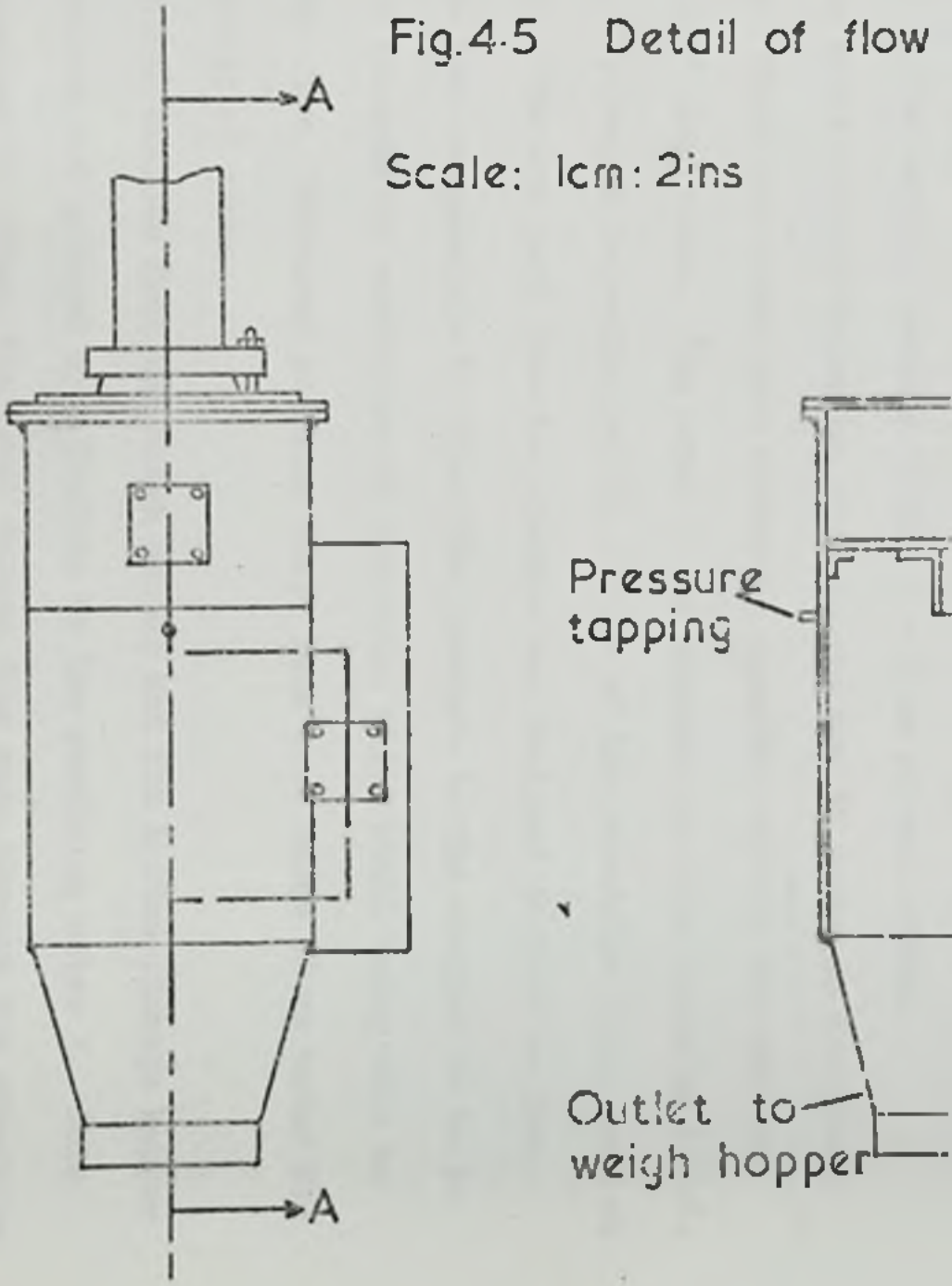

diverter and slide valve assembly

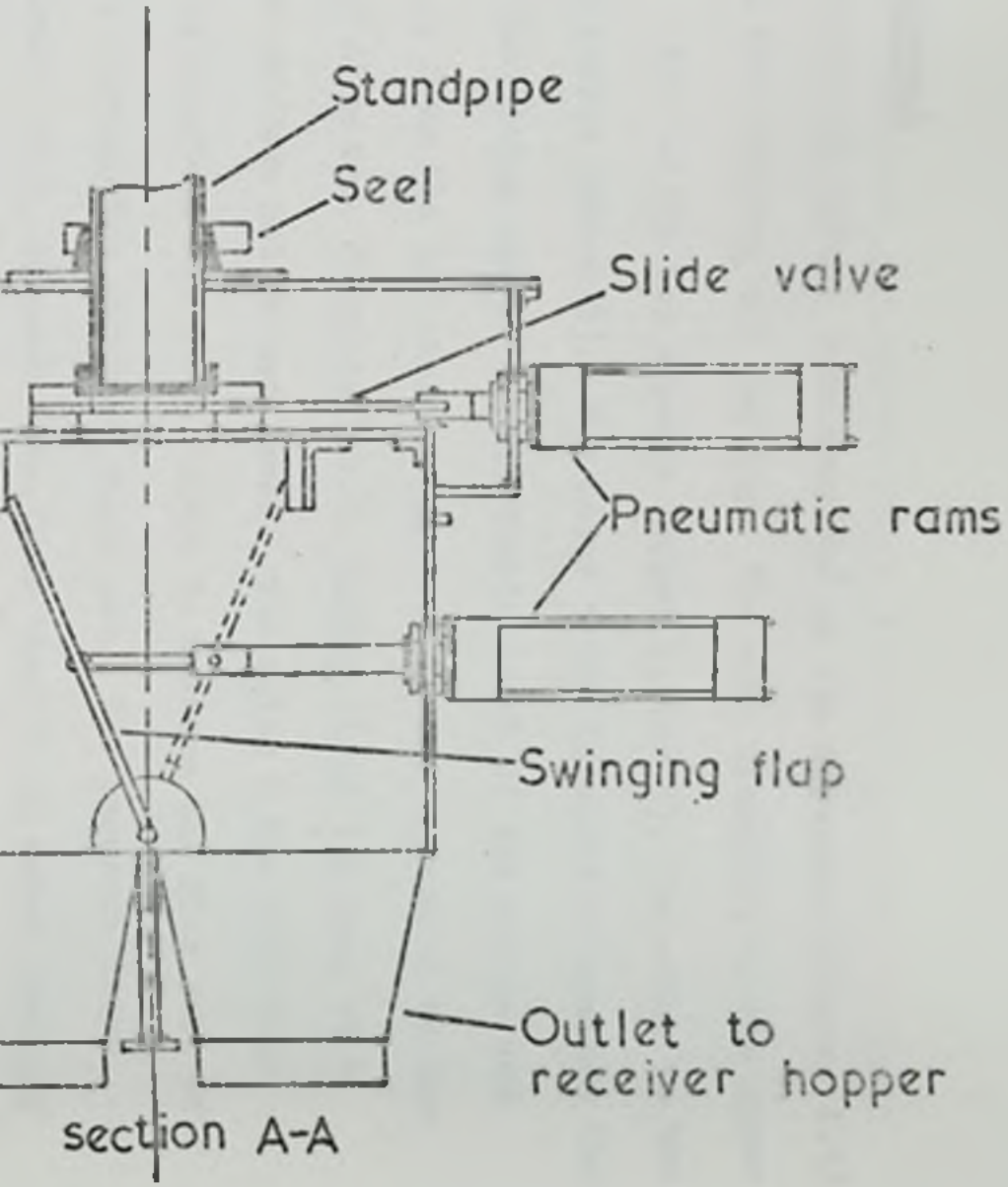

Air Flow Measurement

Three metered air inlets were provided on the apparatus (Figure 4.1) to measure all air entering and leaving. Two were connected to the upper hopper system - one to the top storage hopper (meter 1), the other to the constant depth bunker (meter 2). The meter 1 was intended to measure the air flow into the system caused by the displacement of the solids and interstitial air from the top storage hopper. It was connected to the apparatus by ½" diameter, flexible P.V.C. tubing about 1 m long at a point above the maximum solids bed level. The meter 2 was similarly connected to the constant bed depth bunker to measure the flow rate of percolating air through the constant depth bed. The pressure drops across these meters were, in each case, less than 10 mm water (usually about 1 - 2 mm water), usually within 1 - 2 mm of each other.

The third metered inlet was through the two 1" vents on the glass chamber. These two vents were connected together outside the chamber and to a 2" plug valve. The meter 3 was attached to this valve by P.V.C. tubing, the length depending on the length of the standpipe being used at the time. The air path into the chamber was designed to have as low a pressure drop as possible to allow the pressure in the chamber to be as close to atmospheric conditions as possible, while still being able to meter the flow. Measured pressure drops here were below 10 mm water for the majority of runs.

The air outlets from the weigh hopper and the bottom storage hopper were combined and jointed by a Y-piece to the remaining meter 3. This meter measured in effect the total volume flow rate through the standpipe (both air and solids) and gave some check on the other metered air flows. This meter 4 reading should have been equal to the sum of the readings from meters 1, 2 and 3 (if used).

The magnitude of the air flows was such that it was possible to use test meters accurate to 1% for meter positions 1 and 2, whereas the

larger air flows obtained through positions 3 and 4 necessitated the use of more commercially sized meters (Appendix 2).

Pressure Tappings

Pressure tappings ($\frac{1}{4}$" diameter) were situated at several points on the apparatus (Figure 4.1). For the upper hopper system, tappings were attached to the top storage hopper (P_1) and the constant bed depth bunker (P_2). Further tappings (1/8" diameter) were provided to measure the pressures in the region just above the orifice (P_3), and in the chamber (P_4). Pressure tappings were also fixed at 150 mm intervals down each standpipe, giving a maximum of 31 readings for the longest pipes. A tapping ($\frac{1}{2}$" diameter) was attached to each side of the flow diverter with further tappings in the weigh hopper and bottom storage hopper.

All the pressure tappings were joined to single leg water manometers mounted together on a single, large panel. The water reservoir (situated behind the panel) was a shallow perspex container with a large horizontal cross-sectional area, ensuring negligible depression of the water level during a run (Plate 3). Due to the difficulty of directly reading such a large number of pressures during a run, the manometers were photographed, the pressures being read off the negatives at a later date (Figure 4.6).

Electrostatic Effects

The initial testing of the apparatus showed the presence of electrostatic charges on the glass standpipes; this was not surprising considering the natures of the granular material (sand) and the standpipes (glass) and that the standpipes were, in effect, insulated from the rest of the apparatus (steel) by P.T.F.E. flanges and silicon rubber seals. Since it was recognised that such electrostatic charges could affect the flow of the solids (100) and moreover, since the effects of these charges were unpleasant if the standpipe was touched during a run, copper wire was wound round outside the complete length of each standpipe and earthed to

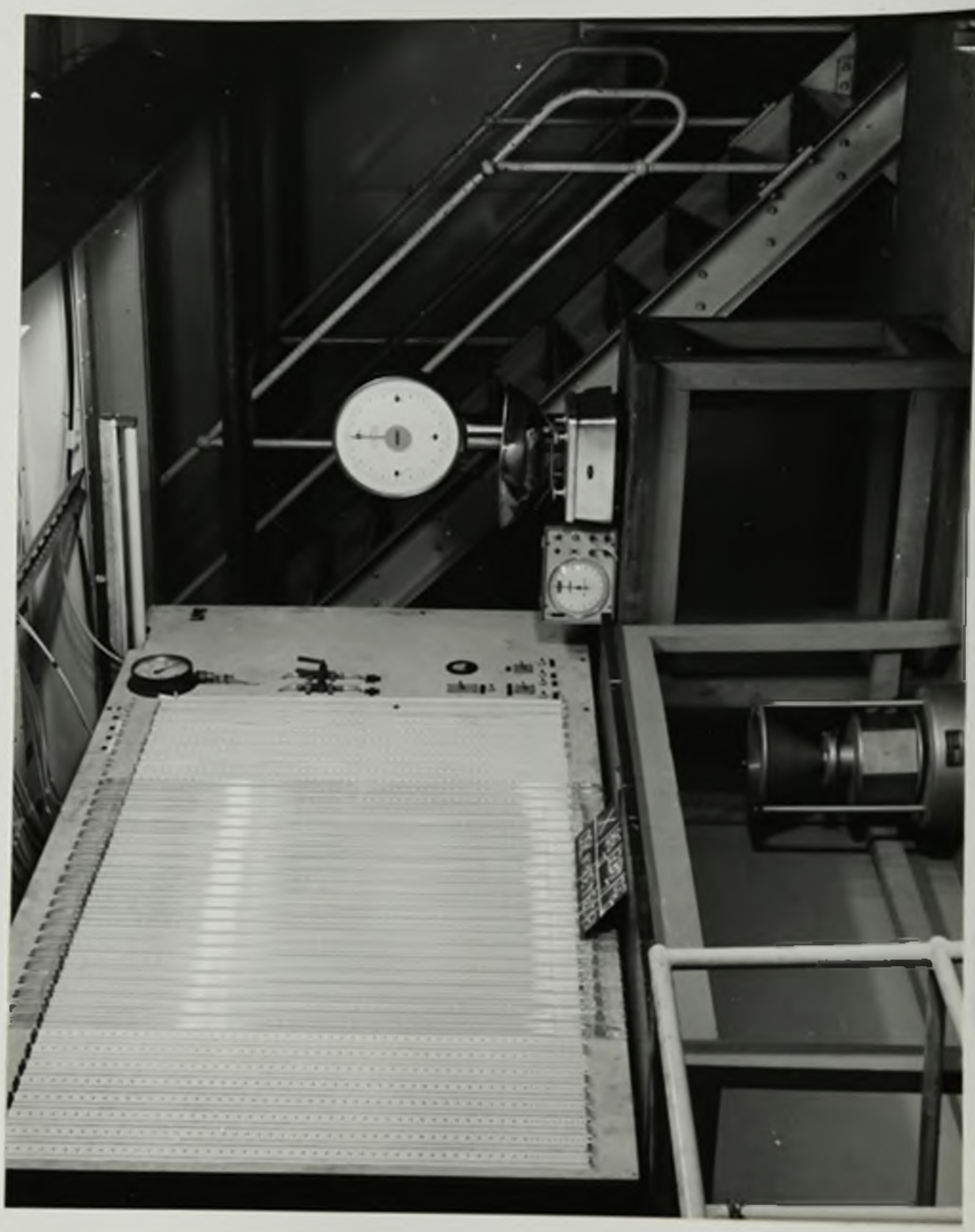

Plate 3. Manometer panel

the metal hoppers and flow diverter. This removed the build-up of charges from the standpipe and resulted in a slight increase in solids mass flow rate. All solids flow rates mentioned subsequently are those carried out with the standpipe earth in place.

Pressure Testing

The apparatus was pressure tested to 1 m of water. The total leakage through the whole apparatus was of the order of 0.00015 m^3/s principally through the 'Mucon' valves. It was noted, however, that the pressures in the hoppers during a run were less than 10 mm of water so that leakage through the 'Mucon' valves was considered to be negligible in such conditions. The seals throughout the rest of the apparatus were found to be sound and no leaks were detected at the standpipe pressure tappings.

Granular Solids

At least two solid materials were required for the test runs. It would have been desirable for each material to have taken the form of monosize spheres, such as glass ballotini, since this would have simplified the problem by eliminating the questions of shape and size range. Unfortunately, for the large quantities of each material needed (about 1,500 kg) glass ballotini proved far too expensive; in addition, it was felt that the use of a 'perfect' material would not be sufficiently relevant to the materials in common industrial usage. There was, moreover, no evidence that the precise measurements of the individual particles was an important bulk parameter for solids flows of this type. The materials eventually chosen were closely graded sands supplied by Joseph Arnold, Ltd. and George Garside, Ltd. (Appendix 3 and Plate 4). Both the sands chosen were described as 'rounded', the particles having no sharp corners or edges, with a large proportion of the particles approximately equi-dimensional and having a fairly narrow size range. Sand had the advantage of good mechanical strength, showing little sign of

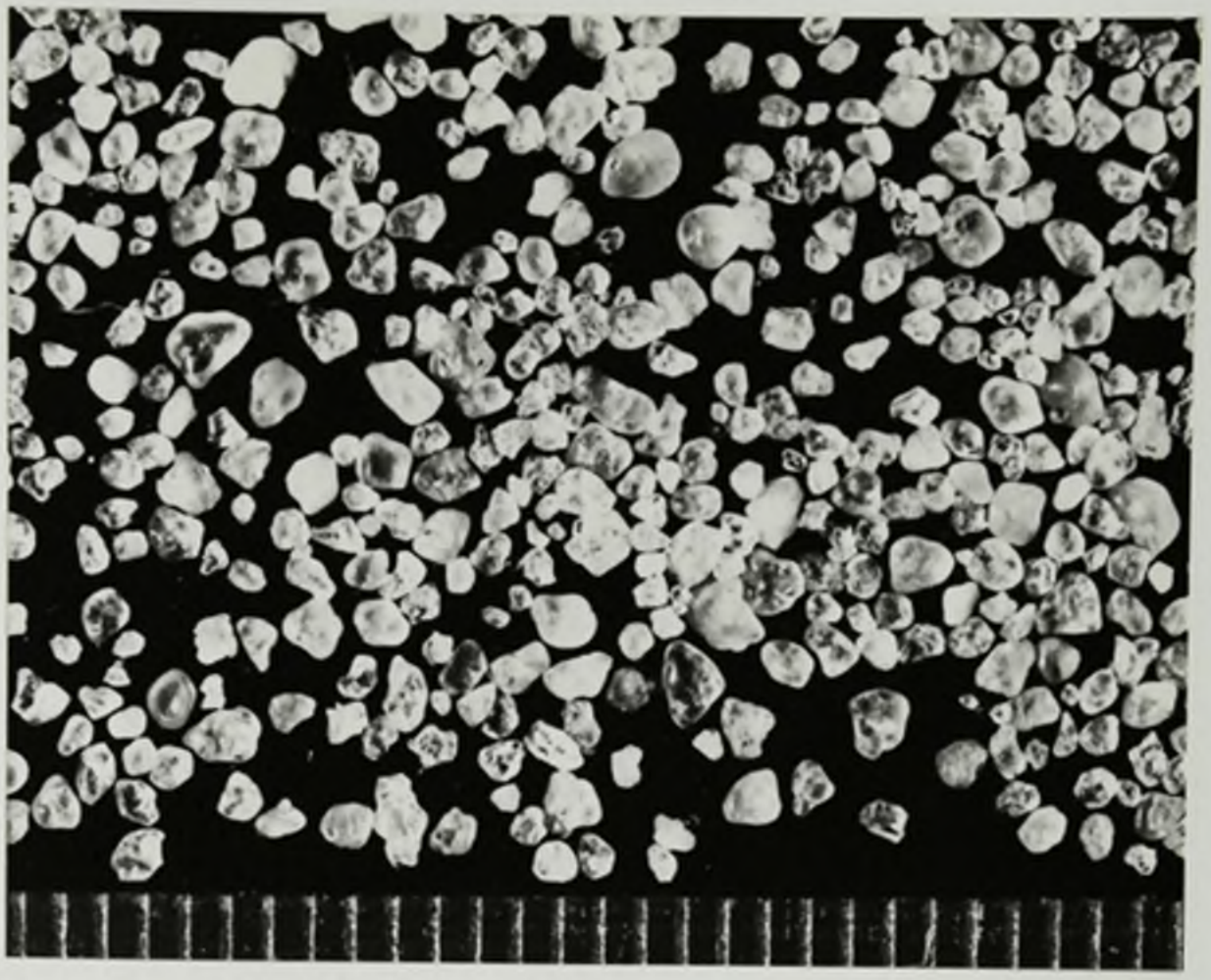

Sand 60

Sand 14/30

Plate 4. Granular solids 1 div = 0.5mm

deterioration with repeated handling.

The physical properties of the solids were determined on representative samples in the laboratory, giving the values used for the subsequent experimental work.

(i) Absolute Density

The absolute densities were found by the immersion method using water and a specific gravity bottle.

(ii) Bulk Density

The bulk density of a solid is a variable property dependent on the amount of compaction or vibration experienced at the time of measurement as well as the container size. Therefore, it was decided to take two measurements of bulk density: (a) the minimum bulk density, (b) the maximum bulk density.

(a) The Minimum Bulk Density

There did not appear to be any absolute value for a minimum bulk density, but it was quite clear that practical systems showed a figure corresponding to the most open packing produced in the given conditions. Thus the measurement needed to be made, and had to involve a reproducible method of producing a comparable packing; the most suitable method appeared to be that proposed by Ridgeway and Rupp (101) which was adopted for this research.

A funnel was fixed at a set height above a flat-topped vessel of known volume (75 ml). The vessel was filled to overflowing via the funnel, the surplus material being scraped off level with a knife blade. Care was taken that there was no external vibrations during the filling of the vessel. The method gave a very good level of reproducibility, the maximum difference in 10 weighings being 0.5 g in 120 g or less than 0.5% on the bulk density value.

(b) The Maximum Bulk Density

Maximum bulk density values are open to criticism in the same way

as minimum values: but equally, they have empirical validity and should be measured. The value of the maximum bulk density was determined by tapping by hand the vessel while being filled with sand. This vibration was continued until no further solids could be added and the vessel and sand remained at a constant weight after the sand level had been topped up, tapped and levelled off. The error in these readings was surprisingly small, the maximum difference in 10 readings being 0.9 g in 120 g or less than 1% on the bulk density value.

(iii) Size Distribution

The size distribution of the solids was found by sieving 500 g samples on 200 mm British Standard sieves with a 'Ro-Tap' machine for 20 minutes. Six samples, taken from the bulk of the solids carefully avoiding segregation (89, 90) were sieved and the results averaged.

(iv) Drained Angle of Repose

The Drained Angle of Repose was found by using a simple apparatus: a perspex box (approximately 8" x 8" x 8") was set up with the top edges horizontal and then filled carefully and evenly. A pinch valve in the base of the box was opened gradually just beyond the point where the solids first started to flow, the apparatus then being left to drain itself. The height of the solids at the centre points of each of the four walls was taken. During the whole operation care was taken to avoid all undue vibration. The type of apparatus used was similar to that recommended by Evans (36) in a survey of methods of measuring the angles of repose; he suggested that wall effects could become significant with the more usual two-dimensional pieces of apparatus.

4.2 Experimental Procedure

Main Runs

The experimental procedure for each run was straightforward. The apparatus was essentially ready to run when the bunker and top hopper were full, the weigh hopper empty and the appropriate orifice plate and

standpipe in position. Then the chamber vent was set open and the readings on the gas meters were taken before starting the flow. Knowles (97) has reported that on starting the flow, the solids rate increased for a very short time, at most a second or so, then rapidly became steady for any given set of conditions. Consequently, the flow diverter was arranged for each run to direct the first part of the solids flow into the bottom storage hopper, changing over to measurement only when the flow became steady.

The run was started by opening the solids (control) valve and simultaneously starting the manual stop clock. The solids fell through the orifice down the standpipe and into the receiver hopper under the influence of gravity. When flow appeared to have steadied, the diverter flap was operated by a fast-acting pneumatic ram, the same action starting the electric stop clock. The run was terminated by just reversing the flap (which stopped the electric clock); secondly, by simultaneously operating the two slide valves at the top and bottom of the standpipe; and thirdly, by shutting off the solids control valve and stopping the manual stop clock. The third part of this procedure followed the second part as quickly as possible to reduce any discrepancies between the measurements of the air flow into and out of the system.

During the run, a succession of photographs was taken of the manometer panel to record the pressures throughout the apparatus (camera details, Appendix 2). After the run, gas meters were read again to find the volumes of air displaced by the movement of the solids, giving in conjunction with the reading from the manual stop clock the values for the air flow rates during the run. The solids isolated in the standpipe by the pneumatic slides were removed and weighed; the weigh hopper and the electric clock readings gave the solids flow rate.

Each individual run was repeated with the same orifice and standpipe, but with the chamber vent closed. Each such pair of runs was repeated

three times and their results averaged. The film recordings of the manometers were developed to the negative stage, the pressures being read from these using a Hilger integral enlarger and screen (courtesy of the Mechanical Engineering Department).

The major part of the experimental work was done using the sand No. 60. Each of the fourteen standpipes were used in conjunction with up to seven orifices depending on the standpipe diameter. The different sets of conditions used are set out in Table 4.1. Similar experiments were carried out using the second sand (14/30), although as these runs progressed it was realised that it was not necessary to repeat the entire experimental programme due to the very noticeable similarity in the behaviour of the two solids. Consequently, for this sand, the full experimental programme was only carried out with the 38.5 mm diameter standpipes (Table 4.2).

On examining the results of the runs carried out with the chamber vent open, it was realised that they were of little direct relevance to the present investigation, serving only to remove the effect of the standpipe on the solids flow through the orifice and to induce a larger volume of air to flow co-currently through the standpipe. The observations of this type of flow were useful, however, and were compared with those made with the solids flowing under the standpipe effect. With this in mind the experimental programme for the 14/30 sand did not include such runs; the runs carried out with the chamber vent closed were replicated three times as before.

Procedure for changing Orifice Plates and Standpipes

The orifice plates were incorporated in the apparatus as shown in Figure 4.3. Thus it was necessary to empty the top hopper system before being able to change the orifice plates. This design feature was inherited with the top hopper system and although it was realised that it was inefficient, no faster methods of changing orifice plates were

TABLE 4.1

Standpipes and Orifices used with Sand 60

Standpipe diameter: 25.5 mm

Standpipe lengths: 1.500, 3.000, 3.650, 4.875 (m)

Orifice diameters: 12.7, 19.01, 25.4, 31.75, 38.1 (mm)

Standpipe diameter: 38.5 mm

Standpipe lengths: 1.500, 2.000, 3.000, 3.650, 4.250, 4.875 (m)

Orifice diameters: 12.7, 19.01, 25.4, 31.75, 38.1, 44.45, 50.8 (mm)

Standpipe diameter: 50.5 mm

Standpipe lengths: 1.500, 2.000, 3.650, 4.875 (m)

Orifice diameters: 12.7, 19.01, 25.4, 31.75, 38.1, 44.45, 50.8 (mm)

TABLE 4.2

Standpipes and Orifices used with Sand 14/30

Standpipe diameter: 38.5 mm

Standpipe lengths: 1.500, 3.000, 3.650, 4.875 (m)

Orifice diameters: 12.7, 19.01, 25.4, 31.75, 38.1, 44.45, 50.8 (mm)

apparent in which the apparatus remained sealed.

The procedure for changing the standpipes was exacting. The top hoppers were emptied and the standpipe stripped of the manometer leads. The seals at each end of the standpipe were loosened and the flow diverter wound down to its lowest posisition, thus removing the top of the standpipe from the upper slide valve unit. The standpipe was then removed and stored vertically in a rack (Plate 1). The top hopper system was attached to the 5 ton crane block and loosened from its guides. It was then raised or lowered to the appropriate position for the next standpipe, tightened up again, and detached from the crane. The new standpipe in place, the flow diverter unit was wound up again to locate the standpipe in the upper slide valve box. The seals were then tightened, holding the standpipe rigid, and finally the manometer leads were attached to the standpipe pressure tappings. The whole operation had to be executed carefully due to the fragility of the standpipes, and needed the assistance of a technician in the handling and accurate location of the standpipes.

4.3 Additional Work

Further experimental work included the determination of the solids flow without the standpipe, i.e. under normal gravity flow conditions, solids flow under the influence of a counter-current air stream and determination of the pressure differences across the orifice which caused the solids flow to cease.

Gravity Flow Runs

The procedure for determining the solids flow under purely gravitational influence was simple. The standpipes were removed, the hopper system set in its lowest position, and a large funnel (0.75 m tall) was connected to the top of the flow splitter. All air meters were disconnected and the chamber vent opened directly to atmosphere. The apparatus was ready to be operated when the top hopper system was full,

the diverter flap positioned to allow the solids to flow into the bottom storage hopper, and when the appropriate orifice plate was in position. To start the run, the solids control valve was opened, then after a short period of time the diverter flap was swung over to let the solids fall into the weigh hopper, starting the electric clock as before; the reverse procedure ended the run.

Counter-current Air Flow Runs

Only small modifications to the apparatus were needed to determine the solids flow rate under the effect of a counter-current air stream. The apparatus was fitted with the shortest (1.5 m) of the largest diameter (50.8 mm) standpipes, the pressure tappings having been previously connected together with short lengths of P.V.C. tubing, thus effectively sealing them off. A dried and filtered air supply (36) was connected to the chamber vent and the chamber and orifice manometer were adapted to read positive pressures. The gas meters were disconnected from the top hopper system and the bottom air outlet from the weigh and storage hoppers blanked off.

Thus, as before, with the top hopper system full and the appropriate orifice plate in position, the appropriate pressure drop conditions were created in the chamber with the solids control valve closed. The valve was then opened, and the necessary adjustments (if any) made to set the pressure difference over the orifice to its predetermined value. The diverter flap was then thrown over for a set length of time and then reversed as before. During the run the pressure above and below the orifice (i.e. in the chamber) was recorded several times.

The runs were repeated for increasing orifice pressure drop values until the solids flow ceased altogether. Several determinations of this pressure drop were made for each orifice and the results averaged. A different and lower orifice pressure drop at which solids flow started again was discovered: several determinations of this pressure drop were

made and averaged. There were, unfortunately, violent oscillations in the solids flow rates under these counter-current conditions, increasing in intensity as the counter-current air flow rate increased, and the average solids flow rate decreased. These oscillations in the solids flow rate created corresponding disturbances in the pressure readings, making accurate determinations of the pressure very difficult. This was especially so at the point of zero solids flow rate, where there was a constant need to adjust the air flow rate to obtain the best estimate of 'stop-flow' pressure drop. Consequently, because of this need to alter the air flow rates, it was not possible to take any measurements of counter-current air flow through the orifice and constant level bed.

CHAPTER 5

The Effect on Solids Mass Flow Rates of an Expansion Chamber between a Hopper Outlet and a Vertical Standpipe

5.1 Introduction

It has been mentioned in Chapter 4 that a glass chamber was interposed between the hopper orifice and the top of the standpipe. The use of such a chamber was based on the results of qualitative work previously performed in the Department (36) and upon the recommendations of Wolf and von Hohenleiten (77). From an inspection of the available literature on the influence of a standpipe on solids flow from a hopper, it was found that the method of connection of the standpipe to the hopper could affect the solids flow. Bulsara et al (50) connected a tube directly to a flat-bottomed bin, and Miles et al (72) attached pipes directly to the outlet of conical hoppers, whereas others (67, 71) used only laboratory funnels fitted directly to small diameter tubing. None of these retained a separate hopper orifice, or even a control valve at the top of the standpipe, and thus in all cases it had been found necessary to start each run with the pipes full of solids. Wolf and von Hohenleiten (77) showed that a tapered cone, while permitting flow when used as a bunker, tended to cause compaction and blockage if used as part of a pipe system due to the powerful wedging action. They recommended the use of a 'breakaway' (an increase of section allowing free space above the solids) if a change of direction or decrease in section or excessive compaction was likely. Experience in the Department (36) also had shown that the inclusion of such a system in the apparatus, in the form of a glass chamber between the hopper orifice and standpipe entrance, allowed the easy insertion of a solids control device between the orifice and the standpipe. The use of such a chamber also enabled orifices of larger diameter than the standpipe to be used.

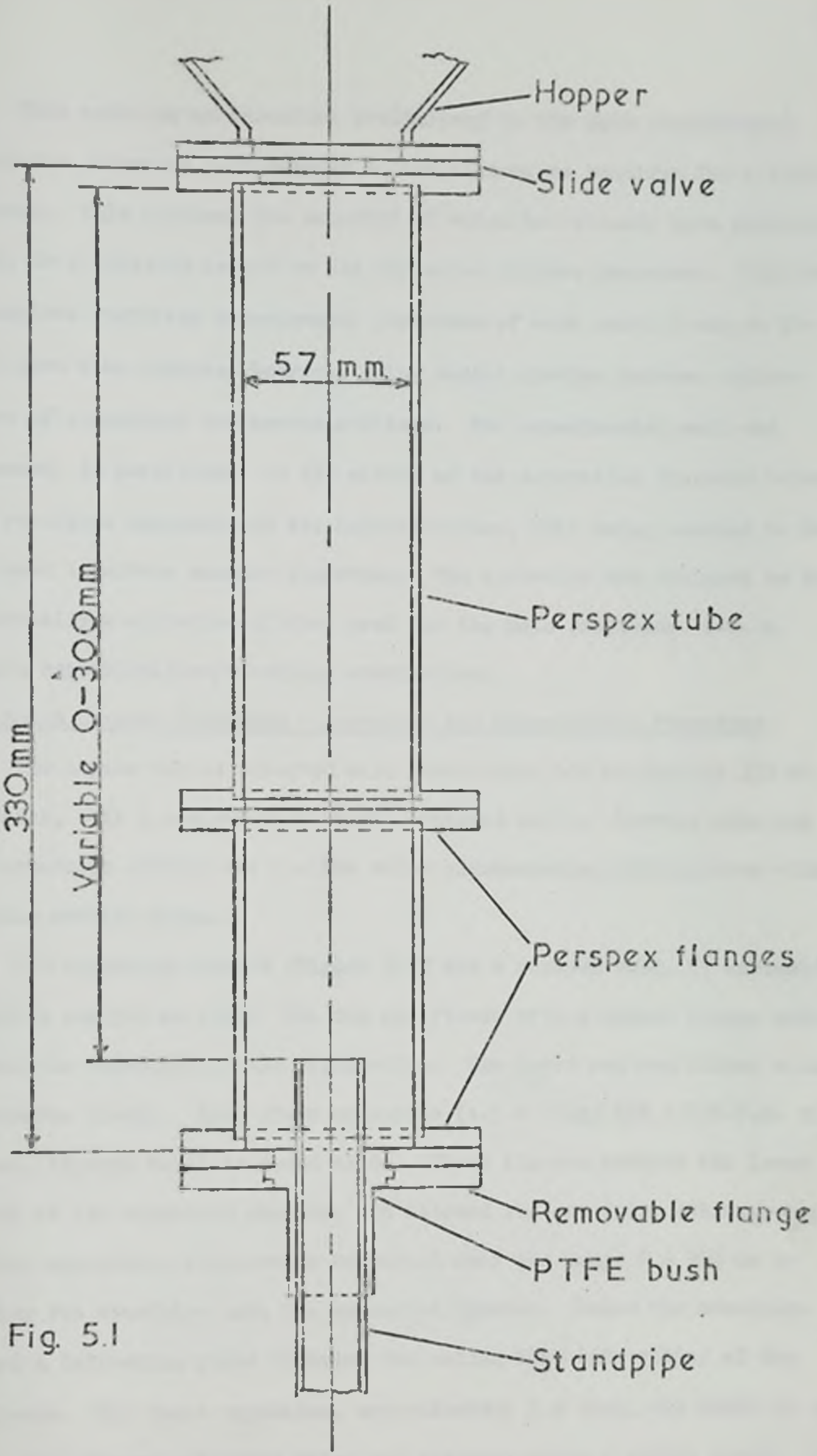

Fig. 5.1

Detail of the Expansion Chamber

This work was an essential preliminary to the main experimental programme, since no data existed on the dimensions required for a suitable chamber. This chapter, the majority of which has already been published (99), is a detailed report on the expansion chamber programme. This was a complete ancillary experimental programme of work carried out on the different flow regimes observed, using such a chamber between various sizes of standpipes and hopper orifices. The experimental work was focussed, in particular, on the effect of the separation distance between the standpipe entrance and the hopper orifice, this being assumed to be the most important chamber dimension. The apparatus was designed to be essentially a miniature of that used for the main programme, i.e. a simple hopper/orifice/standpipe combination.

5.2 Expansion Chamber Programme - Apparatus and Experimental Procedure

The hopper was an inverted mild steel drum, 610 mm high by 350 mm diameter, with a conical neck of 80° included angle. Between this and the expansion chamber was a slide valve accommodating slide plates with varying orifice sizes.

The expansion chamber (Figure 5.1) was a perspex tube, 57 mm inside diameter and 300 mm long. The top was fitted with a square flange which formed the underside of the slide valve. The lower end was fitted with a circular flange. Each glass standpipe (1.5 m long) had a P.T.F.E. flange fitted, through which it could slide. These flanges matched the lower flange of the expansion chamber, and allowed the standpipe entrance hopper orifice separation distance to be varied over the range 0 - 300 mm by raising the standpipe into the expansion chamber. Below the standpipe outlet a deflecting plate diverted the solids flow into either of two receivers. The whole apparatus, approximately 3 m high, was built in a frame, the hopper and tubes being set vertical using a spirit level. The lower end of the glass standpipe was held steady by a clamp (Figure 5.2, Plate 5).

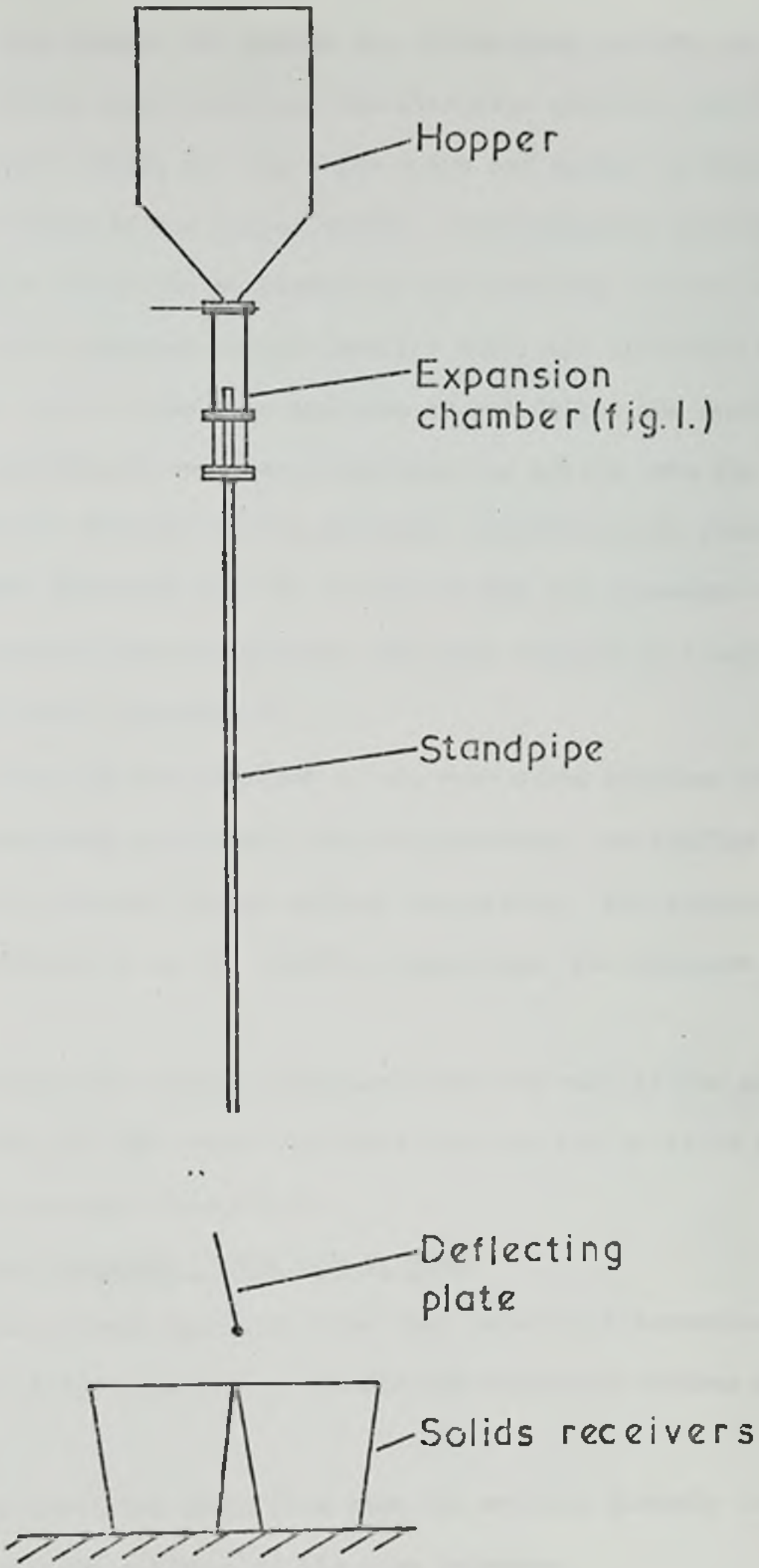

Fig. 5.2

Schematic representation of the apparatus

Operation was simple; the hopper was filled with solids, an orifice plate having been chosen and the standpipe entrance orifice separation distance fixed, and the slide valve was opened to bring the orifice to the centre of the hopper outlet. The deflector had already been positioned to allow the particles to fall into the 'waste' receiver until the flow rate appeared steady (usually until the particles had built up to the level of the pipe entrance or had filled the chamber). The deflector was then thrown over, diverting the solids into the 'sample' receiver. A switch attached to the deflector simultaneously started a centisecond timer (Appendix 2). To finish the run the procedure was reversed. The sample from the receiver was then weighed on a multi-revolution dial scale (Appendix 2).

The mass of solids and duration of run were noted together with the three main experimental variables: the pipe diameter, the orifice diameter and the standpipe entrance hopper orifice separation. For convenience, this last is referred to as the 'orifice separation' for the rest of this chapter.

The total expansion chamber programme involved each of the seven pipes, tested with all the seven available orifices and up to 14 standpipe positions in the chamber (Table 5.1).

5.3 Expansion Chamber Programme - Preliminary Work

At the outset, there appeared to be four possible alternatives for the development of the solids flow through the expansion chamber and into the standpipe:

1. All the particles would flow from the orifice directly into and down the pipe, with no spillage at the pipe entrance.

2. Most of the particles would flow straight down the pipe, but some spillage would occur causing build-up of a stationary bed of particles in the chamber around the pipe until a funnel into the pipe entrance was formed, and thereafter the pipe would be able to carry the full particle

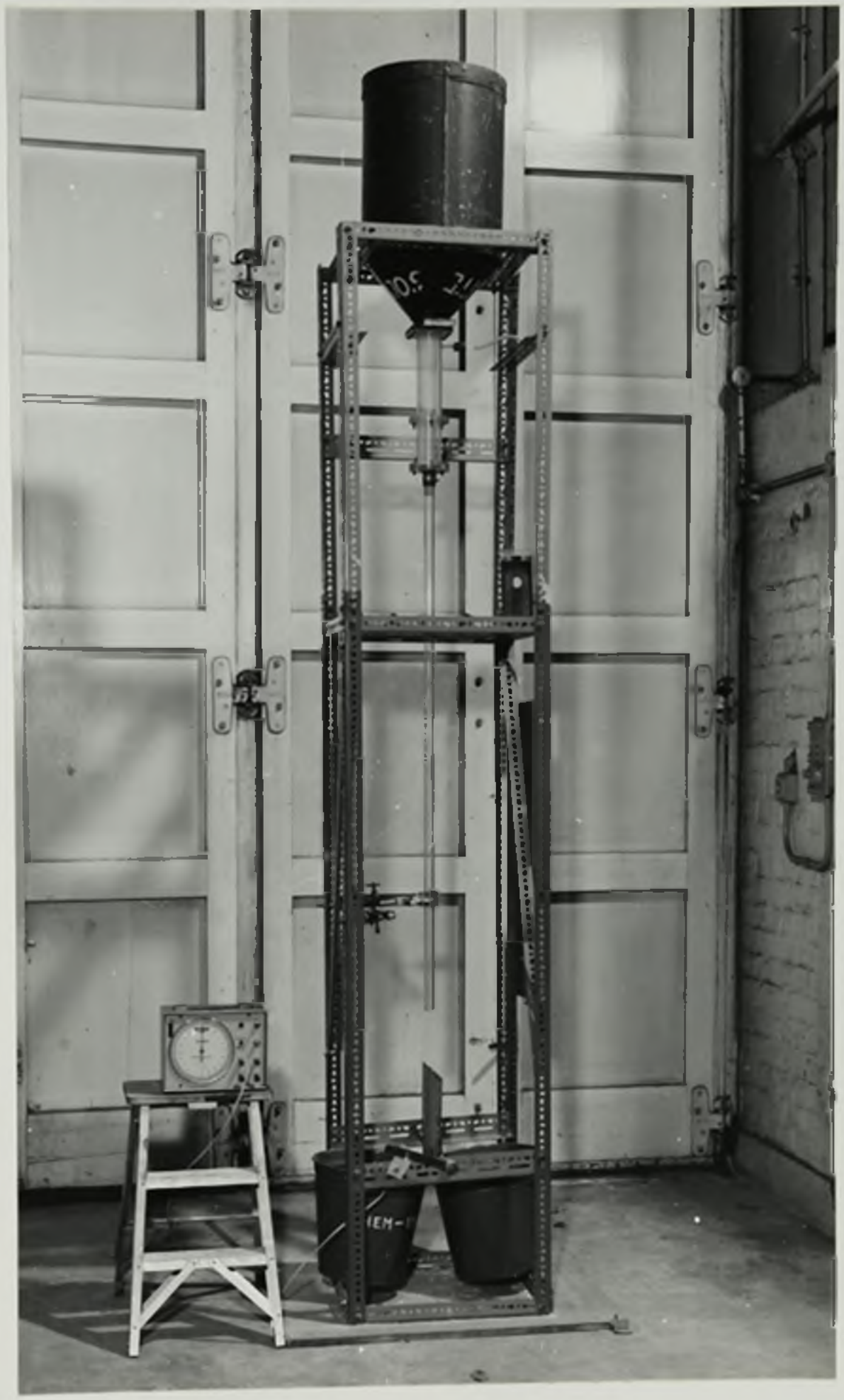

Plate 5. Apparatus - expansion chamber programme

TABLE 5.1

Run Schedule - Mustard Seed - Expansion Chamber Programme

D_o \ D_t	11.0	13.0	15.5	17.0	19.0	20.0	22.5
12.7	8	8	10	9	7	14	14
15.9	8	10	10	9	7	14	14
19.0	8	8	10	10	11	14	14
22.2	8	8	10	11	14	14	14
25.4	8	8	10	11	13	14	14
34.9	8	8	10	10	11	11	14
44.5	8	8	6	10	11	6	14

Number of standpipe positions tested for each orifice diameter (D_o mm) and standpipe diameter (D_t mm), excluding check runs.

TABLE 5.2

Materials Used - Expansion Chamber Programme

Size Distribution

Mustard Seed		Nylon Chips		Sodium Perborate	
µm	% retained	µm	% retained	µm	% retained
2800	tr	2000	tr	600	tr
2000	73.8	1700	50.2	425	56.8
1700	25.6	1400	49.2	355	29.0
1400	tr	1180	tr	base	14.1

Bulk Density

670.5-749.2 kg/m^3	612.8-742.1 kg/m^3	739.2-872.3 kg/m^3

3. There would be spillage as in 2, but the pipe entrance would not be able to carry the particle stream, so that a bed would build up until there was no free space left in the chamber. There would then be continuous moving bed flow (80) between the pipe entrance and the hopper orifice.

4. Similar to 3, but the bed builds up to the orifice, then blocks the pipe entrance, and all flow ceases.

In fact, only flow patterns 1, 2 and 3 were observed in the experimental work. Preliminary work showed that each of the three flow patterns was dependent on the orifice diameter, the pipe diameter and the orifice separation. The experimental work covered 49 diameter ratios (i.e. ratios of orifice diameter to pipe diameter) in the range 0.565-4.04, and it became apparent that this could be conveniently sub-divided into 4 smaller ranges by the nature of the flow phenomena. These were:

1.	Large pipe, small orifice	Diameter ratios	below 0.97
2.	Orifice and pipe of similar diameter	" "	0.97 - 1.10
3.	Orifice just larger than the pipe	" "	1.10 - 1.35
4.	Large orifice, small pipe	" "	above 1.35

5.4 Expansion Chamber Programme - Results

In this preliminary investigation, when the solids to be used in the main programme on the large apparatus had not been decided, it seemed important to use materials as diverse in nature and characteristics as possible. The actual solids used - mustard seed, nylon chips and sodium perborate crystals - were selected (from a very limited range of readily available materials) with this in mind.

Since the three solids (Table 5.2) used in the investigation were all different in character, the results were only compared and contrasted with no attempt at overall correlation. Both the mustard seed and the nylon chips had a narrow size range, but the sodium perborate exhibited a wide size distribution, including a fines element. The mustard seeds were

spheroidal, the nylon chips approximately cylindrical, and the sodium perborate took the form of nodular agglomerates: so that a considerable variety of shapes was represented.

The most comprehensive results were obtained using the mustard seed, varying the orifice separation as well as the orifice diameter and the pipe diameter. The runs with the nylon chips and the sodium perborate used a single fixed orifice separation (150 mm) while varying the orifice and pipe diameters. The mustard seed sample was also used to check the flow relationship for orifices used without standpipes.

To check reproducibility throughout the range of orifice separations, certain runs were repeated at the end of the tests on each orifice/pipe combination. Runs were replicated more frequently at small orifice separations, or wherever a change of flow regime occurred. The general reproducibility was found to be good, generally within $\pm$ 1% on solids flow rates, although this figure increased for the smallest orifices and tubes. Variations were, on the whole, less for 'empty chamber flow' (mean maximum error $\pm$ 0.26% for replicate results from 78 configurations) than for 'full chamber flow' ($\pm$ 0.81% for 80 configurations). Comparing results of two sets of runs with the same conditions, but taken six weeks apart, gave a maximum error of $\pm$ 0.75% through the whole range of orifice/pipe separation distances.

The duration of the runs varied from 20 to 60 seconds, and the total mass throughput of solids from 500 g to 3500 g according to the flow rate. The timer could be read to the nearest 0.01 second and the weighing scale to the nearest 5 g. The main section of the programme, using mustard seed, comprised 706 runs together with 489 runs for the auxiliary tests and the other materials.

The results of the main section of this programme did not clearly show the effect of very small orifice separations of the mass flow rate, and so these were investigated further by using chosen sets of pipes and

orifices characteristic of the different flow patterns. Apart from this, due to the large number of runs needed to complete a programme with variations over the whole range of all three parameters, it was decided to keep the standpipe in one position in the expansion chamber (150 mm separation) for the other solids. This separation was kept fixed for all subsequent runs.

The results are presented graphically in Figures 5.3 to 5.11. Figure 5.3 was typical of the effect of altering the orifice separation on the mass flow rate of mustard seed for one pipe size with all orifice sizes; Figure 5.4 showed, on a larger scale, the effect of very small orifice separations. The results for the mustard seed at the constant 150 mm orifice separation are brought together in Figure 5.5. Similar summary graphs in Figures 5.6 and 5.7 showed the results obtained using the nylon chips and sodium perborate.

Figures 5.8, 5.9 and 5.10 showed the results for the 'free flow' situation represented in the more usual log-log form. The slopes of the lines for constant D_t agree well with earlier results on simple orifice flow (43), and also with the simple orifice runs of the present work - Figure 5.11.

5.5 Expansion Chamber Programme - Discussion of Results

During the course of the experimental work, two major flow regimes were observed: these were termed the 'free flow' regime and the 'restricted flow' regime. The 'free flow' regime was defined as that flow pattern which includes significant free space in the expansion chamber around the compact central core of particle flow between the orifice and the pipe entrance; when the space between the orifice and the pipe entrance was completely filled by a moving bed of solids then the term 'restricted flow' was applied. These two regimes were visually distinct.

The principal aim of this experimental programme was to ascertain the effect on the solids flow rate of altering the orifice separation. Typical

NOTATION

Chapter 5, Figures 3 - 10

Figure 3

	D_o (mm)	Diameter Ratio, D_o/D_t
⊠	12.7	0.67
▲	15.9	0.84
●	19.0	1.00
x	22.2	1.17
□	25.4	1.34
Δ	34.9	1.84
O	44.5	2.34

Figure 4

Diameter Ratios, D_o/D_t				D_t (mm)
Type I - Free Flow		Type II - Restricted Flow		
O	0.99	●	1.98	22.2
Δ	0.74	▲	1.75	20.0
□	1.17	■	1.34	19.0
▽	1.12	▼	2.62	17.0
◇	1.02	◆	1.23	15.0

Figures 5 - 10

D_t (mm)			
●	11.0	O	19.0
▲	13.0	Δ	20.0
■	15.5	□	22.5
x	17.0		

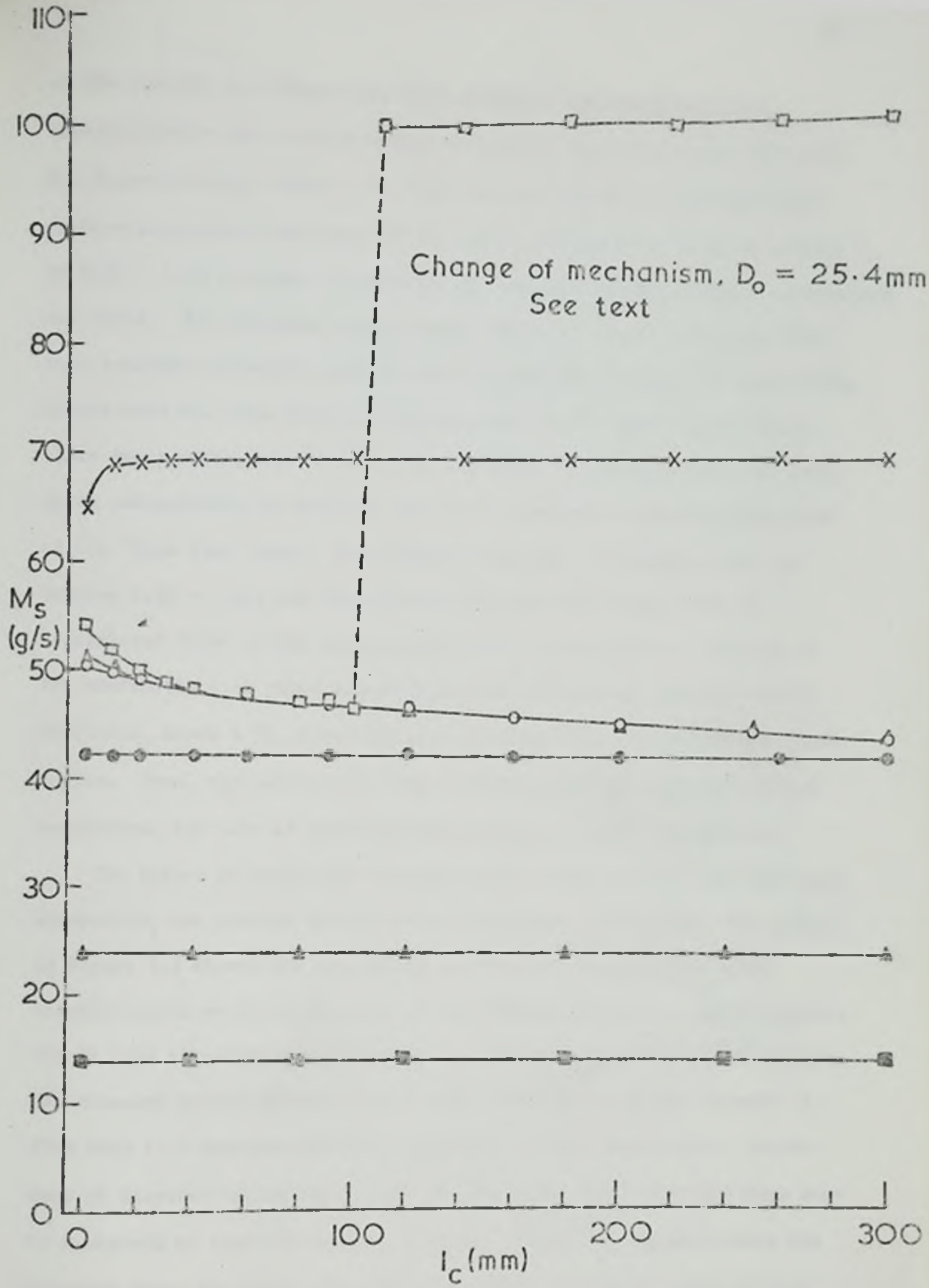

Fig. 5.3 Mass flowrate vs. Separation distance

D_t = 19·0mm Mustard seed

of the results was Figure 5.3, also showing examples of the flow characteristics for various ratios of orifice diameter to pipe diameter. For diameter ratios below 1.10, there was no change of flow rate with orifice separation over most of the range, although for diameter ratios of 0.97 - 1.10 a slight decrease in the solids flowrate at small separations was noted. For diameter ratios chosen between 1.10 and 1.22, the flow rate remained virtually constant and independent of change of separation, except when the pipe entrance was very near to the orifice, whereupon there was a noticeable decrease of flow rate. In general, all the foregoing combinations of orifices and pipes appeared to induce solids flow of the 'free flow' type. With further increase of diameter ratio to between 1.22 - 1.35, the flow pattern changed from 'free flow' to 'restricted flow' as the orifice separation was decreased. The use of the combinations of pipes and orifices for the maximum diameter ratios available, above 1.35, moved the flow entirely into the 'restricted flow' regime. Here, the solids flow rate increased with decrease of orifice separation, the rate of increase being larger at small separations.

The effect of small orifice separations on the solids flow rate was unexpected, and further investigation was thought necessary. The graphs in Figure 5.4 showed the results of this for the larger pipes with selected orifices characteristic of the various phenomena. Three general trends were illustrated by these plots. In the 'restricted flow' regime, for diameter ratios between 1.22 - 1.35, there was a large increase of flow rate to a maximum and then a fall-off at zero separation. In the case of diameter ratios above 1.35, on the other hand, the flow rate rose to a maximum at zero separation. For the 'free flow' regime, where the diameter ratio was below 1.22, there was usually some decrease of flow rate as the separation distance decreased, this tendency increasing as the diameter ratio increased; it was especially noticeable with the diameter ratio of 1.17, where the sharp decrease of flow rate suggested

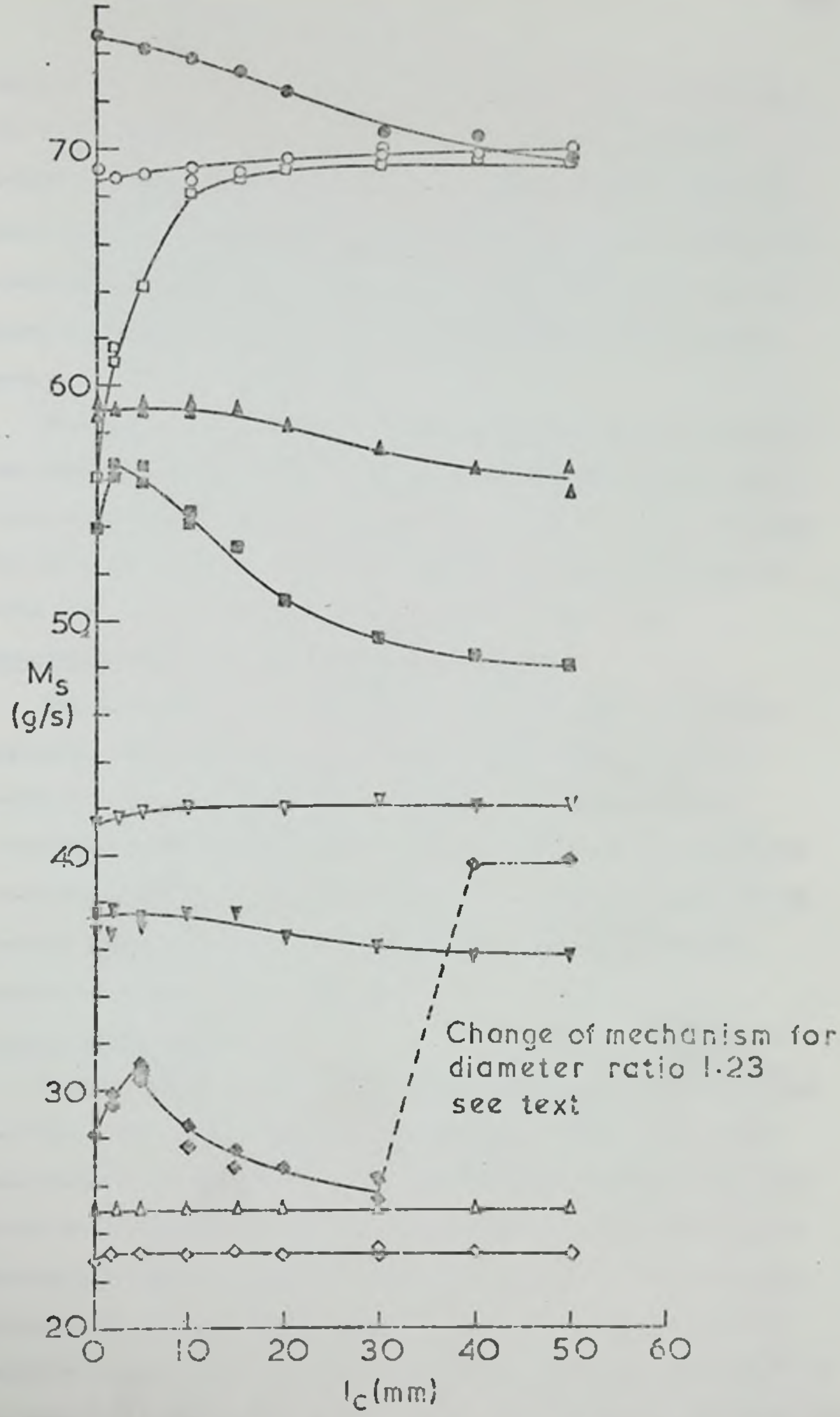

Fig. 5.4 Mass flowrate vs. separation distance at small separation distances

Mustard seed

the possibility of a flow regime change, since the flow rate fell to the values associated with restricted flow. It was not, however, possible to check visually whether such a change actually occurred at these small orifice separations: due to build up of the stationary bed around and above the pipe entrance in the 'free flow' regime, the two types of flow had become visually indistinguishable in the apparatus used.

The test programme thus showed that moving the standpipe entrance away from the hopper orifice by the use of an expansion chamber could increase the solids mass flow rate in the 'free flow' region. It could also have the effect of changing the regime from 'restricted flow' to 'free flow', with a consequent large increase of flow rate.

Expansion Chamber Programme - Suggested Mechanisms

This exploratory study did not lead to any definitive mechanism hypothesis; but it was thought that the detailed descriptions and tentative explanations given below offered at least a qualitative elucidation of the phenomena noted. The clearest way of describing the observations was by dividing the results into categories exemplified by diameter ranges, and considering the effect of varying the orifice separation distance within each range.

Diameter Ratios below 0.97

Diameter ratios in this area at large orifice separations generated the 'free flow' regime, the particles falling in a tight stream with some breakaway at the edges. At the pipe entrance, this breakaway manifested itself initially as spillage around the standpipe, building up a stationary bed and eventually forming a funnel of solids into the pipe, although most of the particles dropped directly into the pipe. Later particles on the edge of the stream fell on to the funnel, while those in the core of the stream fell directly through into the pipe. This resulted in a predominantly downward velocity in the central zone, whereas at the

edges the particles rebounded from the funnel, causing a considerable disturbance. The actual observations of this considerable turmoil of particles in the vicinity of the pipe mouth showed a close visual resemblance to fluidised bed conditions, and for convenience this condition was termed 'solids turbulence'. The pipe then carried all the particles which passed through the orifice without apparent restriction of the flow.

At small separations there was no spillage at all. The particle stream had not been able to spread out sufficiently, all the flow was directly into the standpipe, no stationary bed was built up, and no solids turbulence was observed at the entrance to the standpipe.

Diameter Ratios 0.97 - 1.10

The 'free flow' regime predominated for these diameter ratios at large orifice separations. The situation was as described above for large orifice separations, showing the solids turbulence phenomenon, with the pipe eventually carrying all the solids passing through the orifice, apparently without restriction.

At small separations for these diameter ratios spillage occurred quite readily, as the particle stream was of much the same diameter as the pipe. The stationary bed rapidly built up, reaching the lower side of the orifice plate and obscuring the view. It was assumed that the solids still fell essentially in 'particulate cloud' flow (30) through the orifice, since observed decreases in flow rate were only of the order of 3% at most.

Diameter Ratios 1.10 - 1.35

The 'free flow' regime was again generated with the whole range of orifice separations for diameter ratios at the lower end (1.10 - 1.22). A zone of solids turbulence was noted at the entrance to the pipe even though the orifice diameters were now larger than the pipe diameters. The effect of this solids turbulence was to channel the solids flow from

the larger orifice into the pipe and to maintain 'free flow' conditions. In the case of orifice and pipe combinations with diameter ratios at the larger end of the range (1.22 - 1.35), however, decreasing the orifice separation caused a change of flow regime to 'restricted flow', with the associated moving bed between the orifice and the standpipe entrance. The reason for this was thought to be that at lower values of orifice separation a dynamic arch was formed over the pipe entrance, making this in effect the controlling orifice and resulting in a dramatic decrease in solids flow rate; and that the arch formation was permitted by a reduction in the solids turbulence effect.

In the 'free flow' regime, it was thought that the high energies of the individual particles in the solids turbulence prevented the formation of the dynamic arch at the pipe mouth for large orifice separations, allowing the pipe to carry the solids flow delivered by an orifice of greater diameter. Such solids turbulence probably depended on the spread of the particle stream at the pipe entrance, while the predominently vertical downward motion in the core of the solids turbulence was dependent on the downward velocity at the pipe entrance.

Reducing the orifice separation reduced both the spread of the particle stream and the velocity at the pipe entrance. The combination of less solids turbulence and smaller downward velocity at the pipe entrance was likely to facilitate the formation of a dynamic arch over the mouth of the pipe. As soon as this was formed, the flow rate through the pipe would drop, but that through the orifice would remain unchanged: consequently, the particle bed would build up above the standpipe entrance and reach the underside of the orifice plate, causing a change to moving bed flow between the orifice and the pipe entrance, and giving the overall effect of the 'restricted flow' regime. Conversely, this implies that if flow through the orifice were too great for the solids turbulence to handle, then the particles would not be conveyed into the pipe at a sufficient rate to

maintain 'free flow'.

It was seen that there was very little variation of flow rate (2%) with decrease of orifice separation in the 'free flow' regime. This also was probably due to the existence of the solids turbulence at the entrance to the standpipe. Although this solids turbulence may have decreased as the standpipe was moved nearer to the orifice, it still appeared to enable the pipe to carry all the orifice flow until the critical condition was reached which allowed the formation of a dynamic arch and consequent flow restriction. Thus, at levels of solids turbulence above the critical condition, the flow through the standpipe would be expected to remain fairly constant, as was observed.

Diameter Ratios above 1.35

These combinations of orifices and pipes always generated 'restricted flow'. The particle flow rate apparently exceeded the carrying capacity of the pipe, there was spillage at the pipe entrance and formation of a stationary bed, as before. But the flow rate was now too great for the solids turbulence to deal with, so that the dynamic arch quickly appeared and a moving bed built up to the orifice plate. The increase of flow rate with decrease of orifice separation was probably due to the decrease of the mean particle path length between the orifice and the pipe entrance, with consequent decrease of the total particle-wall and particle-particle frictional losses.

Diameter Ratios above 1.10 for Small Orifice Separations

When the diameter ratio was in the range 1.10 - 4.04 and the flow patterns at the very small orifice separation were rather complex. It was noted that for those combinations with a diameter ratio between 1.10 - 1.35, which were in the 'free flow' regime for the whole range of separations, the flow rate decreased at small values of orifice separation, while for those in the 'restricted flow' regime the flow rate rose to a maximum in this area and then decreased suddenly at zero separation. No

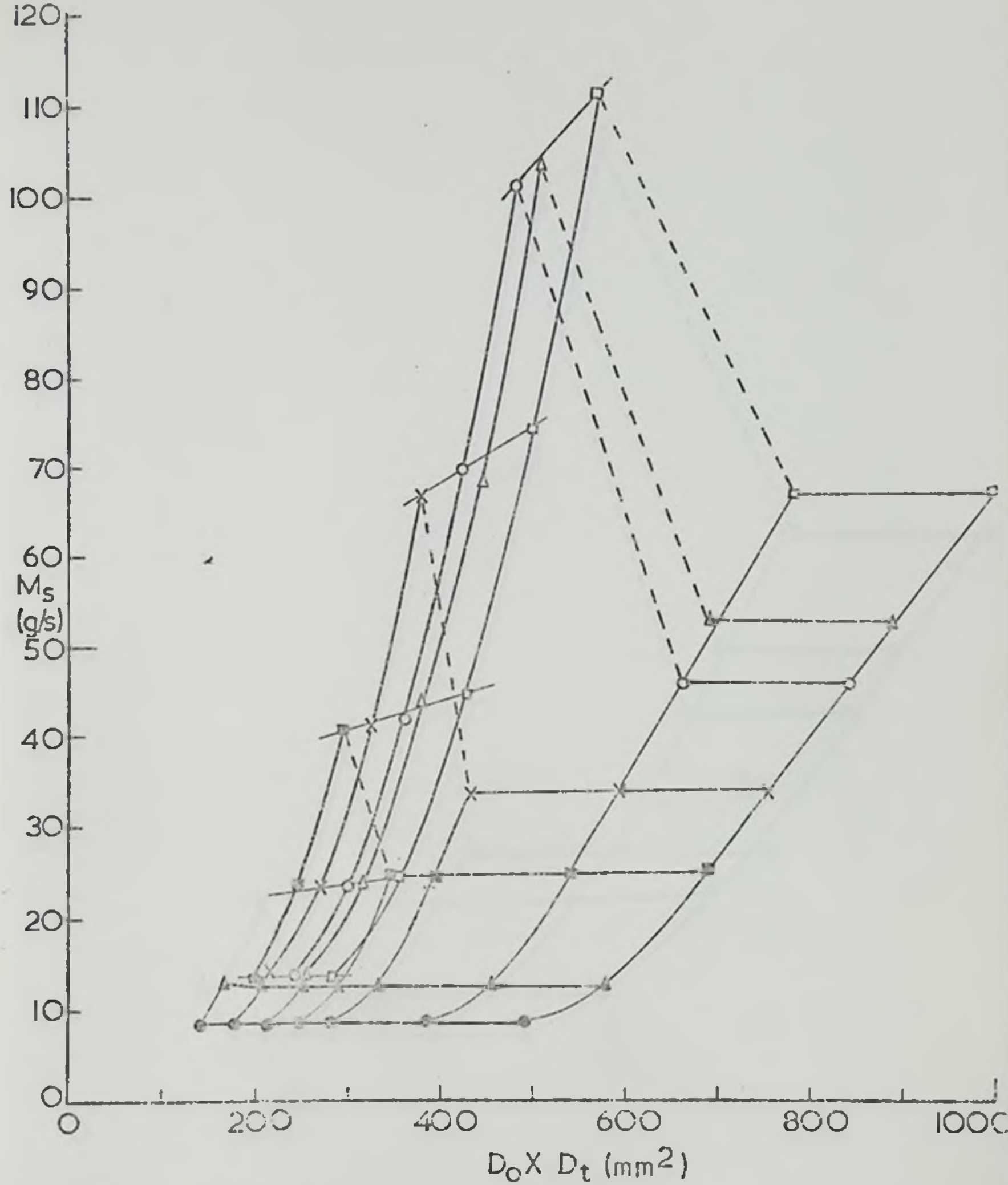

Fig. 5.5 Mass flowrate vs. orifice diameter x pipe diameter for l_c = 150mm. Mustard seed

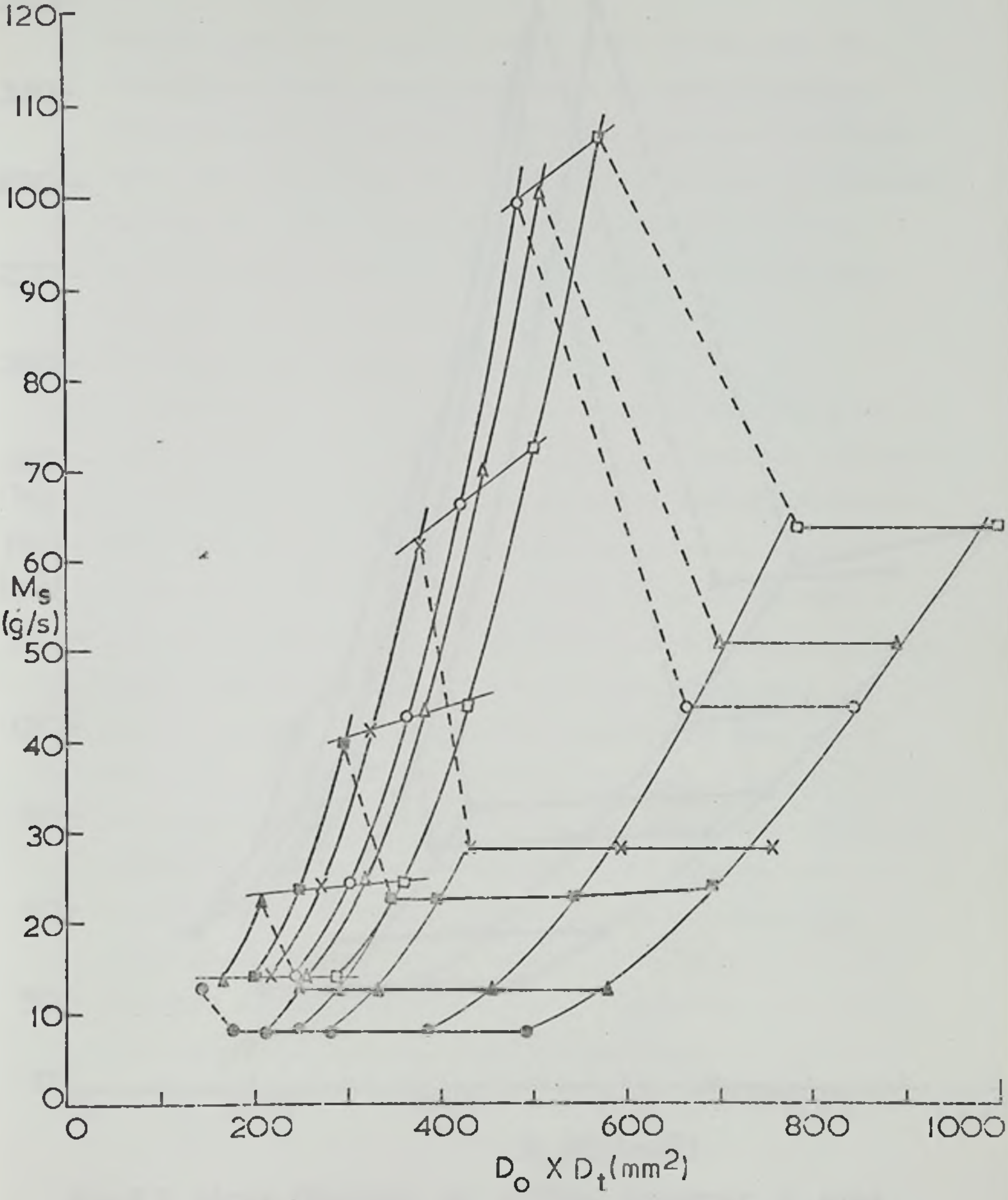

Fig. 5.6 Mass flowrate vs. orifice diameter x pipe diameter. $l_c = 150mm$. Nylon chips.

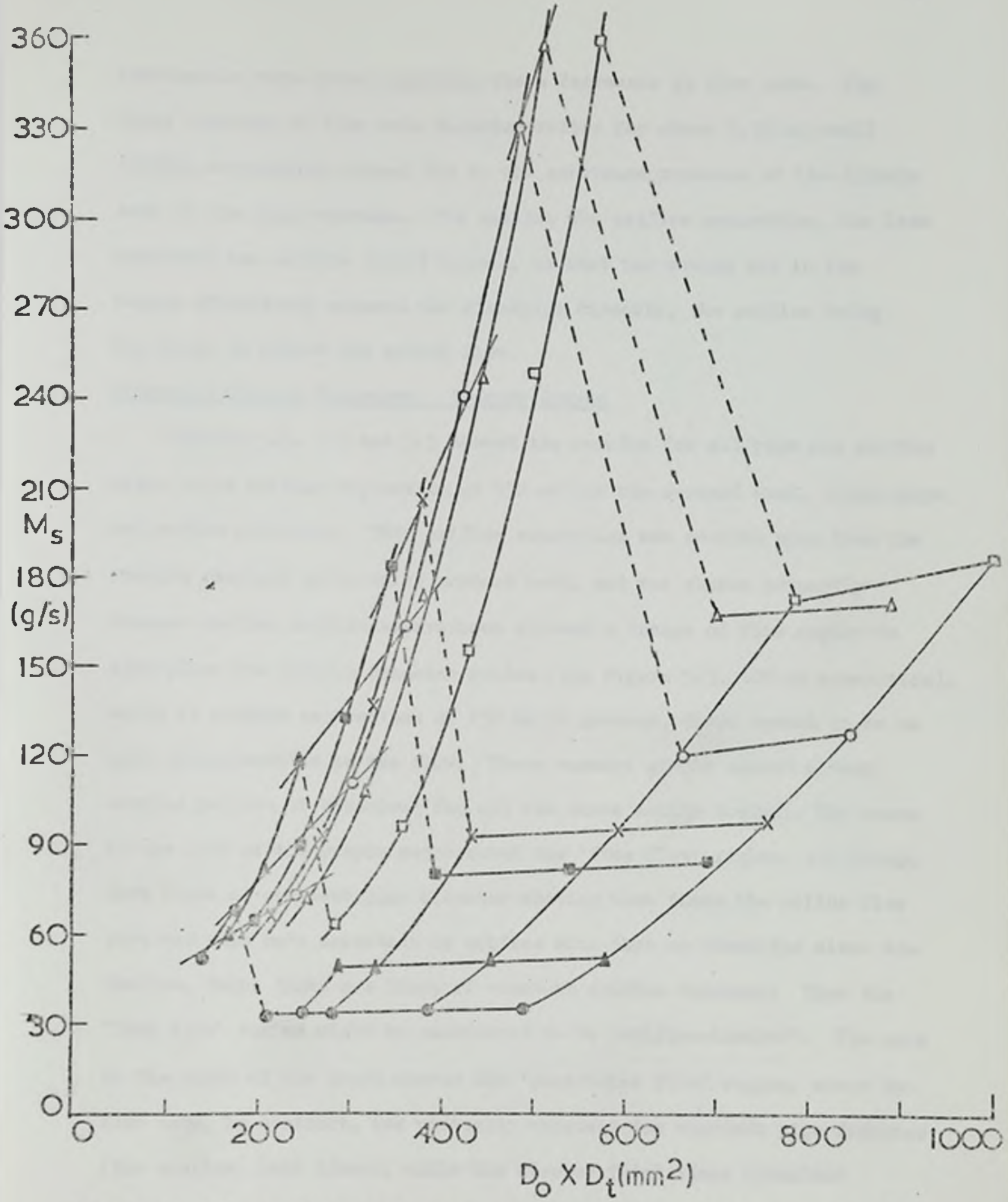

Fig. 5.7 Mass flowrate vs. orifice diameter x pipe diameter. l_c = 150mm. Sodium perborate.

conclusions were drawn regarding these decreases in flow rate. The large increase of flow rate diameter ratios for above 1.35 at small orifice separations seemed due to the continued presence of the dynamic arch at the pipe entrance. The smaller the orifice separation, the less important the orifice itself became, so that the moving bed in the hopper effectively entered the standpipe directly, the orifice being too large to affect the solids flow.

Expansion Chamber Programme -- Summary Graphs

Figures 5.5, 5.6 and 5.7 showed the results for all pipe and orifice sizes at an orifice separation of 150 mm for the mustard seed, nylon chips and sodium perborate. This orifice separation was decided upon from the results obtained while using mustard seed, and was chosen primarily because smaller orifice separations allowed a change of flow regime to take place for certain diameter ratios (see Figure 5.3, 100 mm separation), while at orifice separations of 150 mm or greater, there seemed to be no such irregularities in the flow. These summary graphs showed a very similar pattern of behaviour for all the three solids tested. The areas to the left of the graphs represented the 'free flow' regime, the steep, dark lines of constant pipe diameter showing that there the solids flow rate was much more dependent on orifice size than on standpipe size: the shallow, feint lines are lines of constant orifice diameter. Thus the 'free flow' regime might be considered to be 'orifice-limited'. The area to the right of the graph showed the 'restricted flow' regime, where the flow rate, by contrast, was virtually constant for constant pipe diameter (the shallow, dark lines), while the steeper feint lines (constant orifice diameter) showed much greater dependence on pipe diameter. This 'restricted flow' regime was thus regarded as 'pipe-limited'. The broken lines on the graphs join constant pipe diameter plots between the two flow regimes, showing the marked decrease in flow rate characteristic of the change from 'free flow' to 'restricted flow'. The similarity exhibited

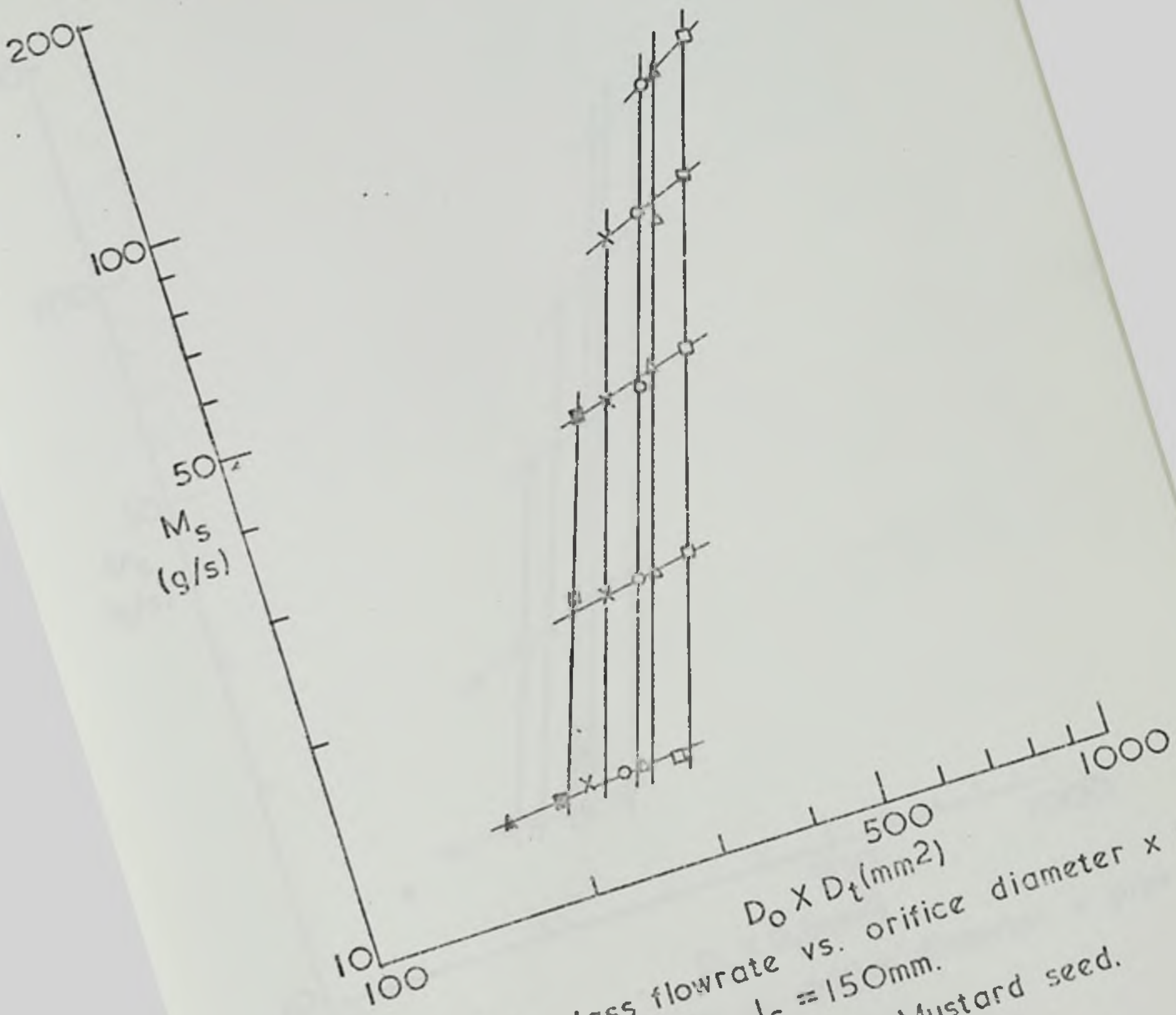

Fig.5.8 Mass flowrate vs. orifice diameter x pipe diameter. l_c = 150mm.
Free flow region. Mustard seed.

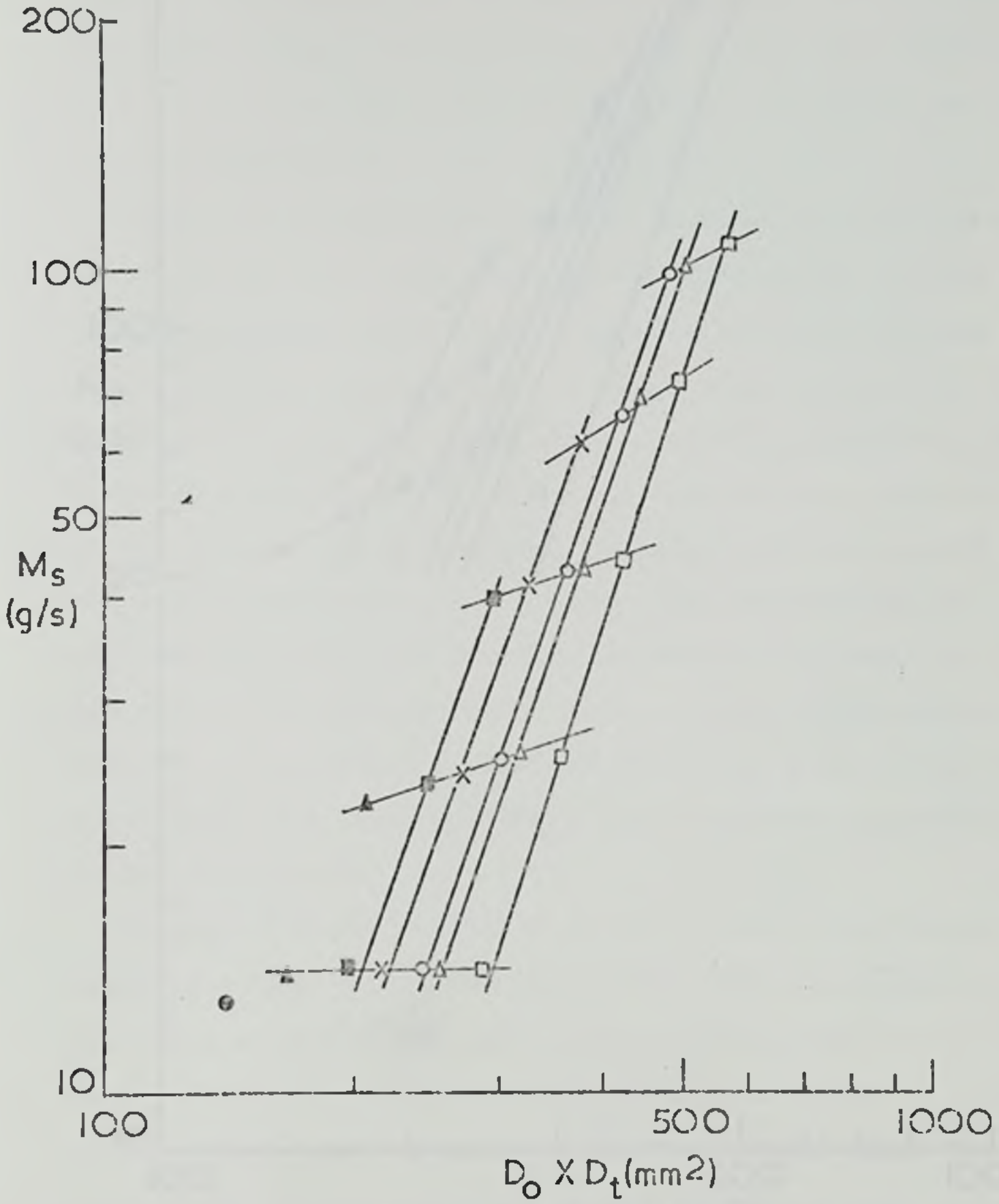

Fig.5.9 Mass flowrate vs. orifice diameter x pipe diameter. $i_c = 150mm.$
Free flow region. Nyion chips.

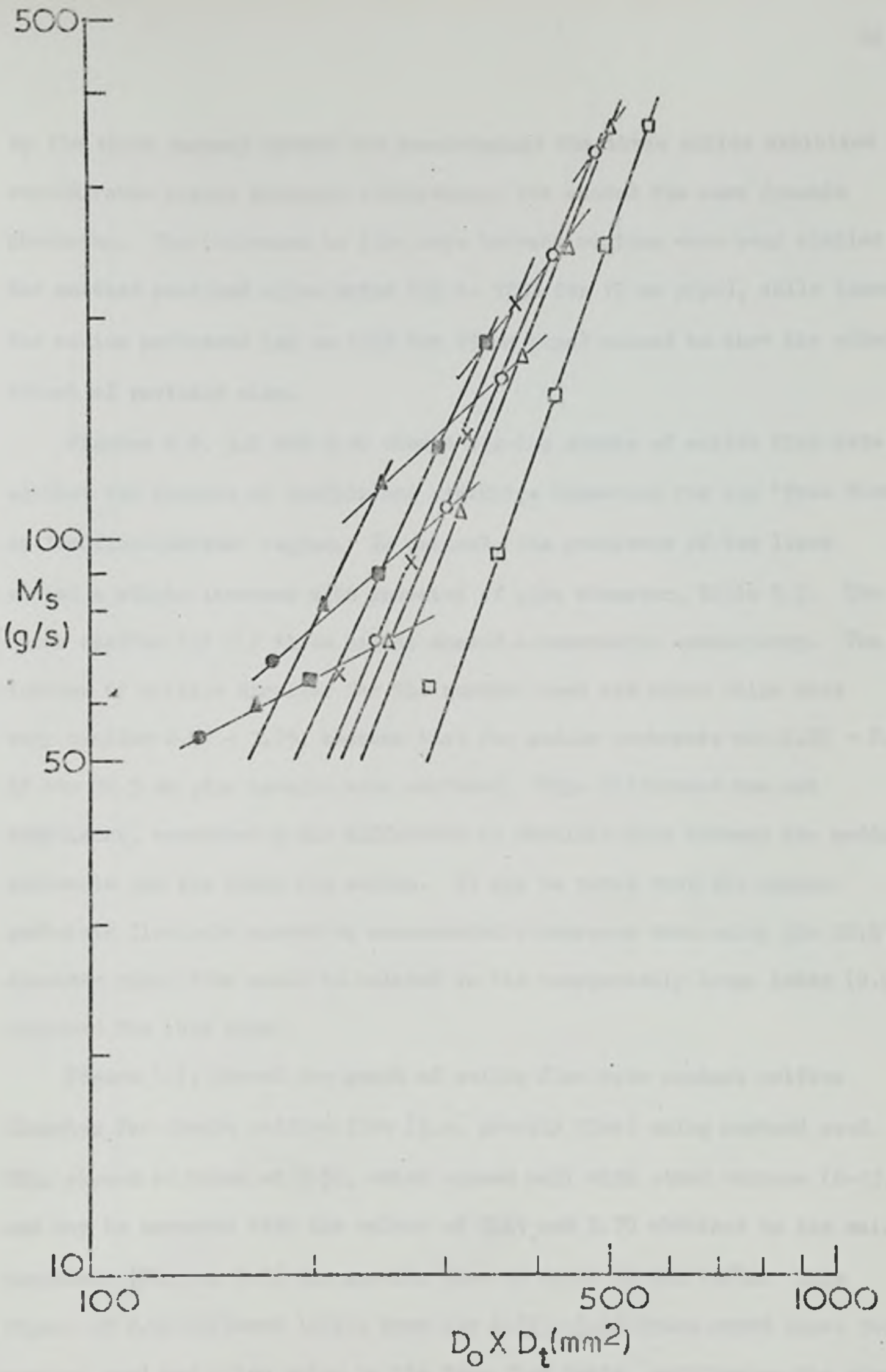

Fig. 5.10 Mass flowrate vs. orifice diameter x pipe diameter. $l_c = 150mm$.
Free flow region. Sodium perborate

by the three summary graphs was encouraging: the three solids exhibited considerable static property differences, but showed the same dynamic phenomena. The increases in flow rate between regimes were very similar for mustard seed and nylon chips (up to 125% for 19 mm pipe), while those for sodium perborate (up to 175% for 19 mm pipe) seemed to show the added effect of particle size.

Figures 5.8, 5.9 and 5.10 showed log-log graphs of solids flow rate against the product of orifice and standpipe diameters for the 'free flow' or 'orifice-limited' regime. In general, the gradients of the lines showed a slight increase with increase of pipe diameter, Table 5.3. The check results for all three solids showed a remarkable consistency. The indices of orifice diameter for the mustard seed and nylon chips were very similar 2.77 - 3.25, whereas that for sodium perborate was 2.05 - 2.53, if the 22.5 mm pipe results were excluded. This difference was not surprising, considering the difference in particle size between the sodium perborate and the other two solids. It may be noted that the sodium perborate flow rate showed an unaccountable decrease when using the 22.5 mm diameter pipe; this could be related to the unexpectedly large index (2.91) observed for this pipe.

Figure 5.11 showed the graph of solids flow rate against orifice diameter for simple orifice flow (i.e. gravity flow) using mustard seed. This showed an index of 2.98, which agreed well with other workers (6-13), and may be compared with the values of 2.61 and 2.70 obtained in the main programme (Chapter 6.5) for gravity flow of sands 60 and 14/30. This figure of 2.98 differed little from the 2.77 - 3.25 index noted above for mustard seed and nylon chips in the free flow tests, reinforcing the view that the orifice was the main factor in the solids flow rate in that regime. Table 5.4 compared the mustard seed flow rates for simple gravity flow with those for all orifice/pipe combinations which allowed the 'free flow' regime at an orifice separation of 150 mm. A comparison of the two sets of results

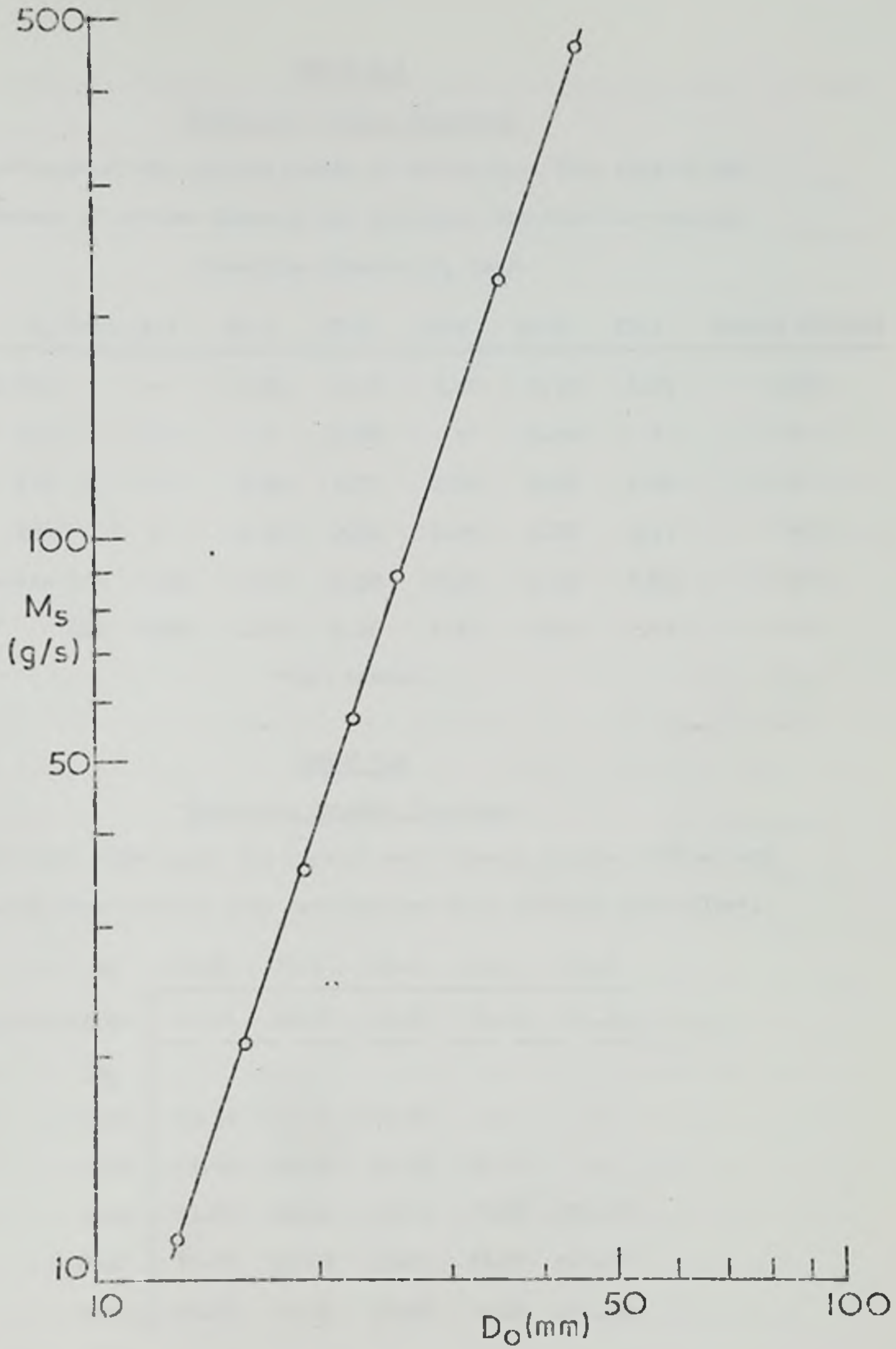

Fig. 5.11 Mass flowrate vs. orifice diameter
Gravity flow – Mustard seed

TABLE 5.3

Expansion Chamber Programme

Gradients of the log-log graphs of solids mass flow rate vs the product of orifice diameter and standpipe diameter for constant standpipe diameter D_t (mm).

D_t (mm)	13.0	15.5	17.0	19.0	20.0	22.5	Simple Orifice
Mustard Seed (1)	-	2.85	3.10	3.10	3.12	3.25	2.98
" " (2)	-	*	2.98	*	3.10	*	*
Nylon Chips (1)	-	2.84	2.77	2.86	2.89	3.10	*
" " (2)	-	2.92	2.84	2.83	2.88	3.11	*
Sodium Perborate (1)	2.05	2.14	2.38	2.39	2.53	2.85	*
" " (2)	2.09	2.22	2.48	2.42	2.47	2.91	*

* Not tested.

TABLE 5.4

Expansion Chamber Programme

Solids flow rates (g/s) for mustard seed through simple orifices and through those orifice pipe combinations which allowed 'free flow'.

D_o	12.7	15.9	19.0	22.2	25.4
Simple Orifice	11.31	20.70	35.57	57.06	89.39
D_t					
15.5	13.50	24.00	41.00	-	-
17.0	14.00	23.50	41.50	67.15	-
19.0	13.85	23.65	42.15	70.25	102.00
20.0	14.00	24.00	44.25	68.00	104.00
22.5	13.75	24.75	45.00	74.25	112.00

revealed a significant increase of solids flow rate over that for simple orifice flow in each case.

It was well known that the use of a simple vertical standpipe with a hopper increased the solids flow rate. The present apparatus simulated this situation when the orifice separation was reduced to zero: Table 5.5 showed such flow rates, predicted from Figure 5.11, for orifice sizes interpolated to be equal to the standpipe diameters: and also maximum flow rates through the standpipes for the 'restricted flow' regime. It was seen that the flow rates for the standpipes were, in all cases, higher than for the corresponding simple orifices. The solids flow rates through the pipes in the 'free flow' regime at 150 mm separation, given in the third column of Table 5.5, showed the beneficial additional effect of promoting this type of flow regime. This regime was, however, only possible if an expansion chamber, interposed between the hopper outlet and the pipe entrance, could run with free space above the pipe entrance. This proved impossible when the flow was initiated from the exit of the standpipe, for in this case both the pipe and expansion chamber started full, and this invariably gave 'restricted flow'; to achieve 'free flow' the controlling orifice must be positioned above the expansion chamber and pipe entrance to ensure that both are empty before flow commences. The use of an orifice at the base of the standpipe to control the flow increased the likelihood of producing moving bed flow throughout the length of the standpipe and the hopper (50). It was noticed in the present work, when this method was used to start the flow, that the initial moving bed flow produced in the standpipe tended to be unstable, so that after a very short time the pipe had emptied itself in a surge, and thereafter the standpipe showed individual particle cloud flow. The overall effect was thus to produce a 'restricted flow' situation in the expansion chamber, and a total flow rate somewhat higher than that through the corresponding simple orifice. Miles et al (72) have noted similar phenomena with sand.

TABLE 5.5

Expansion Chamber Programme: Mustard Seed

D_t	(i)	(ii)	(iii)
11.0	7.2	8.5	-
13.0	11.5	16.0	13.0
15.5	18.0	31.0	41.0
17.0	26.0	37.5	67.0
19.0	35.5	56.5	102.0
20.0	42.0	65.5	104.0
22.5	60.0	78.5	112.0

(i) Solids flow rate (g/s) through simple orifices of diameter equivalent to standpipe diameter D_t.

(ii) Solids flow rate through standpipe at zero separation (restricted flow).

(iii) Solids flow rate (g/s) through standpipe at 150 mm separation (free flow).

5.6 Expansion Chamber Programme - Comments and Conclusions

As shown in Chapter 4, a chamber interposed between the hopper orifice and the standpipe entrance was incorporated into the main apparatus and, since it was considered inappropriate to test its effect on the solids flow on that apparatus, this supplementary experimental programme was carried out. It must be noted, however, that this small apparatus had some deficiencies; in particular, that the slide valve was not completely air-tight, and consequently the standpipe was not able to develop its full influence on the solids flow. Nevertheless, a pressure tapping incorporated in the chamber showed a reduction in pressure below the orifice and the standpipes increased the solids mass flow rates significantly in all cases (Table 5.5). Visual observations of the solids streams in the standpipes showed that core flow of solids was not so evident as in the later work with sands in the large scale apparatus (Chapter 6.8), although the sodium perborate showed a tendency to form a core with larger mass flow rates. The small orifices and standpipes relative to the particle size probably accounted for the lack of core flow with the mustard seed and nylon chips.

In general, visual observations made of the flow in the chamber were believed to be characteristic of this type of system, and hence applicable for sands in the large apparatus. This was subsequently confirmed by the change of regime from 'free flow' to 'restricted flow', shown in the runs with the large apparatus, and by the apparently similar conditions noted at the standpipe entrance (Chapter 6.8). In contrast, it may be noted that the use of orifice-standpipe diameter ratios in the explanation of the small apparatus results was largely a matter of convenience. Although found to have some meaning in connection with regimes of flow and the change-over point, the range of diameter ratio values associated with the change of flow regime for this apparatus was not expected to have generality, since the orifice separation was also clearly an important factor. The general conclusions drawn from the results of this small apparatus are as follows:

The addition of a standpipe to a hopper outlet always gave increased throughput compared to that for simple orifice flow. If the flow through the standpipe was initiated from the base of the standpipe, then there would invariably be 'restricted flow'. Hence, to obtain maximum flow rates, the controlling orifice should be placed between the hopper and the standpipe entrance; the easiest way to realise this was by the use of an expansion chamber.

Interposition of an expansion chamber introduced a further variable - the orifice separation. This programme elucidated the effect of the orifice separation and showed that the total effect on flow rate was a complex function of the separation and the orifice-pipe diameter ratio. It was to be expected that there would prove to be an orifice-limited flow region where flow depended on the size of the orifice, and that this would give way to a pipe-limited region when the orifice was large. The further reasonable expectations that the change-over would occur when the orifice and pipe diameters were equal, and that the pipe-limited region would exhibit the maximum solids flow rate, were shown to be incorrect.

For the large scale apparatus, it was concluded that the chamber length should be sufficient to allow free flow conditions for the majority of orifice/standpipe combinations, but the small apparatus work did not prove capable of giving an exact chamber specification. However, since the orifice and standpipe diameter ranges necessarily would consist of discrete values, it was considered that the actual chamber dimensions would not be critical. It was, therefore, decided to use as the chamber 0.230 internal diameter by 0.457 m long, since this was available in the Department. From the experience gained in the supplementary experimental programme on the small apparatus, and the previous work done in the Department (36), these dimensions seemed suitable. The results from the large apparatus confirmed the correctness of this conclusion.

CHAPTER 6

Results from Experimental Work and Discussion of Results

6.1 Introduction

The main part of the experimental work was carried out using the sand No. 60, with a further series of confirmatory runs using the sand No. 14/30. These two solids differed only in particle size, their absolute densities and average particle shape being virtually identical. In all, a total of 582 runs, including replications, were performed with the sand 60 and 97 runs with the sand 14/30. Each run at a given set of conditions was repeated three times to ensure accuracy and reproducibility, the logical order of experimentation based on increasing orifice diameter and standpipe length being randomised as much as possible. In the case of counter-current flow and stop-flow tests, more replications were performed, where necessary, due to difficulties of measurement in the presence of wildly fluctuating solids flow.

The results from each set of replications were averaged arithmetically and are presented in Appendix 6.

Three sets of experimental runs were performed using each solid. These consisted of:

1. the bulk of the experimental work. This was carried out using the standpipes and orifices to determine the air and solids flow rates induced by the presence of the standpipe. A large amount of experimental data during each run was collected in this section: the duration, the total air flows through the various parts of the apparatus, the mass of solids in the weigh hopper, the duration of the solids flow into the weigh hopper, the mass of solids isolated in the standpipe, the various pressures in the upper and lower hopper systems and, depending on the length, up to thirty-one pressure readings along the standpipe, the latter being recorded by photography.

2. the gravity flow rate of solids: used as a datum or fixed point with which to compare the solids flow rates obtained using the standpipes - the physical measurements here being only the mass of the solids sample and the duration of its collection.

3. the counter-current solids flow rates and the 'stop-flow' pressures. These were carried out to test previous work on the subject of air-assisted solids flow through orifices (49, 52). The mass of the solids sample, the duration of its collection and the pressures above and below the orifice were recorded.

An examination of the apparatus and the results from the experimental programme showed that each section could be considered independently and that a complete investigation into solids and air flow through the apparatus could be achieved by analysing each section independently, starting from the top feed hopper and progressing down to the exit of the standpipe.

The main aims of the experimental work were: to investigate the effect of the standpipe dimensions on the solids mass flow rate, and to construct a mathematical model of the flow of the solids and air through the standpipe: to investigate the influence of interstitial fluid pressure on the rate of flow of particulate solids through an orifice, and in doing so, to clarify the forms of correlation presented in the literature (Chapter 2). The comprehensive nature of the apparatus made possible subsidiary investigations into the voidage of a moving solids bed, the flow of air through a moving solids bed, and the conditions around the orifice.

The experimental results from this apparatus and the previous work (Chapter 5) indicated two distinct phases in the discharge of solids from an orifice followed by flow through a glass chamber and down a standpipe: a 'free flow' condition in which there was no solids hold-up in the glass chamber, and 'restricted flow' in which the solids flow rate through the orifice was greater than the standpipe could accommodate. In the latter case, the glass chamber filled up and the flow was controlled by the

entrance to the standpipe, whereas with the 'free flow' conditions the orifice was the controlling factor. Only the 'free flow' phase was considered in the main investigation, since only under these conditions could the air flows in the various sections of the apparatus be analysed fully, although comparisons between the solids flow rates for the two phases were made in certain cases (Table 6.7)

6.2 The Physical Characteristics of the Solids

The Particle Size Distribution

As mentioned above, the solids chosen were both sands. These were chosen because of their ready availability, mechanical strength, and reasonable cost. Both were free-flowing materials and, although they were considered to be a good approximation to many commercially used materials they had the disadvantage, from the experimental point of view, of not being monosize. The actual size distributions were typical of many naturally occurring solids, exhibiting the usual logarithmic-normal distribution (89). Figures 6.1 and 6.2 and Appendix 3 show that the size range was fairly narrow and that consequently a mean particle size could be used to characterise the solids.

Several mean particle diameters have been developed to represent various particular features, for example, the size of the particles with the mean weight or mean surface of the particles. Dallavalle (89) and others (90, 91, 92) have recommended the use of the surface-mean diameter (volume-surface mean diameter) when the determination of the specific surface of the particles was of prime importance.

On a mass basis, this was given as:

$$d_p = \frac{\Sigma_i W_i}{\Sigma_i \left(\frac{W_i}{d_i}\right)} \qquad (6.1)$$

where $d_i = \frac{d_{os} + d_{us}}{2}$, i.e. the arithmetic average of the oversize and

Fig.6.1 Particle size distribution.
Histogram plot.

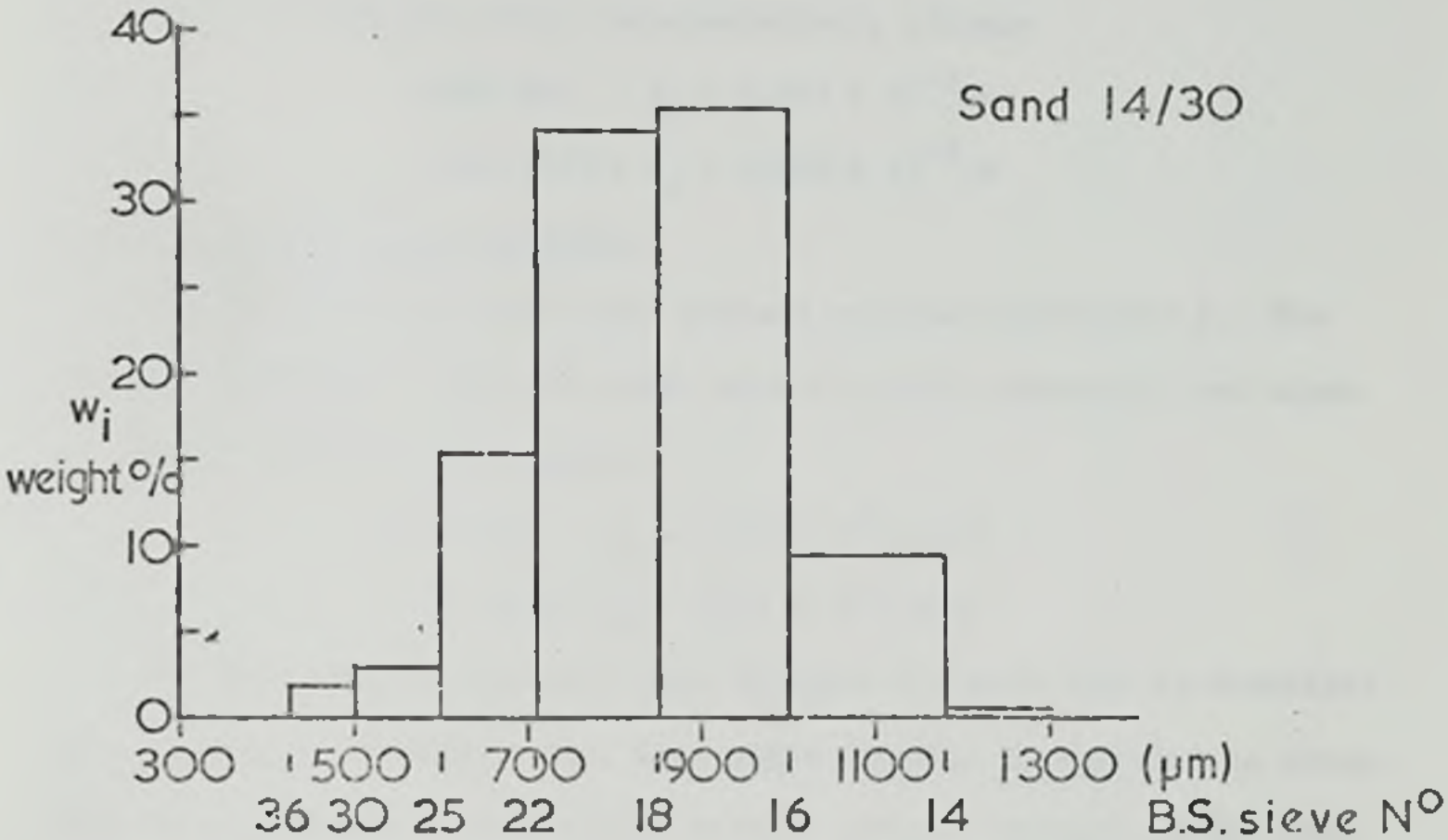

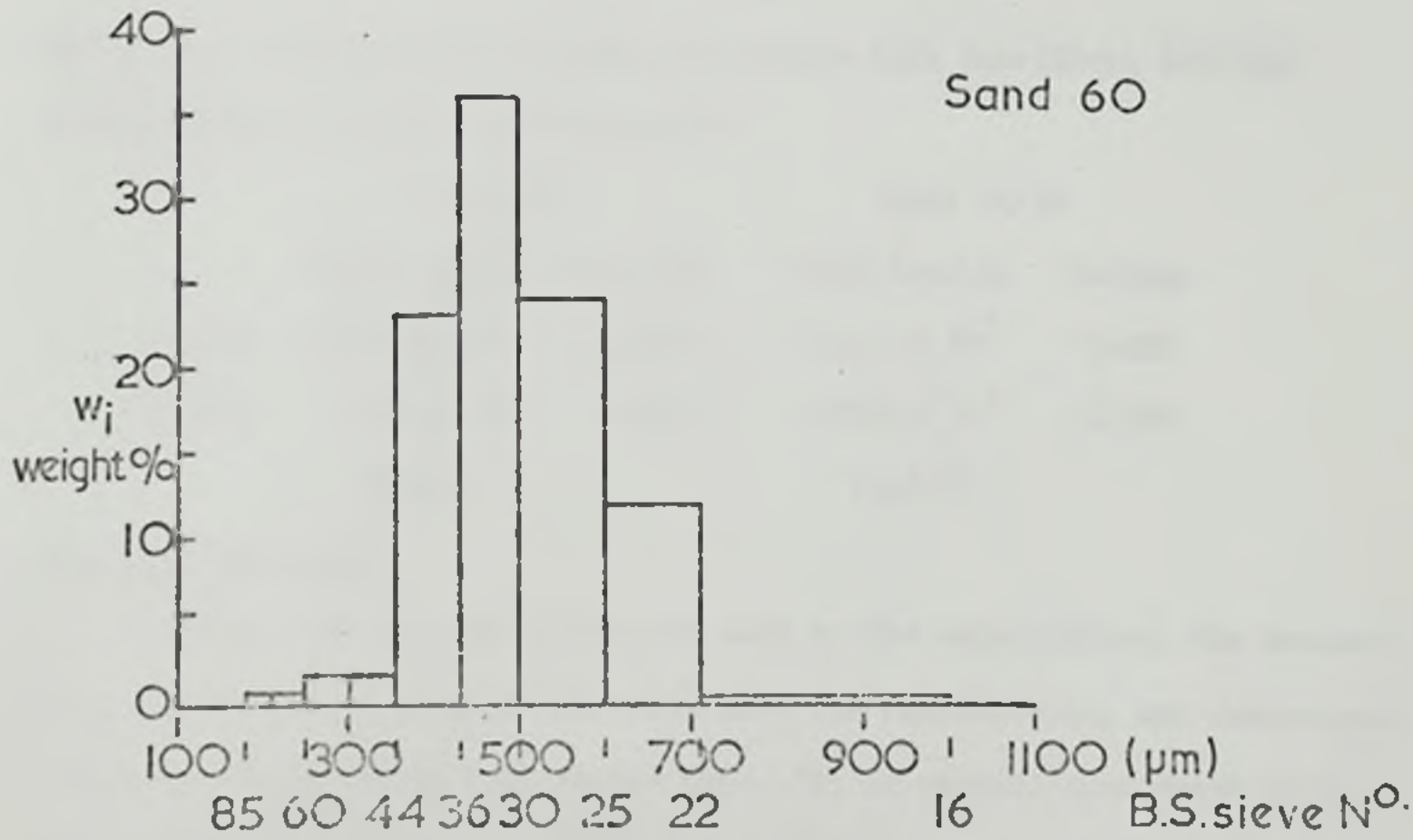

undersize sieve dimensions, and W_i = the mass fraction retained on the undersize sieve.

The values of the particle diameters for both sands were determined in accordance with the above recommendations, giving:

Sand 60: $d_p = 0.461 \times 10^{-3}$ m

Sand 14/30: $d_p = 0.806 \times 10^{-3}$ m

The Absolute and Bulk Densities

These were determined by the methods outlined in Chapter 4. The absolute densities of the two sands were virtually identical, and close to the average for silica sands:

Sand 60: $\varphi_s = 2.64 \times 10^3$ kg/m^3

Sand 14/30: $\varphi_s = 2.65 \times 10^3$ kg/m^3

Two values of bulk density were obtained for each sand as described above, covering the whole range that might normally be expected to occur. From the bulk density and absolute density values, voidages of the bulk solids were determined in each case.

$$e_B = 1 - \frac{\varphi_B}{\varphi_s} \qquad (6.2)$$

The values determined for minimum and maximum bulk densities, and the corresponding voidages are given below:

	Sand 60		Sand 14/30	
	Bulk density	Voidage	Bulk density	Voidage
Poured	1.588×10^3	0.399	1.517×10^3	0.428
Tapped	1.718×10^3	0.350	1.728×10^3	0.348
	(kg/m^3)		(kg/m^3)	

The Angle of Repose

Although this was not in the end used in the calculations, the drained angle of repose was measured for each sand for completeness, and comparison with other work. Evans (36) stated that, "it is usually considered that solids with an angle of repose less than 40° flow easily, whereas those with

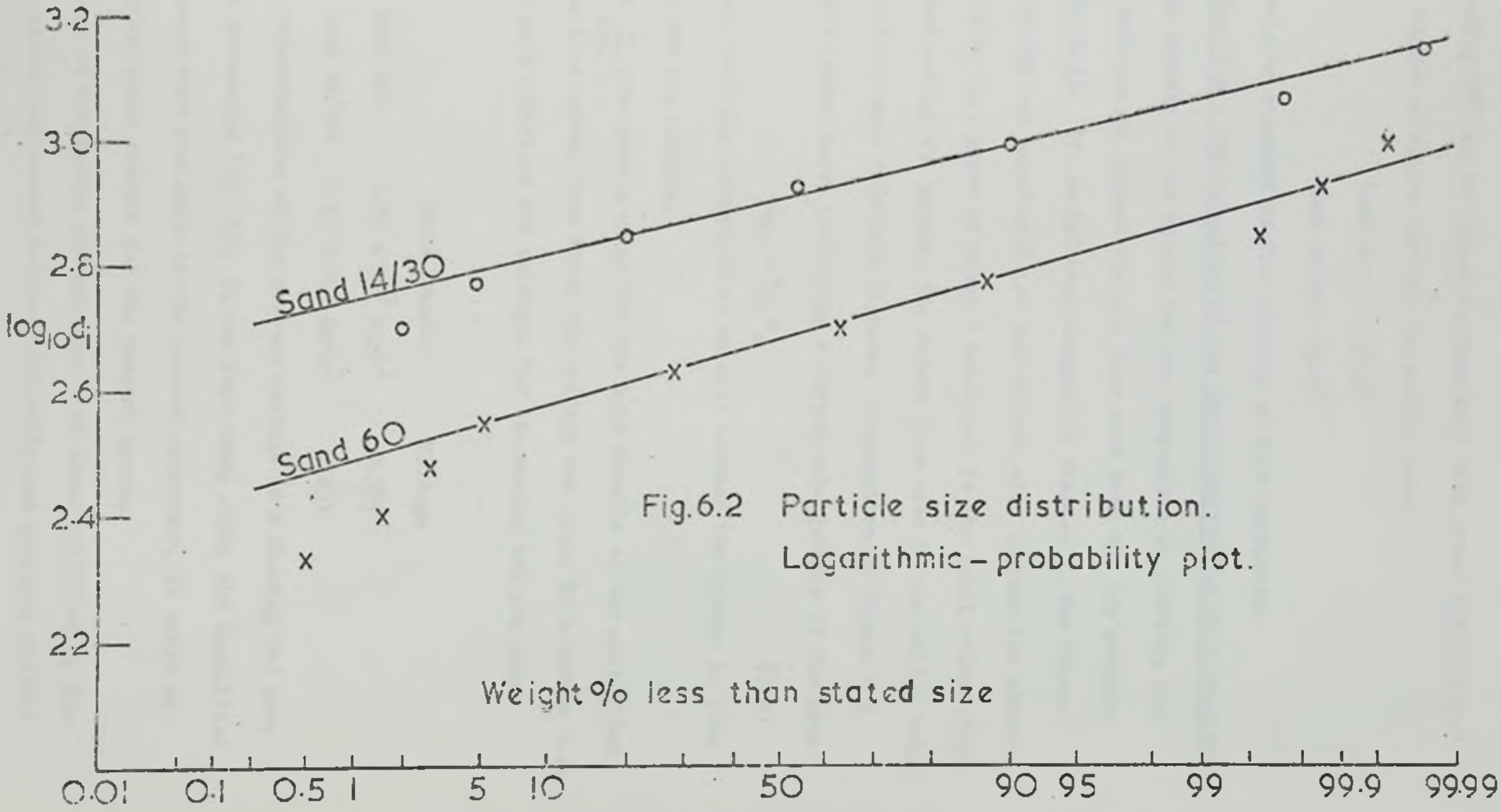

Fig.6.2 Particle size distribution.
Logarithmic – probability plot.

angles exceeding 50° can be caused to flow only with great difficulty."
The drained angles of repose for the two solids were:

Sand 60: 37.0°

Sand 14/30: 35.5°

Thus both would be regarded as free flowing on this criterion.

6.3 The Solids Feed Bed - Determination of the Moving Solids Bed Bulk Density

The bulk density of the moving bed was determined by plotting the solids flow rate out of against the air flow rate into the top storage hopper (Figure 6.3). If, as had been assumed in Chapter 3, the interstitial air in the bed moved with the bed without slip between the phases, then the air flow rate given by meter 1 was equal to the total volume flow rate of the bed out of the hopper, the volume flow rate of the solids being determined from the mass flow rate figures. Examination of Figure 6.3 showed a simple linear curve indicating a direct relationship of the type:

$$Q_{fb} = k_{fb} M_s \qquad (6.3)$$

which confirmed that the assumption of no slip between the phases in this moving solids bed was correct.

The term $\frac{1}{k_{fb}}$ thus gave a value for the bulk density of the moving bed for all solids flow rates, from which the voidage was given by equation 6.2. Values of the bulk densities and voidages for the moving bed are shown below:

	Bulk Density	Voidage
Sand 60:	1.59×10^3 kg/m^3	0.399
Sand 14/30:	1.51×10^3 kg/m^3	0.431

Although determinations of the average voidage in a flowing bed have been published previously (33, 93), it was felt that, since the facilities for the experiment were available in the present apparatus, it would be desirable to check these results for the present system.

A comparison of the moving bed voidages with those exhibited by the loosely packed static bed showed a close similarity and provided further

Fig.6·3 Feed hopper.

Sand 60 Air flowrate vs. solids mass flowrate.

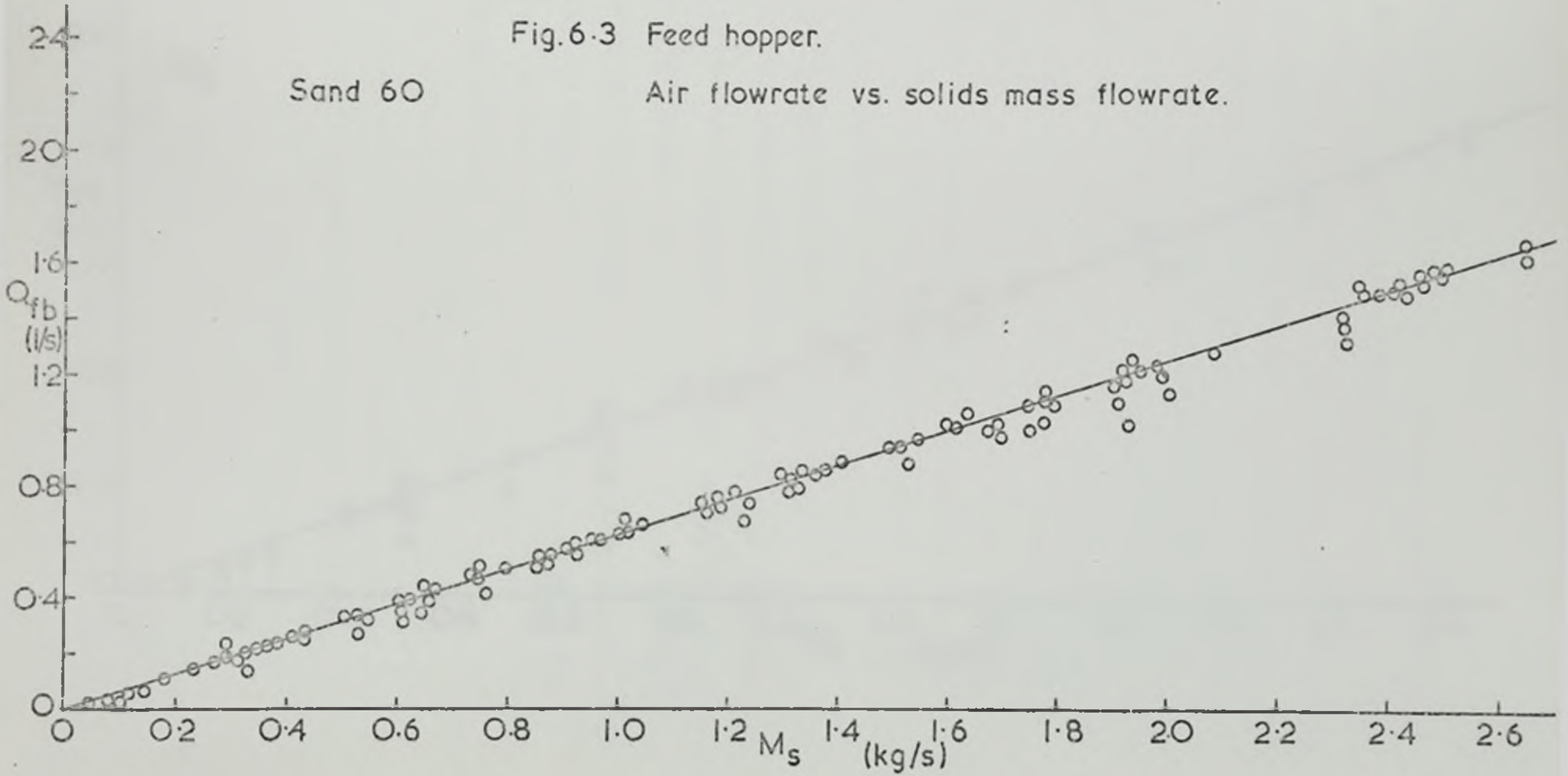

Fig.6.3 Feed hopper.

Sand 14/30 Air flowrate vs. solids mass flowrate.

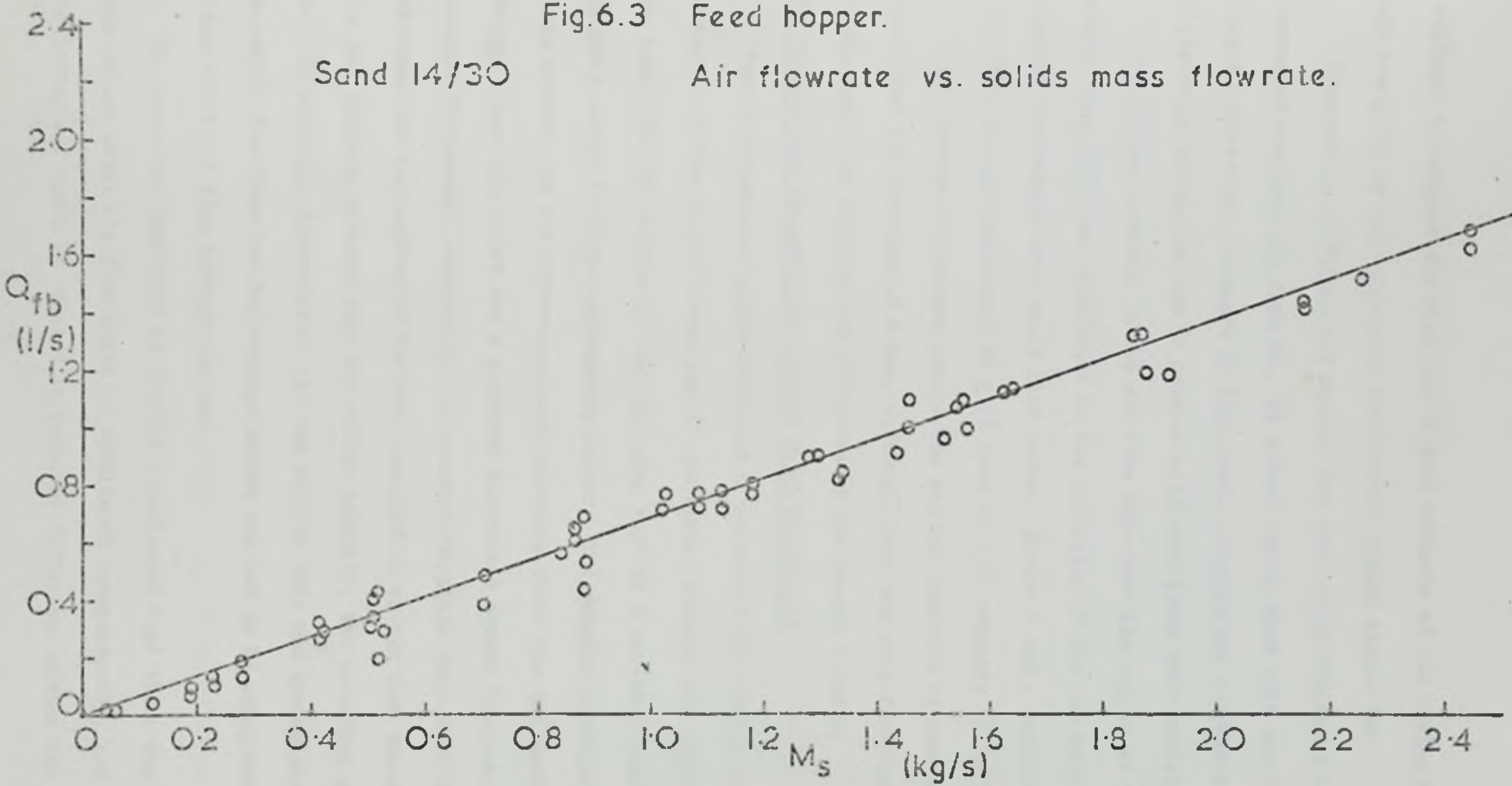

evidence to support the view that a good estimate of the moving bed voidage was given by the voidage of the loosest packed static bed.

Examination of Figure 6.3 showed that sand 14/30 exhibited a wider degree of scatter than sand 60. It seemed likely that this was due to the larger interstitial passages in this sand, allowing any transient pressure differences during the run to produce slip conditions more readily.

The slight decrease in the air flow rate into the hopper at very low solids flow rates was attributed to the inability of the gas meter to register accurately such small flow rates. (Meter 1 had a capacity of 1.57 l/s, and was guaranteed to ± 1% down to 1/20 capacity or 0.075 l/s).

The pressure difference across the bed was regarded as zero on average throughout the duration of a run, although there was some fluctuation due to the small but varying back pressures of gas meters 1 and 2.

6.4 The Flow of Air through the Constant Depth Moving Bed

The flat-bottomed bunker contained a constant depth moving solids bed: during a run the solids flowed out of the bunker through the orifice set in the base, the top surface of the bed being kept at a constant level by incoming solids from the top storage hopper. The reduced pressure in the glass chamber and the near-atmospheric pressure above the top surface of the bed meant that there was a pressure difference across the bed. This pressure difference, measured by the pressure tappings just above the orifice and above the top surface of the bed, resulted in an air flow through the bed at a net velocity greater than the solids velocity, the so called percolating air. In addition, interstitial air was carried into the system along with the solids flow from the top storage hopper and had to be considered as part of the total air flow through the bed.

The equations developed in Chapter 3 indicated that these two constituent parts of the total air flow could be considered independently, and that the percolating air could be related to pressure difference across the bed by

means of a Kozeny-Carman type equation:

$$Q_{ap} = \frac{1}{k''} \frac{e_B^3}{(1 - e_B)^2} \frac{A_B}{S^2} \frac{\Delta P_B}{\mu l_B} \qquad (6.4)$$

for $Re'_1 > 2.0$, where $Re'_1 = \frac{U'_a \varphi_a}{S(1 - e_B)}$ (6.4a)

assuming that the voidage in the bed remained constant for all solids and air flow rates. This has been shown to be the case for the flowing solids bed in the top storage hopper (Section 6.3) and consequently was also reasonably expected to be the case in the constant depth bed. Thus, for all solids and air flow rates, equation 6.4 could be reduced to:

$$Q_{ap} = k_B \Delta P_B \qquad (6.5)$$

where $$k_B = \frac{1}{k''} \frac{e_B^3}{(1 - e_B)^2} \frac{A_B}{S^2} \frac{1}{\mu l_B} \qquad (6.5a)$$

Graphs showing the percolating air flow rate plotted against the bed pressure drop are given in Figure 6.4 A line drawn with a slope of unit fitted the experimental data very well, confirming the form of equation 6.5.

The maximum values of the particle Reynolds' number in the bed were given by the maximum air flow rate through the bed. These were, from Figure 6.4:

Sand 60: Q_{ap} (max.) = 4.6×10^{-3} m^3/s

Sand 14/30: Q_{qp} (max.) = 3.8×10^{-3} m^3/s

The particle Reynolds' number in the bed was defined as:

$$Re'_1 = \frac{U'_a \varphi_a}{S(1 - e_B)\mu} \qquad (6.4a)$$

where U'_a was the superficial air velocity.

Thus, for the two sands, the maximum values of the Reynolds' number were:

Sand 60: $$Re'_1 = \frac{4.6 \times 10^{-3} \times 1.218}{0.164 \times 13.7 \times 10^3 \times 0.601 \times 17.8 \times 10^{-6}} = 0.233$$

Sand 14/30: $$Re'_1 = \frac{3.8 \times 10^{-3} \times 1.218}{0.164 \times 7.84 \times 10^3 \times 0.569 \times 17.8 \times 10^{-6}} = 0.355$$

Fig. 6.4 Percolating air flowrate vs. solids bed pressure drop Sand 60

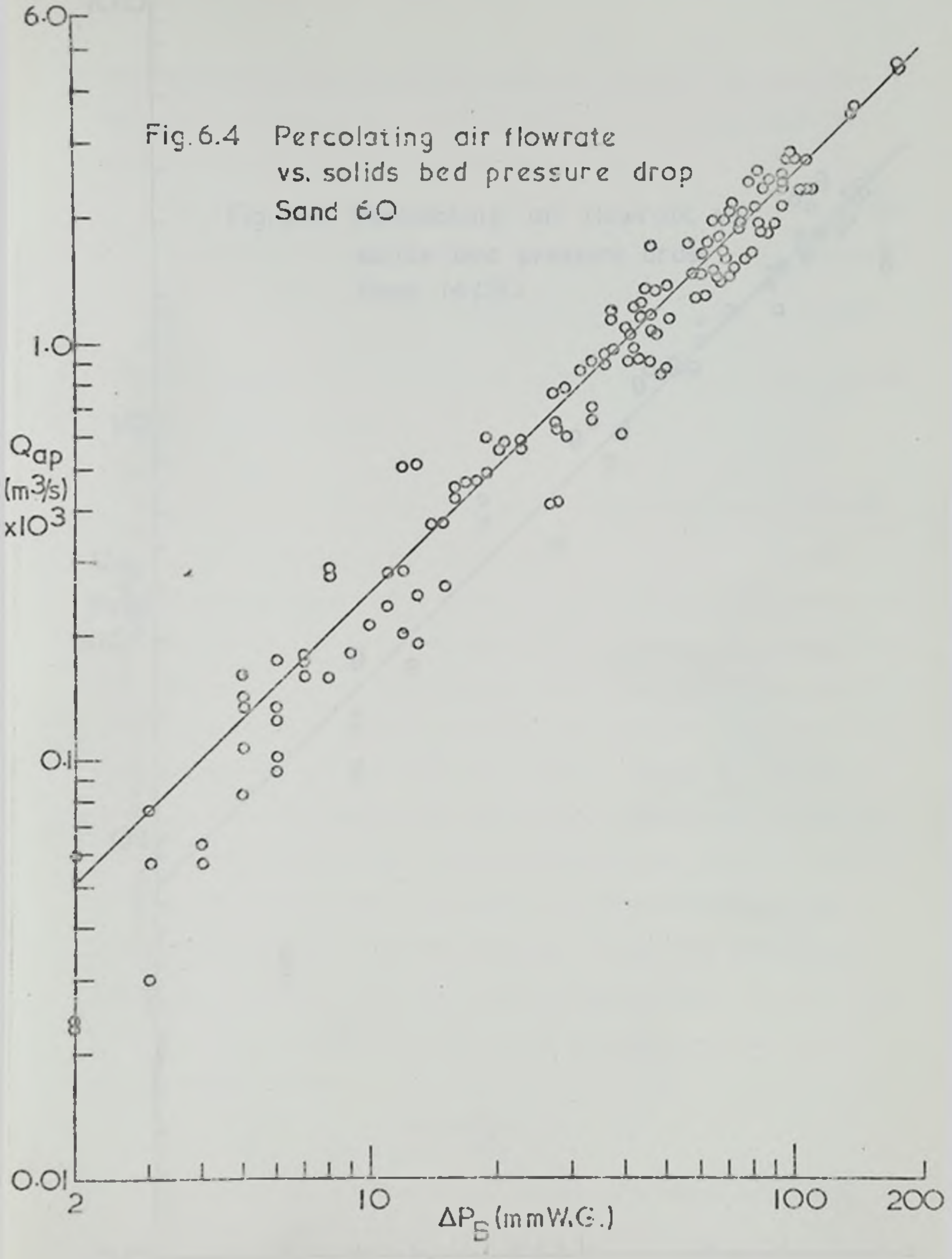

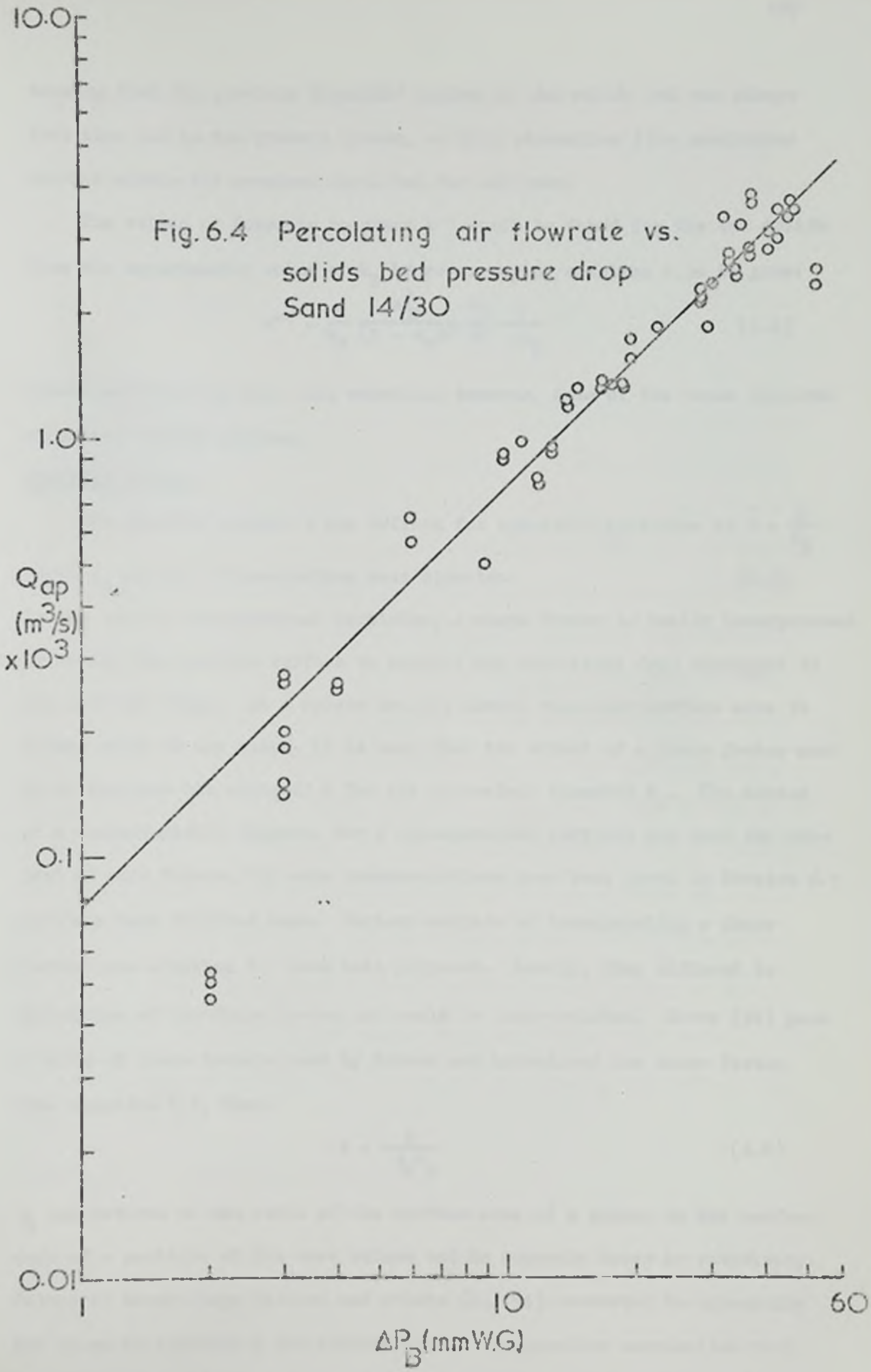

Fig. 6.4 Percolating air flowrate vs. solids bed pressure drop Sand 14/30

showing that the particle Reynolds' number in the solids bed was always less than 2.0 in the present system, so that streamline flow conditions existed within the constant depth bed for all runs.

The values of Kozeny's constant k'' could be found for the two solids from the experimental value of k_B by re-arranging equation 6.5a to give:

$$k'' = \frac{1}{k_B} \frac{e_B^3}{(1 - e_B)^2} \frac{A_B}{S^2} \frac{1}{\mu l_B} \qquad (6.6)$$

Before substitution into this equation, however, some of the terms involved warranted further mention.

Specific Surface

The specific surface S was defined for spherical particles as $S = \frac{6}{d_p}$ where d_p was the volume-surface mean diameter. (6.7)

In the case of non-spherical particles, a shape factor is usally incorporated to modify the specific surface to account for deviations from spherical in the particle shape. As a sphere has the lowest value for surface area to volume ratio of any shape, it is seen that the effect of a shape factor must be to increase the value of S for any equivalent diameter d_p. The choice of a characteristic diameter for a non-spherical particle has been the subject of much debate, but some recommendations have been noted in Section 6.1 and have been followed here. Various methods of incorporating a shape factor into equation 6.7 have been proposed. Mostly, they differed in definition of the shape factor and could be inter-related. Morse (92) gave a table of shape factors used by Carman and introduced the shape factor into equation 6.7, thus:

$$S = \frac{6}{\Phi_s d_p} \qquad (6.8)$$

Φ_s was defined as the ratio of the surface area of a sphere to the surface area of a particle of the same volume and is commonly known as sphericity. Values of these shape factors and others (43, 94) converted to sphericity are shown in Appendix 4 for various sands. Comparative examination with the photographs of the sands used by Morse (92) and Fair and Hatch (94)

suggested that a value of 0.95 would be reasonable as the shape factor for the present sands. The values of specific surface for both sands are given below using this value in equation 6.8:

$$\text{Sand 60} : S = \frac{6}{0.95 \times 0.461 \times 10^{-3}} = 13.700 \times 10^{3}\ m^{-1}$$

$$\text{Sand 14/30}: S = \frac{6}{0.95 \times 0.806 \times 10^{-3}} = 7.836 \times 10^{3}\ m^{-1}$$

Bed Height

The shape of the moving solids bed did not lend itself to a precise measurement of the bed depth. The incoming solids from the top storage hopper formed a conical section at the upper surface of the bed, while at the base of the bed the solids flowed in an inverted conical core towards the orifice, leaving static solids in the surrounding space between the bunker walls and that core. It was felt that a reasonable approximation of an upper level of the bed was a point half-way up the upper conical section. The depth of the bed was taken as the distance from this level to the orifice, the tapering of the moving bed at this level not being taken into account. This assumption was in accordance with those made in Chapter 3, i.e. that constant air and particle velocities and voidage existed throughout the bed. It was recognised that these assumptions were not strictly true with respect to the situation occurring at the orifice but, since there was a lack of detailed information on this topic, it was felt that adoption of these assumptions was justified for a first approximation to describe the whole bed. The representative depth of the bed was thus taken as 0.842 m.

Determination of Kozeny's Constant k''

The value of Kozeny's constant k'' was found by substitution for the terms in equation 6.6. The values of k_B for both sands were found from Figure 6.4. For air flow rate in m^3/s and bed pressure drop ΔP_B in mm H_2O, the values of k_B were:

Sand 60: $k_B = 25.24 \times 10^{-6}$ $(m^3/s)/(mm\ H_2O)$

Sand 14/30: $k_B = 76.0 \times 10^{-6}$ $(m^3/s)/(mm\ H_2O)$

Substitution of these figures and the values for the remaining variables (Appendix 5) in equation 6.6 gave, for sand 60:

$$k'' = \frac{1}{25.24 \times 10^{-6}} \frac{0.399^2}{0.601^2} \frac{0.164}{(13.7 \times 10^3)^2} \frac{9.8067}{17.8 \times 10^{-6} \times 0.842} = 4.0$$

and similarly for 14/30, $k'' = 5.7$.

These two values for k'', although not identical, compared well with those available in the literature for static beds. For example, Bird, Stewart and Lightfoot (95) recommended a value of 4.2 for k'', and whereas Coulson and Richardson (96) said that a value of 5.0 was a more likely value, they also presented values for various particle shapes ranging from 3.5 to 5.5. It was not possible to draw any definite conclusions on the values of k'' determined in the present work, except to say that the results obtained supported the view that the Kozery-Carman equation was suitable to describe the flow of air percolating through a moving solids bed.

Examination of equation 6.6 showed that the value of the Kozony constant was dependent on several variables for which only estimated values were available. These were: the particle specific surface, the solids bed depth, the bed voidage and the factor k_B; errors may have been present in the determination of any or all of these components. Due to the presence of a size distribution of the solids, the non-spherical shape of the particles, and the approximation inherent in the use of a shape factor, the determination of the specific surface was especially prone to error and, moreover, its inclusion in equation 6.6 as a squared term would have magnified any such errors present. Further errors may have been introduced by the values of the bed depth adopted and by the assumptions of constant velocities and voidage throughout the bed. Moreover, k_B and the voidage e_B were average values determined from graphs (Figures 6.3 and 6.4) exhibiting some degree of scatter.

Further consideration of the values of the Kozeny constant obtained in the light of the possible errors present only confirmed the suitability of the use of the Kozeny-Carman equation for the present system.

Examination of the graphs of Figure 6.4 showed that the experimental points at low air flow rates and bed pressure drops fell away from the 'best fit' lines. This was attributed to errors in the gas meter readings at such low values, as already noted in Section 6.3, and to the errors inherent in reading low air pressures subject to some oscillation.

The Total Air Flow Rate

Equation 3.9 indicated that the total air flow rate through the constant depth bed was given by the sum of the interstitial air flow rate and the percolating air flow rate. The total air flow rate was found experimentally from the sum of the air flow rate through meter 1 (Q_{ai}) and that through meter 2 (Q_{ap}) minus the solids volume flow rate, i.e.

$$Q_{at} = Q_{ai} - \frac{M_s}{\varphi_s} + Q_{ap} \qquad (6.9)$$

interstitial percolating.

In Section 6.3, it was found that $Q_{ai} = \frac{M_s}{\varphi_s}$ (6.10)

so: $$Q_{ai} - \frac{M_s}{\varphi_s} = M_s \left(\frac{1}{\varphi_B} - \frac{1}{\varphi_s}\right) = \frac{M_s}{\varphi_s}\left(1 - \frac{\varphi_B}{\varphi_s}\right) \qquad (6.11)$$

Equation 6.2 showed that $e_B = 1 - \frac{\varphi_B}{\varphi_s}$

which could be re-arranged to $\varphi_B = \varphi_s (1 - e_B)$.

Substitution for φ_B and $(1 - \frac{\varphi_B}{\varphi_s})$ into equation 6.11 revealed:

$$Q_{ai} - \frac{M_s}{\varphi_s} = \frac{M_s}{\varphi_s} \frac{e_B}{(1 - e_B)} \qquad (6.12)$$

Previously in this section it was shown that $Q_{ap} = k_B \Delta P_B$ (equation 6.5).

The combination of equations 6.12 and 6.5 gave the total air flow rate:

$$Q_{at} = \frac{M_s}{\varphi_s} \frac{e_B}{(1 - e_B)} + k_B \Delta P_B \qquad (6.13)$$

identical to equation 3.9 developed in Chapter 3.

Fig.6.5 Total air flowrate.
Experimental values vs.
theoretical values
Sand 60

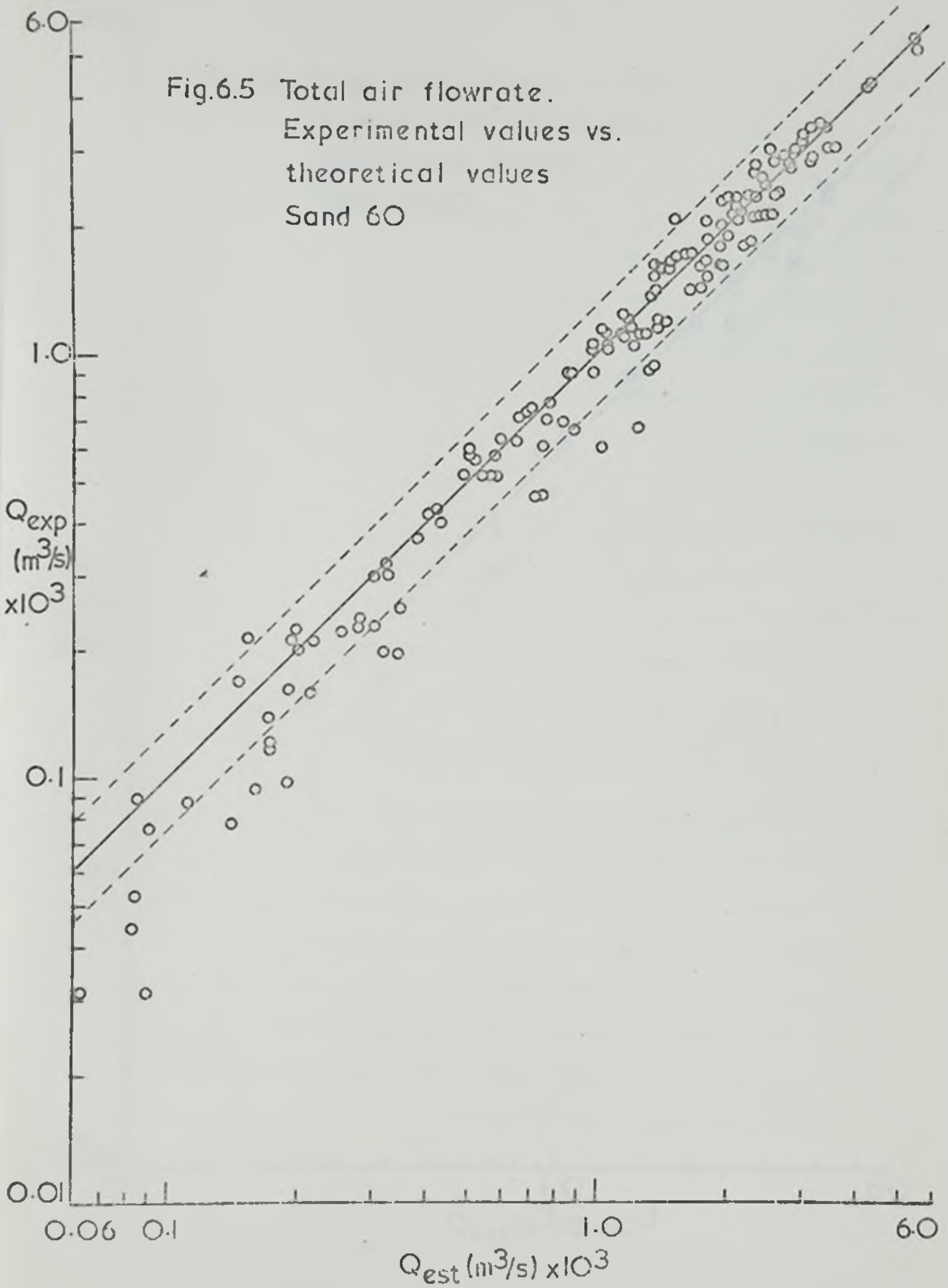

Fig.6.5 Total air flowrate
Experimental values vs.
theoretical values
Sand 14/30

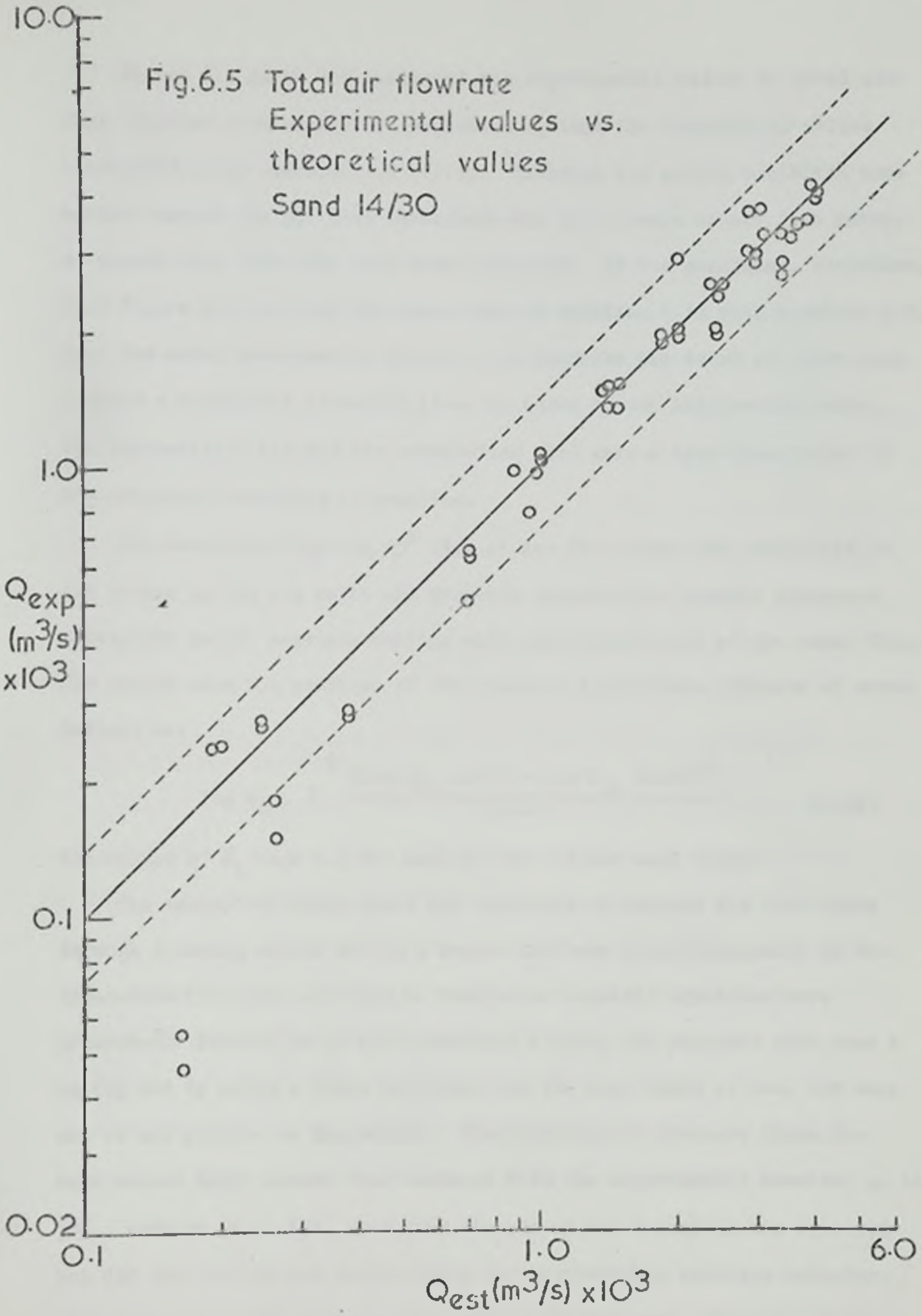

Figure 6.5 shows the graphs of the experimental values of total air from computed from equation 6.9 plotted against the theoretical values calculated using equation 3.9 (6.13). Although the graphs exhibited some scatter around the 45° line throughout the whole range of air flow rates, no trends away from this line were perceived. It was concluded, therefore, from Figure 6.5 and from the comparison of equation 6.13 with equation 3.9, that the model developed in Chapter 3 to describe the total air flow rate through a moving bed of solids (i.e. in terms of two independent parts, the interstitial air and the percolating air) gave a true description of the situation occurring in practice.

The deviation from the 45° line at low flow rates was attributed to the errors in the gas meter and pressure measurements already discussed previously in the sections dealing with each constituent of the total flow. The graphs show the position of the standard logarithmic estimate of error defined as:

$$\log S_L = \sum^{N} \frac{(\log Q_{at}\ (est) - \log Q_{at}\ (exp))^2}{(N - 2)} \qquad (6.14)$$

The values of S_L were 1.3 for sand 60 and 1.4 for sand 14/30.

The concept of using fixed bed equations to measure air flow rates through a moving solids bed in a hopper had been noted previously in the literature (50, 51), although no results or explicit equations were presented. Bulgara et al (50) mentioned finding the pressure drop over a moving bed by using a fixed bed model for the same depth of bed, but were not at all precise on the method. Their calculated pressure drops for sand showed large errors when compared with the experimental results; up to 58%. Resnick et al (51) mentioned the use of the Kozeny-Carman equation but did not mention any modification for particle/air relative velocity: they showed that the pressure drop across the bed was a function of bed height at constant air flow rate, and that the solids discharge rate was independent of the bed depth at any given air flow rate: this confirmed

the original findings of Kuwai (49) who, similarly, had not attempted any further correlation. Miles et al (46), in their analysis of the fluid drag effects on normal gravity discharge, suggested modelling the situation at the orifice by using a simple Darcy's Law equation modified to account for particle-air relative velocity. Thus, although the concept of using a fixed bed equation to describe the flow of air through moving solids beds had been noted previously, no specific results or full correlations had been presented, especially for solids flowing through a hopper. It was recognised that data and a correlation had been published for fluid flow through moving solids beds (93) in large tubes, but it was felt that the use of the better known Kozeny-Carman equation in the present study was likely to be more useful in practical engineering applications: and further, the observation that the total flow rate could be considered as two separate air flows was felt to be particularly useful.

6.5 The Flow of Granular Solids through the Hopper Orifice under the Influence of a Co-current Air Stream

The particulate solids flow through the orifice under the influence of a co-current air stream (more conveniently referred to as pressurised solids flow) was, in the present apparatus, due to the reduced air pressure in the chamber caused by the flow of the solids down the standpipe. The system under consideration consisted of an orifice set into the base of a flat-bottomed bunker containing a constant depth bed. During a run, the solids discharged from this bunker through the orifice. As noted in the previous section, there was an air pressure difference between the top level of the bed and the glass chamber below the orifice. This pressure difference was considered as the sum of two parts, that across the orifice and that across the bed, the orifice pressure drop being measured by tappings placed in the chamber (P_4) and just above the orifice (P_3). The pressure difference across the orifice and the constant level bed resulted in a co-current air flow through the bed and orifice, in addition to the interstitial air flow normally associated with a flowing solids bed.

Fig.6.6 Solids mass flowrate vs. orifice pressure drop
Sand 60

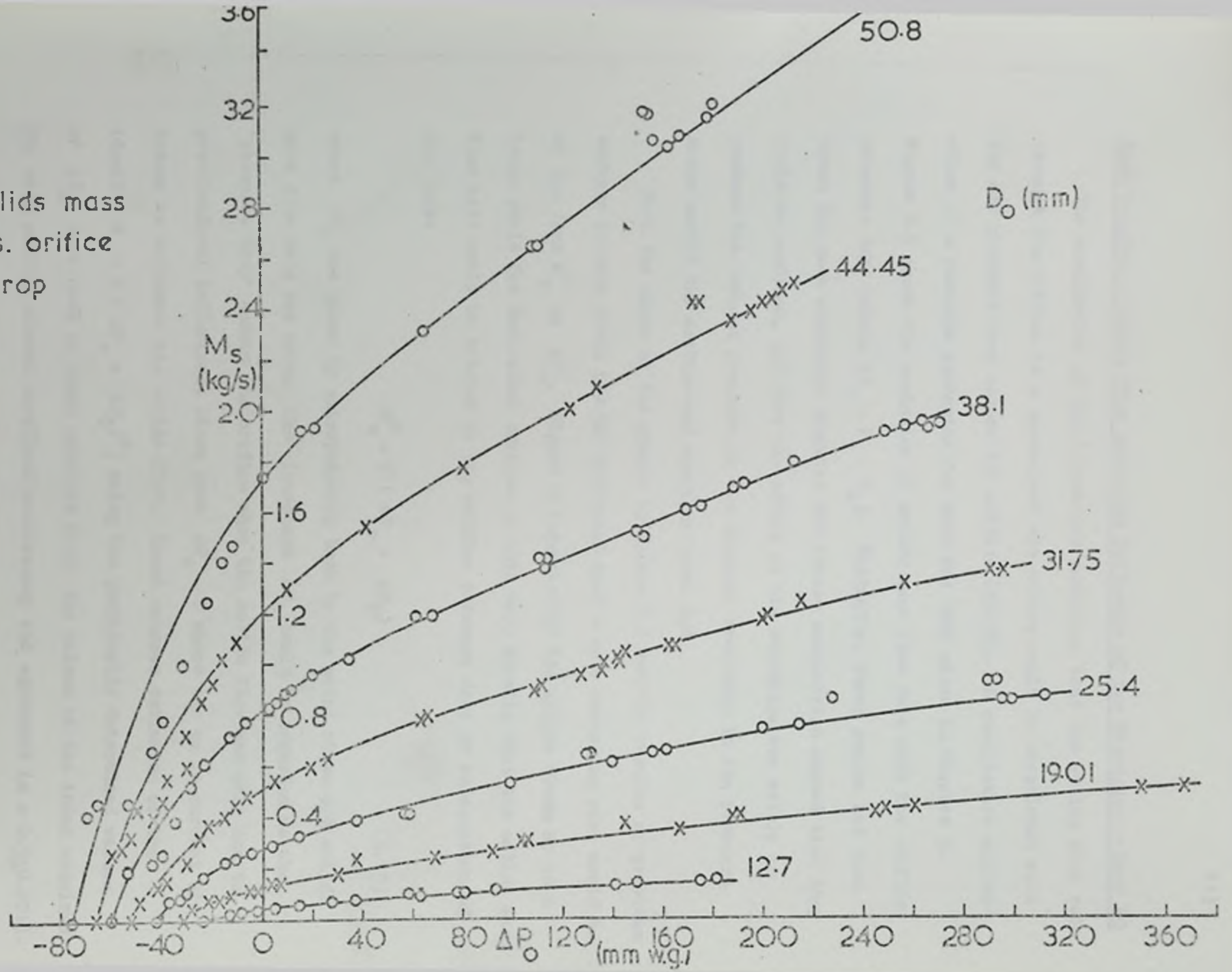

Main Results - Solids Flow under the Influence of the Standpipe - Sand 60

The examination of the literature indicated that the solids flow rate through the orifice in a co-current air stream could be correlated with the air pressure drop across the orifice (49-52). A qualitative explanation of a possible mechanism for this has been given in Chapter 3. Figure 6.6 shows the variation of solids mass flow rate with the orifice pressure drop (where $\Delta P_o = P_3 - P_4$). Initially, these graphs had been drawn for each standpipe diameter but closer examination showed that they could be combined, and that the effect of the standpipe was solely to produce the reduced pressure in the chamber, resulting in the pressure drops across the orifice and constant level bed.

Both the shape of the graphs in Figure 6.6 and the results of previous workers in this field (49-52) indicated that a more revealing plot would be of the form M_s^2 vs ΔP_o. Figure 6.7 summarises the graphs drawn up on a large scale for individual orifice in this way, showing that the solids mass flow rate could be related to the orifice pressure drop by an equation of the form:

$$M_s^2 = C (\Delta P_o + \Delta P_C) \qquad (6.15)$$

where ΔP_C was given by extrapolating back to the point where the solids mass flow rate was zero. The intercept ΔP_C could be regarded as the 'pressure drop' across the orifice when the solids flow was only due to gravitational influences, since when $\Delta P_o = 0$ where was no co-current air stream to influence the solids flow. Least squares estimates of the identity $M_s = C (\Delta P_o + \Delta P_C)^n$, using the graphically determined values of ΔP_C, were used to check equation 6.15: the values of the index obtained for each orifice showed excellent consistency and agreement ($n = 0.5 \pm 0.001$).

According to the method of development, in Chapter 3, of equations to describe the pressurised flow of solids from a hopper, the total solids flow rate could be considered as composed of two constituent parts: that due to gravitational influence, and that due to co-current air flow. The form of

Fig.6·7 Solids mass flowrate squared vs. orifice pressure drop Sand 60

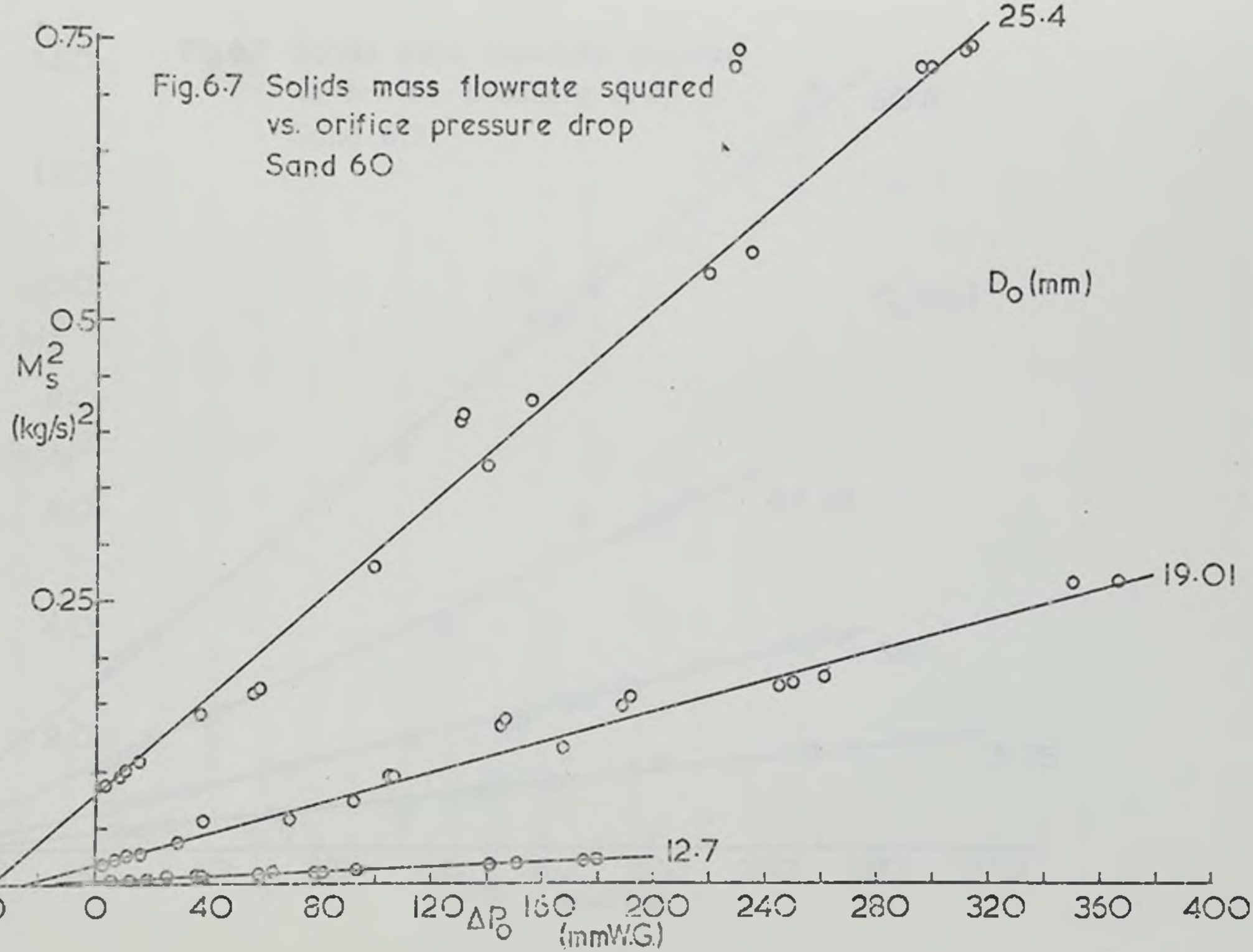

Fig.6.7 Solids mass flowrate squared vs. orifice pressure drop Sand 60

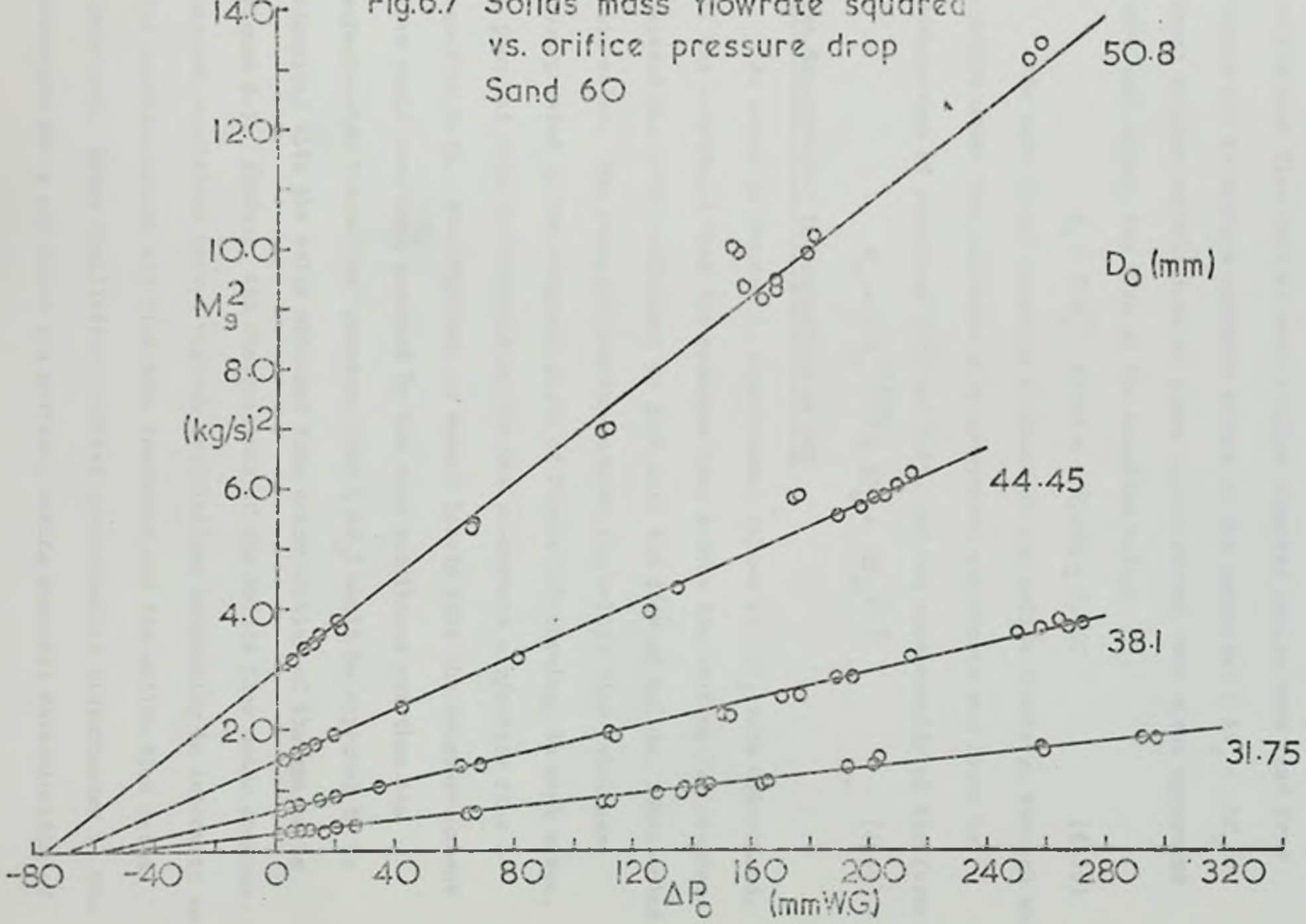

equation 6.15 seemed to support this view, the total solids flow being dependent on the sum of two separate terms; ΔP_o for the pressurised flow and ΔP_C for the gravity flow term.

Figure 6.8 shows the correlation of the solids mass flow rate against the orifice diameter (the fixed parameter in Figure 6.7), the values of solids mass flow rate at each orifice diameter having been read from Figure 6.7 at various constant values of the parameter ($\Delta P_o + \Delta P_C$). Least squares correlations of these points showed very close agreement with each other, the form of the equation being:

$$M_s = C\, D_o^m \quad \text{where } m = 2.095 \pm 0.002 \qquad (6.16)$$

The form of the equation to describe the solids discharge through an orifice under the influence of a co-current air stream was found by combination of equations 6.14 and 6.15, and was consequently of the form:

$$M_s = C\, D_o^{2.095} (\Delta P_o + \Delta P_C)^{0.5} \qquad (6.17)$$

The Experimental Determination of ΔP_C

As noted in Chapter 4, experimental values of ΔP_C were determined. It was considered that the pressure drop across the orifice for counter-current air flow, sufficient to just halt the flow of solids, represented this value. The observed counter-current air/solids flow rates were incorporated in the original plots of Figure 6.7 showing, in most cases, a poor fit with the correlation for the co-current air/solids flow - equation 6.15. Nevertheless, it seemed likely that the counter-current flow would have been governed by the same conditions and thus the experimental 'stop-flow' pressure drop (ΔP_C) would be expected to be identical with the value obtained from extrapolation of the graphs in Figure 6.7. However, the observations of the solids flow under counter-current conditions showed violent oscillations increasing in intensity as the counter-current air flow rate increased and the solids flow rates decreased. These oscillations created corresponding disturbances in the pressures above and below the orifice, making accurate determination of

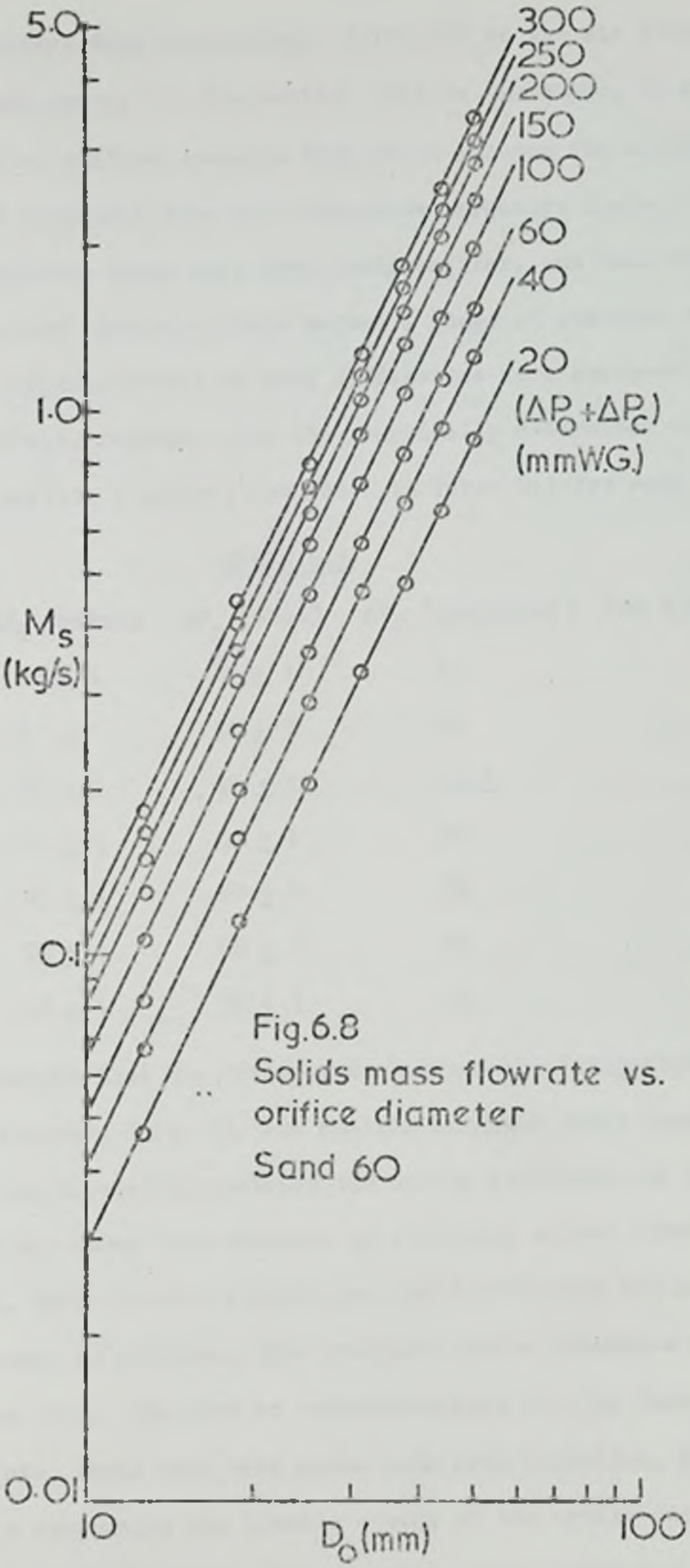

Fig.6.8
Solids mass flowrate vs. orifice diameter
Sand 60

the orifice pressure drop increasingly difficult as the air flow rate increased. Furthermore, for the smaller orifice diameters, it was found that the values of orifice pressure drop which allowed the solids flow to restart were different from the 'stop-flow' pressure drops. These 'start-flow' pressure drops were invariably smaller, and thus together with the 'stop-flow' pressure drops marked a range of possible values for ΔP_C; for the larger orifices no such differences were observed. These experimental values, together with the graphically determined values of ΔP_C for each orifice diameter, are shown in Table 6.1 for sand 60.

TABLE 6.1

D_o(mm)	ΔP_C (start)	ΔP_C (stop)	ΔP_C (graphical) ($mm\ H_2O$)
12.7	20 ± 1	24 ± 1	17
19.01	31 ± 1	36 ± 1	24
25.4	39 ± 1	42 ± 1	36.5
31.75	51 ± 1	53 ± 1	48
38.1	60 ± 1	60 ± 2	59
44.45	66 ± 1	66 ± 1	68
50.8	76 ± 1	76 ± 1	76

It was thought that the differences between the 'stop-flow' and the 'start-flow' pressure drops for the smaller orifices could possibly have been explained by the interaction between the solids particles and the small orifices. It was known that unstable or free-fall arches existed above an orifice which, under certain conditions, could stabilise and halt the solids flow; and, in addition, that smaller orifice diameters facilitated this formation (75). The flow of counter-current air, by decreasing the solids flow rate, could only have aided such arch formation, the air flow rate initially overcoming the kinetic energy of the moving particles and then when the solids flow rate was reduced to zero, balancing the weight of the particles at the orifice. An unstable or partial arch at the

orifice would clearly have supported the weight of the solids to some extent as well, thus reducing the air flow rate (and orifice pressure drop) needed to support the solids. Moreover, in the case of the larger orifices, where arch formation would have been less likely, the values of the two orifice pressure drops were identical. It was also considered likely that the violent oscillations in solids flow were due to the formation and disruption of short-lived stable arches above the orifice which, as the orifice pressure drop increased, tended to become stable for longer periods until at the critical pressure drop they stabilised fully. It was, therefore, decided to use the graphically determined values for all orifice sizes.

As has already been noted, these two methods for finding a suitable value of 'stop-flow' orifice pressure drop had been previously investigated separately: Kuwai (49) used the extrapolation method, while Knowles (52) investigated the experimental determination of ΔP_C. Neither of these workers determined ΔP_C by the other's method, and consequently there had been no direct comparison. Neither Kuwai nor Knowles had attempted to correlate the pseudo-pressure values: examination of the form of their equations for the discharge of solids through an orifice showed a possible reason for this. Thus:

$$M_s = D_o^{2.5} \left(\Delta P_o + \Delta P_C \right)^{0.5} \frac{\pi}{4} C \sqrt{2g \varphi_B} \qquad (3.16)$$

which, on re-arranging, showed up the two flow contributions:

$$M_s^2 = D_o^5 \, \Delta P_o \left(C \sqrt{2g \varphi_B} \frac{\pi}{4}\right)^2 + D_o^5 \, \Delta P_C \left(C \sqrt{2g \varphi_B} \frac{\pi}{4}\right)^2 \qquad (6.18)$$

pressure flow gravity flow

Comparison of this gravity flow term with that obtained from simple gravity flow investigations, i.e.

$$M_s^2 = D_o^5 \left(C \frac{\pi}{4} \varphi_B \sqrt{2g}\right)^2 \qquad (3.13)$$

implied that $\Delta P_C = \varphi_B$ which was dimensionally inconsistent. Thus the

Fig.6.9 'Pseudo-pressure' vs. orifice diameter

Sand 60

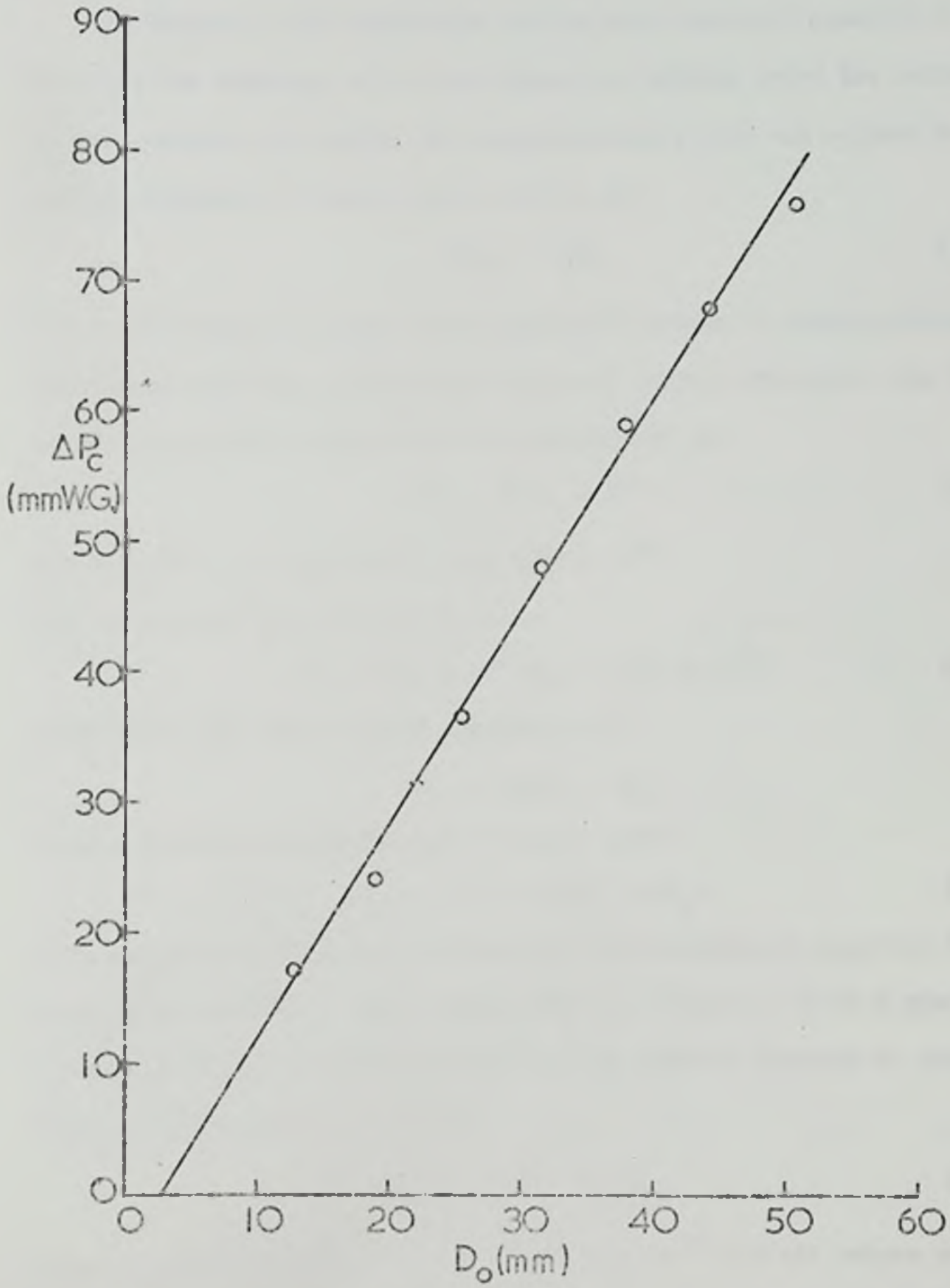

discharge coefficient C had been credited with the dimensions $L^{-\frac{1}{2}}$ which again was not consistent with the definitions of orifice coefficients used in fluid flow (97), a fact which would severely limit any attempt at correlation.

Correlation of ΔP_C

In Chapter 3, the derivation of the semi-empirical equation to describe the discharge of solids through an orifice under the influence of a co-current air stream, the pseudo-pressure term was related to the orifice diameter and solids bulk density by:

$$\Delta P_C = \varphi_B D_o \qquad (3.19a)$$

Figure 6.9 shows the graphically determined values of pseudo-pressure plotted against the corresponding value of orifice diameter. The form of the graph could conveniently be represented by:

$$\Delta P_C = \alpha(D_o - \beta) \qquad (6.19)$$

For sand 60 $\alpha = 1.63 \times 10^3$, $\beta = 2.87 \times 10^{-3}$

for ΔP_C in mm H_2O and D_o in m, i.e.

$$\Delta P_C = 1.63 \times 10^3 (D_o - 2.87 \times 10^{-3}) \qquad (6.20)$$

This was of the same form as equation 3.23:

$$\Delta P_C = \varphi_B(D_o - kd_p)$$

which, on substituting for bulk density, gave:

$$\Delta P_C = 1.59 \times 10^3(D_o - kd_p) \qquad (6.21)$$

This equation implied that the appropriate parameter in equation 6.17 should have been $(D_o - kd_p)$ rather than D_o. Figure 6.10 is a graph of (solids mass flow rate)$^{0.5}$ plotted against orifice diameter at constant $(\Delta P_o + \Delta P_C)$, showing the form:

$$\mu_s^{0.5} = C(D_o - kd_p) \qquad (6.22)$$

where kd_p lies between 1.0×10^{-3} and 1.5×10^{-3} for all values of $(\Delta P_o + \Delta P_C)$. Thus, for the experimental value $d_p = 0.461 \times 10^{-3}$ m, the value of k lies between 2.17 and 3.25. Least squares tests on the data

Fig. 6.10 (Solids mass flowrate)$^{0.5}$ vs. orifice diameter Sand 60

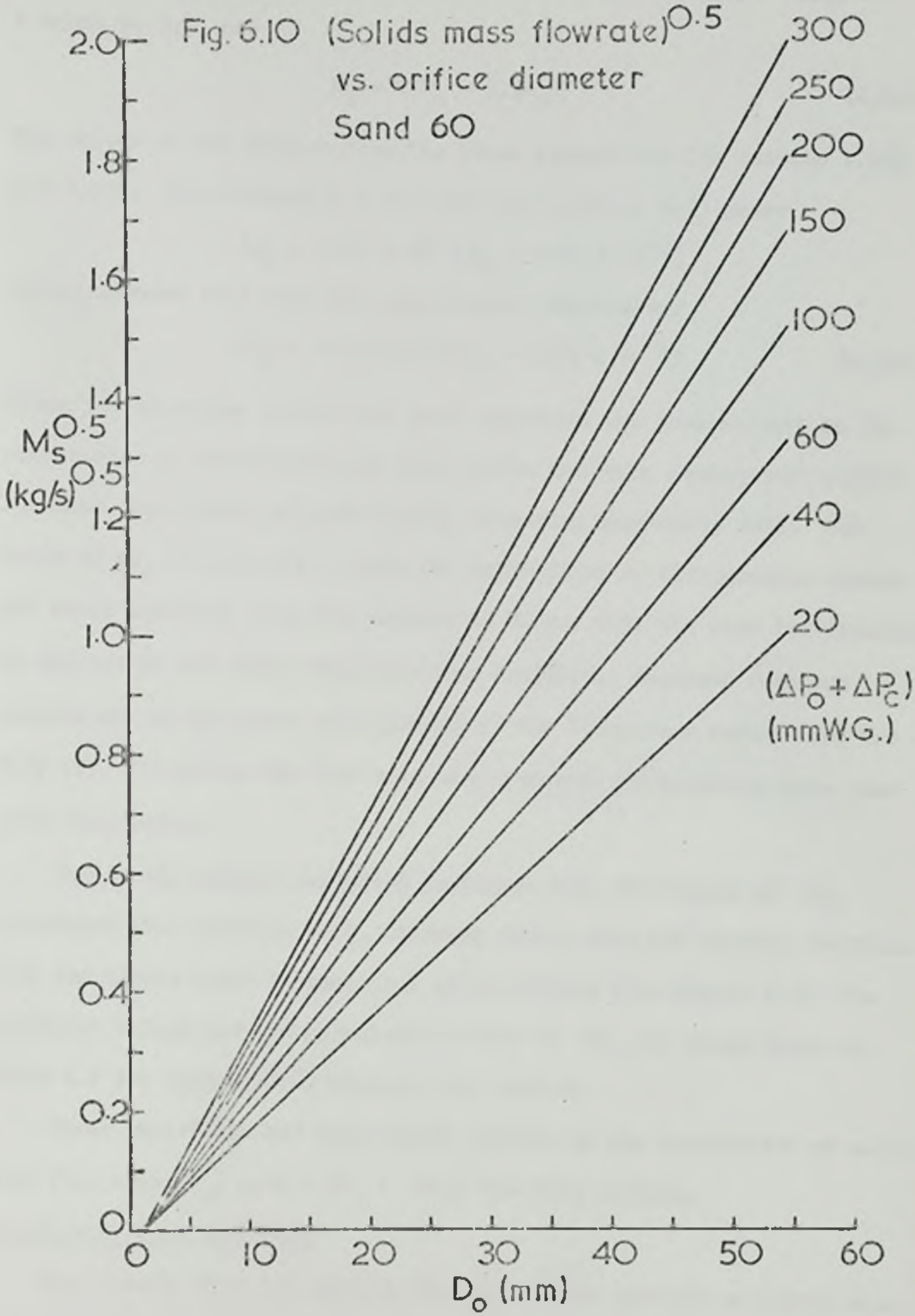

showed that the best fit for all orifices was given using a value of k equal to 2.5, or:

$$M_s = C(D_o - 2.5d_p)^n \qquad (6.23)$$

The values of the index n from the least squares fit lie between 1.993 and 1.995. Substituting k = 2.5 into the equation 6.21 gave:

$$\Delta P_c = 1.59 \times 10^3 \ (D_c - 1.15 \times 10^{-3})$$

which compared well with the experimental expression:

$$\Delta P_c = 1.63 \times 10^3 \ (D_o - 2.87 \times 10^{-3}) \qquad (6.20)$$

These two equations showed very good agreement and gave support to the correlation of pseudo-pressure with solids bed bulk density and orifice diameter, the values of bulk density comparing especially well. The value of kd_p did not fit so well but examination of the possible causes for error involved, i.e. the scatter in Figure 6.9, the size distribution of the solids and their characteristic dimension, together with the uncertainty in the value of k (values in the literature varied from 1.4 - 2.9) (19, 37) led to the view that the agreement achieved was here also quite favourable.

Due to the scatter exhibited in Figure 6.9, the values of ΔP_c calculated from equation 6.20, although close, were not exactly identical with the values found by graphical extrapolation from Figure 6.7. The graphical values and the calculated values of ΔP_c are given below in Table 6.2 for each orifice diameter for sand 60.

These variations had only slight effects on the correlation of solids mass flow rate (M_s) with (ΔP_o + ΔP_c) for each orifice.

The Gravity Flow of Solids

The results from the gravity flow tests were plotted as solids mass flow rate against orifice diameter and exhibited a relationship of the form:

$$M_s = C D_o^{2.61} \qquad (6.24)$$

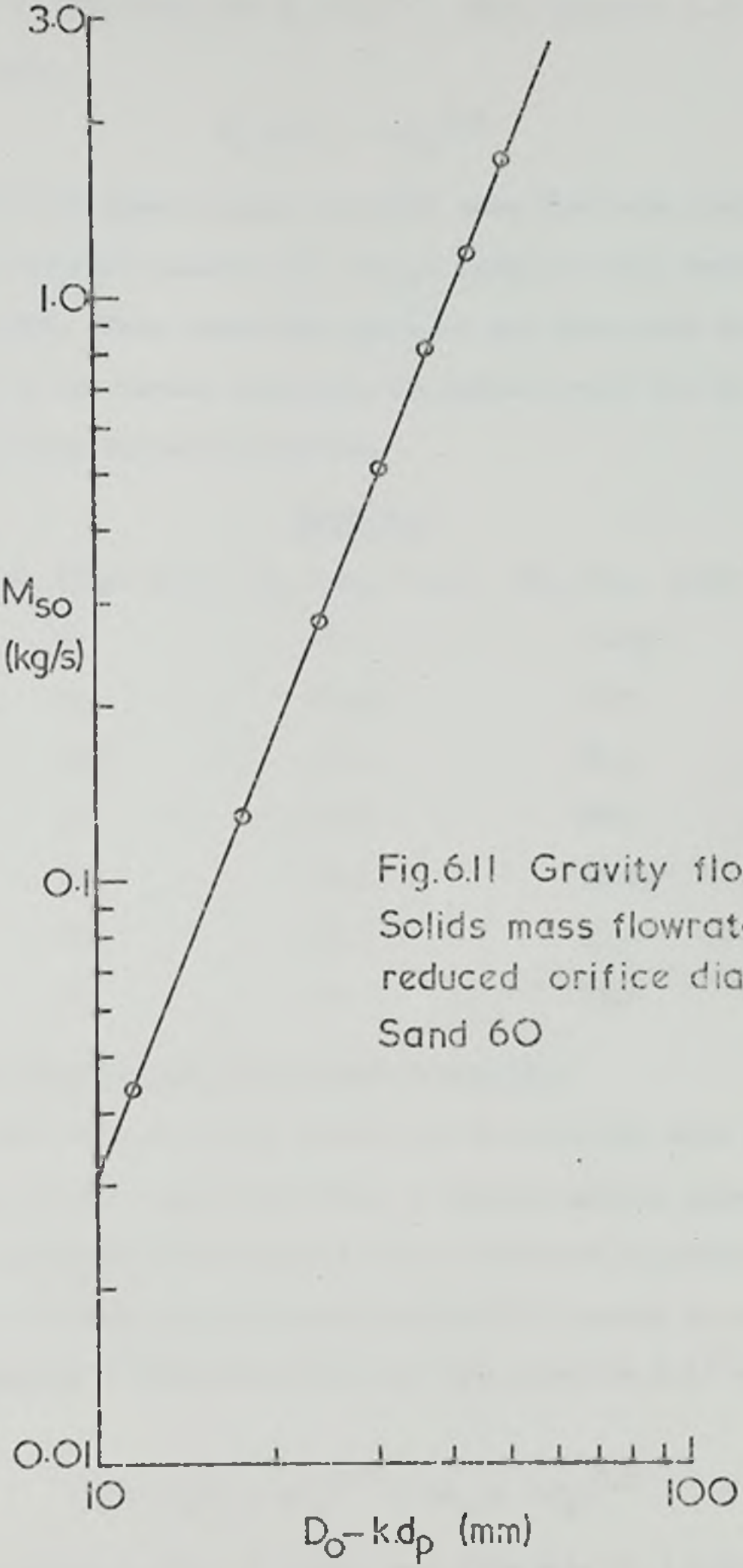

Fig.6.11 Gravity flow
Solids mass flowrate vs.
reduced orifice diameter
Sand 60

Equation 3.13 indicated that $M_s \propto D_o^{2.5}$, while equation 3.14 suggested the preferable:

$$M_s \propto (D_o - kd_p)^{2.5} \qquad (6.25)$$

Figure 6.11 shows a graph of solids mass flow rate plotted against the reduced orifice diameter $(D_o - kd_p)$, using k = 2.5, exhibiting a slope of 2.495. Thus, excellent agreement was given with the proposed equation 3.14 and further supported the overall model for the pressurised solids flow rate through an orifice.

TABLE 6.2

D_o (mm)	ΔP_c (Fig. 6.7)	ΔP_c (equ. 6.20)	ΔP_c (equ. 3.23) ($mm H_2O$)
12.7	17	16	18.25
19.01	24	26.25	28.5
25.4	36.5	36.5	38.5
31.75	48	47.0	48.5
38.1	59	57.25	58.75
44.45	68	67.5	69.0
50.8	76	78	79.0

The Overall Equation for Pressurised Solids Flow

It seemed from the above results and correlations that the use of the 'empty annulus' concept to define a reduced orifice diameter was a necessary empirical modification to the theoretical equations developed to describe the flow rate of pressurised solids through an orifice. Thus, on consideration of equations 6.23 and 6.25, equation 6.17 was modified to:

$$M_s = C_1(D_o - kd_p)^{2.0} (\Delta P_o + \Delta P_c)^{0.5} \qquad (6.26)$$

Figure 6.12 shows a graph of solids mass flow rate (M_s) plotted against $(D_o - 2.5\, d_p)^{2.0} (\Delta P_o + \Delta P_c)^{0.5}$. A least squares fit on the data showed that the constant from equation 6.26 was equal to 79.27, giving the full correlation:

Fig.6.12 Solids mass flowrate correlation
Sand 60

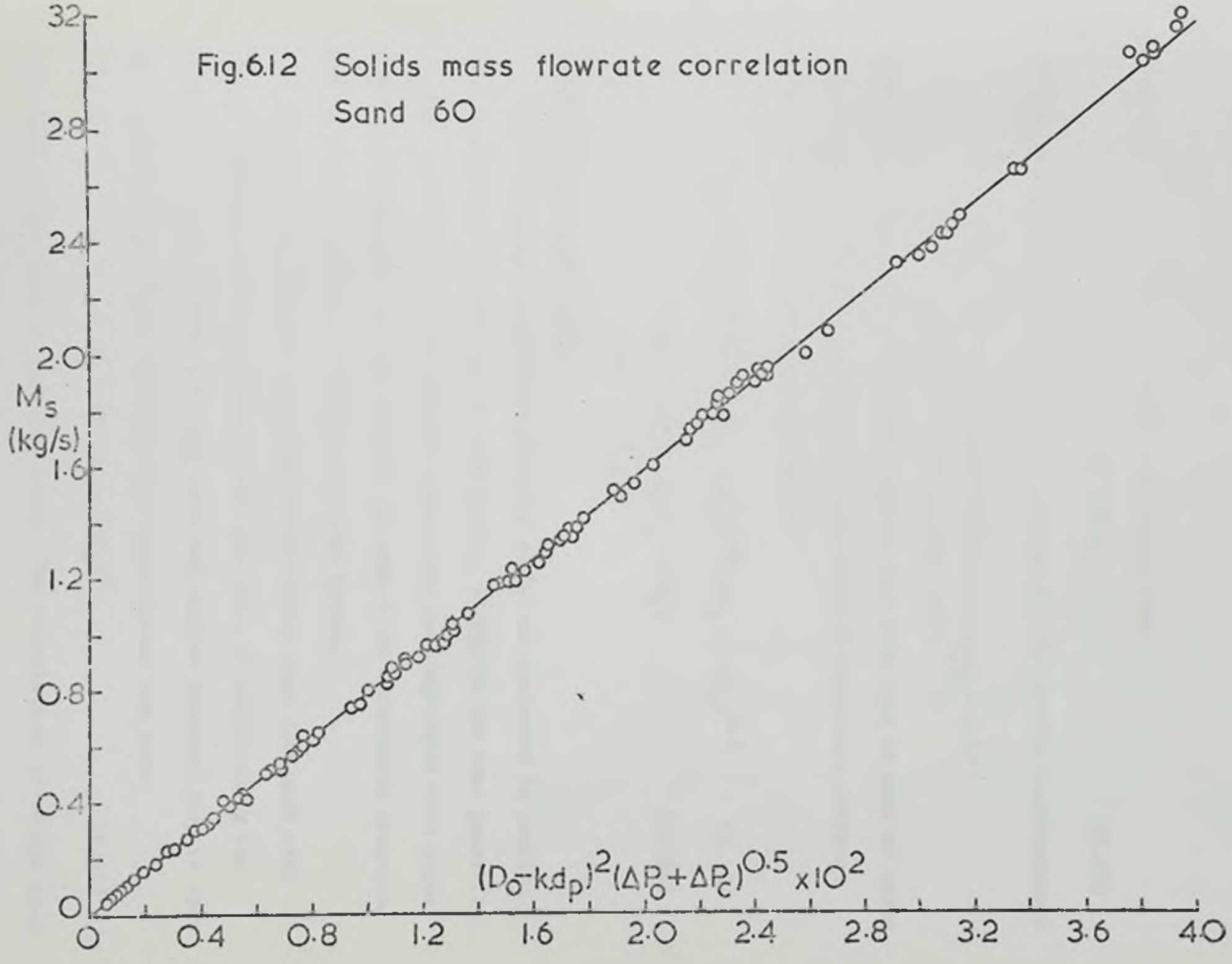

$$M_s = 79.27(D_o - 2.5d_p)^2 \, (\Delta P_o + \Delta P_C)^{0.5} \qquad (6.27)$$

where ΔP_o, ΔP_C were in (mm H_2O)

D_o, d_p were in (m)

M_s was in (kg/s)

Comparison of equation 6.27 with 3.22 showed that:

$$C_1 = C \frac{\pi}{4} \sqrt{2g \varphi_B} \qquad (6.28)$$

Substitution into this equation gave a value for the orifice coefficient C

$$C = \frac{79.27 \times 4}{\pi \times (2 \times 9.8067 \times 1.59 \times 10^3)^{0.5}} = 0.57$$

Thus the full equation relating the solids mass flow rate of sand 60 under the influence of a co-current air stream through a horizontal orifice set in the base of a hopper was given by:

$$M_s = 0.57 \frac{\pi}{4} \sqrt{2g \varphi_B} \, (D_o - kd_p)^{2.0} (\Delta P_o + \Delta P_C)^{0.5} \qquad (6.29)$$

$$\text{where} \quad \Delta P_C = \varphi_B (D_o - kd_p) \qquad (6.29a)$$

$$\text{and} \quad k = 2.5$$

<u>The Results for Sand 14/30</u>

The experimental programme for sand 14/30 was performed to confirm the results for sand 60 and, to some extent, to try to add some generality to the investigation. The results showed very good agreement with those for sand 60 and hence it was possible to conduct an abbreviated programme and to treat the data collected in the same manner.

Figure 6.13 shows the variation of the solids mass flow rate with orifice pressure drop and indicates the same form of relationship for sand 14/30 between solids mass flow rate and orifice pressure drop as that for sand 60. The graphs in figure 6.14 again showed the form:

$$M_s = C(\Delta P_o + \Delta P_C)^n \qquad (6.30)$$

The value of the index n was 0.5 ± 0.005. The correlations of solids mass flow rate against the orifice diameter for various constant values of

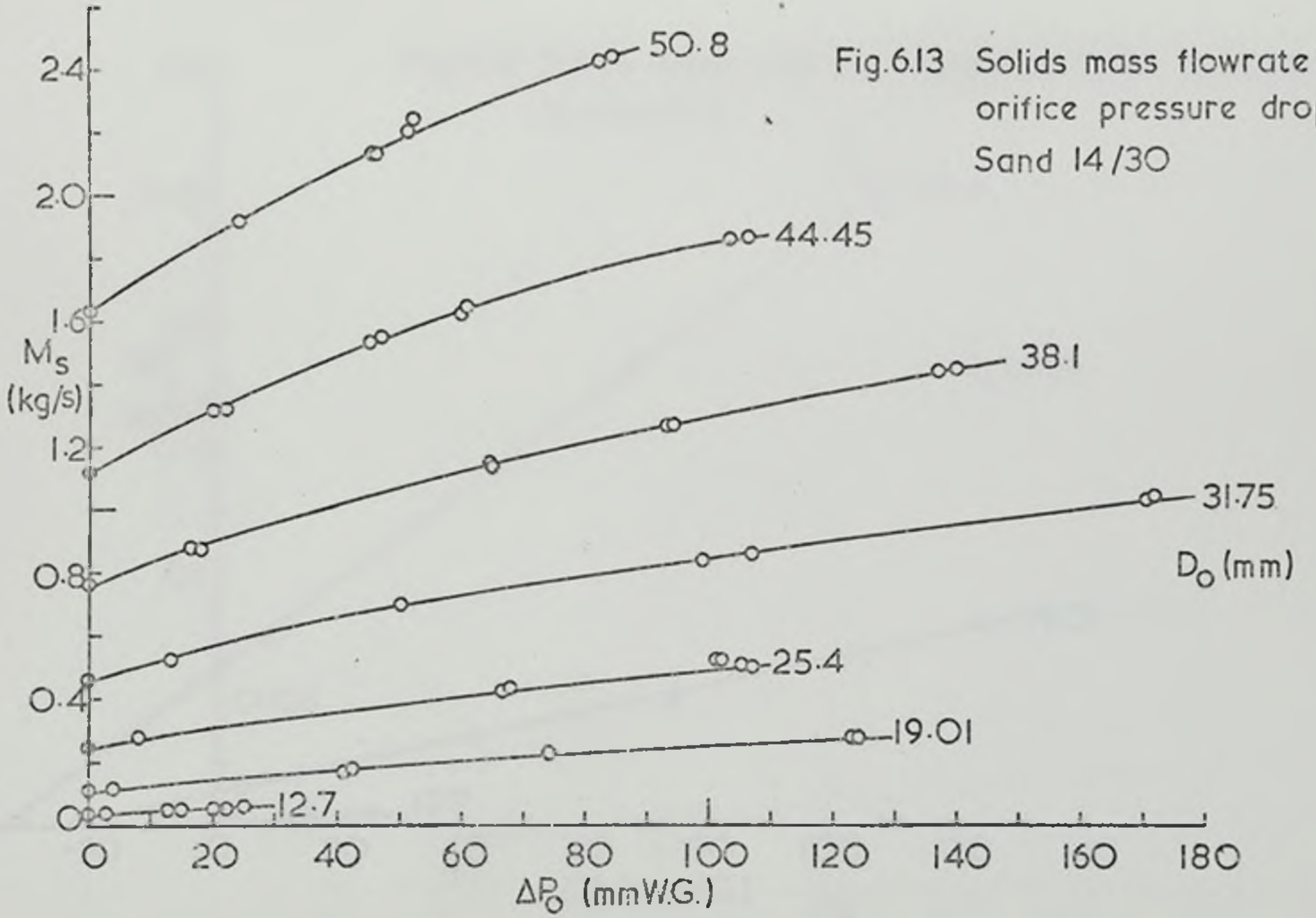

Fig.6.13 Solids mass flowrate vs. orifice pressure drop Sand 14/30

Fig.6.14

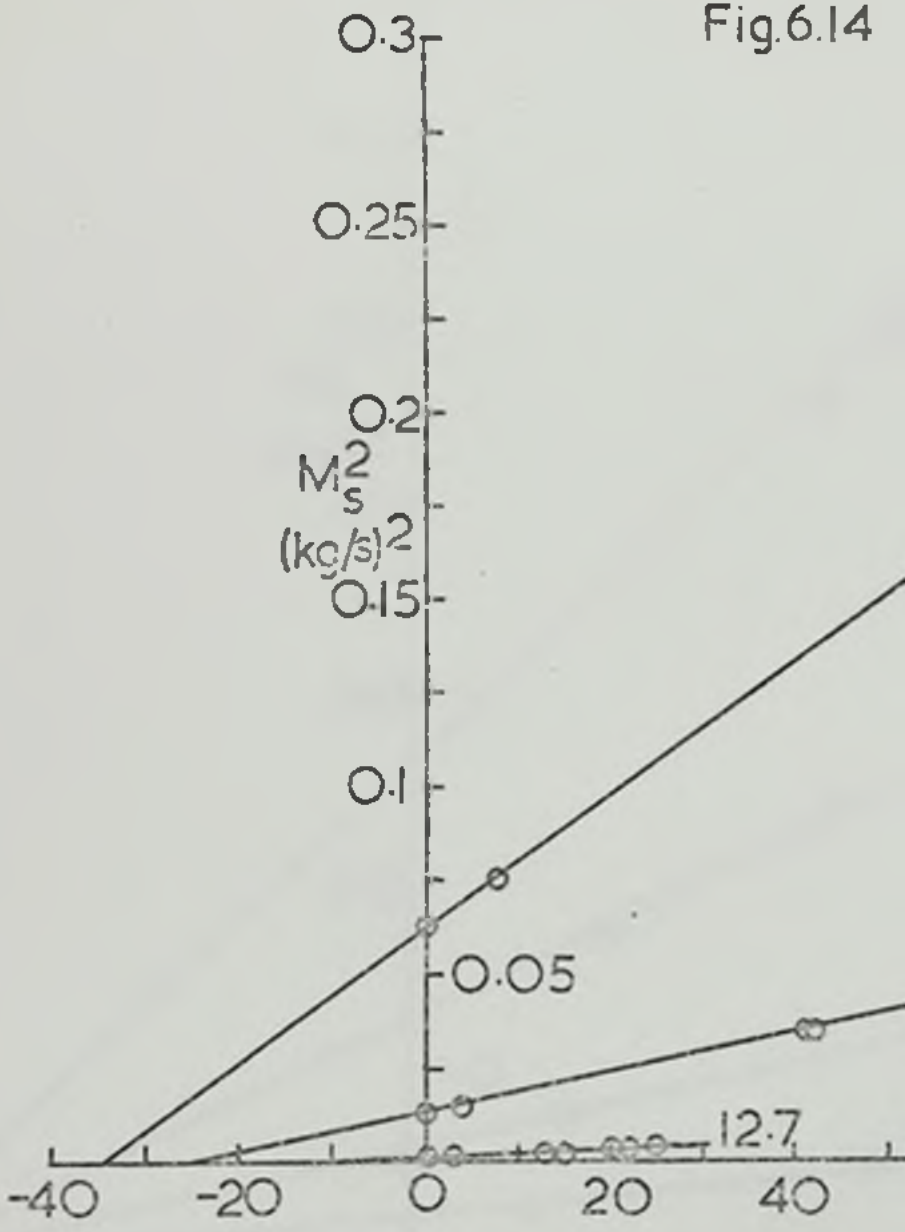

Solids mass flowrate squared vs. orifice pressure drop
Sand 14/30

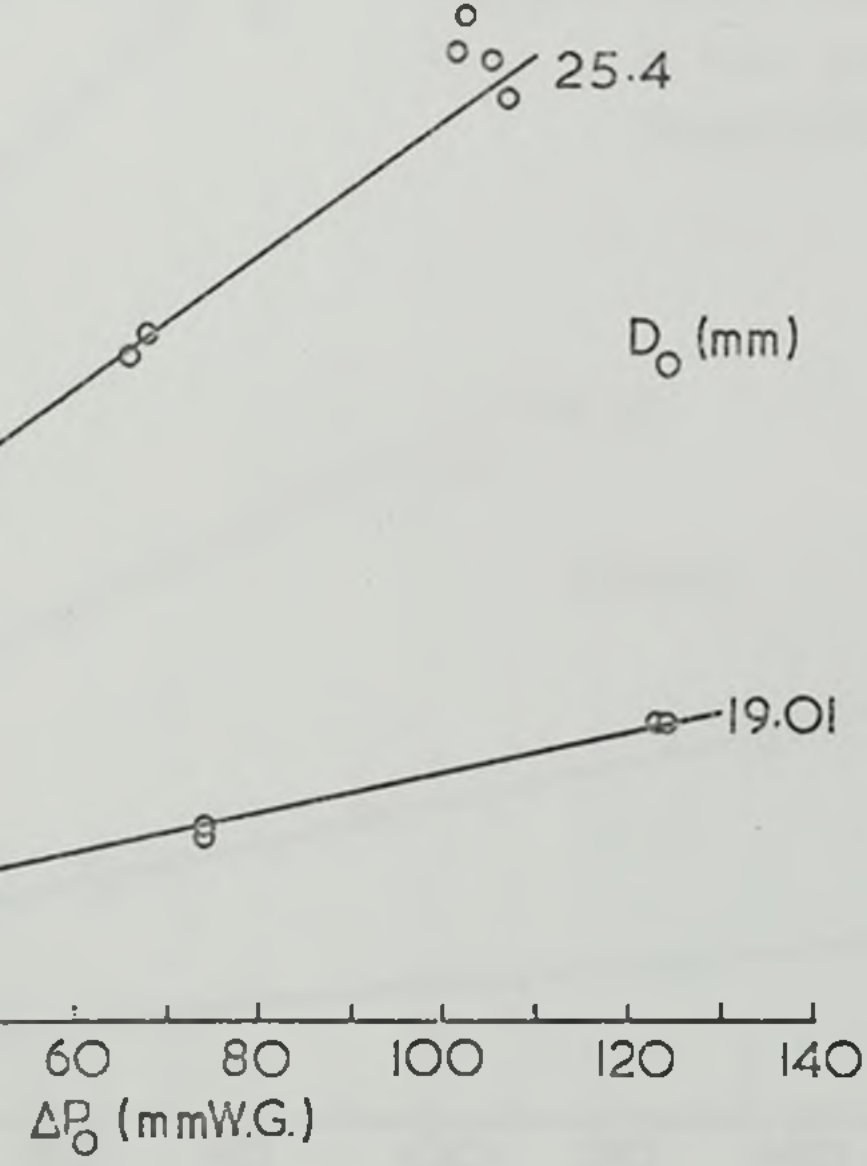

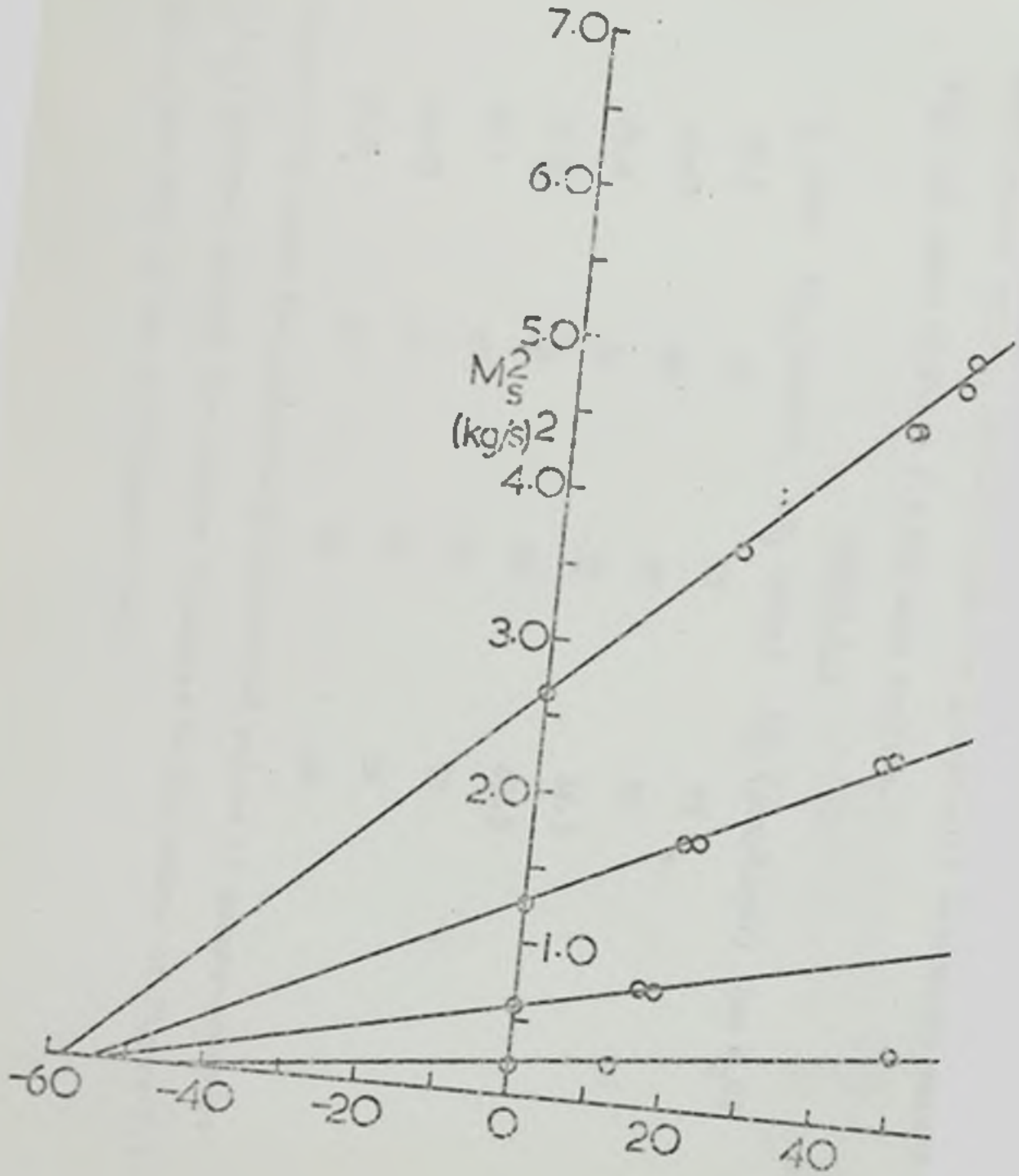
7.0
6.0
5.0
M_s^2
(kg/s)2
4.0
3.0
2.0
1.0
-60
-40
-20
0
20
40

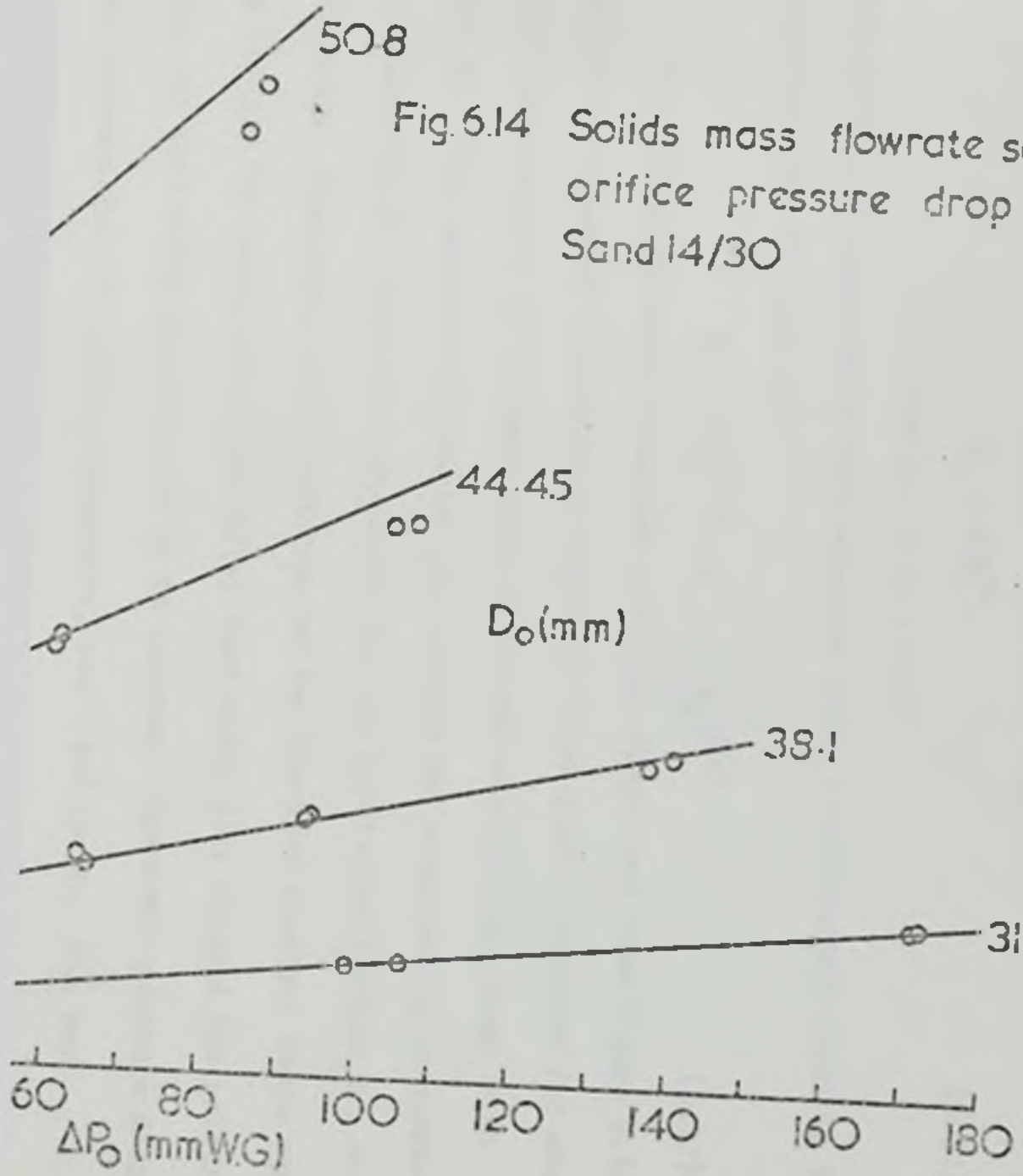

Fig. 6.14 Solids mass flowrate squared vs. orifice pressure drop
Sand 14/30

($\Delta P_o + \Delta P_c$), summarised Figure 6.15, showed the form:

$$M_s = C D_o^m \qquad (6.31)$$

where $m = 2.30 \pm 0.01$

and giving, on combination with equation 6.30, a relationship similar to equation 6.17 for sand 60:

$$M_s = C D_o^{2.3} (\Delta P_o + \Delta P_c)^{0.5} \qquad (6.32)$$

The values of pseudo-pressure used were those read from Figure 6.14. The observations of experimental values of 'stop-flow' pressures for sand 14/30 were subject to the same sort of violent oscillations found with sand 60. They were, on the whole, more marked and consequently accurate determination of 'stop-flow' pressures for any particular orifice was very difficult. There was, again, evidence of two distinct pressure drops over the orifice for zero solids flow rate; that which just stopped the solids flow, and that which just allowed it to restart. These two pressure drops were apparent for all orifice diameters, small and large. The two experimental values, together with the graphically determined values of ΔP_c, are shown in Table 6.3 for each orifice.

TABLE 6.3

D_o (mm)	ΔP_c (start)	ΔP_c (stop)	ΔP_c (graphical) ($mm\ H_2O$)
12.7	10	12	19
19.01	26	30	25
25.4	32	37	34.5
31.75	36	45	43.5
38.1	40	55	52
44.45	44	60	54
50.8	60	74	58

Figure 6.16 shows the graphically determined values of pseudo-pressure (ΔP_c) plotted against the orifice diameters in the manner of Figure 6.9. Again, the form of the relationship was:

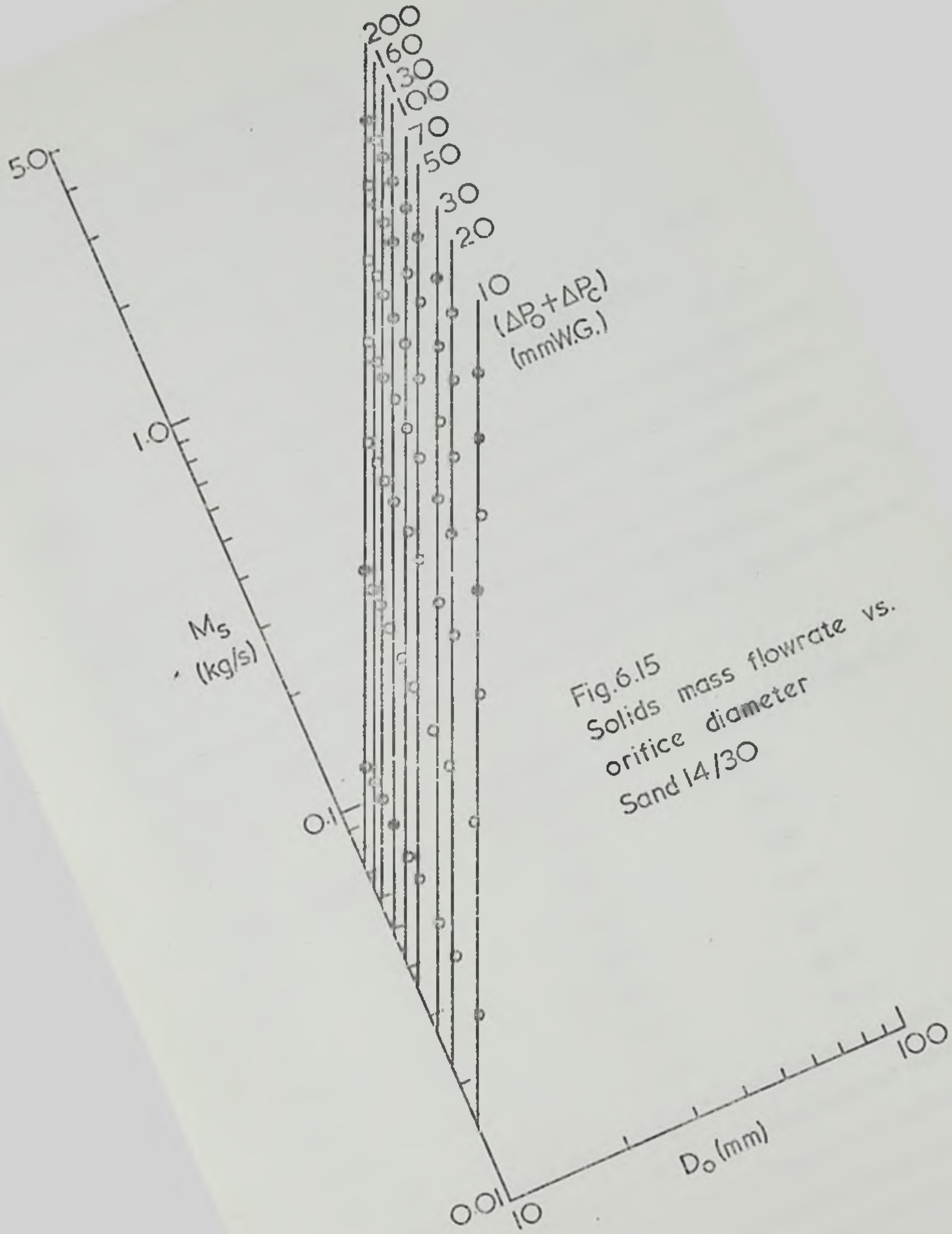

Fig.6.15
Solids mass flowrate vs. orifice diameter
Sand 14/30

$$\Delta P_C = \alpha_1(D_o - \beta_1) \qquad (6.33)$$

where $\alpha_1 = 1.456 \times 10^3$ and $\beta_1 = 1.79 \times 10^{-3}$

i.e. $$\Delta P_C = 1.456 \times 10^3 (D_o - 1.79 \times 10^{-3}) \qquad (6.34)$$

compared to the equation 3.23

$$\Delta P_C = \varphi_B(D_o - kd_p)$$

which, on substituting for bulk density, gave:

$$\Delta P_C = 1.51 \times 10^3(D_o - kd_p) \qquad (6.35)$$

Using the same value as before ($k = 2.5$), this equation became:

$$\Delta P_C = 1.51 \times 10^3(D_o - 2.01 \times 10^{-3}) \qquad (6.36)$$

The agreement between the experimental and the derived equations for pseudo-pressure was not quite so good with this sand but, since the difference in the slope of the equations was only 3.5%, it was felt that these results gave further support to the method of determining the pseudo-pressure (ΔP_C) from the orifice diameter and particle properties. The graphical values and the calculated values (from equation 6.34 and 6.36) of ΔP_C are given in Table 6.4.

TABLE 6.4

D_o (mm)	ΔP_C (graphical)	ΔP_C (equ. 6.34)	ΔP_C (equ. 6.36) (mm H_2O)
12.7	19	16.5	16.0
19.01	25	25.0	25.5
25.4	34.5	34.5	35.5
31.75	43.5	45.5	45.0
38.1	52	52.5	54.5
44.45	54	62.0	64.0
50.8	58	71.5	73.5

It was seen from Table 6.4 that for the two largest orifices there was some discrepancy between the values of pseudo-pressure determined graphically from Figure 6.14 and those predicted by Figure 6.16 (equation 6.34). It was not possible to find a precise explanation for these low figures. It has been noted in Chapter 3, however, that it was expected that the effect of

Fig.6.16 'Pseudo pressure' vs. orifice diameter
Sand 14/30

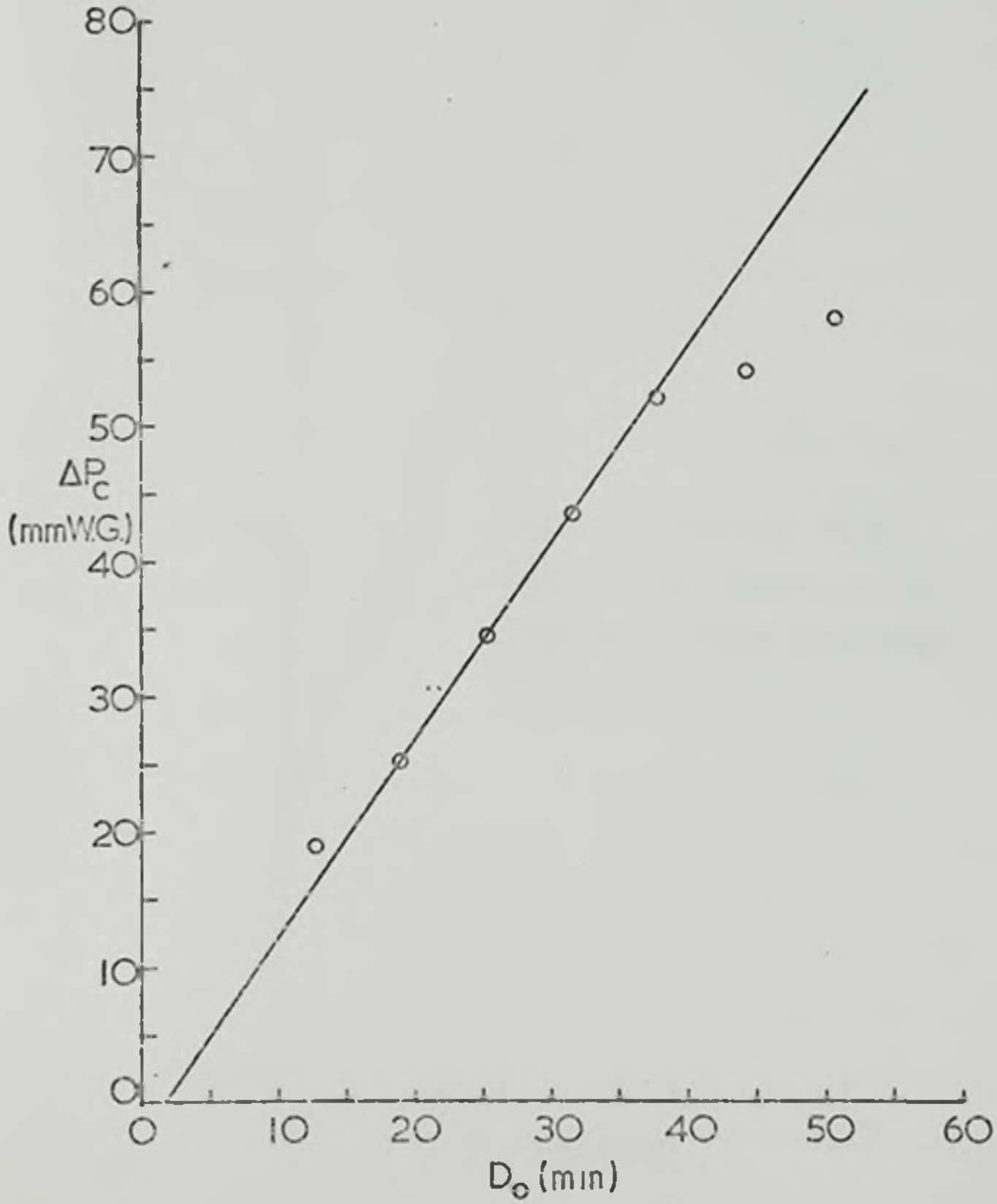

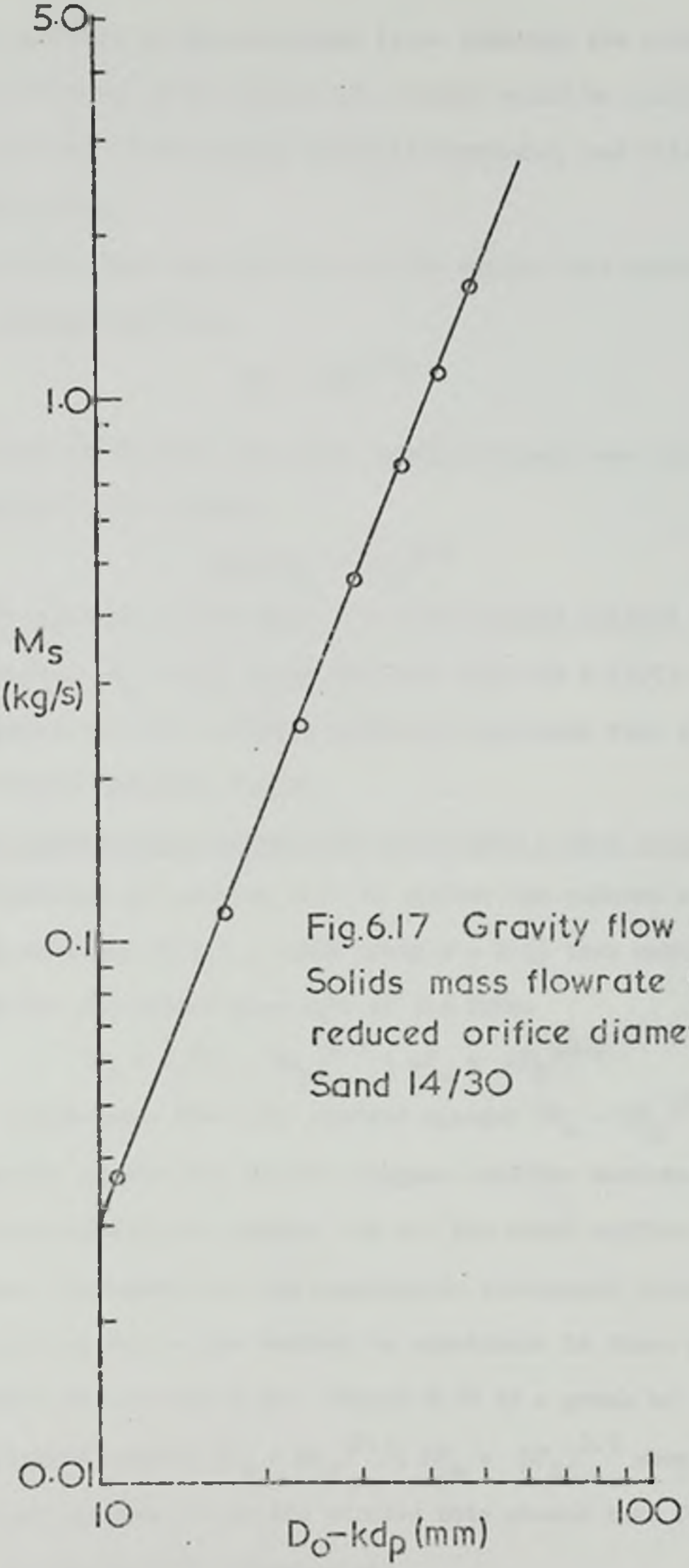

Fig.6.17 Gravity flow
Solids mass flowrate vs.
reduced orifice diameter
Sand 14/30

co-current air flow on the particles (i.e. inducing the solids to flow through the orifice in the manner of a fluid) would be reduced as the particle size (and consequently inertia) increased, and this might account for the difference.

The gravity flow runs were plotted as solids mass against orifice diameter, showing the form:

$$M_s = C D_o^{2.70} \qquad (6.37)$$

As in the case of sand 60, the empty annulus concept was introduced to modify equation 3.13, giving:

$$M_s \propto (D_o - kd_p)^{2.5} \qquad (6.25)$$

Figure 6.17 shows the solids mass flow rate plotted against the reduced orifice diameter $(D_o - kd_p)$ using the same value of k (2.5); the slope of the correlation was 2.51, showing excellent agreement with the proposed form of relation (equation 6.25).

The Overall Equation for Pressurised Solids Flow - Sand 14/30

Modifications of equation 6.31 to include the reduced orifice diameter resulted in an index of 2.1 ± 0.005 using k = 2.5, thus making the final correlation for the solids flow rate of the form:

$$M_s = C_1(D_o - kd_p)^{2.1} (\Delta P_o + \Delta P_C)^{0.5} \qquad (6.38)$$

A graph of solids mass flow rate plotted against $(D_o - kd_p)^{2.1}(\Delta P_o + \Delta P_C)^{0.5}$ showed that the results for the two largest orifices deviated from the average correlation of the results for all the other orifices. Examination of this trend indicated that the graphically determined values of ΔP_C used could be too low; and it was decided to substitute in these cases values of ΔP_C predicted by equation 6.34. Figure 6.18 is a graph of the solids mass flow rate plotted against $(D_o - kd_p)^{2.1}(\Delta P_o + \Delta P_C)^{0.5}$ showing the improvement. A least squares fit in the amended data showed that $C_1 = 56.37$ in this case, giving the full correlation:

$$M_s = 56.37(D_o - kd_p)^{2.1}(\Delta P_o + \Delta P_C)^{0.5} \qquad (6.39)$$

Fig. 6.18 Solids mass flowrate correlation
Sand 14/30

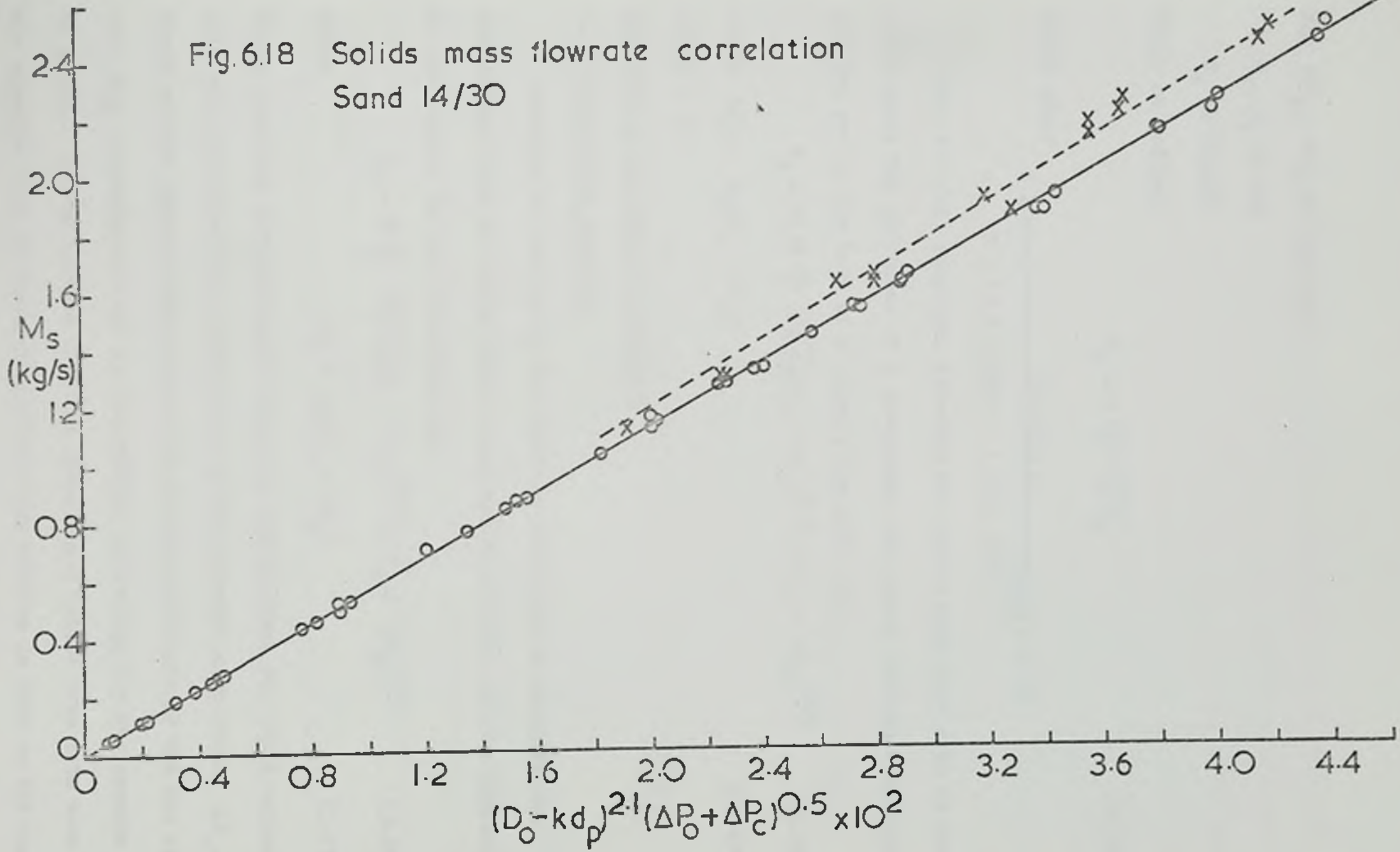

for ΔP_o, ΔP_C in (mm H_2O)

D_o, d_p in (m)

M_s in (kg/s)

Thus, as before:

$$C_1 = C \frac{\pi}{4} \sqrt{2g \varphi_B} \qquad (6.28)$$

which gave:

$$C = \frac{56.37 \times 4}{\pi \times (2 \times 9.8067 \times 1.51 \times 10^3)^{0.5}} = 0.35$$

Thus the full equation, relating the solids mass flow rate of sand 14/30 under the influence of a co-current air stream through a horizontal orifice set in the base of a hopper, was given by:

$$M_s = 0.35 \frac{\pi}{4} \sqrt{2g \varphi_B} (D_o - kd_p)^{2.1} (\Delta P_o + \Delta P_C)^{0.5} \qquad (6.40)$$

where $\Delta P_C = \varphi_B (D_o - kd_p)$ (6.40a)

and $k = 2.5$

Comments on the Results and Model

1. Theoretical equation

According to Chapter 3, the equation developed to describe the pressurised flow of solids from a consideration of the various approaches to the subject in the literature was:

$$M_s = C \frac{\pi}{4} \sqrt{2g \varphi_B} (D_o - kd_p)^{2.0} (\Delta P_o + \Delta P_C)^{0.5} \qquad (3.22)$$

where $$\Delta P_C = \varphi_B (D_o - kd_p) \qquad (3.23)$$

These equations were developed using the concept that the total solids flow rate was determined by a combination of two pressure components; ΔP_o, the fluid orifice pressure drop accounting for the influence of the air stream, and ΔP_C, a pseudo-pressure at the orifice accounting for the gravity flow of solids. It was noticed that the pressurised solids flow rate term in the expanded form of equation 3.22 was very similar in form to the equation proposed by Evans (36): it was, however, recognised that the theory route was quite different, Evans having based his reasoning on a direct fluid analogy.

The concept of pseudo-pressure had been noted by Kuwai (49) and Knowles (52) to account for the gravity flow contribution to the total solids flow rate. Examination of the equations in Chapter 3 showed that the pseudo-pressure should be related to the particle and bed properties, where previously it had only been found by experiment. Further examination showed that the coefficient was dimensionless in the present equations (6.29, 6.40), whereas the previous forms of expression for pressure solids flow rate had inferred a dimension of $L^{-\frac{1}{2}}$.

2. Experimental correlation

The equations resulting from the experimental work on the pressurised flow of solids through orifices gave very good agreement with the theoretical equation 3.22 above:

$$M_s = 0.57 \frac{\pi}{4} \sqrt{2g \varphi_B}(D_o - kd_p)^{2.1}(\Delta P_o + \Delta P_c)^{0.5} \quad \text{for sand 60} \quad (6.29)$$

$$M_s = 0.35 \frac{\pi}{4} \sqrt{2g \varphi_B}(D_o - kd_p)^{2.1}(\Delta P_o + \Delta P_c)^{0.5} \quad \text{for sand 14/30} \quad (6.40)$$

where $\Delta P_c = \varphi_B(D_o - kd_p)$ and $k = 2.5$.

As explained above, the ΔP_c values were obtained by graphical extrapolation from plots of solids mass flow rate against orifice pressure drop (e.g. Figure 6.7). The experimental values of ΔP_c were considered less reliable due to the oscillations in solids flow rate and pressure readings under counter-current flow conditions.

The slightly high value of the index of the reduced diameter term $(D_o - kd_p)$ for the sand 14/30 (equation 6.40), and the deviations from equation 6.34 of the graphically determined values of ΔP_c for the two largest orifices, were in accordance with the expected limitations on the analysis of the effect of co-current air on the flow of solids through an orifice.

The correlations of the experimental data showed the need to include a constant correction factor in the orifice diameter terms (Figures 6.9, 6.10 and 6.16). The values of this factor were compared with the values

obtained by using Brown's concept of an empty annulus at the edge of the orifice (38). Although there were no specific observations of the existence of such an annulus in the present work, the values of the correction factors agreed reasonably well.

Finally, the proportionality factors C were described as orifice discharge coefficients in the manner of fluid flow. The experimentally derived values of orifice coefficient, although not identical, were encouraging in that the value for sand 60 was very close to those values published in the literature for flow of fluidised solids streams through vertical orifices. Stemerding (60) correlated a wide range of particle sizes and orifice dimensions using a value of 0.5 for the orifice coefficient, whereas de Jong (57) showed that with some modification to the results of Jones et al (61) a value of 0.53 was likely: Massimilla et al (58) also reported similar values. The results of Jones et al (61) showed that the orifice coefficient was dependent on the relative values of particle diameter and orifice diameter; generally, the larger the value of the ratio $\frac{d_p}{D_o}$, the smaller the discharge coefficient - see Table 6.5.

TABLE 6.5

$d_p : D_o$	C (Jones et al)
1:11.5	0.28
1:21	0.34
1:32	0.38
1:32	0.42
1:42.5	0.47
1:63.5	0.49
1:210	0.50

Although the individual discharge coefficients were not found in the present work, the experimental value of C could be considered as an average value for all orifices. The range of particle to simple orifice diameter ratios for sand 14/30 was 1:16 to 1:63 which was included in the range used by

Jones et al. Averaging the orifice coefficients for this equivalent range showed a value of 0.4, similar to that found from the present work on sand 14/30. Similar analysis for sand 60 (diameter 1:27.5 to 1:111) gave an average value of 0.45 which was rather low compared with the value in the present work.

Generally speaking, it was seen that the present values of orifice discharge coefficient compared well with those in the literature, and that the seemingly low valuesfor the sand 14/30 were, in fact, in line with the results of a more rigorous investigation into the values of orifice coefficients (61).

Orifice Pressure Drop and Moving Solids Bed Pressure Drop

In the vast majority of the measurements made in this work the fluid pressure drop over the solids orifice greatly exceeded that over the moving solids bed in the hopper (Appendix 6), the exceptions being some readings taken with the shortest standpipe and the smallest orifice where the measurement of the low fluid pressures may have involved some error, as noted previously (Sections 6.3, 6.4). Attempts to relate together the two pressure drops did not prove satisfactory, although it had been considered that there might have been some proportionality, since in the case of a static bed and an orifice, assuming no mutual interference, it was thought very likely that the respective pressure drops would show some correlation if tested for a range of air flow rates. Clearly, in the present case, the presence of the moving solids in the orifice, and the fact that the solids bed was in motion, affected the magnitudes of the two pressure drops and since the solids flow rate was in turn affected by air flow rates and fluid pressure drops, any direct proportionality between the bed and orifice pressure drops was unlikely. Rausch (34), in testing the effect of counter-current air flow, similarly observed that the orifice pressure drop was substantially larger than the solids bed pressure drop, concluding that the head of solids above the orifice had little effect on solids flow

rate and that the orifice pressure drop was the controlling factor on the effect of fluid flow on solids flow rate; he showed also that a relatively small flow of air was sufficient to cause cessation of the solids flow. The present work substantiated these conclusions both directly in the counter-current flow tests for the determination of 'stop-flow' pressures and in reverse in the results of the main experiments (i.e. co-current flow), showing that the co-current flow of air profoundly affected the flow rate of the solids. This effect has previously been suggested as a method for directly controlling solids flow rates (80). The relationship between orifice pressure drop and bed pressure drop was not investigated in the present work, but it was considered that further work should be carried out to find the effect of bed height on the air-induced flow of solids.

6.6 The Estimation of the Voidage at the Orifice

A description of the physical situation at the orifice has already been given in Section 6.5. The pressure drop over the orifice was taken from the measurements of pressures in the chamber and just above the orifice. As already stated (Sections 6.4 and 6.5), this pressure drop, in conjunction with the pressure drop over the constant level bed, resulted in a flow of percolating air through the orifice at a net velocity greater than the solids velocity. In order to determine the air and particle velocities at the orifice, it was found necessary to estimate the voidage of the flowing stream of solids.

From work on the estimation of a moving bed voidage for the gravity flow situation by Delaplaine (33), Evans (36) proposed that the voidage at the orifice could be taken as the bulk value for the moving bed. Direct measurements of the voidages in a moving bed at Warren Spring (45) indicated that the voidage of the flowing solids increased as the orifice was approached, but no values or methods of evaluation of the voidage were given. In connection with the flow of fluidised solids streams through

orifices set in the walls of a fluidised bed container, both Massimilla et al (58) and Jones et al (61) were able to estimate the values of the voidage at the orifice. Massimilla (58) reported for sand essentially constant values of orifice voidage about 0.5, whereas Jones (61) showed that the orifice voidage was dependent on the orifice diameter and, to some extent, the pressure drop over the orifice. De Jong (57) was able to show that with some modification of the diameter of the solids stream, a virtually constant value of orifice voidage of 0.53 was obtainable using Jones' results for sand. Thus, although it seemed likely that the orifice voidage would be greater than the bulk value in the present system, it was not possible to ascertain whether the results of Massimilla or Jones were directly applicable. Consequently, it was decided, as shown in Chapter 3, to adopt the method of Massimilla to determine the values of the orifice voidage for all air and solids flow rates in the present work.

The values of orifice voidage were calculated from equation 3.31:

$$\Delta P_o = \frac{k_1 Q}{\pi r_o} + \frac{k_2 Q^2}{3 \pi^2 r_o^2} \qquad (3.31)$$

by Newton-Raphson iteration and checked by substitution back into the equation. Figure 6.19 shows these calculated voidages of the solids stream at the orifice, plotted against the solids mass flow rate for both solids. This graph supported the view of a virtually constant voidage at the orifice for all orifices.

The average voidage at the orifice calculated for sand 60 was lower than that for sand 14/30, being approximately 0.46 and 0.49 respectively, and these values were consistent with the results for the static bed and moving bed voidages (Section 6.1, 6.2). The average values of orifice voidages were similar to those found for sands by Massimilla (58) and de Jong (57). There was no reason to suppose that the sands used in the present work had identical properties to those used earlier, and thus the figures of Massimilla or de Jong could not be used. Thus it was felt that

Fig. 6.19 Orifice voidage vs. solids flowrate
Sand 60

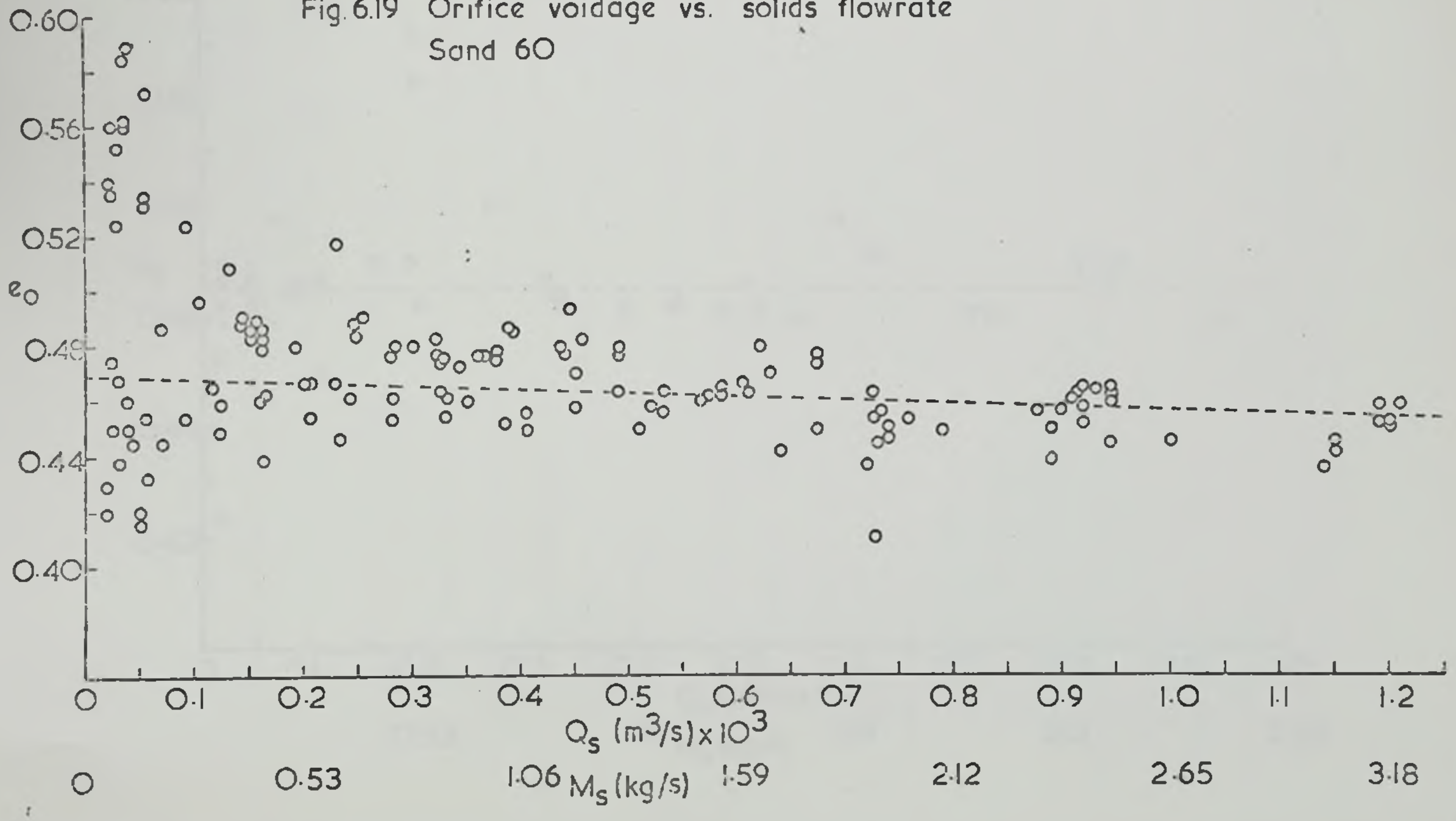

Fig.6.19 Orifice voidage vs solids flowrate
Sand 14/30

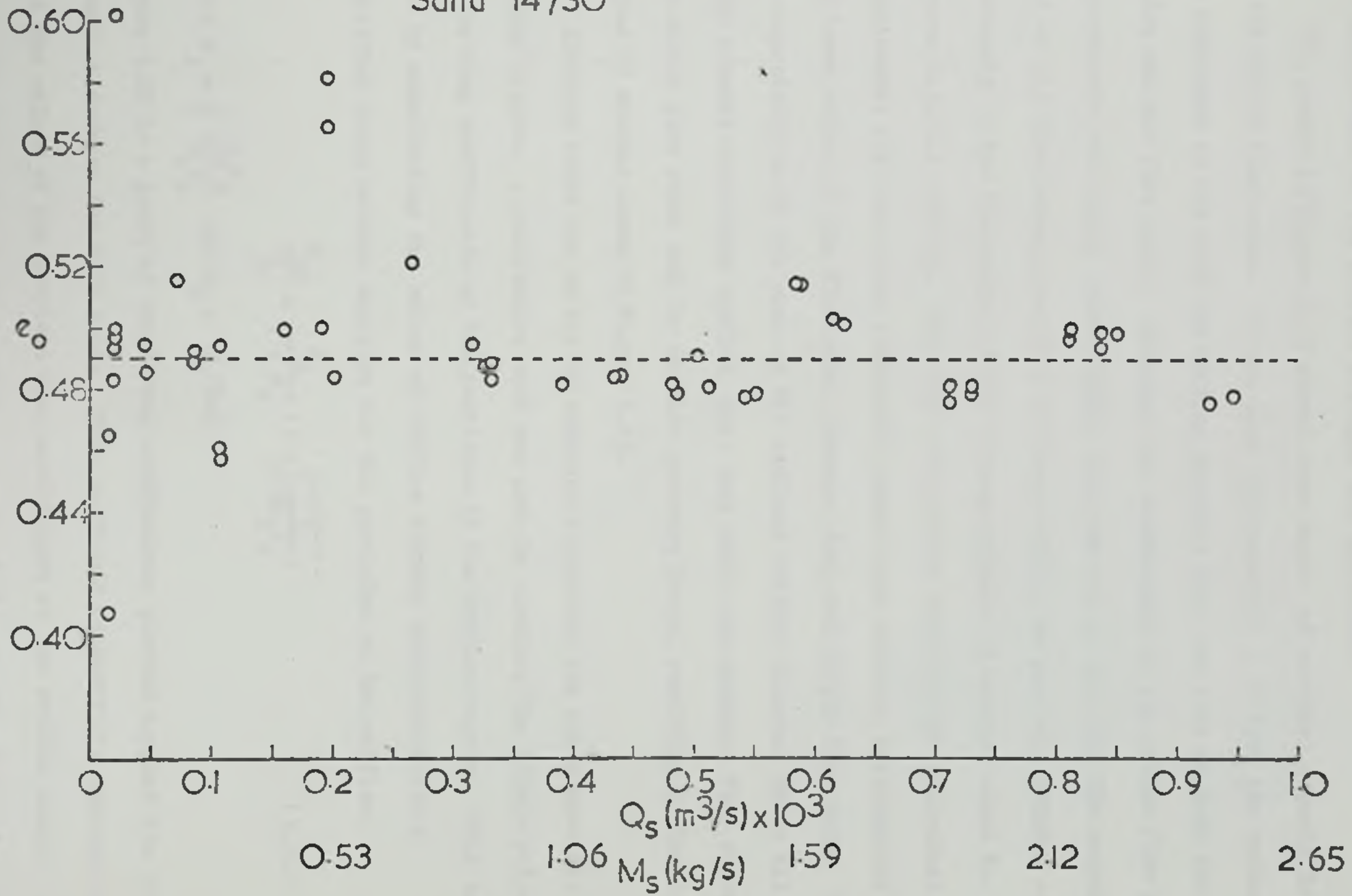

the calculation of the orifice voidages was justified.

The graphs in Figure 6.19 showed some degree of scatter, especially at low solids flow rates. It was seen from equation 3.31 that the voidage was dependent on not only the orifice pressure drop but also on both the solids and air flow rates. Although the measurement of the solids flow rate was accurate and highly reproducible, this was not so true for the measurement of air flow rates, especially at lower values: as has been pointed out previously in the discussion of the various degrees of scatter shown in Figures 6.3, 6.4 and 6.5. Thus any calculations based on the individual experimental air flow rates inherently showed some scatter, particularly for the lower values of air flow rate, pressure drop and solids flow rate. This was especially so in the case of the smallest orifice diameter where all three adverse conditions applied, i.e. very small air measured flow rates, low solids flow rates and low orifice pressure drops, resulting in the large degree of scatter shown in Figure 6.19.

Although there was no way of accurately checking the calculated orifice voidage figures, a qualitative test was made by checking the likely values of the drag coefficients of the particles in the orifice region. This was done by substituting the values of orifice voidage into Massimilla's simplified force balance equation for the particles at the orifice.

$$\frac{Q_{at}}{Q_s} = \frac{e_o}{1 - e_o}\left(1 + \sqrt{\frac{3}{2k_3 r_o}}\right) \qquad (3.34)$$

where $k_3 = \frac{3}{4}\frac{\varphi_n k_D}{\varphi_c d_p}$ and $k_D = f_n(Ro)$

Figure 6.20 is a graph of these drag coefficients plotted against the particle Reynolds' numbers for both sands. This confirmed Massimilla's conclusions that the values of the particle drag coefficient at the orifice should be much larger than the single particle value, and also confirmed Rowe's (105, 106) demonstration that particle drag coefficients related to the flow of fluids past a group of spheres can be one order of magnitude greater than the drag coefficient for a single sphere. This check indicated that the

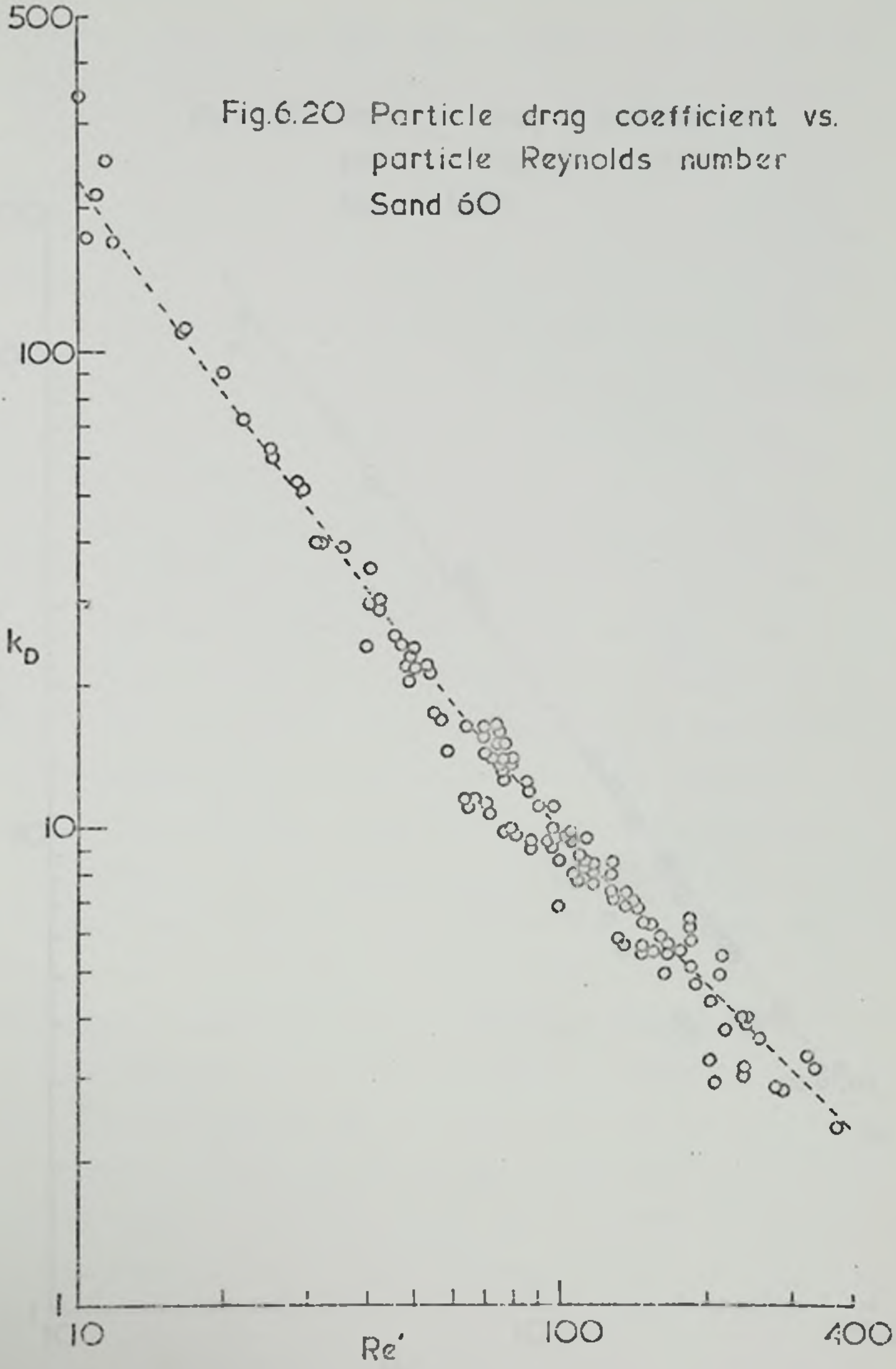

Fig.6.20 Particle drag coefficient vs. particle Reynolds number
Sand 60

Fig.6.20 Particle drag coefficient vs. particle Reynolds number
Sand 14/30

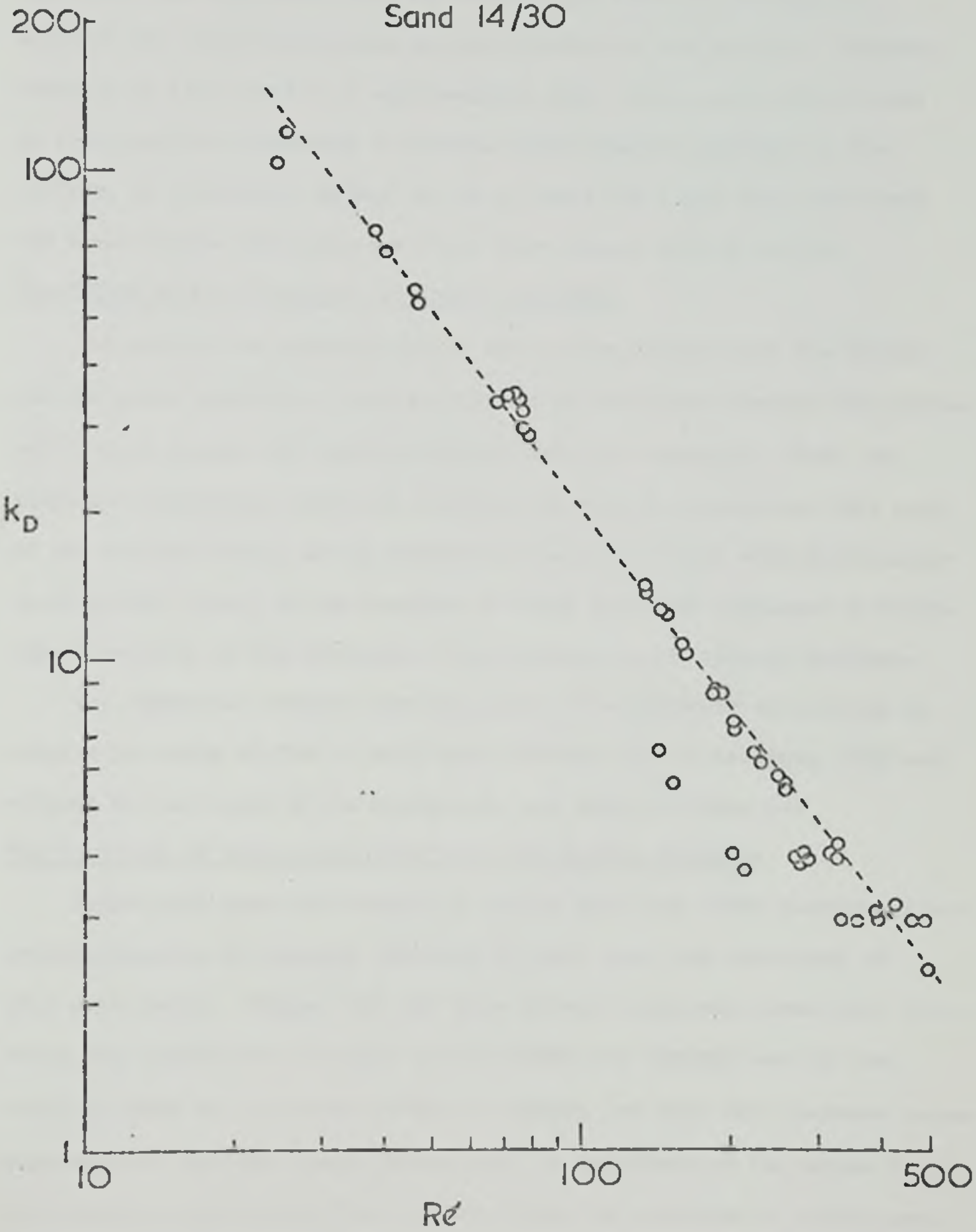

calculated orifice voidage values were at least reasonable, and well in line with the previous work. In addition, Holland et al (46), in their analysis on the effect of the ambient fluid on solids discharge, proposed the use of the Richardson-Zaki expressions for hindered settling to estimate the fluid drag forces on the particles at the orifice. However, Shook et al (47) noted in a supplementary paper that, as the drag forces on fine particles generated an adverse fluid pressure gradient at the orifice, an alternative method was to estimate the fluid drag force from the Kozeny-Carman equations for fluid flow through beds of solids.

6.7 The Effect of the Standpipes on Solids Flow Rate

The part of the apparatus below the orifice consisted of the chamber and the glass standpipe. During a run the solids flowed through the orifice and dropped through the chamber directly into the standpipe. Thus, by running the apparatus with each standpipe in turn in conjunction with each of the orifice plates, and by performing a series of runs with no standpipe (i.e. gravity flow), it was possible to study fully the influence of standpipe dimensions on the discharge of particulate solids through orifices.

The summarised results from the series of experiments carried out to compare the rates of flow of both sands through all the orifices, with and without the influence of the standpipes, are shown in Table 6.6.

The Variation of Solids Mass Flow Rate with Orifice Diameter

Figure 6.21 shows one example of solids mass flow rates plotted against orifice diameter for gravity flow and, in this case, for standpipes of 38.5 mm diameter. Figure 6.21 and these curves in general showed that there was a very significant increase in the solids flow through each of the orifices under the influence of the standpipes, and that this increase became more apparent with the longer standpipes. A comparison of the curves for the standpipe and gravity flow suggested that the variation of solids mass flow rate with orifice diameter was similar for both gravity and standpipe flow. Further examination of the graphs on log-log paper, however, showed

Fig.6.21
Solids mass flowrate vs. orifice diameter
Sand 60
D_t = 38.5mm.
⊗ Average for
L_t = 3.650m., 4.250m., 4.875m

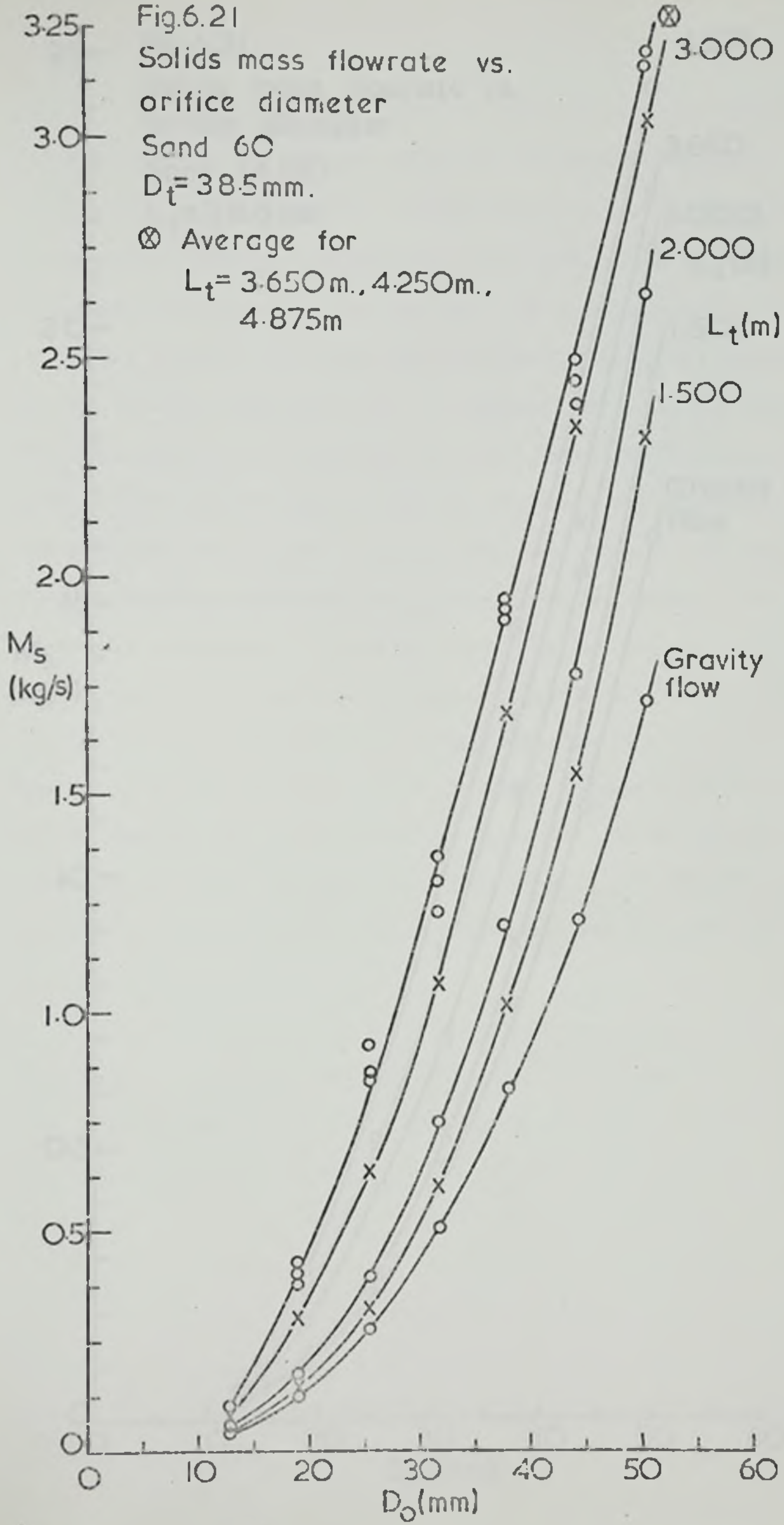

Fig.6.21
Solids mass flowrate vs. orifice diameter
Sand 14/30
L_t = 38.5 mm

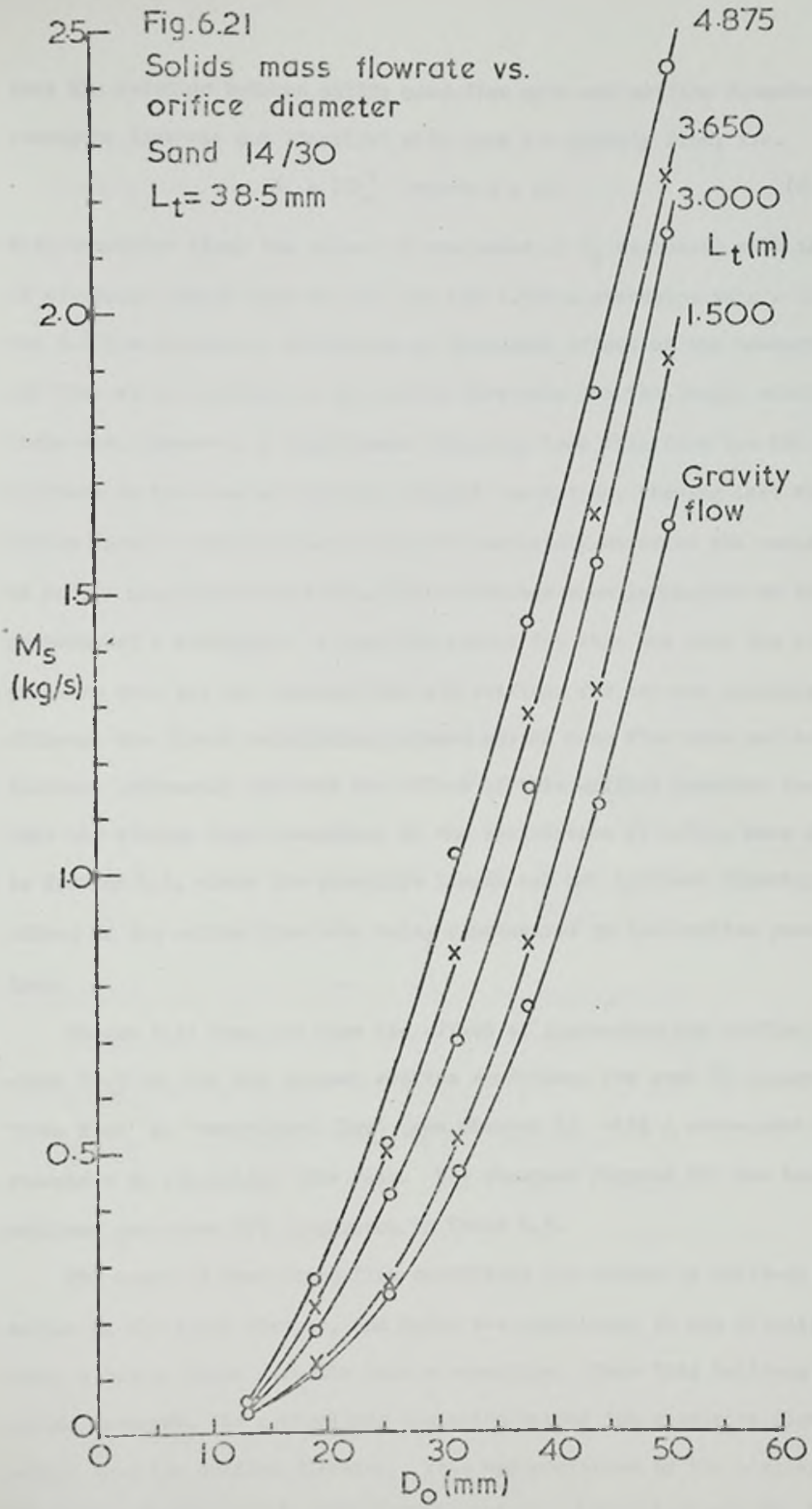

that the relation between solids mass flow rate and orifice diameter for standpipe flow was not identical with that for gravity flow, i.e.

$$M_s = C D_o^n \quad \text{where } n = 2.7 \qquad (6.41)$$

With standpipe flow, the values of the index of D_o decreased with increase of standpipe length from n = 2.7 for the 1.500 m standpipe to n = 2.0 for the 4.875 m standpipe, indicating an increased effect of the co-current air flow at the orifice on the solids flow rate for the longer standpipes. There was, moreover, a significant deviation from this form for the small orifices in the case of the four longest standpipes, showing that the simple form of equation 6.41 could not completely describe the variation of solids mass flow rate with orifice diameter when influenced by the presence of a standpipe. A possible reason for this was that the orifice pressure drop was not constant for all orifices for any one standpipe, although the direct correlation between solids mass flow rate and orifice diameter inherently included the effect of this orifice pressure drop. This had already been recognised in the correlation of solids mass flow rate in Section 6.6, where the standpipe length was not included directly, its effect on the solids flow rate being represented by the orifice pressure drop.

Figure 6.21 does not show the effect of increasing the orifice diameter above 50.8 mm, for the largest orifice conditions for sand 60 changed from 'free flow' to 'restricted flow' (see Chapter 5), with a consequent sharp reduction in the solids flow rate. The observed figures for the two largest orifices are shown for comparison in Table 6.7.

The onset of restricted-flow conditions was marked by build-up of solids in the glass chamber, and hence was equivalent to the situation where a hopper feeds directly into a standpipe. Once this build-up of solids occurred, the controlling dimension became the standpipe diameter rather than the orifice diameter. This was confirmed by the similarity of the flow rate for gravity flow through the 38.1 mm orifice and the flow

rate through the 1.500 standpipe in the restricted-flow regime:

Gravity flow: D_o = 38.1 (mm) M_s = 0.823 (kg/s)

Restricted flow: D_t = 38.5 (mm) M_s = 0.897 (kg/s) L_t = 1.500

The slight difference in these flow rates was probably due to the effect of the standpipe, since it could be seen from Table 6.7 that the standpipe still had some influence in the restricted-flow regime: the mass flow rate still increased with increase in standpipe length.

A comparison of the results in Table 6.6 and Figure 6.21 for the two solids indicated differences in the increase in solids flow rate due to the presence of the standpipe, thus showing that particle size - as would be expected - had some effect on the influence of the standpipe on the solids mass flow rate.

TABLE 6.7

Solids Flow Rates (kg/s)

	Standpipe lengths (diameter 38.5 mm)						
D_o (mm)	1.500	2.000	3.000	3.650	4.250	4.875	L_t (m)
50.8	2.320	2.649	3.070	3.173	3.200	3.600	
63.5	0.897	0.949	1.114	1.334	1.392	1.620	

The Variation of Solids Mass Flow Rates with Standpipe Length

Examples of the variation of the solids mass flow rate with standpipe length are given in Figure 6.22. These graphs, which show the results for all orifices in conjunction with all the standpipes of 38.5 mm diameter, depict a characteristic 'S' shaped curve which was common to all plots of solids mass flow rate against standpipe length. In the case of sand 60, the curves for all the standpipe diameters showed that the solids mass flow rates, for any one orifice, were nearing a maximum value with the longest standpipes and that any further increase in standpipe length was unlikely to have much effect on the solids flow rate. Moreover, in the case of the 38.5 mm diameter standpipes, it was seen that the mass flow rates for each orifice were virtually constant for the three longest standpipes, and thus

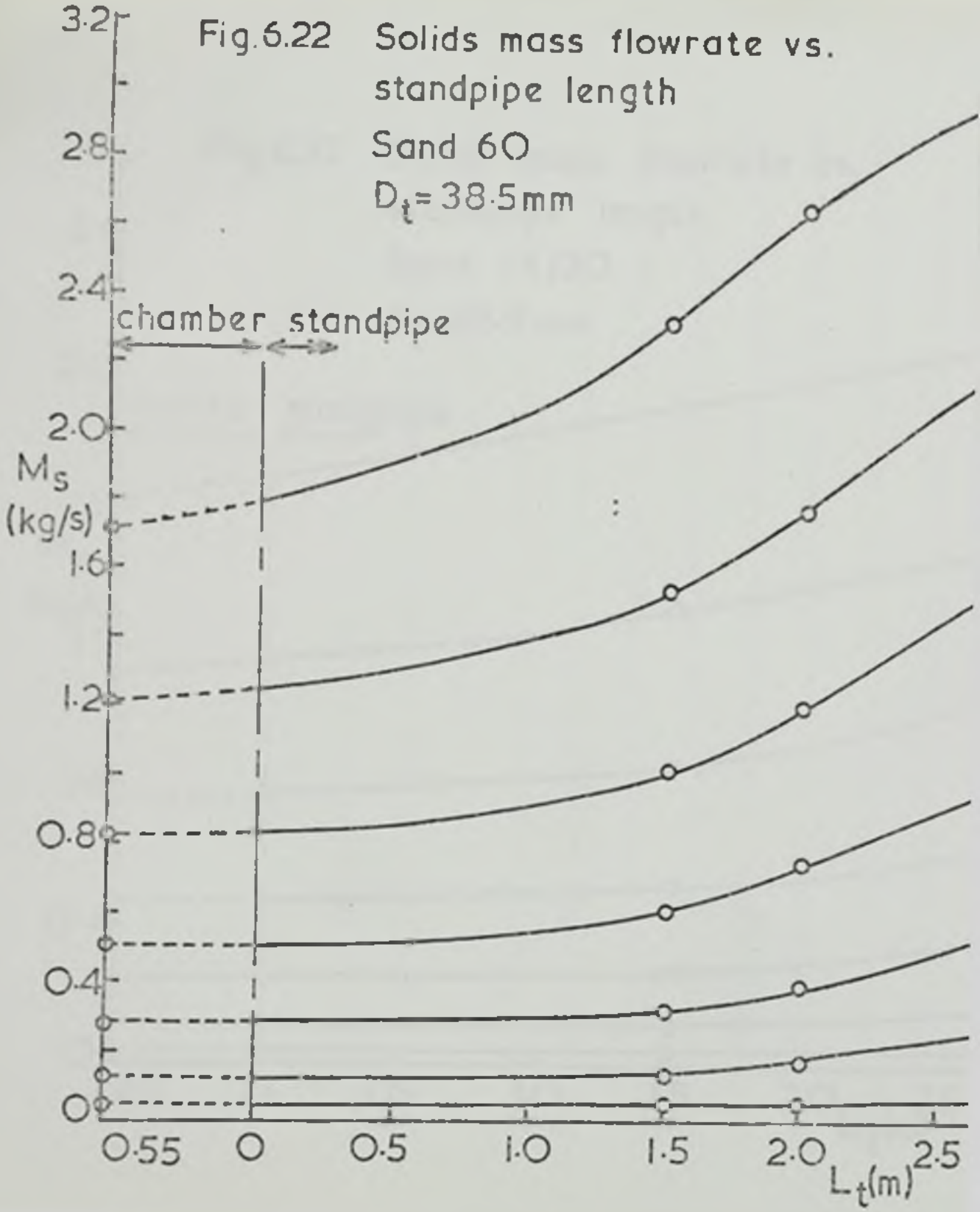
Fig.6.22 Solids mass flowrate vs. standpipe length
Sand 60
D_t = 38.5mm
chamber
standpipe
M_s (kg/s)
3.2
2.8
2.4
2.0
1.6
1.2
0.8
0.4
0
0.55
0
0.5
1.0
1.5
2.0
2.5
L_t(m)

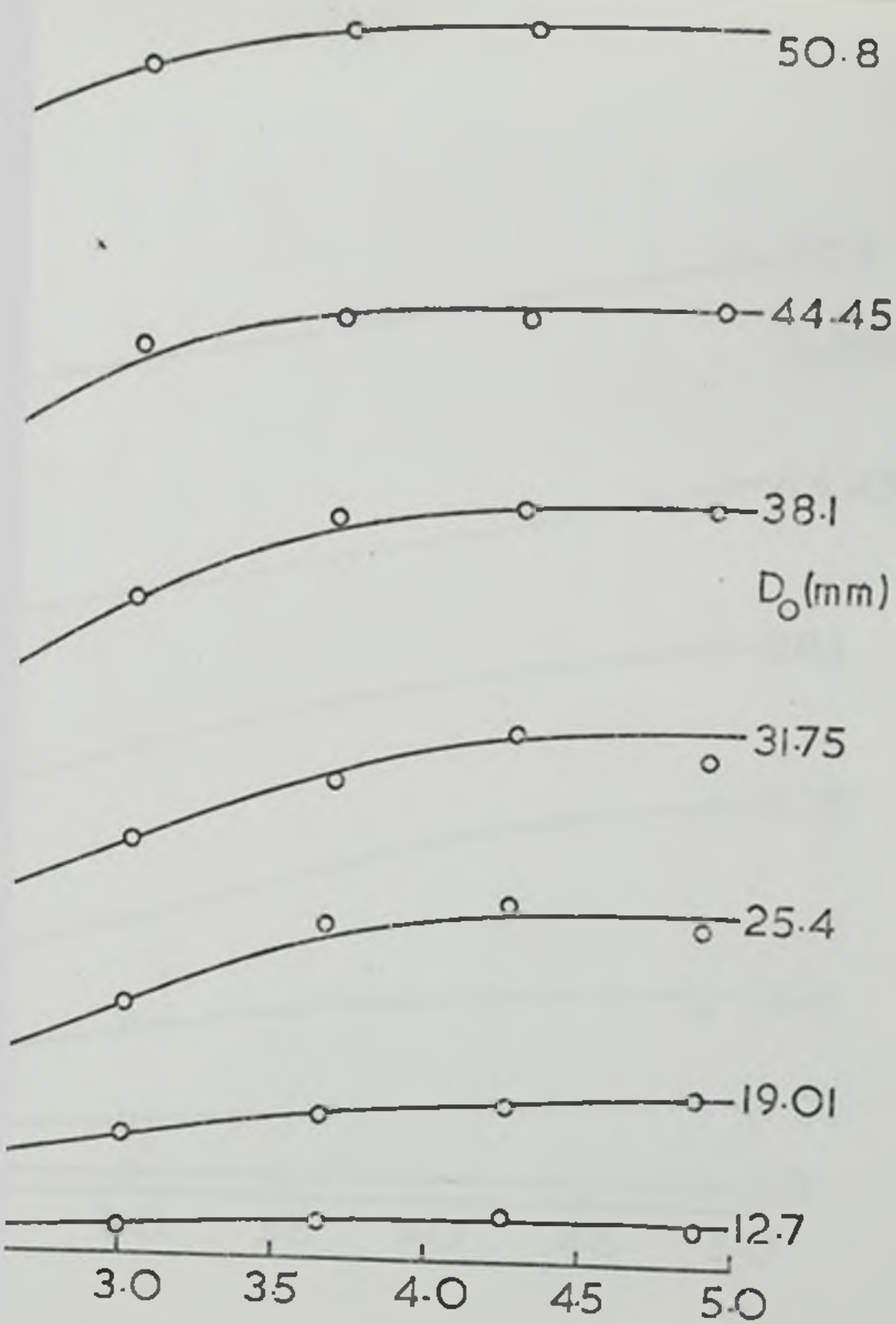
50.8
44.45
38.1
D_o(mm)
31.75
25.4
19.01
12.7
3.0
3.5
4.0
4.5
5.0

Fig.6.22 Solids mass flowrate vs. standpipe length
Sand 14/30
D_t = 38.5 mm

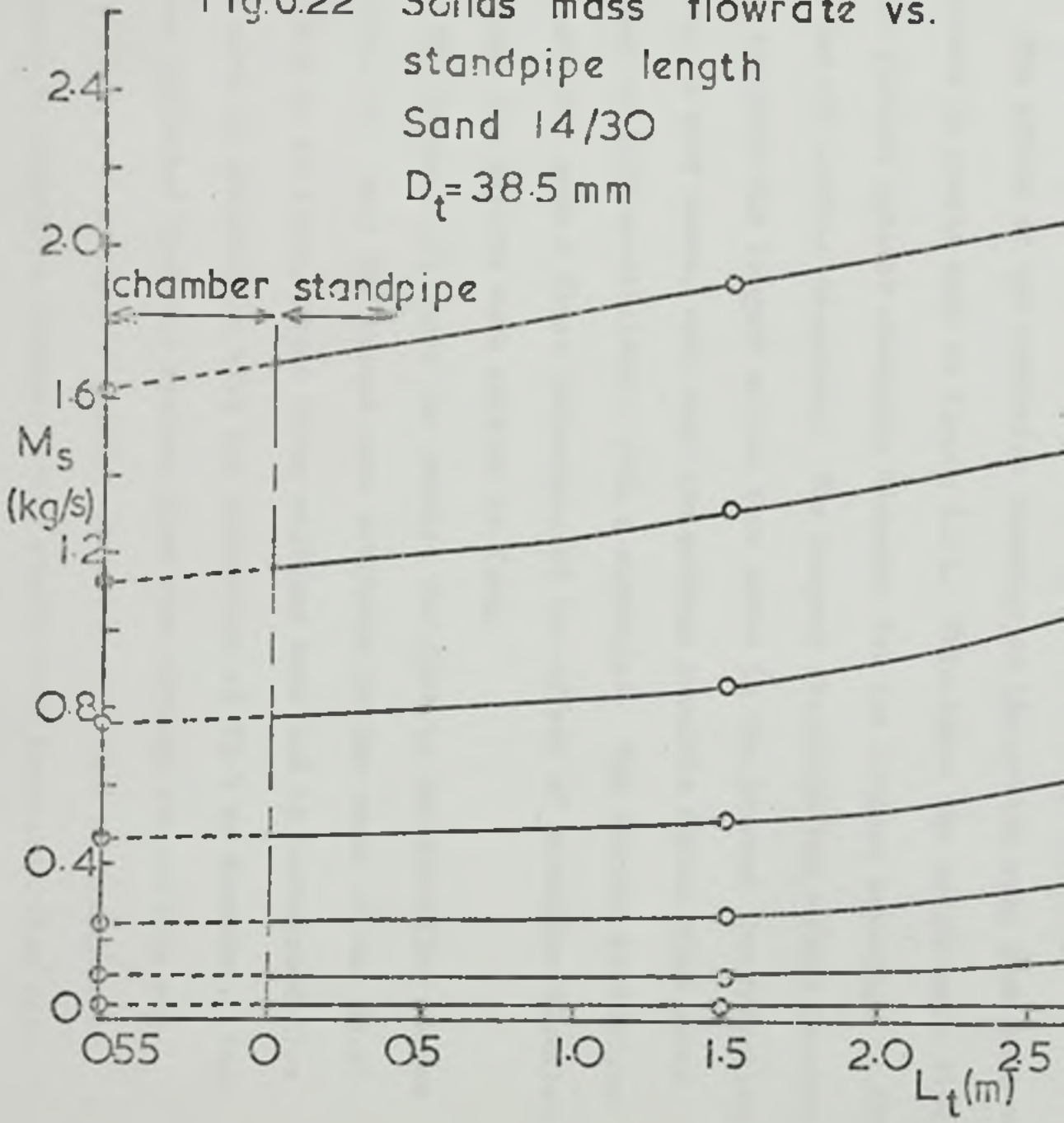

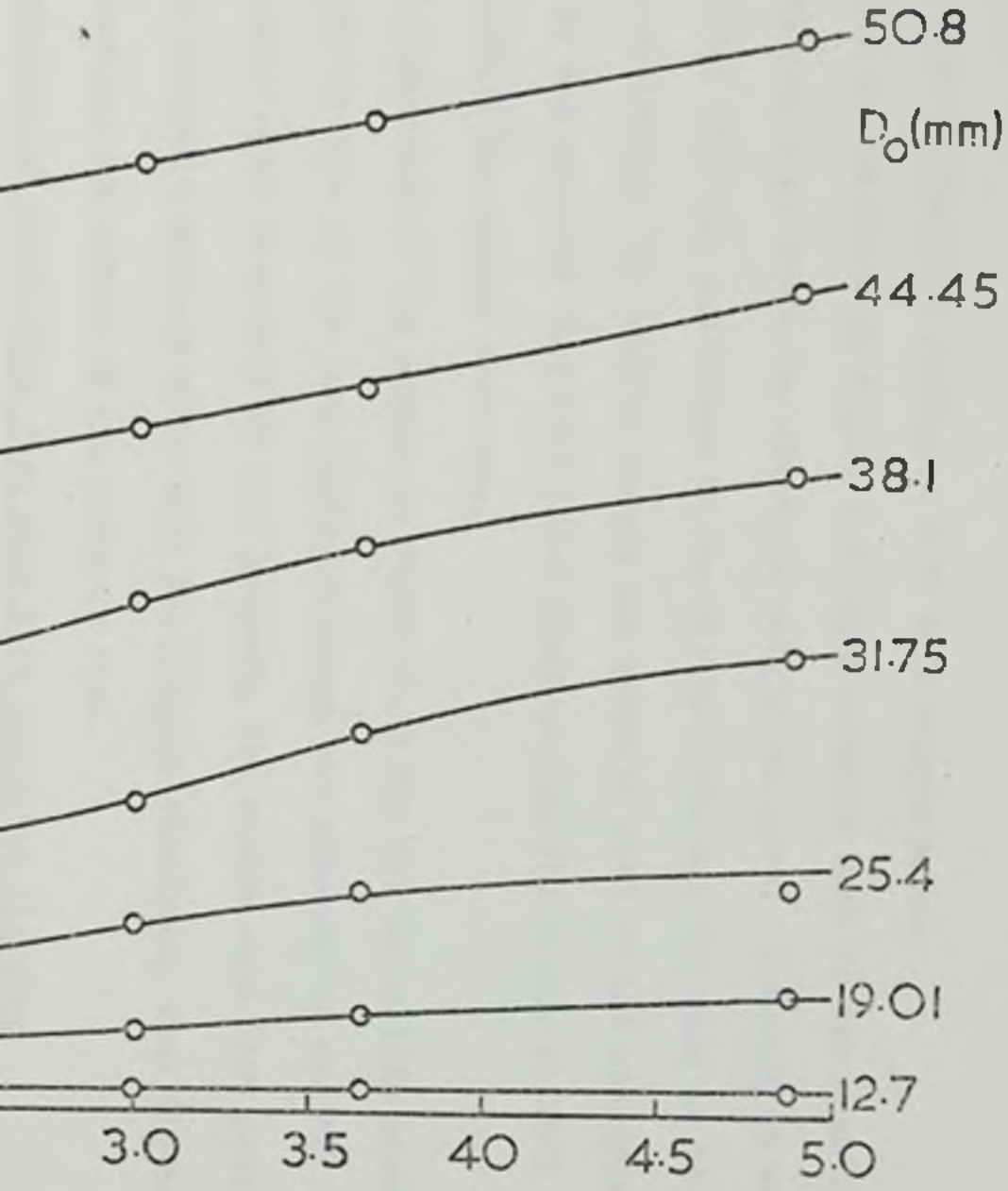
50.8
D_o(mm)
44.45
38.1
31.75
25.4
19.01
12.7
3.0
3.5
4.0
4.5
5.0

these were represented in Figure 6.21 by a single curve.

The curves shown in Figure 6.22 were extended back to the gravity flow values, i.e. where the standpipe length was zero. Although it was recognised that the conditions in the chamber were not the same as those in the standpipe, the chamber length was taken as part of the standpipe, since it was expected that this added distance for the solids to fall would affect the solids flow rate.

A comparison of the graphs in Figure 6.22 for the two solids showed that, in the case of the sand 14/30, although the elements of the 'S' shape curve shown with sand 60 were present, the solids mass flow rate had not reached a maximum value with the longest standpipe, thus further demonstrating the effect of the particle size.

The Variation of Solids Mass Flow Rate with Standpipe Diameter

The effect of the standpipe diameter on the solids mass flow rate was depicted in graphs such as Figure 6.23. This shows the solids mass flow rates plotted against standpipe diameter for the longest standpipe (4.875 m) and for all orifice diameters. The longest standpipe was chosen because this produced the largest solids flow rates in the present investigation which, in many cases, were near the maximum possible solids flow rates through an orifice attainable with a standpipe. The shorter standpipes did not give such a clear indication of the effect of standpipe diameter, although the results were similar in form.

The Figure 6.23 shows the results for flow in the free-flow regime for sand 60. Only two points were available in the cases of the 44.45 and 50.8 mm orifices, since these orifices resulted in restricted-flow when used in conjunction with the standpipes of 25.5 mm diameter. The curves indicated that the maximum flow rate through the orifice was achieved by a standpipe of similar diameter, and that an increase or decrease in standpipe diameter would result in a decreased flow rate through that orifice. Thus, following this trend, the graphs were freely

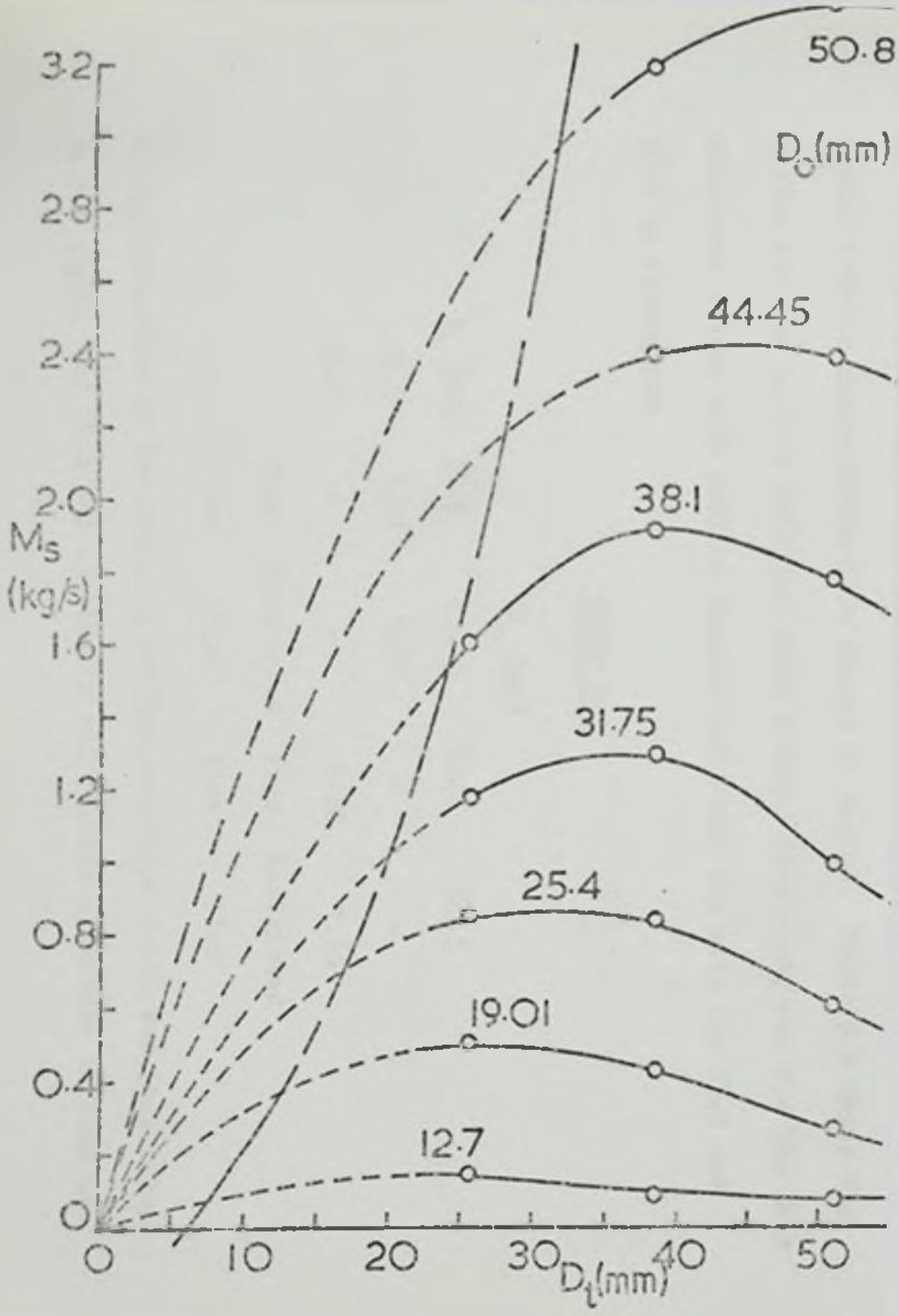
3·2
2·8
2·4
2·0
1·6
1·2
0·8
0·4
0
M_s (kg/s)
0
10
20
30
40
50
D_i(mm)
D_o(mm)
50·8
44·45
38·1
31·75
25·4
19·01
12·7

Fig.6.23 Solids mass flowrate vs. standpipe diameter
Sand 60 L_t = 4.875 m

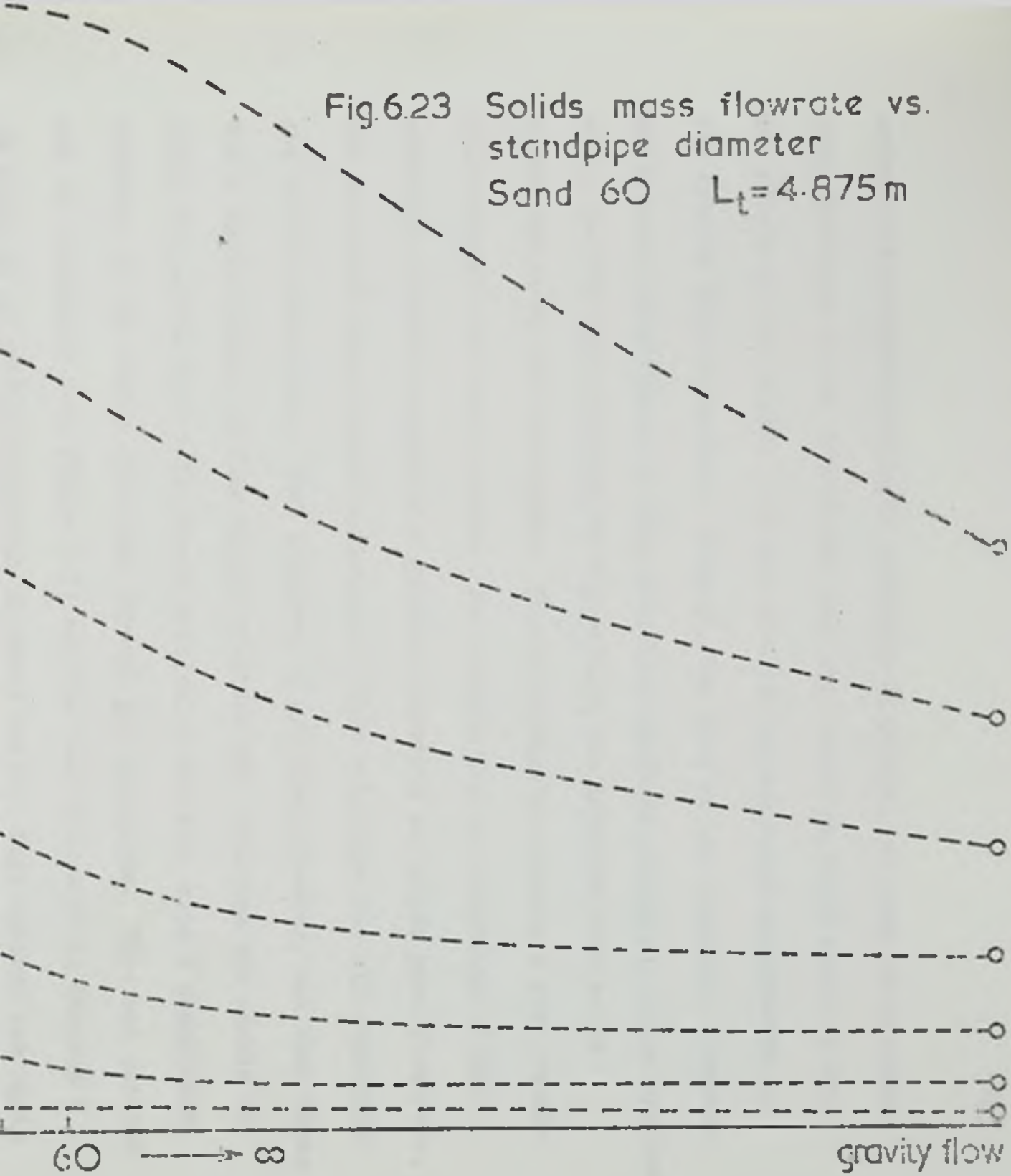

extrapolated towards infinite standpipe diameter. At such large standpipe diameters it was considered that the standpipe would cease to have any effect on the solids flow and that the system would approximate to the gravity flow situation. Clearly, the size of the standpipe diameter which would approximate to this situation would be dependent on the orifice size, and the extrapolation in Figure 6.23 was intended only as an illustration of this principle. The extrapolation towards a zero standpipe diameter was not so clear. The results for the reduction of the standpipe diameter suggested a gradual reduction in solids mass flow rate, and the graph shows an extrapolation of this situation for all standpipe and orifice diameters. What occurred in practice, however, was that there was a sudden change of flow regime wherever the standpipe was unable to carry the solids flow rate from a particular orifice, with a consequent decrease in the solids flow rate through the apparatus. This was pointed out in connection with Figure 6.21 and has been discussed in Chapter 5 in terms of an orifice/standpipe diameter ratio. This concept was again useful here to characterise this change of regime. Table 6.8 shows the ratios for the largest orifices which allowed free flow, and for the next available larger size orifice (restricted flow) for both the 25.5 and 38.5 mm standpipes.

TABLE 6.8

	D_o (mm)			
D_i (mm)	38.5	44.45	50.8	63.5
25.5	1.51	1.75	-	-
38.5	-	-	1.32	1.65
	Free flow	Restricted flow	Free flow	Restricted flow

An approximation of the limiting orifice/standpipe ratio was thus taken as 1.6 (8/5), and this was applied to all orifice diameters to find the

corresponding standpipe diameter which just allowed free flow. This resulted in the vertical curve on the left of Figure 6.23, showing the approximate lower limits of standpipe allowing free flow through each orifice diameter.

The Variation of Orifice Pressure Drop with Standpipe Dimensions

Figure 6.24 shows typical examples of the variation of orifice pressure drop with standpipe length for the whole range of orifices. The curves generally exhibited an 'S' shape in the same way as the plots of solids mass flow rate against standpipe length in Figure 6.22. This similarity in form between the curves in Figures 6.22 and 6.24 could not, however, be extended to show any definite dependence of the orifice pressure drop on the standpipe length since, as could be seen from Figure 6.24, the shapes of the curves for the orifices were not sufficiently uniform to lend themselves to further correlation.

The variation of the orifice pressure drop with orifice diameter did not show the same form as the variation of solids mass flow rate with orifice diameter (Figure 6.21). Since it was felt that the permeability of the constant level solids bed above the orifice also had an important effect, in conjunction with the standpipe dimensions, on the air flow rate through the system (see below), it seemed likely that the orifice pressure drop was not only dependent on the standpipe length, but also on the orifice diameter and the solids bed permeability.

Comments on the Effect of the Standpipe

Although it was apparent from these graphs that it was unlikely to be possible to predict the solids mass flow rate through the systems from the consideration of the standpipe and orifice dimensions alone, some general conclusions could be drawn about the discharge of the solids through the system. Figure 6.21 showed that the solids mass flow rate dependency on orifice diameter was similar to that for gravity flow, and that the maximum solids flow rate was determined by standpipe considerations rather than

Fig.6.24 Orifice pressure drop vs standpipe length
Sand 60
D_t = 38.5mm

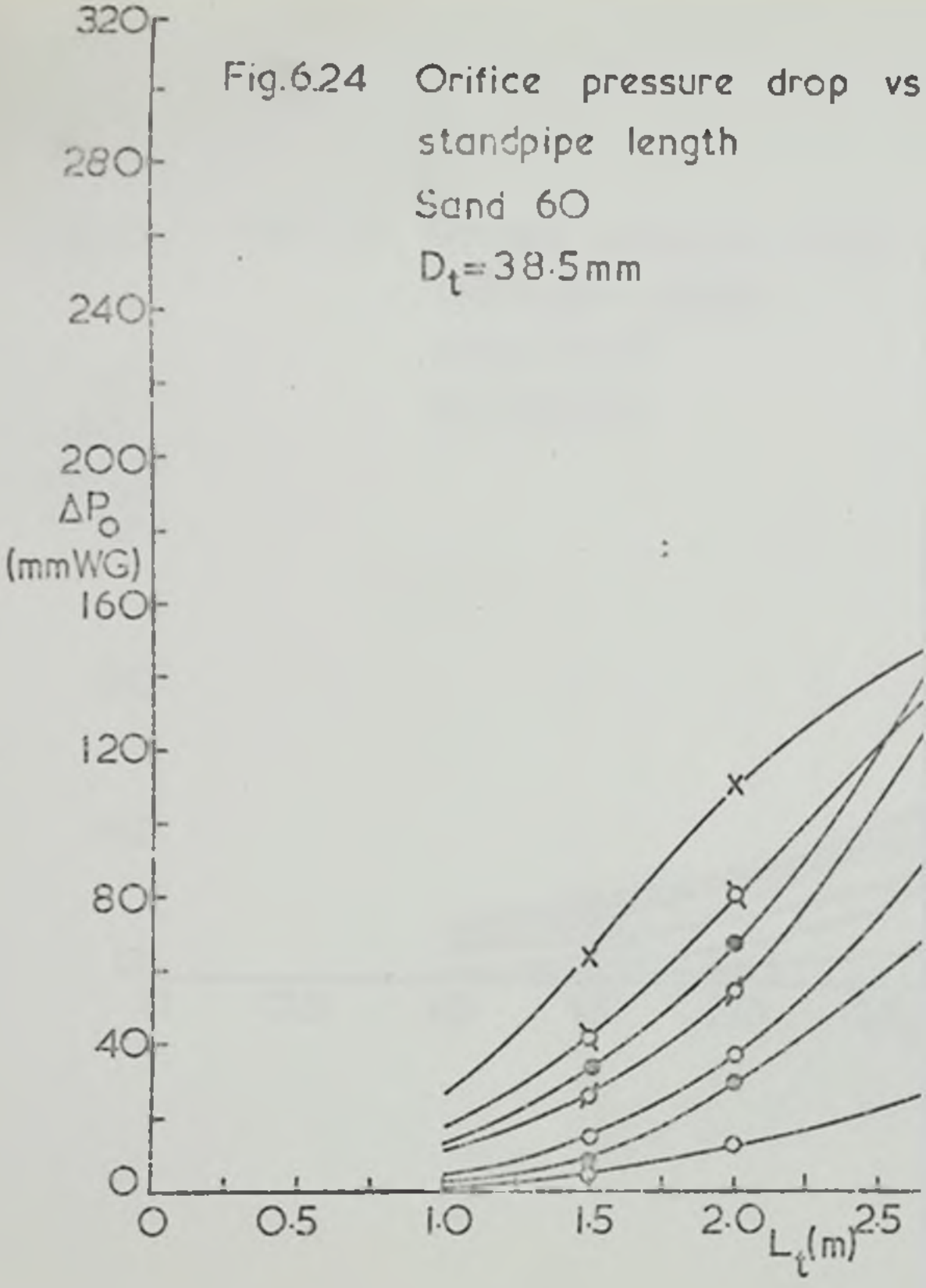

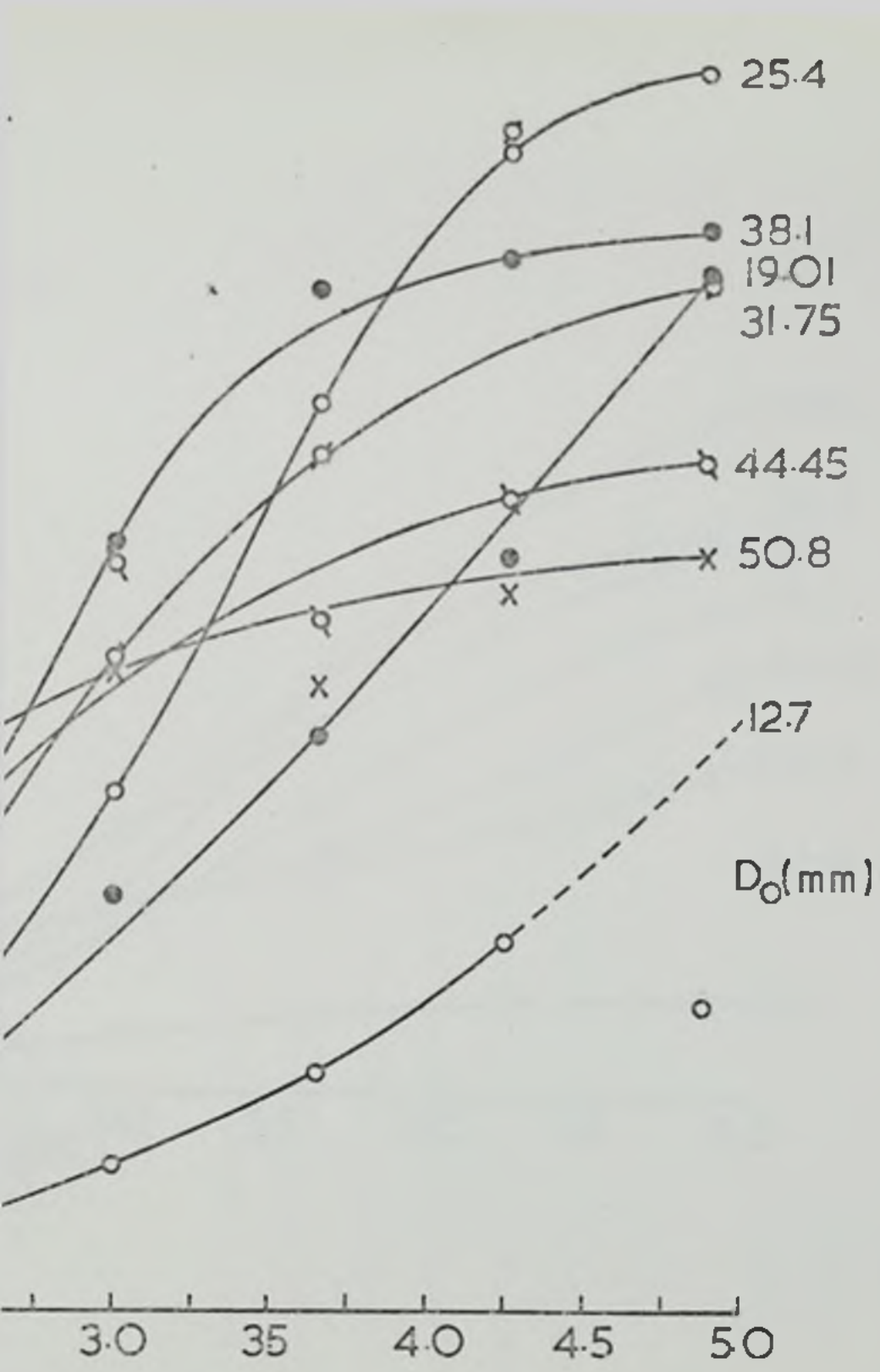
25·4
38·1
19·01
31·75
44·45
50·8
12·7
D_o(mm)
3·0
3·5
4·0
4·5
5·0

Fig.6.24 Orifice pressure drop standpipe length
Sand 14/30
D_t = 38.5mm

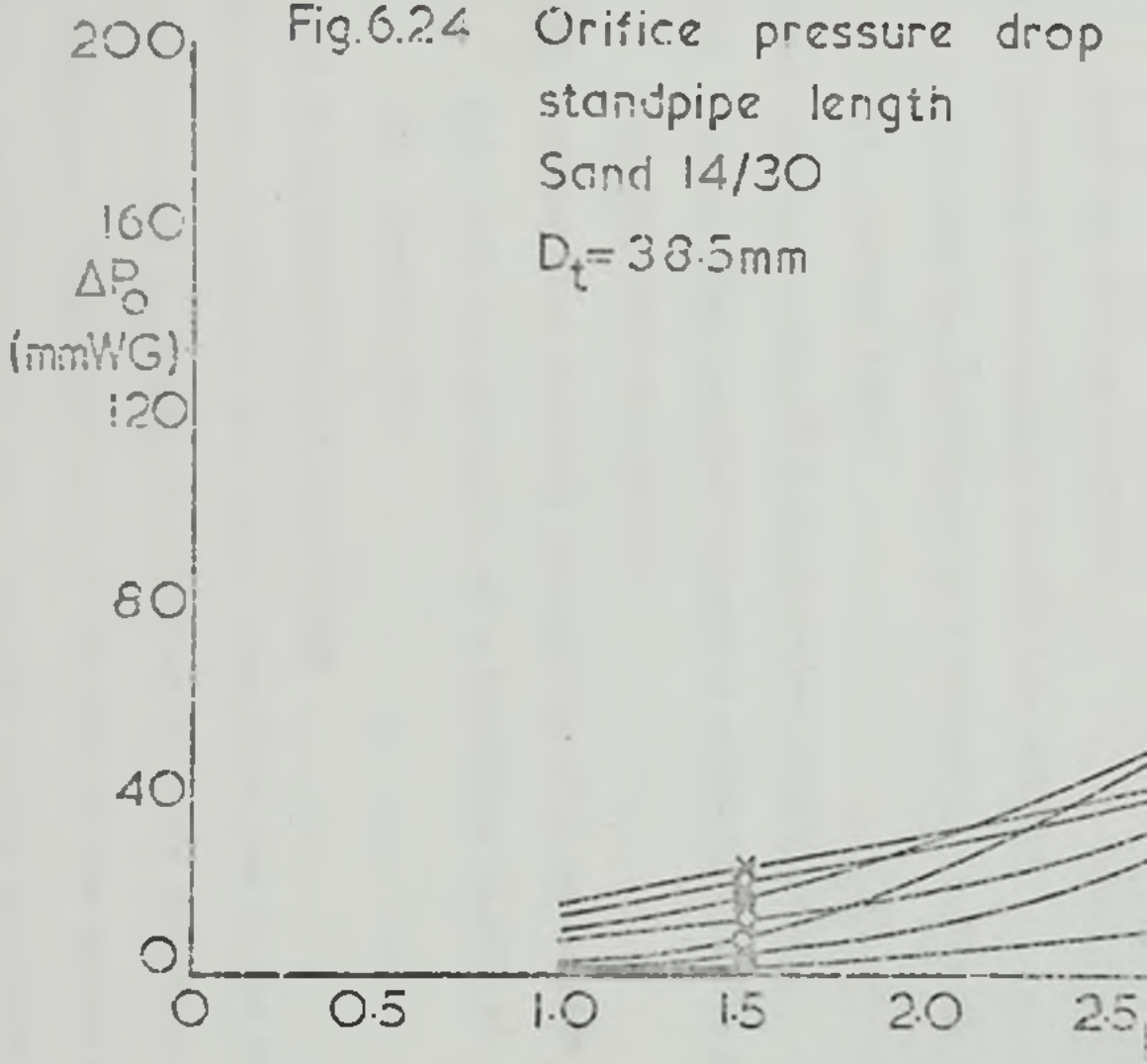

vs.

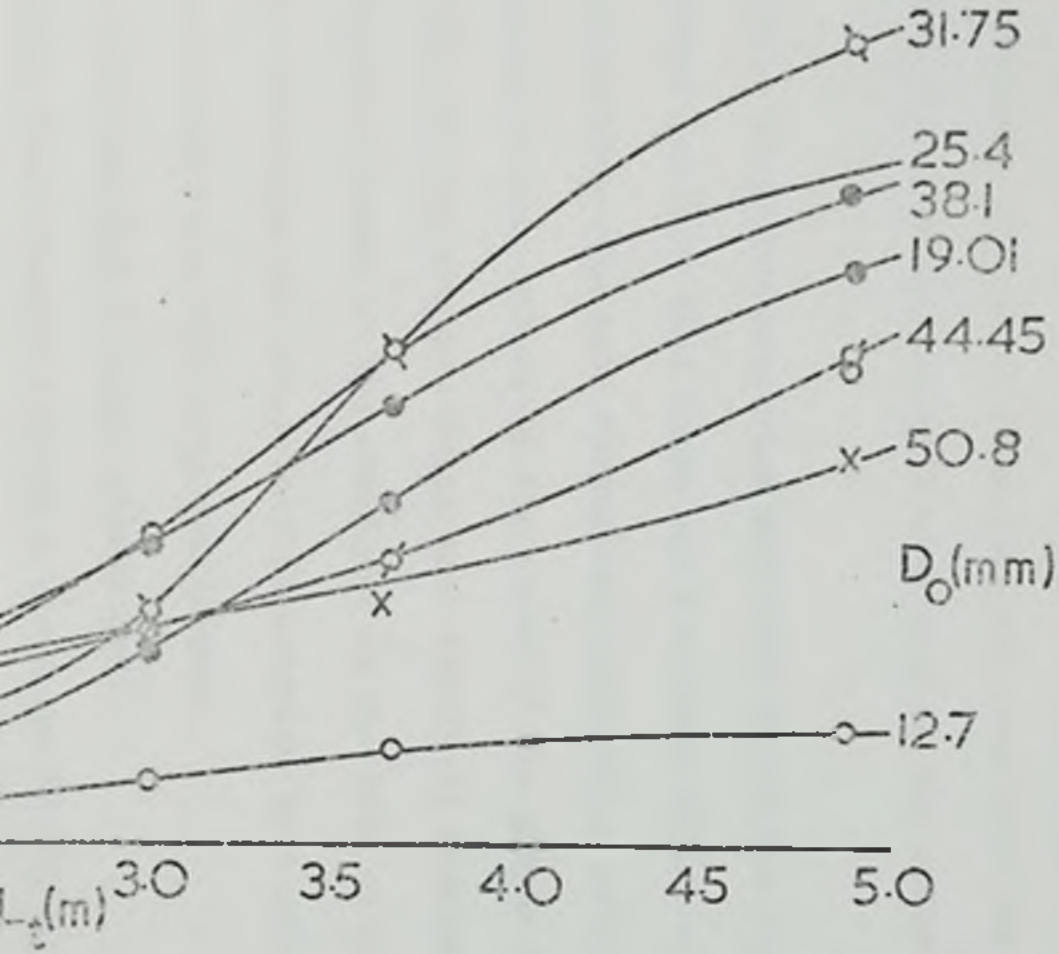

any limitations of flow due to the orifice. The graphs in Figure 6.23 gave some confirmation of this, since for any orifice diameter less than the standpipe diameter the solids flow rate was less than the maximum attainable (at $D_o/D_t = 1$) indicating a reduction in the effect of the standpipe.

The variation of solids mass flow rate with standpipe length in Figure 6.22 showed evidence that there was a maximum effect of the standpipe on the solids mass flow rate through any particular orifice diameter. This was confirmed to some extent by the shape of the graphs in Figure 6.24, showing that the orifice pressure drops were similarly tending to a maximum.

The profound influence of the standpipe on the rate of discharge of solids through an orifice was adequately illustrated by a comparison of solids flow rates under the following conditions:

Sand 60 - for the 38.5 diameter standpipes:

(1) Maximum flow recorded through a standpipe (4.875 m long with the 50.8 mm orifice) 3.20 kg/s

(2) Maximum flow through the 38.1 mm orifice

(a) with the influence of a standpipe (4.875 m) 1.95 kg/s

(b) gravity flow 0.82 kg/s

Sand 14/30 - for the 38.5 mm diameter standpipes:

(1) Maximum flow recorded through a standpipe (4.875 m long with the 50.8 mm orifice) 2.44 kg/s

(2) Maximum flow recorded through the 38.1 mm orifice

(a) with the influence of a standpipe (4.875 m) 1.45 kg/s

(b) gravity flow 0.761 kg/s

Suggested Flow Mechanism for the System

In order to achieve the higher flow rates due to the standpipe effect, the particles must be moving faster than in their discharge through a simple orifice. A consideration of the flow of the solids and air through the system was able to cast some light on how the standpipe affected the

flow rate of the solids. The suction effect of solids falling through a standpipe has previously been recognised (36, 67, 73) and, although there have been various attempts at an explanation, it was felt that a further clarification of the effect of the standpipe on the solids flow rate was necessary in the present work.

The total effect of the solids falling through the standpipe was, of course, to induce an air stream flowing co-currently with solids away from the chamber and thus creating a reduced pressure within the chamber. The resistance (i.e. permeability) of the constant depth solids bed above the orifice controlled the size of this reduced pressure in the chamber, hence producing a pressure difference across the orifice and the solids bed, and inducing an air flow through the bed at a net velocity greater than the initial solids velocity - the percolating air. The effect of this percolating air flow was to increase the solids velocity (and hence the solids mass flow rate) due to the drag effects between a faster moving current of air and the solids particles. After discharge from the hopper, gravitational forces were free to act on the solids in the orifice, the chamber and the standpipe. Thus, due to gravitational acceleration, the particle velocity exceeded the air velocity after some short distance, whereupon the mutual solids-air drag forces reversed and acted against the solids motion, creating the co-current air flow through the standpipe. The increased solids mass flow rate due to the influence of the air flow at the orifice created a further increase in co-current air flow rate which, in turn, reduced air pressure in the chamber and increased the air and solids flow rates through the orifice. The system came to equilibrium when the resistance of the constant depth solids bed and the orifice to the air flow was balanced by the drag forces inducing the air flow in the standpipe. In the practical situation, this dynamic equilibrium was reached almost instantaneously at the start of each run, the pressures in the chamber and throughout the standpipe remaining stable (except for slight oscillations

due to inhomogeneities in the solids flow) throughout the duration of each run. Clearly then, the effect of the standpipe on the solids flow rate could not be described from a consideration of the system within the standpipe alone, since the air flow rate (which determined the pressure in the chamber) was dependent not only on the solids flow rate but also on the resistance of the solids bed and orifice to air flow. With this in mind, it was not surprising that it was not possible to produce any direct correlation from the graphs of orifice pressure drop and solids mass flow rate with standpipe dimensions - Figure 6.24.

Using this tentative description of the system and the observations of the solids flow, further elucidation could be offered for the results presented in Figures 6.21 and 6.24.

From Section 6.6, it was seen that the increase in solids mass flow rate through the standpipe was dependent on the increased orifice pressure drop, and consequently on the increased air flow rate. Since these were both observed to increase with the standpipe length, it was felt that the resulting increased air flow rate went some way to explaining the fluid-like nature of the solids flow rate correlation shown with the longer standpipes in the discussion of Figure 6.21. This was also seen to be consistent with the explanation of the air-induced flow of solids through the orifice given in Chapter 3.

Visual observations of the solids stream in the chamber showed that it seemed to flow from the orifice to the standpipe entrance in a fairly compact core, with only a little scatter at the edges. At the entrance to the standpipe there was some 'solids turbulence' (Chapter 5) thought to be due to this slight scatter from the stream passing through the chamber, although there was no solids build-up observed in the chamber. In the case of certain orifices of larger diameter than the standpipe diameters, the stream core in the chamber was observed to decrease in diameter during its passage, so entering the standpipe, and with apparently

a similar degree of 'turbulence' to that observed for the smaller orifices. Still further increase of orifice diameter showed a decrease in solids flow rate, the flow regime changing from free flow to restricted flow (Figures 6.21, 6.23 and Chapter 5).

In the case of restricted flow, it was observed that the decrease in diameter of the stream core was not sufficient to allow all the solids to enter the standpipe directly. The solids which then collected in the chamber about the entrance to the standpipe apparently interfered further with the stream core, in effect interposing an additional resistance before the standpipe entrance, causing the build-up in the chamber. As a result of this solids build-up and the separation of the solids core from the standpipe, the flow stabilised and the controlling dimension became the standpipe diameter.

It was tentatively suggested that the change-over from free flow to restricted flow had two possible causes, the diameter of the stream core at the standpipe entrance and the intensity of the solids scatter at the entrance of the standpipe due to wayward particles at the edge of the core. The tendency of such particles to build up was usually counteracted by the co-current air flow, which in most cases overcame the stray velocities and induced the solids to flow into the standpipe. This, in turn, seemed dependent on the chamber length which could also affect the diameter of the stream core at the standpipe entrance, and the standpipe length which could affect both the co-current air flow rate and the solids flow rate. These observations and effects have been discussed more fully in Chapter 5 in connection with the influence of the chamber on the solids flow rate.

The examination of the effect of the standpipe length on the solids mass flow rate and orifice pressure drop gave further insight into the conditions within the standpipe. As shown above, it was possible for both solids flow rate and orifice pressure drop to achieve maximum values with increase in standpipe length, and thus the total drag effects of the solids and air

in the standpipe also tended to a maximum. If, at these limiting values of standpipe length, the total drag effect of the solids flow in the standpipe could be regarded as 'drag effect per unit length of standpipe', then clearly, for standpipe lengths above the limiting value, this 'drag effect per unit length' must show a decrease with increasing standpipe length.

Comparison of these results with those of previous workers in this field was not very rewarding - many of the features observed had not been previously reported, although some rather general agreement was shown. Only Evans (36) used a similar apparatus both in terms of size and the inclusion of a chamber between the orifice and the standpipe. Although he only used one length of standpipe (3.650 m), the form of his plots of solids mass flow rate against orifice diameter was in good agreement with present results. Other workers connected the standpipes directly to the base of the hopper, thus making the controlling orifice the standpipe diameter. Using funnels and capillary tubes connected in this way, Bingham and Wikoff (67) demonstrated a linear relationship between solids flow rate and standpipe length and a dependence on the standpipe diameter of the form:

$$M_s = C D_t^{2.65}$$

which was similar to that generally accepted in normal gravity flow (equation 3.11). Since their apparatus was so small (max. D_t = 2.5 mm, L_t = 200 mm), and since the standpipe diameter acted as the orifice diameter, the similarity between this dependence of solids diameter in gravity flow was not surprising. Bulsara et al (50) merely noted the effect of the standpipe, while Miles et al (72) with a larger scale apparatus, but using only two different standpipe lengths, showed that there was some tendency for the solids flow rate toreach a maximum value with increase in standpipe length. Yuasa et al (74), with a small scale

TABLE 6.6

Solids Mass Flow Rates (kg/s)

Sand 60

D_o	Gravity	D_t = 25.5					
		1500	2000	3000	3650	4250	4875
12.7	0.044	0.072	-	0.103	0.136	-	0.147
19.01	0.129	0.235	-	0.348	0.420	-	0.506
25.4	0.282	0.414	-	0.651	0.742	-	0.858
31.75	0.508	0.798	-	0.962	1.034	-	1.192
38.1	0.823	1.187	-	1.373	1.504	-	1.608
44.45	1.213	*	-	*	*	-	*
50.8	1.716	*	-	*	*	-	*
		D_t = 38.5					
		0.049	0.058	0.077	0.101	0.115	0.095
		0.144	0.180	0.308	0.372	0.404	0.430
		0.326	0.390	0.645	0.860	0.923	0.855
		0.610	0.750	1.070	1.230	1.363	1.306
		1.020	1.197	1.688	1.910	1.953	1.945
		1.546	1.780	2.351	2.424	2.440	2.480
		2.320	2.649	3.070	3.173	3.200	3.600
		D_t = 50.5					
		0.045	-	0.058	0.060	-	0.075
		0.134	-	0.190	0.238	-	0.272
		0.295	-	0.409	0.529	-	0.608
		0.543	-	0.671	0.909	-	1.003
		0.878	-	1.159	1.409	-	1.787
		1.301	-	1.652	2.046	-	2.410
		1.925	-	2.501	3.045	-	4.343

* Restricted flow

TABLE 6.6 (contd.)

Solids Mass Flow Rates (kg/s)

Sand 14/30

D_o	Gravity	D_t = 38.5			
		1500	3000	3650	4875
12.7	0.037	0.039	0.049	0.053	0.059
19.01	0.113	0.123	0.186	0.225	0.275
25.4	0.249	0.275	0.424	0.502	0.513
31.75	0.464	0.524	0.700	0.860	1.035
38.1	0.761	0.876	1.157	1.285	1.448
44.45	1.12	1.328	1.555	1.643	1.869
50.8	1.62	1.923	2.145	2.247	2.440

apparatus showed similar 'S' shaped curves in graphs of solids flow rate against standpipe length to those of the present work. Their investigations with different sized glass ballotini also showed higher solids mass flow rates for the smaller sizes, indicating an increased standpipe effect for smaller particles. It was also noted in the present work that the results from the main apparatus agreed well in form with those from the small apparatus (Chapter 5), although no direct comparison was possible due to the different solids used and the inherent limitations of the small apparatus.

6.8 The Flow of Solids through the Standpipe

As previously described, after discharge from the orifice the solids flowed directly through the chamber and into the standpipe set vertically below the orifice. The upper and lower ends of the standpipe were attached to the chamber and flow diverter respectively, via two pneumatically controlled slide valves. During a run, the static pressures throughout the chamber, standpipe and flow diverter were recorded, and the solids hold-up in each standpipe was found by activating the slide valves simultaneously to isolate the standpipe. Thus, by running the apparatus with each standpipe

in conjunction with each of the orifice plates, the effects on the standpipe static pressure profile and the solids hold-up of different solids and air flow rates were found.

The Experimental Determination of Particle Velocities in the Standpipe

Values of pipe solids hold-up (m_p) for both solids are shown in Figure 6.25, plotted against orifice diameter for all standpipes of 38.5 mm diameter (Appendix 6).

The values of standpipe solids hold-up showed a small degree of scatter about the 'best fit' lines (more noticeable in the case of sand 60) which could be attributed, in part, to interference in the slide valve motion by the solids particles. Moreover, these values of standpipe solids hold-up were also dependent on the solids mass flow rate, so that deviations from the curves shown in Figures 6.22 and 6.23 appeared again as similar deviations in Figure 6.26.

At the outset of the present work it had been hoped to obtain detailed experimental information on the particle velocities in the standpipe. Various methods of determining these velocities were considered at that time but all rapidly proved impracticable on closer examination.

It had been hoped to obtain photographic records of the solids stream throughout the whole length of the standpipes during the runs. Again, this proved impracticable owing to the dimensions of the field of interest - the standpipe lengths ranged from 1.500 to 4.875 m with diameters up to 0.05 m, hardly compatible with the cameras and film formats available. Moreover, the difficulties of even illumination over such lengths and the lens effects of such glass tubing added to the problems. In addition, the size of the field of view necessitated the camera being placed a considerable distance from the apparatus (even with the use of a wide-angle lens) which, due to the construction of the laboratory and the relatively short duration of the experimental run time, would have been impracticable.

Since the solids were thought to be accelerating throughout the length

Fig.6.25

Standpipe solids holdup vs. orifice diameter

Sand 60

D_t=38.5mm

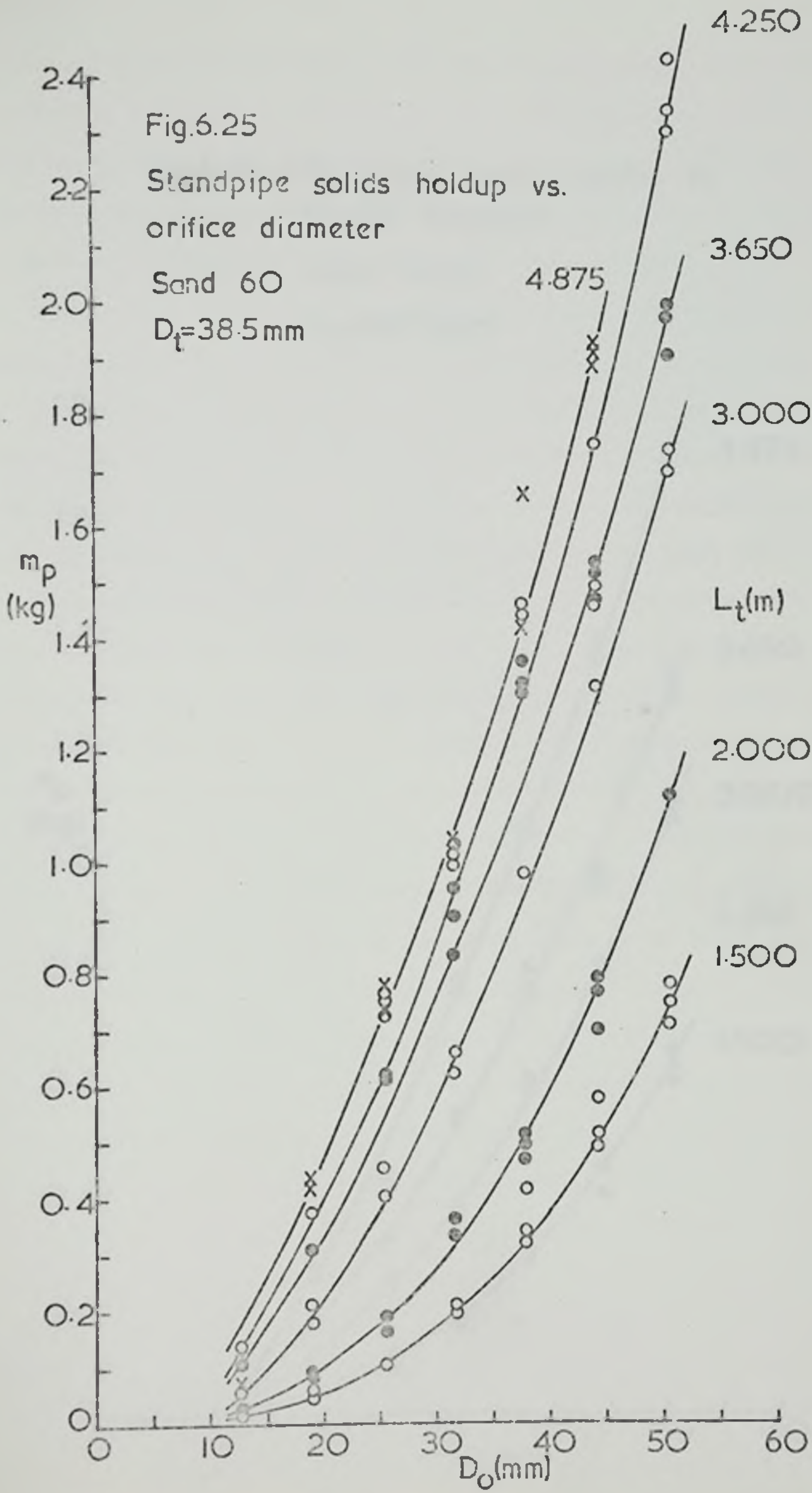

Fig.6.25 Standpipe solids holdup vs. orifice diameter

Sand 14/30

L_t=38.5(mm)

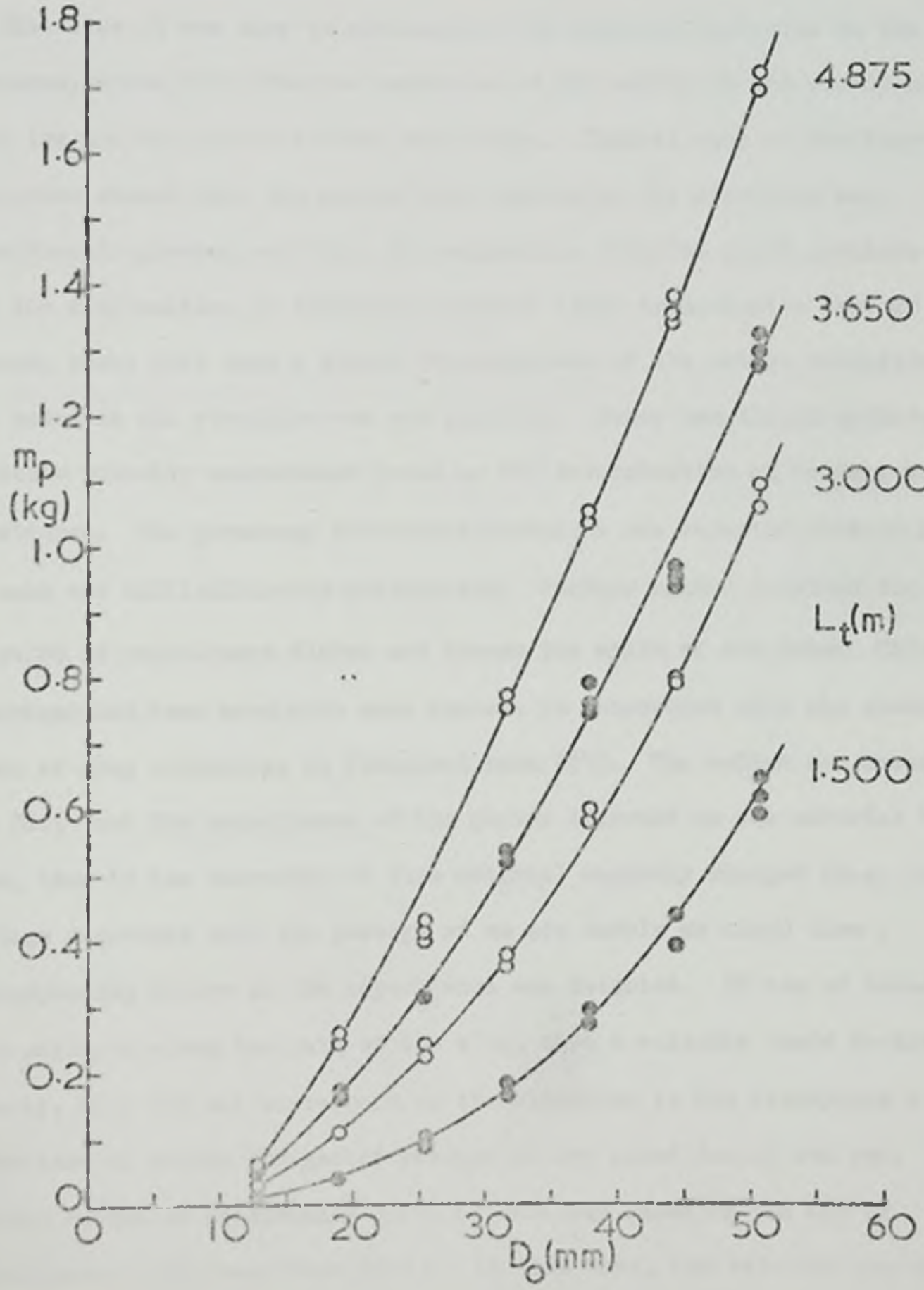

of the standpipe, it was realised that several simultaneous determinations of particle velocity were needed at various positions along the standpipe. This was a major factor in deciding against attempting determination of the solids velocity profile along the standpipe, since the multiplication of the equipment seemed to necessitate prohibitive expenditure.

Double-flash photography had already been tested at one position on a standpipe in conjunction with the small apparatus described in Chapter 5. In that case it was easy to distinguish the separate particles in the pictures, since the effective densities of the solids in the standpipes were very low and the particle sizes were large. Initial runs on the large apparatus showed that the solids bulk density in the standpipe was considerably greater and this, in conjunction with the small particle size and the difficulties of effecting suitable light transmission through the stream, meant that such a direct determination of the solids velocities at any point in the standpipe was not possible. Other non-direct methods of particle velocity measurement based on the determination of voidage were considered. The gamma-ray absorption technique was rejected both on grounds of cost and difficulties in calibration. Another method involved the use of pairs of capacitance plates set across the walls of the tube. This technique had been used with some success in connection with the determination of slug velocities in fluidised beds (88). The method was based on the fact that the capacitance of the plates depended on the material between them, thus if the character of this material suddenly changed (e.g. the voidage decreased with the passage of an air bubble or slug) then a corresponding change in the capacitance was detected. If two of these sets were employed along the path of the slug, then a velocity could be determined. Clearly, this did not correspond to the situation in the standpipes since there were no sudden changes of voidage at any point during the run. A further method of determining particle velocity based on the use of capacitance plates was found (111). In this work, the velocity was derived

from the transit time of the naturally occurring noise pattern between capacitance transducers at two positions along the pipe axis. The method involved extensive use of an on-line digital computer, the facility for which did not exist in the Department at that time.

Thus, since it proved impracticable to obtain detailed information of the solids velocity profile down the standpipe, it was decided to determine the average particle velocity throughout the standpipe. The method of isolating the standpipe by fast-acting valves was based on the methods successfully used to determine the particle velocities in the constant velocity region of pneumatic flow systems (100). From the mass of solids isolated in the standpipe, a value of the average voidage could be found. The volume of the standpipe was $A_t L_t$ and the volume of the solids in the standpipe was given by $\frac{m_p}{\varphi_s}$

so the average standpipe voidage was given by:

$$\bar{e}_p = \frac{A_t L_t - \frac{m_p}{\varphi_s}}{A_t L_t} \qquad (6.42)$$

$$\text{or } m_p = \varphi_s A_t L_t (1 - \bar{e}_p) \qquad (6.43)$$

Now the voidage in any element of the volume $A_t dx$ was related to the solids in that volume by:

$$dm_p = \varphi_s A_t (1 - e_x) dx \qquad (6.44)$$

which for the whole tube gave:

$$m_p = \varphi_s A_t \int_o^{L_t} (1 - e_x) dx \qquad (6.45)$$

so equating equations 6.43 and 6.45:

$$(1 - \bar{e}_p) = \int_o^{L_t} \frac{(1 - e_x) dx}{L_t} \qquad (6.46)$$

The integration of the equations developed in Chapter 3 to model the flow in the standpipe yielded values of the voidage at various points along the standpipes. Thus, from these values, an estimate of the average voidage

in the standpipe could be found and compared with those experimental values. The computation also yielded particle velocities at points along the standpipe and from those values the average particle velocity was similarly calculated. The experimental average particle velocity in the standpipe was found from the continuity equation, using the experimental average voidage.

$$\bar{U}_s = \frac{M_s}{(1 - \bar{\varepsilon}_p) A_t \varphi_s} \qquad (6.47)$$

or, by substituting equation 6.45

$$\bar{U}_s = \frac{M_s L}{\bar{m}_p} \qquad (6.48)$$

Thus the experimental determination of the pipe solids hold-up gave a method for checking the computed voidages and particle velocities in the standpipe from the model developed in Chapter 3.

The Static Pressure Profiles in the Standpipe

The values of the static pressures throughout the apparatus were recorded by photography during the run, and then subsequently read off the film negatives. Figure 6.25 shows examples of these profiles, as obtained throughout the experimental programme. The reproducibility of the pressures throughout the standpipe was generally very good, the final values of the pressures being the average of the three replications at each set of operating conditions. The pressure tappings were set at 150 mm intervals along the standpipe, starting from the top: where these were not a whole number of such intervals, the second interval from the bottom was adjusted as necessary. The pressure at the top of the standpipe was taken as the chamber pressure, while the pressure in the flow diverter box was taken as the pressure at the exit of the standpipe (virtually at atmospheric pressure).

Curve A of Figure 6.26 is typical of the near linear pressure profiles obtained with the smallest orifices (12.7 and 19.01), particularly with the larger particle sand 14/30. This was not a hard and fast rule, of course, and some of the profiles produced with the 19.01 mm orifices tended towards

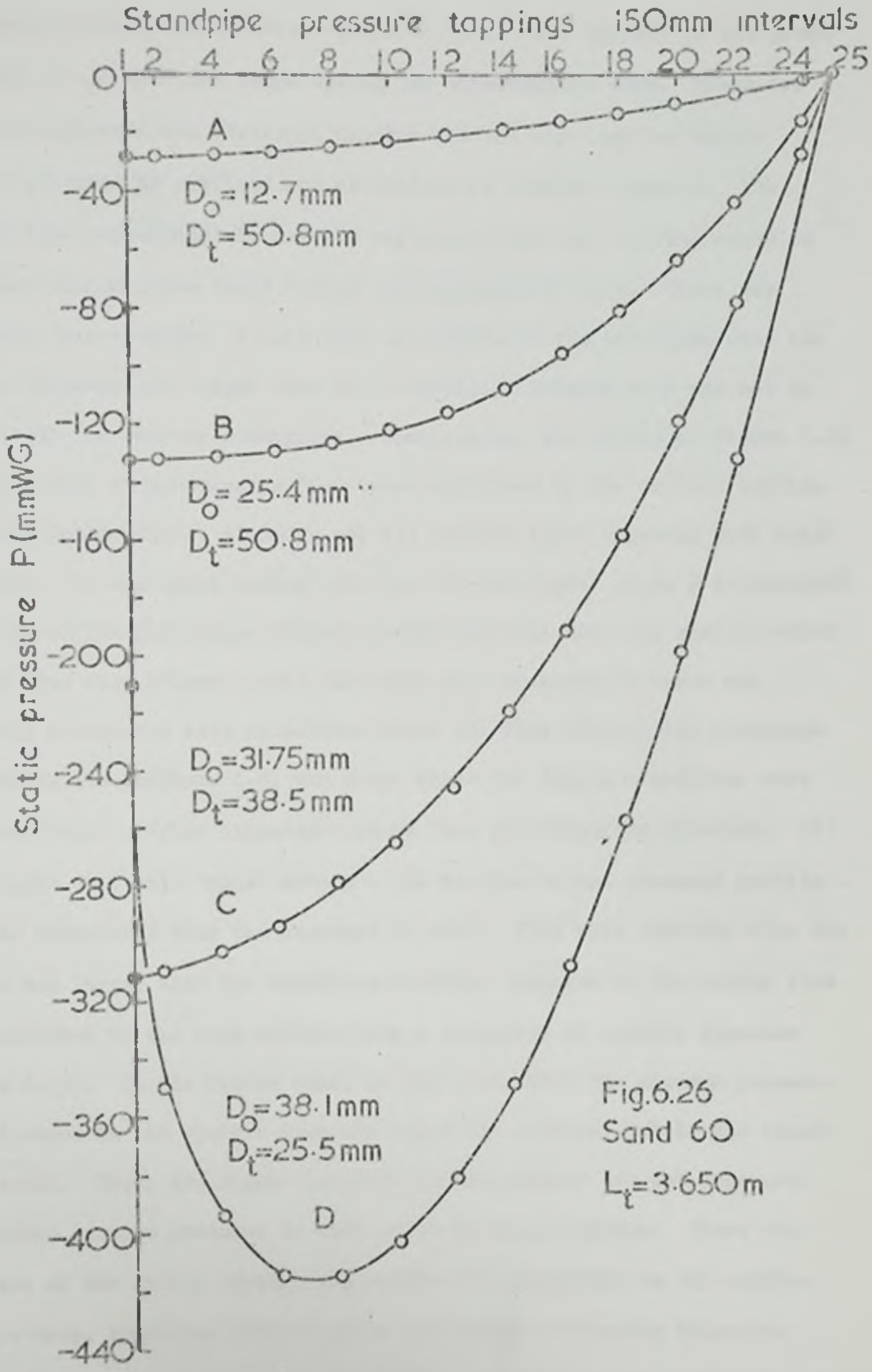

Fig.6.26
Sand 60
L_t=3·650m

the shapes illustrated by curves B and C, which were typical of the great majority of the profiles found during the experimental work. These two curves illustrated the flattened profile and the more regular curves profile produced by orifices and standpipes of similar diameter. The profile type represented by curve D was one of the most extreme examples of a hook-shaped curve found during the experimental work. There was generally some evidence of this type of profile in the standpipe when the orifice diameter was larger than the standpipe, although this was not so marked with the shorter standpipes. Summarising, the curves of Figure 6.26 show the range of pressure profile types exhibited by the various orifice standpipe combinations, although not all profile types appeared with every standpipe. It was worth noting that for the particular curve D illustrated here, the orifice/standpipe diameter ratio was very near the maximum which allowed free flow (Figure 6.23), and that this hook-shaped curve was generally associated with situations where the flow through the standpipe was nearing its maximum, i.e. the cases where the longer standpipes were associated with orifice diameters larger than the standpipe diameter. It was thought that this 'hook' effect - the reverse in the pressure profile - could be associated with the decrease in solids flow rate observed when the orifice was larger than the standpipe diameter compared to the solids flow rate exhibited by the same orifice with a standpipe of similar diameter (Figure 6.23). In the former case, it was clear that the minimum pressure did not occur in the chamber directly below the orifice, but in the standpipe itself. Thus, the higher pressure in the chamber did not represent the maximum suction produced by the solids in the standpipe. Since the flow rate of the solids through the orifice was dependent on the orifice pressure drop, which was determined by the pressure directly below the orifice (i.e. in the chamber), this higher chamber pressure would have the effect of reducing the solids flow rate for the same orifice diameter. It was also thought that the inclusion of the chamber between the top of the

standpipe and the orifice possibly removed this hook effect from the other standpipe-orifice combinations due to its large volume acting as a reservoir and evening out the pressures produced between the standpipe and the orifice. This would have the effect of producing a lower average pressure in the chamber, with a consequent increase in the solids flow rate through the orifice, and may help to explain the lower solids flow rate obtained in the restricted-flow regime compared with those observed in the free-flow regime where the orifice and standpipe diameter were of similar size. An example of this could be seen by looking at Figure 6.21 and Table 6.7, and by comparing the flow through orifices and standpipes of similar diameter under free-flow conditions with the flow through the same standpipe in the restricted-flow regime (this corresponded to the situation where the standpipe joined directly to the base of the hopper), for example:

Sand 60: $L_t = 3.650$

Free flow: $D_o = 38.1$, $D_t = 38.5$ mm, $M_s = 1.91$ kg/s

Restricted flow: $D_o = D_t = 38.5$, $M_s = 1.33$ kg/s

A similar situation was shown in connection with the experimental work on the small apparatus (Chapter 5). Moreover, the paper of Yuasa et al (74), in which the standpipe was shown attached directly to the hopper base, gave hook-shaped pressure profiles in all cases, thus providing some confirmation of the present suggestions.

The Solids Velocities at the Orifice and the Standpipe Inlet

The values of the solids and the air velocities at the orifice were estimated from the calculated voidage values at the orifice (Section 6.6), using equation 3.32:

$$U_{so} = \frac{M_s}{A_o(1 - \epsilon_o)\,\rho_s}$$

$$U_{so} = \frac{Q_{at}}{A_o \epsilon_o}$$

Typical values of the estimated velocities at the orifice are shown in Table 6.9 for various orifice diameters and standpipes for both solids.

TABLE 6.9

Examples of Solids and Air Velocities at the Orifice

Sand 60

D_t = 25.5 (mm)

D_o (mm)							
25.4	L_t (m)	1.500	3.000	3.650	4.875		
	U_{so} (m/s)	0.602	0.946	1.062	1.230		
	U_{ao} (m/s)	2.87	5.96	7.33	8.96		

L_t = 4.875 (m)

D_o (mm)	12.7	19.01	25.7	31.75	38.1
U_{so} (m/s)	1.024	1.298	1.230	1.112	0.997
U_{ao} (m/s)	12.8	11.7	8.96	6.39	4.53

D_t = 38.5 (mm)

D_o = 19.01 (mm)	L_t (m)	1.500	2.000	3.000	3.650	4.250	4.875
	U_{so} (m/s)	0.345	0.431	0.768	0.985	1.038	1.060
	U_{ao} (m/s)	0.706	1.70	4.87	6.87	7.81	8.84

L_t = 2.000 (m)

D_o (mm)	12.7	19.01	25.7	31.75	38.1	44.45	50.8
U_{so} (m/s)	0.320	0.431	0.567	0.635	0.735	0.788	0.892
U_{so} (m/s)	1.32	1.70	2.13	2.16	2.28	2.28	2.58

D_t = 50.8 (mm)

D_o = 38.1 (mm)	L_t (m)	1.500	3.000	3.650	4.875
	U_{so} (m/s)	0.537	0.738	0.866	1.129
	U_{ao} (m/s)	0.757	2.33	3.29	5.52

L_t = 3.650 (m)

D_o (mm)	12.7	19.01	25.7	31.75	38.1	44.45	50.8
U_{so} (m/s)	0.384	0.581	0.740	0.824	0.866	0.910	1.015
U_{ao} (m/s)	2.41	3.33	3.91	3.82	3.29	3.19	3.35

Range of solids velocity at the orifice: 0.257 - 1.298 m/s.

TABLE 6.9 (contd.)

Examples of Solids and Air Velocities at the Orifice

Sand 14/30

D_t = 38.5 (mm)

D_o = 44.45 (mm)	L_t (m)	1.500	3.000	3.650	4.875		
	U_{so} (m/s)	0.629	0.777	0.804	0.876		
	U_{ao} (m/s)	2.04	3.76	4.24	5.42		
L_t = 3.000 (m)	D_o (mm)	12.7	19.01	25.4	31.75	38.1	44.45	50.8
	U_{so} (m/s)	0.286	0.512	0.634	0.704	0.742	0.772	0.798
	U_{ao} (m/s)	3.00	5.45	5.90	4.85	4.44	3.75	3.29

Range of solids velocity at the orifice: 0.207 - 0.955 m/s.

TABLE 6.10

Examples of Solids Velocities at the Entrance to the Standpipe

Sand 14/30

D_t = 38.5 (mm)

D_o = 44.45 (mm)	L_t (m)	1.500	3.000	3.650	4.875			
	U_{si} (m/s)	3.34	3.38	3.38	3.40	no drag		
	U_{si} (m/s)	3.00	3.03	3.03	3.05	with drag		
L_t = 3.000 (m)	D_o (mm)	12.7	19.01	25.4	31.75	38.1	44.45	50.8
	U_{si} (m/s)	3.30	3.32	3.35	3.36	3.37	3.38	3.38 no drag
	U_{si} (m/s)	2.95	2.98	3.00	3.01	3.02	3.03	3.03 with drag

Range: 3.29 - 3.42; 2.95 - 3.06.

TABLE 6.10 (contd.)

Examples of Solids Velocities at the Entrance to the Standpipe

Sand 60

D_t = 25.5 (mm)

D_o = 25.4 (mm)	L_t (m)	1.500	3.000	3.650	4.875			
	U_{si} (m/s)	3.34	3.42	3.45	3.51	no drag		
	U_{si} (m/s)	2.60	2.65	2.68	2.71	with drag		
L_t = 4.875 (m)	D_o (mm)	12.7	19.01	25.4	31.75	38.1		
	U_{si} (m/s)	3.44	3.53	3.51	3.47	3.43	no drag	
	U_{si} (m/s)	2.66	2.72	2.71	2.69	2.67	with drag	

D_t = 38.5 (mm)

D_o = 19.01 (mm)	L_t (m)	1.500	2.000	3.000	3.650	4.250	4.875	
	U_{si} (m/s)	3.30	3.31	3.37	3.43	3.44	3.45	no drag
	U_{si} (m/s)	2.56	2.58	2.62	2.66	2.66	2.67	with drag
L_t = 2.000 (m)	D_o (mm)	12.7	19.01	25.4	31.75	38.1	44.45	50.8
	U_{si} (m/s)	3.30	3.31	3.33	3.35	3.36	3.38	3.40 no drag
	U_{si} (m/s)	2.57	2.58	2.60	2.61	2.62	2.63	2.66 with drag

D_t = 50.8 (mm)

D_o = 38.1 (mm)	L_t (m)	1.500	3.000	3.650	4.875
	U_{si} (m/s)	3.33	3.37	3.40	3.47 no drag
	U_{si} (m/s)	2.59	2.62	2.65	2.70 with drag

L_t = 3.650 (m)	D_o (m)	12.7	19.01	25.4	31.75	38.1	44.45	50.8	
	U_{si} (m/s)	3.31	3.34	3.37	3.39	3.40	3.41	3.44	no drag
	U_{si} (m/s)	2.58	2.60	2.62	2.64	2.65	2.66	2.68	with drag

Range of solids velocity at the standpipe entrance: 3.29 - 3.53 no drag

2.57 - 2.72 with drag

The values of solids velocity at the orifice provided the starting point for the subsequent calculations of the velocities throughout the chamber and the standpipe. To determine the solids velocities at the entrance to the standpipe, two different assumptions were made in Chapter 3:

1. The particles fell individually through the chamber with no mutual interference, and their motion was described in terms of a single particle drag coefficient and the relative velocity between the particles and air. This gave a low limit for the particle velocity at the entrance to the standpipe. The solids velocities were calculated from equation 3.35:

$$\frac{dU_s}{dx} = \frac{b - a\,(U_s - U_a)^2}{U_s} \qquad (3.35)$$

where $b = g(1 - \frac{\varphi_a}{\varphi_s})$, $a = \frac{3}{4}\frac{C_D\,\varphi_a}{d_p\,\varphi_s}$

with initial values $U_s = U_{so}$ the particle velocity at the orifice

at $x = 0$ the orifice level.

2. The solids accelerated in the chamber solely under gravitational forces, the fluid drag forces and inter-particle interference being considered negligible (this is the usual assumption made when calculating solids velocities after discharge from a hopper into free space) (14, 87). In this case the solids velocities were calculated from the simple dynamic equation 3.36:

$$U_s^2 = U_{so}^2 + 2gl_c \qquad (3.36)$$

giving a high limit for the particle velocities at the standpipe entrance. Table 6.10 shows a comparison of some typical values of the solids velocity at the standpipe entrance on each hypothesis. The most striking fact shown by this table was the narrow range of particle velocities at the standpipe entrance for both solids and with both methods of calculation. The difference between the pairs of calculated values of solids velocity at the standpipe entrance were, as expected, smaller in the case of sand 14/30, since the particle size was greater than the sand 60, consequently giving

a smaller drag term in equation 3.35. As described previously observations of the solids stream in the chamber showed that in fact it flowed as a tightly packed core with little dispersion during its passage through the chamber. This form of flow was similar to that normally associated with solids discharge from a hopper, except that the stream in this case was not so subject to dissipation (72). In describing this situation, Boothroyd (87) noted, "usually the density of the falling suspension is so high that the solids fall with negligible resistance from the surrounding air. The size of the particles is not very important in this respect." Thus, with this and other (44) recommendations in mind, in conjunction with the observations in the present case, it was decided to adopt the hypothesis assuming no fluid drag in the chamber and calculate the solids velocity at the standpipe from equation 3.36. These values of solids velocity at the entrance to the standpipe were then taken as the initial values for the calculations of velocities lower down the standpipe.

The Integration of the Standpipe Equations

Having obtained values of the initial solids velocities at the standpipe entrance, the equations developed in Chapter 3 were integrated to determine the voidage and solids and air velocities down the length of the standpipe.

$$U_s \frac{dU_s}{dx} = b + a(U_a - U_s)^2 - \frac{f_s U_s^2}{D_t} \quad \text{for } U_a > U_s \qquad (3.46)$$

$$U_s \frac{dU_s}{dx} = b - a(U_s - U_a)^2 - \frac{f U_s^2}{D_t} \quad \text{for } U_s > U_a \qquad (3.47)$$

where $b = g(1 - \frac{\varphi_a}{\varphi_s})$, $a = \frac{3}{4} \frac{C'_D \varphi_a}{d_p \varphi_s}$, $C'_D = C_D(1 - e^{-\frac{wx}{L_t}})$

C_D = single particle drag coefficient.

$$e_o = 1 - \frac{W_s}{A_t \varphi_s U_{sx}} \qquad (3.49)$$

$$U_{ax} = \frac{Q_{at}}{A_t e_x} \qquad (3.49a)$$

these equations were integrated numerically using a Runge-Kutta-Merson routine on the departmental IBM 1130 computer. The external step length was taken as 0.15 m - corresponding to the positions of the pressure tappings on the standpipe - giving an internal (Runge-Kutta-Merson) step length of 0.03 m. Checks using shorter step lengths showed no difference in the results. Initial values of the friction factor f_s and the drag coefficient parameter w were provided and the pressure profile along the standpipe was found by numerically integrating the equation 3.43, using Simpson's Rule.

$$P_x = g\,\varphi_s \int_o^x (1 - o_x)dx + g\,\varphi_a \int_o^x o_x dx - \frac{M_s}{A_t}(U_{sx} - U_{si}) - \frac{M_a}{A_t}(U_{ax} - U_{ai})$$

$$- 2f_a\,\varphi_a \int_o^x o_x U_{ax}^2\,dx - 2f_s\,\varphi_s \int_o^x (1 - o_x)\,U_{sx}^2\,dx$$

Since this integration assumed atmospheric pressure at the top of the standpipe, the pressures along the standpipe appeared as positive with the maximum value at the standpipe exit. The air at the exit of the standpipe was, in practice, at atmospheric pressure, so the true pressure profile was found by subtracting the calculated pressure at the standpipe exit from the pressure value at each point along the standpipe. In this form the calculated pressures and the experimental pressures could be compared.

The average velocity throughout the standpipe was also calculated and compared to the experimental value for the average particle velocity found from equation 6.48. Thus, by comparing both the experimental and calculated pressures in the standpipes and the experimental and calculated average particle velocities, it was possible to obtain new estimates of the two unknown factors f_s and w. The drag coefficient parameter w was adjusted from the comparison of the average solids velocities, since it was seen from the initial runs that the particle velocities were more dependent on the drag term in equation 3.46 and 3.47 than on the friction term. Since one end of the pressure profile was regarded as fixed (i.e. at the exit from the standpipe the air pressure was regarded as at atmospheric for all

runs) it was decided to find the new estimates of the friction factor from a comparison of the calculated and experimental pressure values at the entrance to the standpipe. In practice, the first pressure reading in the standpipe (P_2) was used for this comparison since it was noticed that the pressure reading at the entrance to the standpipe (i.e. the chamber pressure) did not lie on the smooth curve drawn through the other pressure readings in the standpipe, even showing a discontinuity in some cases (Figure 6.27). The final solution of the equations for each run was thus obtained by an iterative process until the limits set on the accuracy were reached. These accuracy limits were set slightly better than the expected experimental accuracy, being 1 mm H_2O for the pressure valve P_2 and 0.1 m/s for the average particle velocity. Thus, from the numerical solution of the equations for each standpipe and orifice diameter, the pressure profiles, the solids and air velocities' profiles, the voidage profile and the parameter w and friction factor f_s were found.

The Standpipe Pressure and Velocity Profiles

Figure 6.27 shows graphs of the experimental and calculated standpipe pressure profiles for each run. The shapes of the pressure profiles lay within the range illustrated by Figure 6.26 and showed the change of pressure profile shape with increasing orifice diameter/standpipe diameter ratio (or increasing flow rate). It was seen that for any one standpipe the slope of the experimental profiles at the top of the standpipe decreased as the solids mass flow rate (orifice diameter) increased. This decrease of the slope of the pressure profile progressed further until, in some cases, the slope became negative at the entrance to the standpipe and a 'hook' shape profile was formed. As previously stated, this 'hook' shape was associated with those orifice-standpipe combinations in which the orifice diameter was larger than the standpipe diameter and in which the longer standpipes were used. Examination of the calculated solids and air velocities in the chamber for such a combination showed that, at the entrance to the standpipe, as had been

NOTATION

Chapter 6, Figure 6.27

Pressure Profiles along the Standpipes

Graph	Orifice diameter (D_o)
A	12.7 (mm)
B	19.01 "
C	25.4 "
D	31.75 "
E	38.1 "
F	44.45 "
G	50.8 "

Experimental Pressure Readings marked O

Theoretical Pressure Profile marked ⌣

Static Pressure P (mm W.G.) below atmospheric against

Standpipe Tapping Positions at 150 mm intervals

measured from the upper (chamber) end of the standpipe.

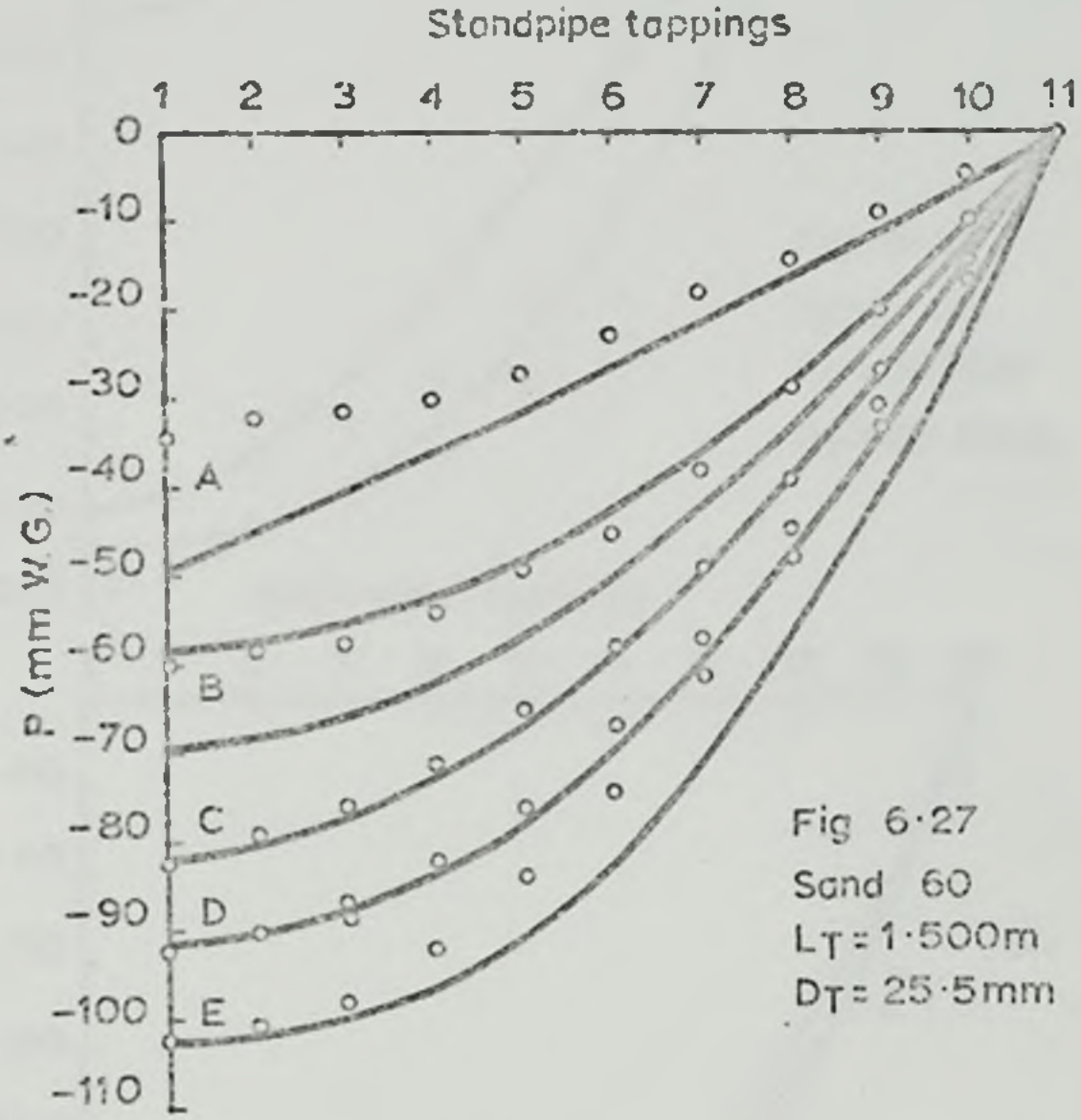

Fig 6·27
Sand 60
L_T = 1·500m
D_T = 25·5mm

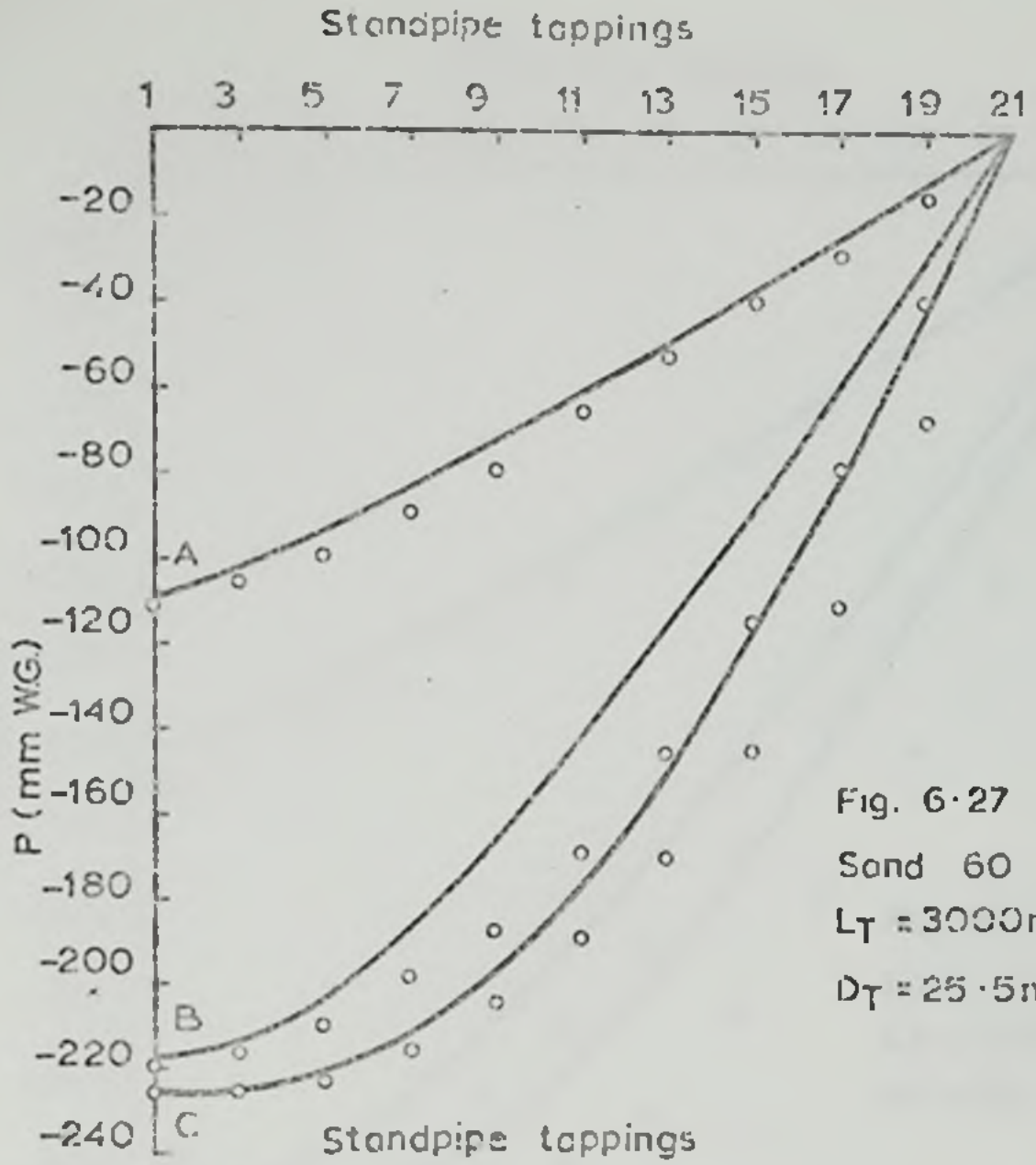

Fig. 6·27

Sand 60

L_T = 3000m

D_T = 25·5mm

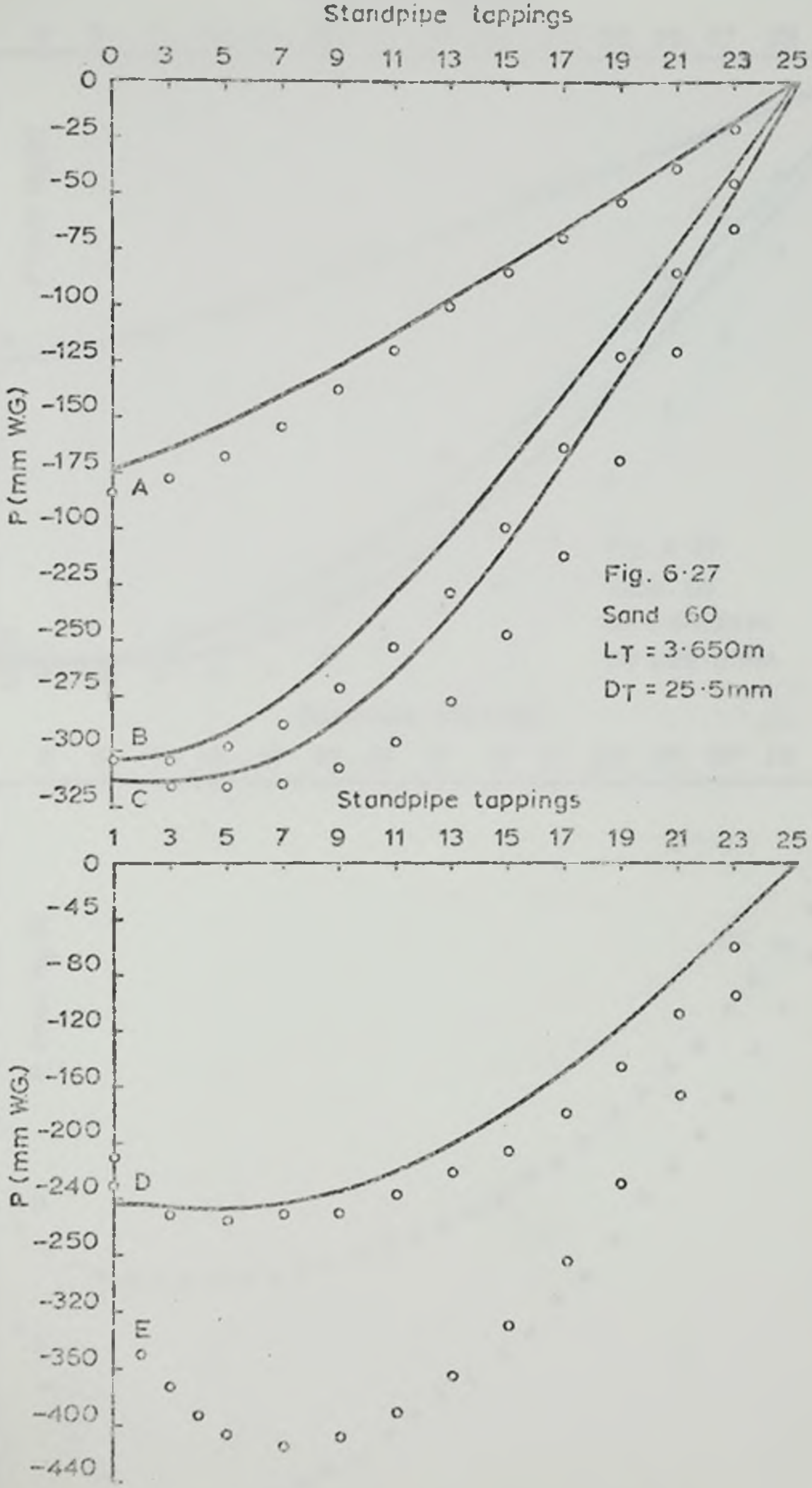

Fig. 6·27

Sand GO

L_T = 3·650m

D_T = 25·5mm

Standpipe tappings

1 3 5 7 9 11 13 15 17 19 21 23 25 27 29 31 33

0 -40 -80 -120 -160 -200 -240 -280 -320 -360 -400 -440

P (mm H_2O)

A

B

C

C

D

Fig 6·27

Sand 60

L_T = 4·875 m

D_T = 25·5 mm

Standpipe tappings

1 3 5 7 9 11 13 15 17 19 21 23 25 27 29 31 33

-50 -100 -150 -200 -250 -300 -350 -400 -450 -500 -550 -600 -650

P (mm H_2O)

D

E

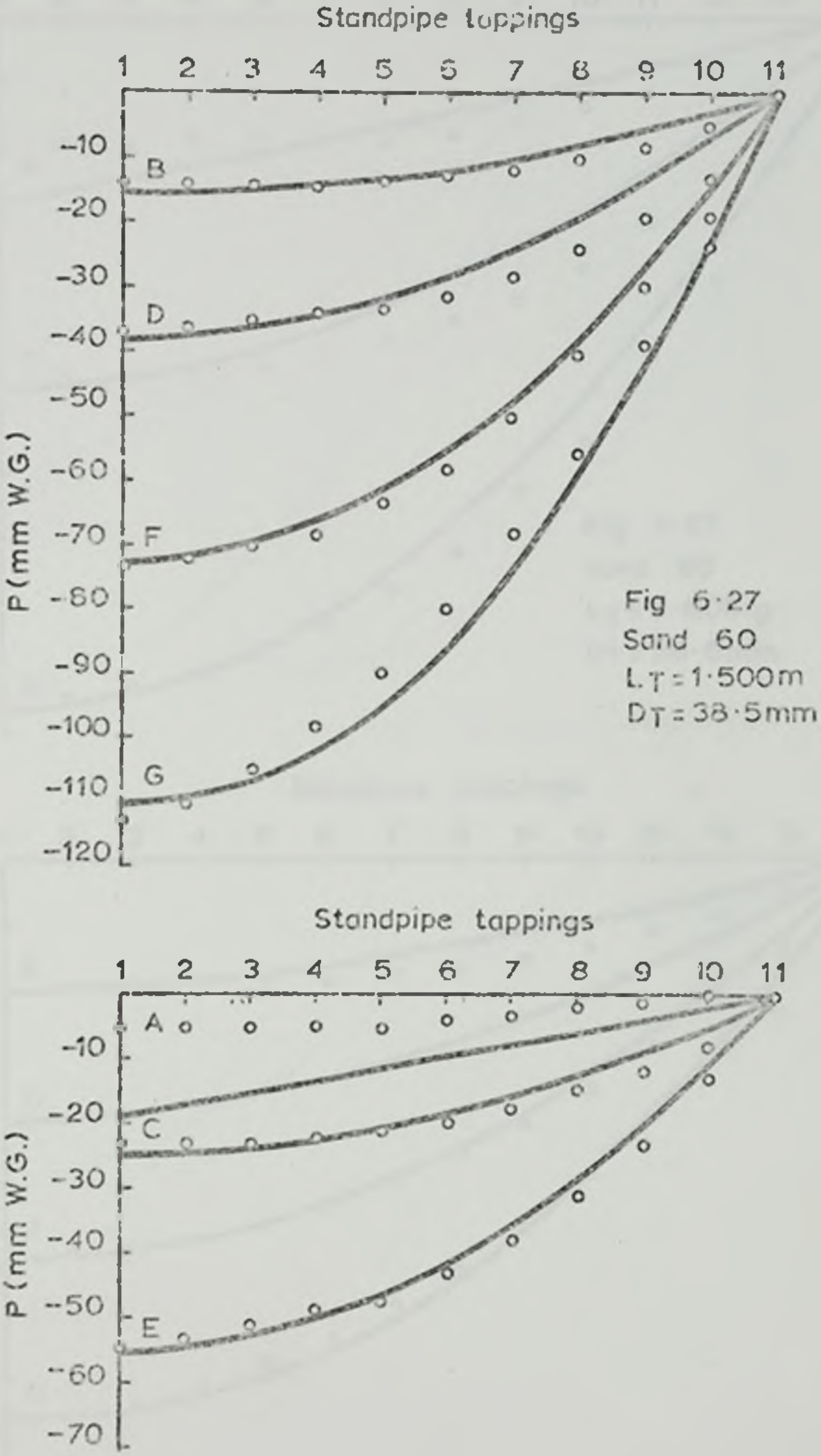

Fig 6·27
Sand 60
L_T = 1·500m
D_T = 38·5mm

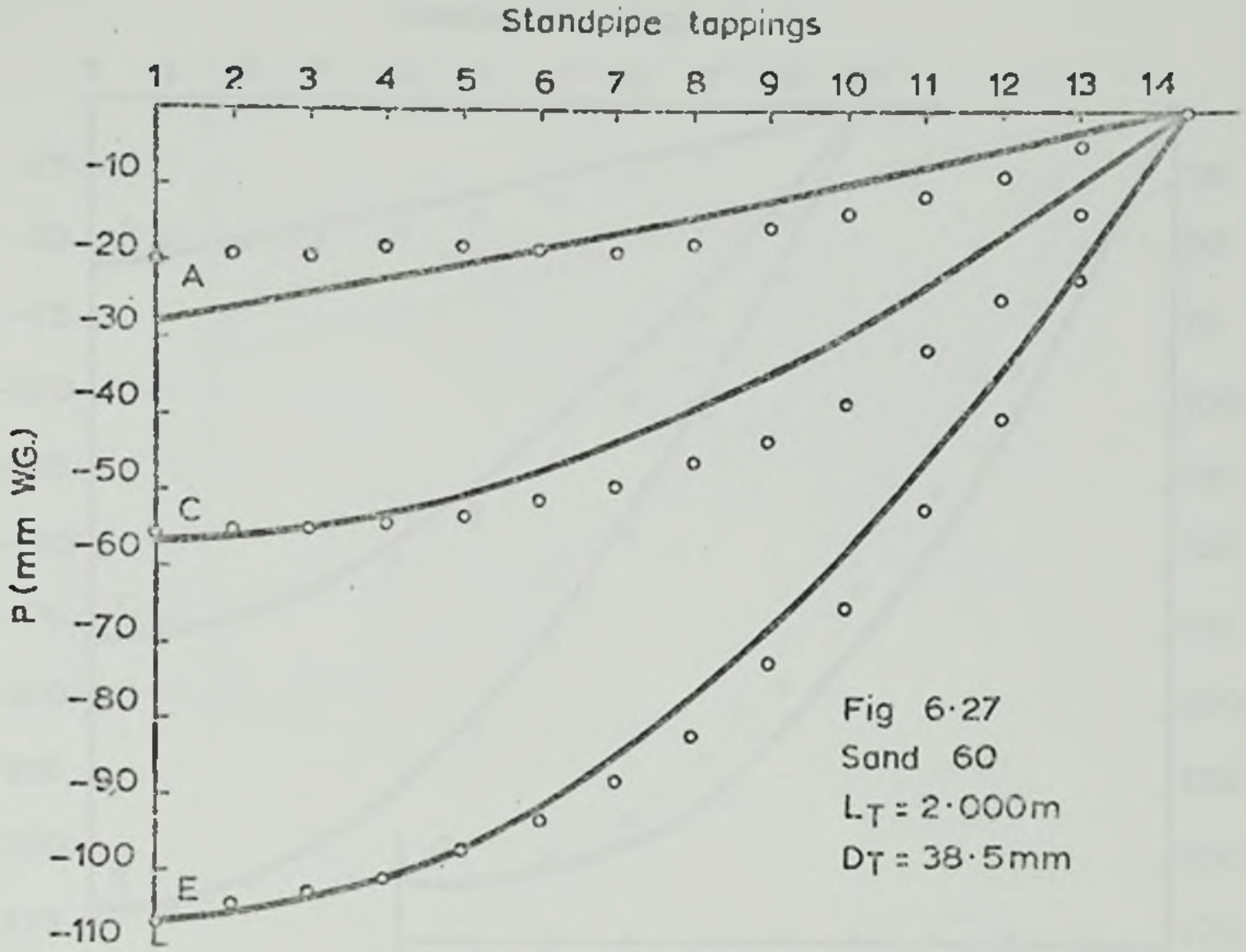

Fig 6·27
Sand 60
L_T = 2·000m
D_T = 38·5mm

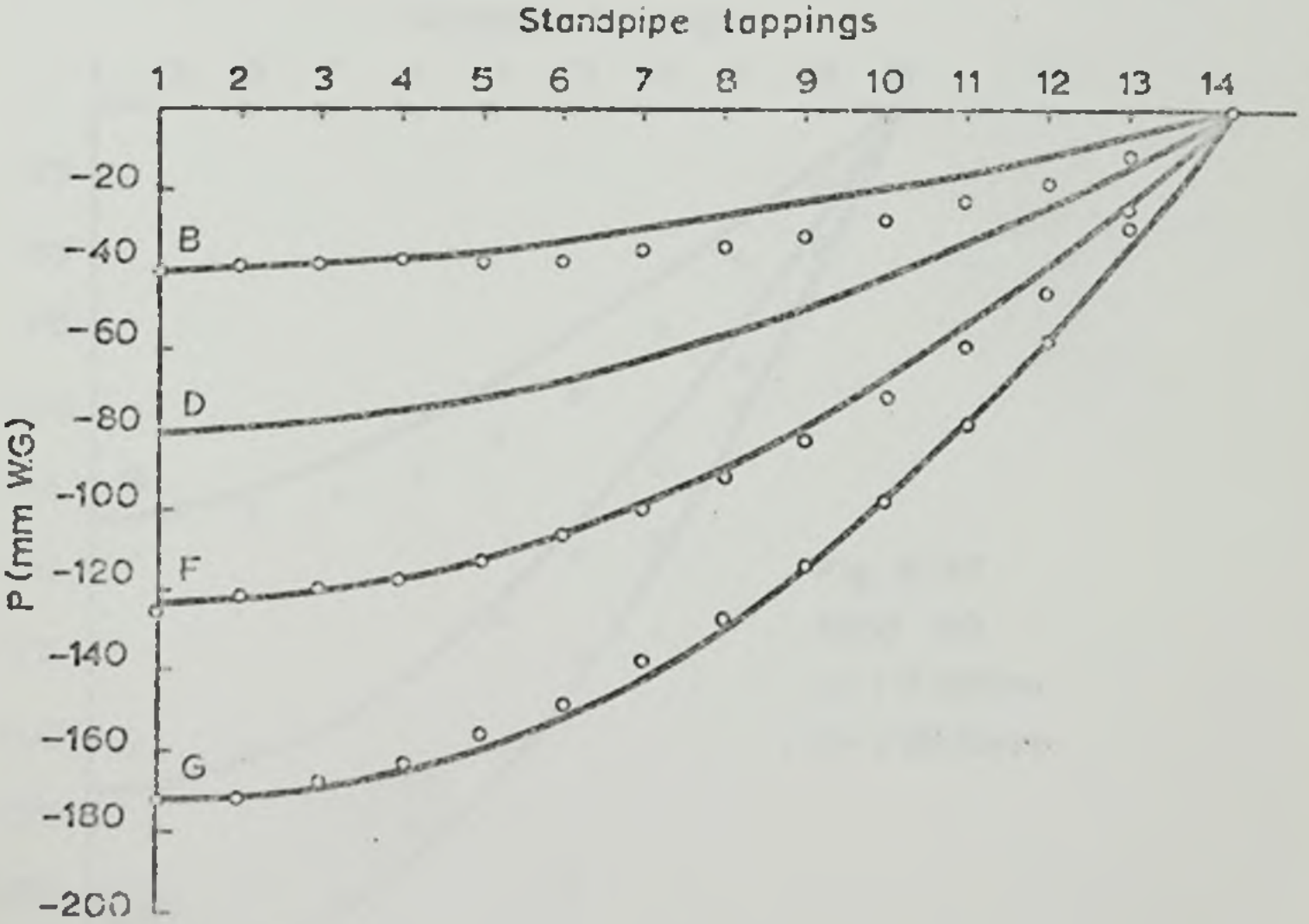

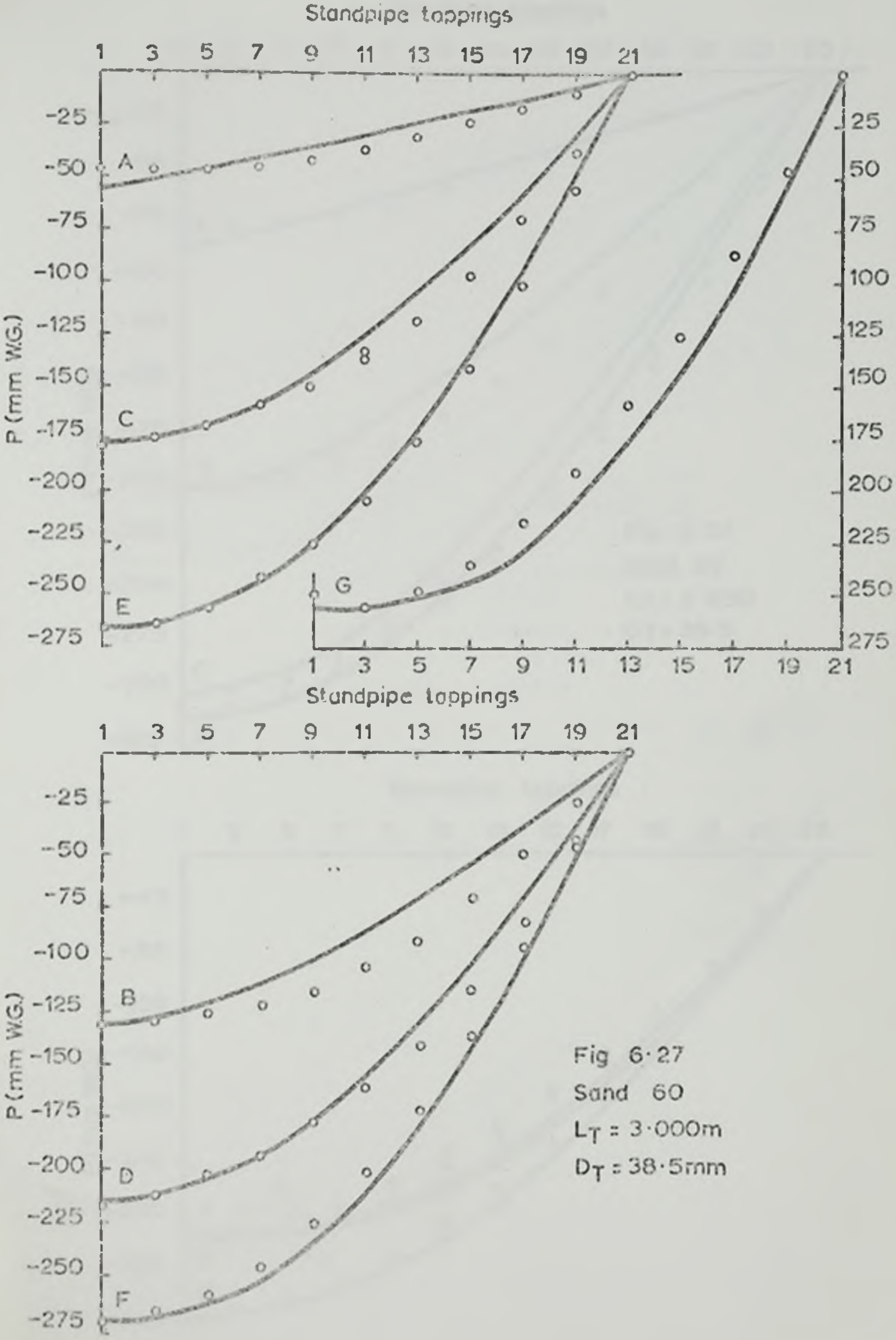

Fig 6·27
Sand 60
L_T = 3·000m
D_T = 38·5mm

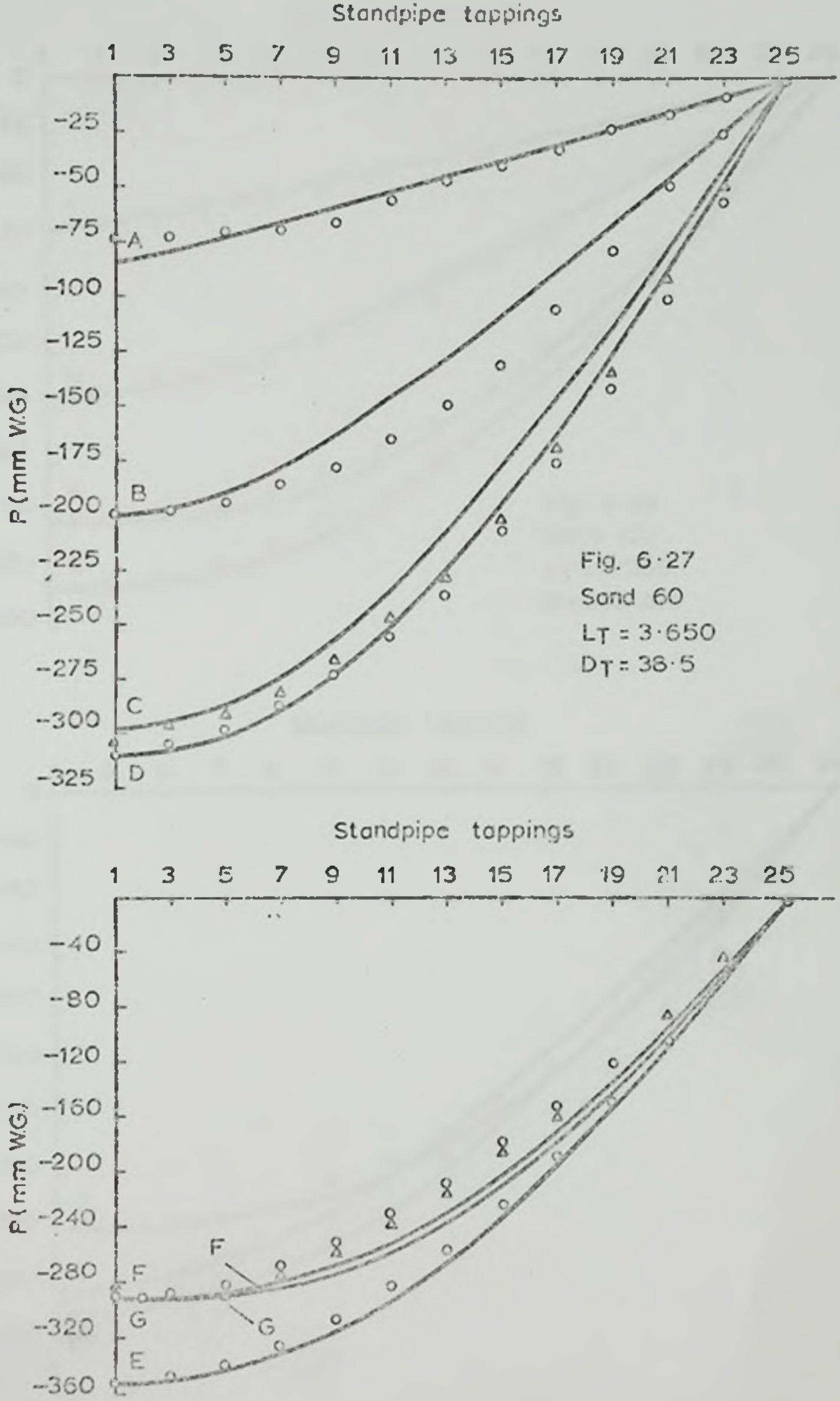
Standpipe tappings
1 3 5 7 9 11 13 15 17 19 21 23 25
-25
-50
-75
-100
-125
-150
-175
-200
-225
-250
-275
-300
-325
P (mm W.G)
A
B
C
D
Fig. 6·27
Sand 60
LT = 3·650
DT = 38·5
Standpipe tappings
1 3 5 7 9 11 13 15 17 19 21 23 25
-40
-80
-120
-160
-200
-240
-280
-320
-360
P (mm W.G.)
F
F
G
G
E

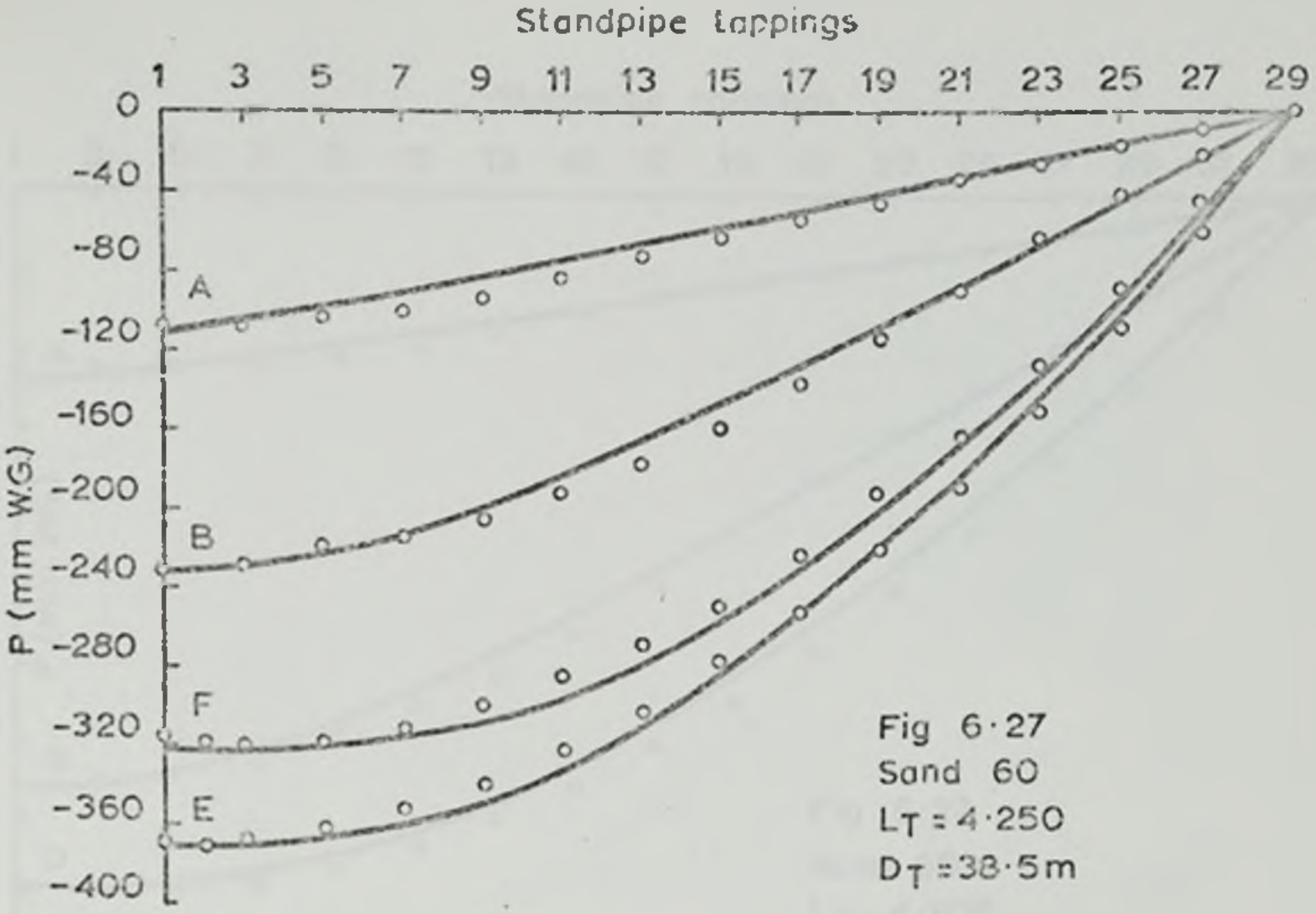

Fig 6·27
Sand 60
L_T = 4·250
D_T = 38·5 m

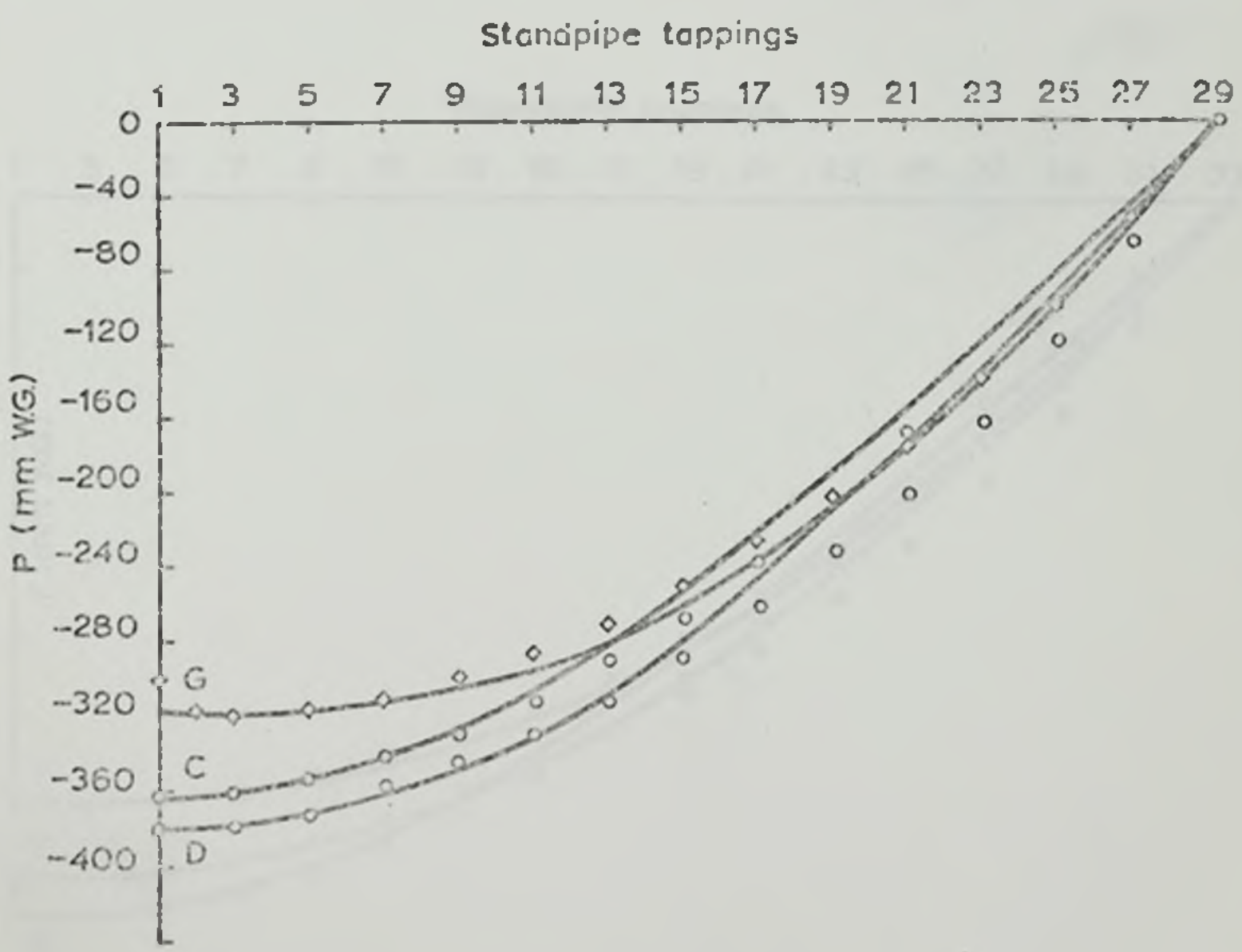

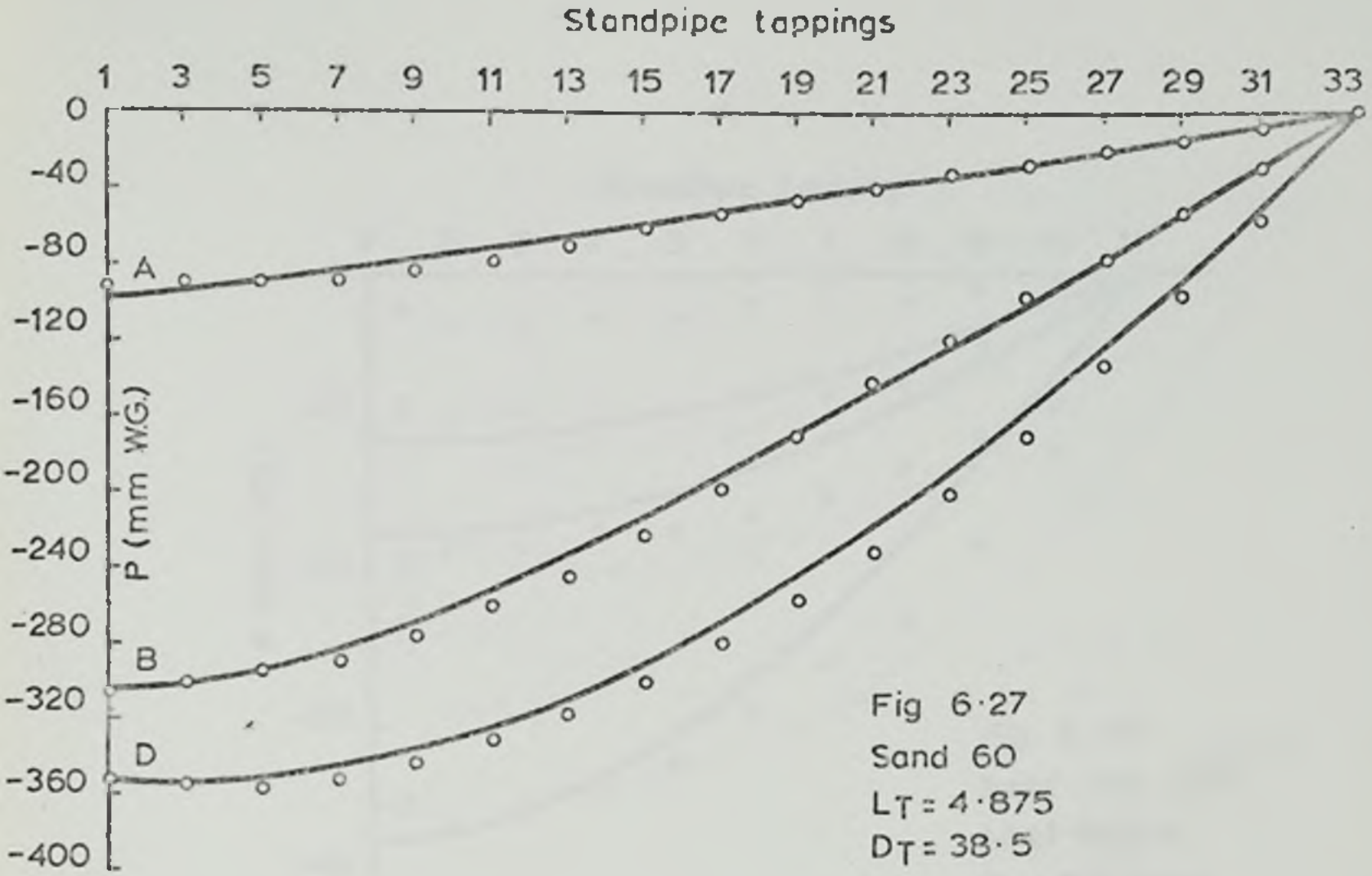

Fig 6·27
Sand 60
$L_T = 4·875$
$D_T = 38·5$

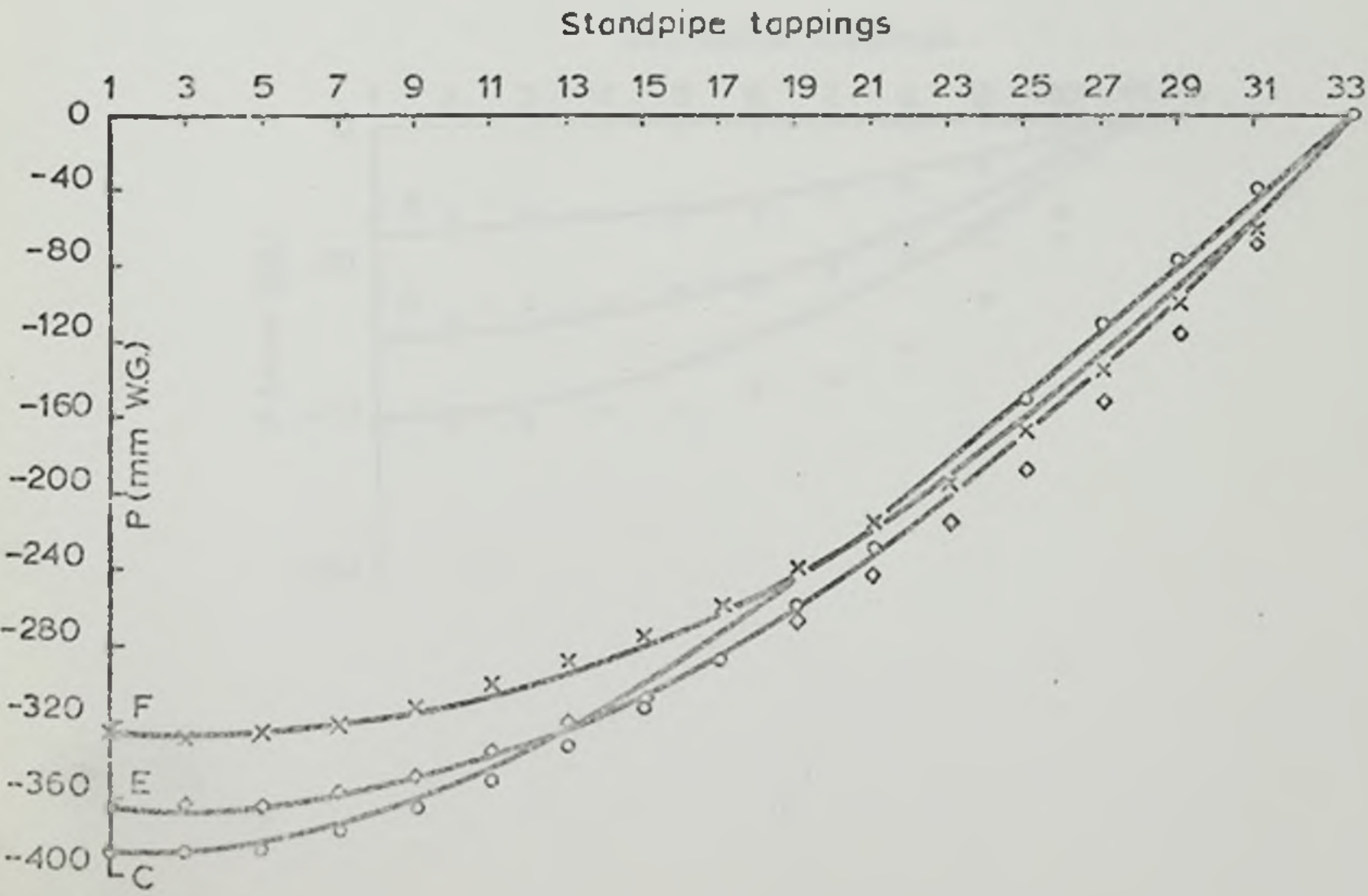

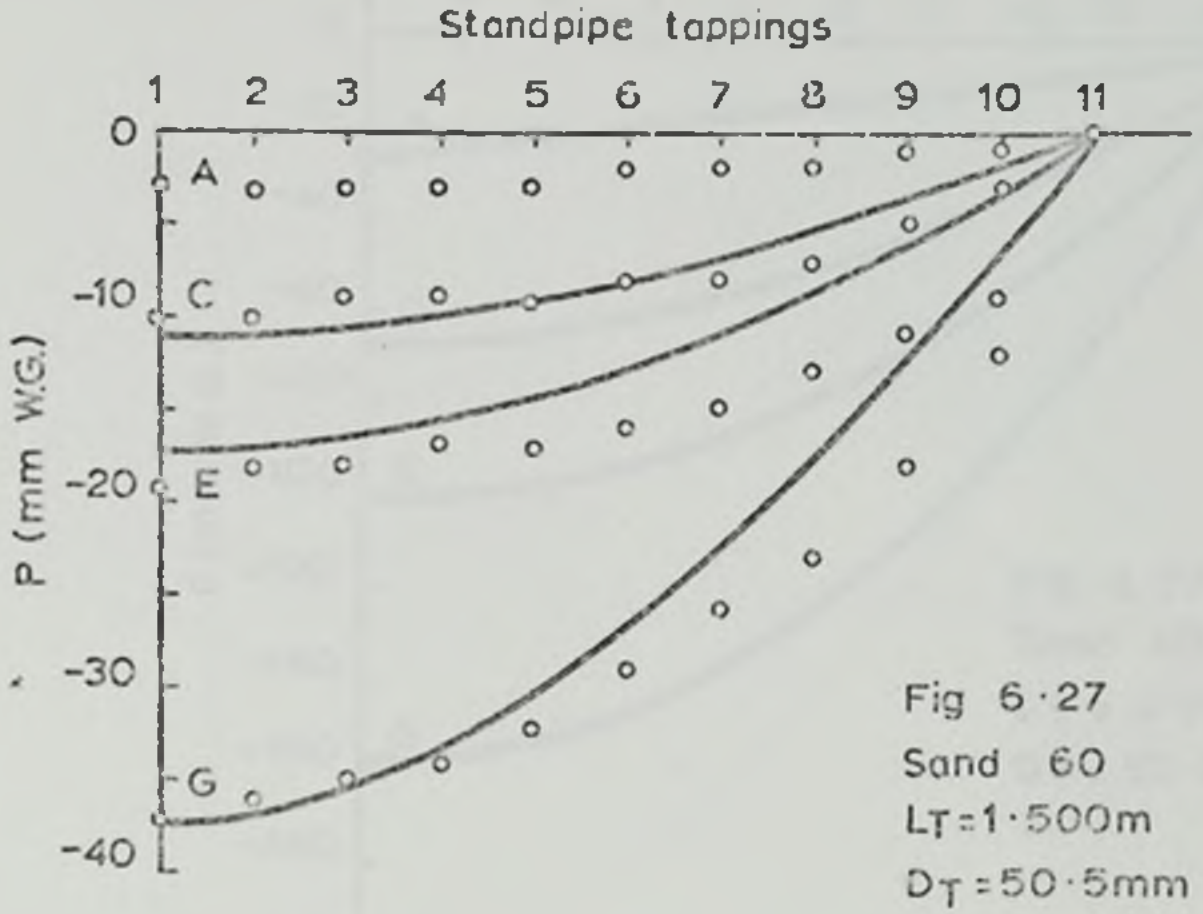

Fig 6·27
Sand 60
L_T = 1·500m
D_T = 50·5mm

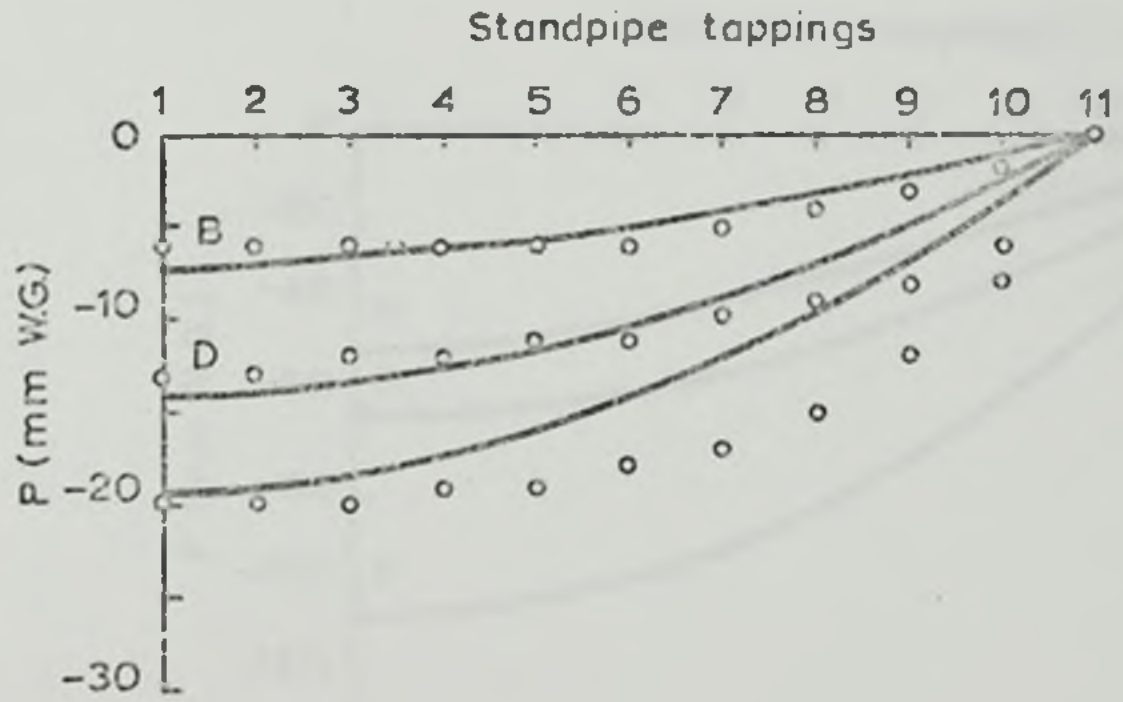

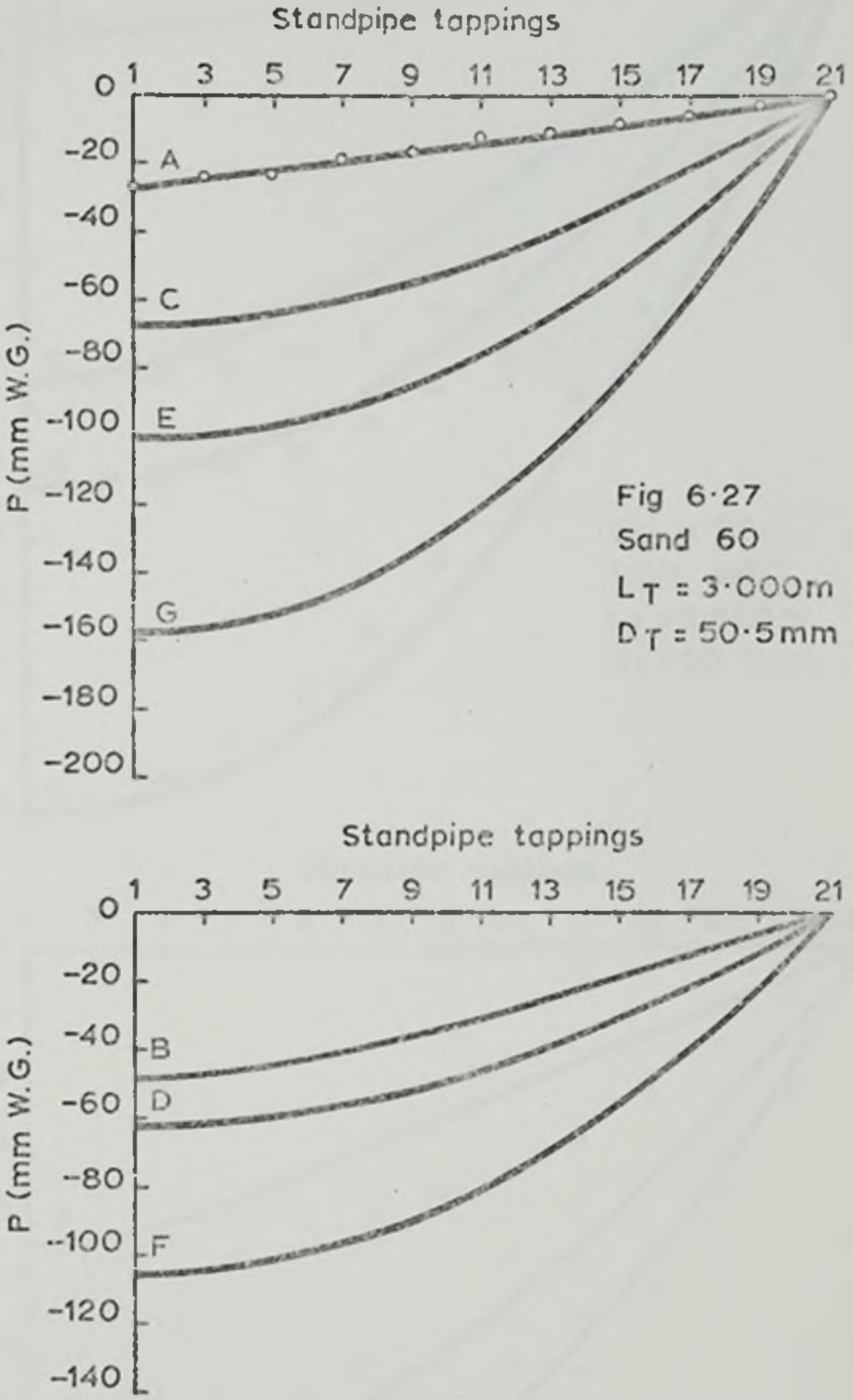

Fig 6·27
Sand 60
L_T = 3·000m
D_T = 50·5mm

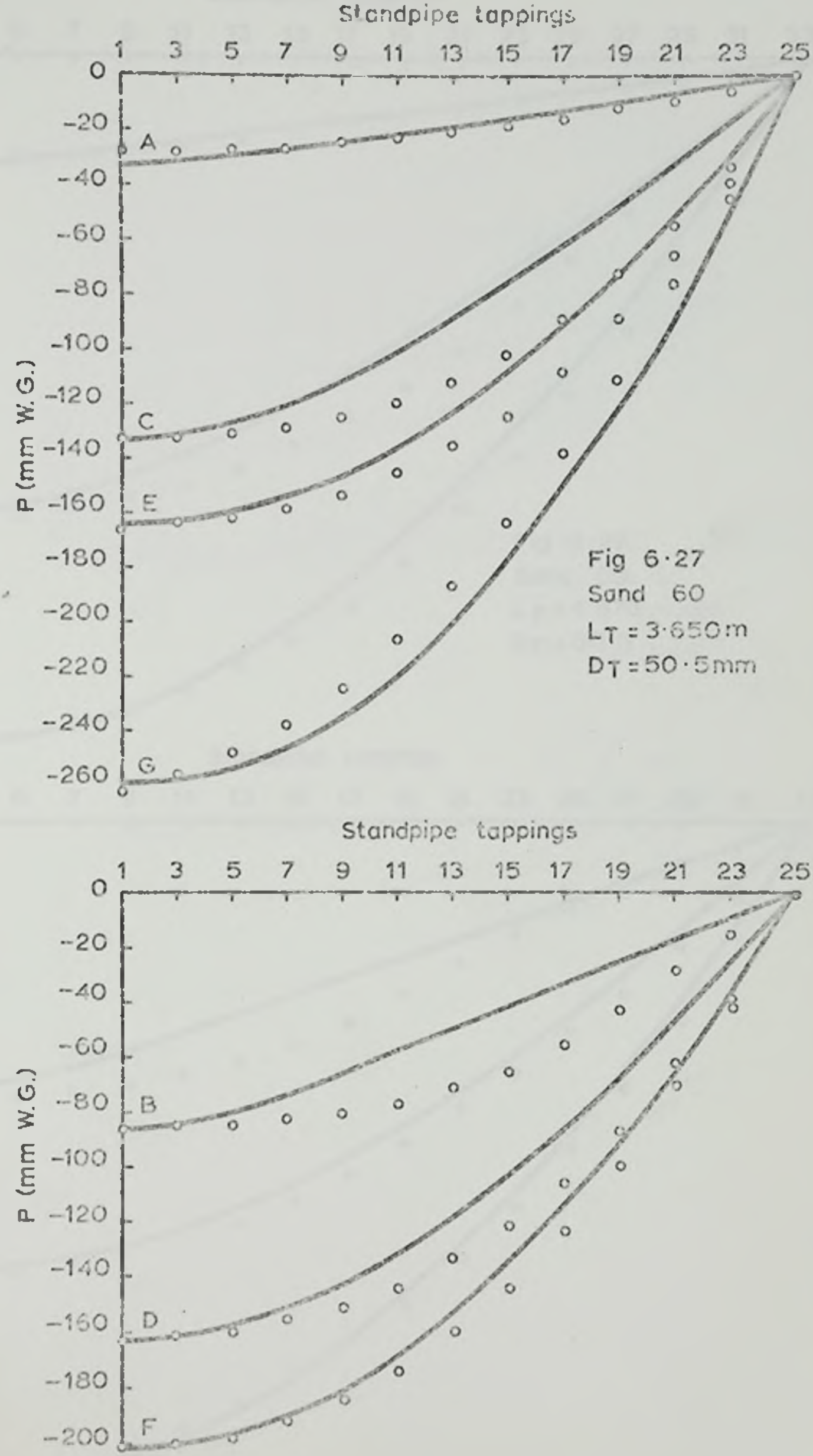
Standpipe tappings
1 3 5 7 9 11 13 15 17 19 21 23 25
0 -20 -40 -60 -80 -100 -120 -140 -160 -180 -200 -220 -240 -260
P (mm W.G.)
A
C
E
G
Fig 6·27
Sand 60
LT = 3·650m
DT = 50·5mm
Standpipe tappings
1 3 5 7 9 11 13 15 17 19 21 23 25
0 -20 -40 -60 -80 -100 -120 -140 -160 -180 -200
P (mm W.G.)
B
D
F

Standpipe tappings

1 3 5 7 9 11 13 15 17 19 21 23 25 27 29 31 33

0 -25 -50 -75 -100 -125 -150 -175 -200 -225 -250 -275 -300

P (mm W.G)

A

C

E

Fig 6·27
Sand 60
$i_T = 4·875$
$D_T = 50·5$

Standpipe tappings

1 3 5 7 9 11 13 15 17 19 21 23 25 27 29 31 33

0 -50 -100 -150 -200 -250 -300

P (mm W.G)

B

D

F

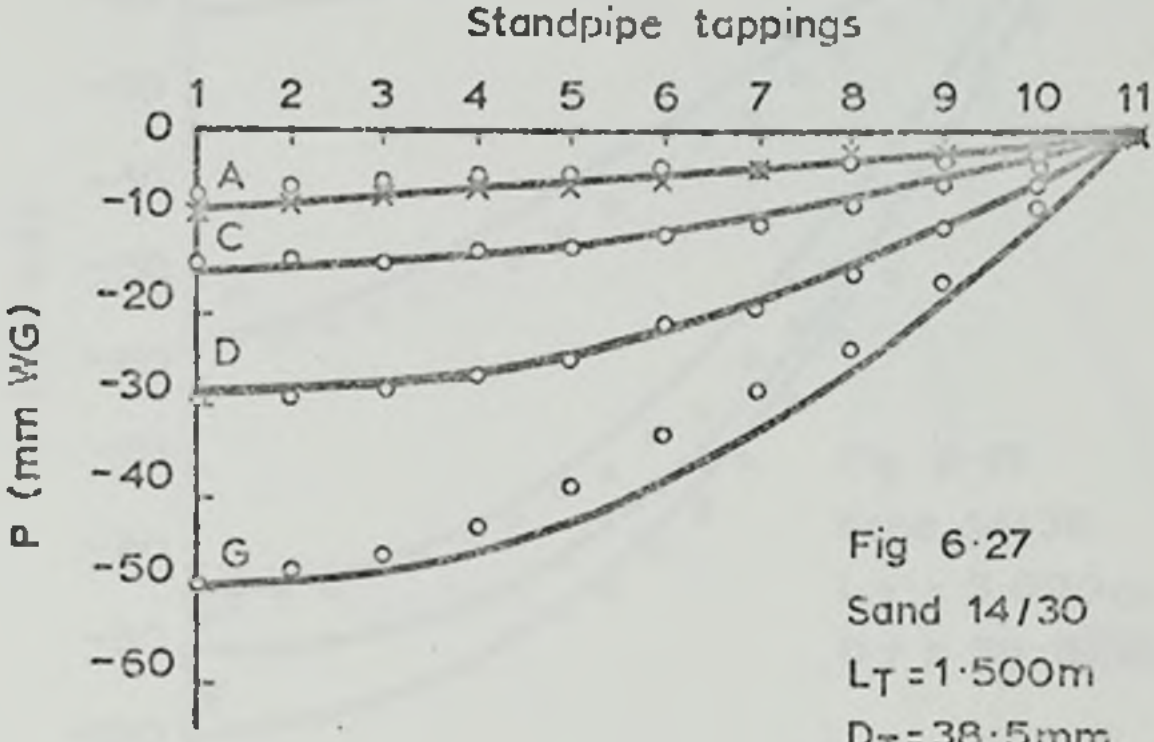

Fig 6·27
Sand 14/30
L_T = 1·500m
D_T = 38·5mm

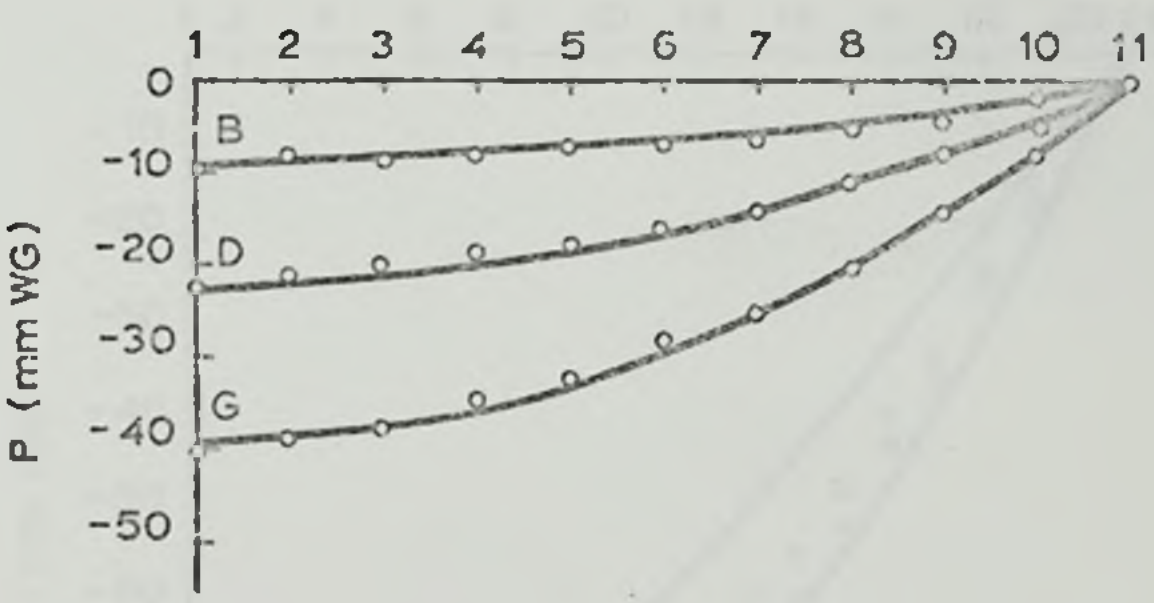

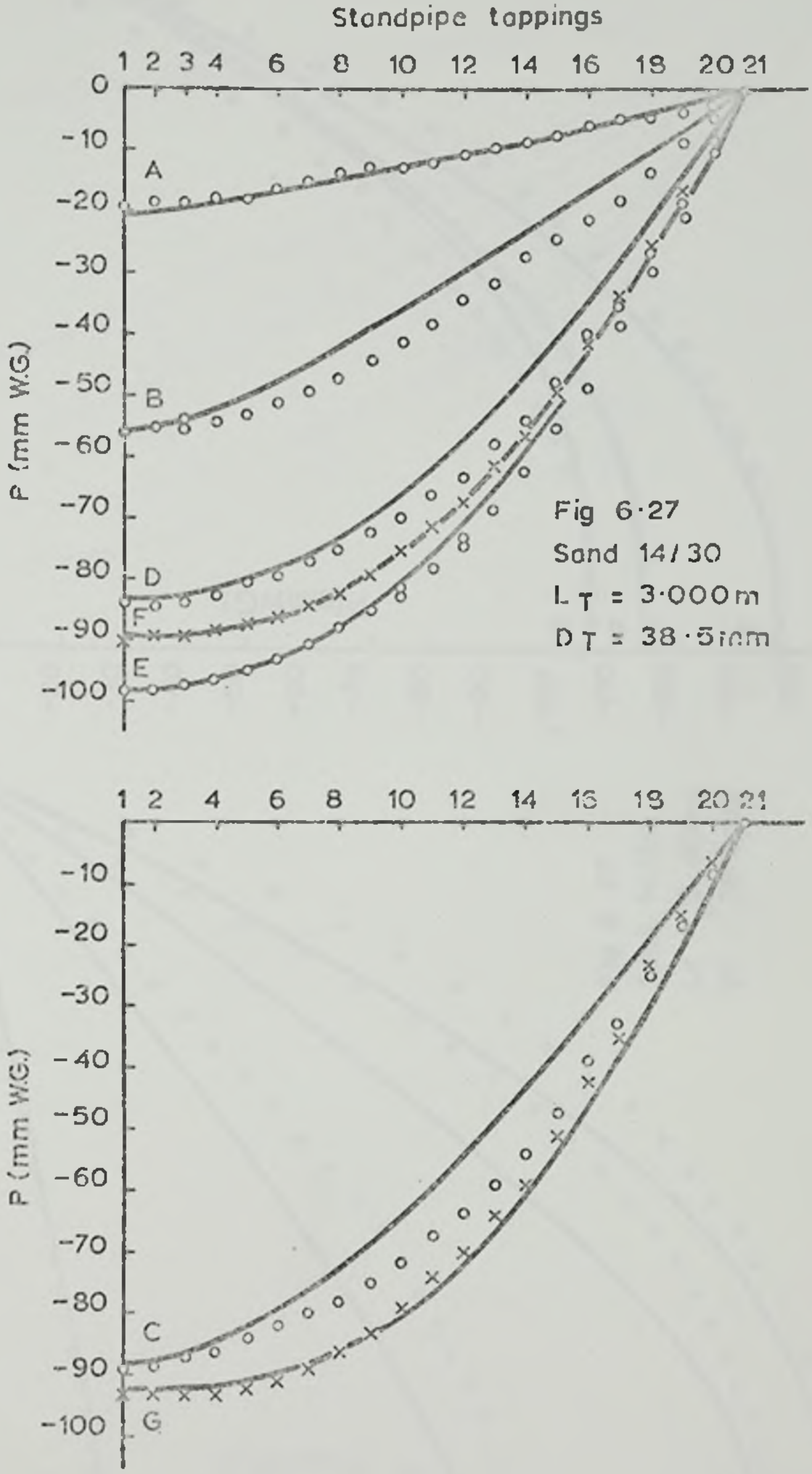

Fig 6·27
Sand 14/30
L_T = 3·000 m
D_T = 38·5 mm

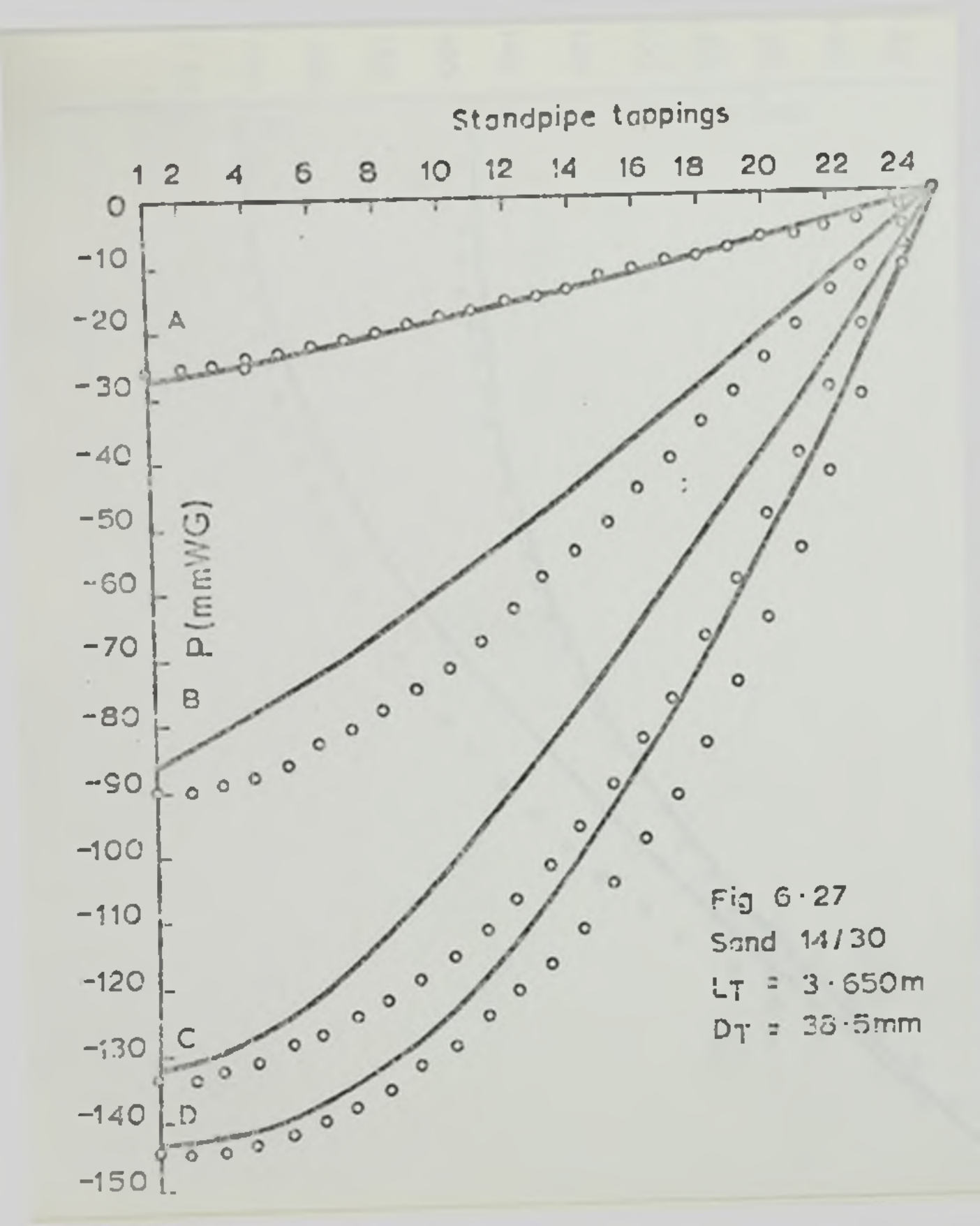

Fig 6·27
Sand 14/30
L_T = 3·650m
D_T = 38·5mm

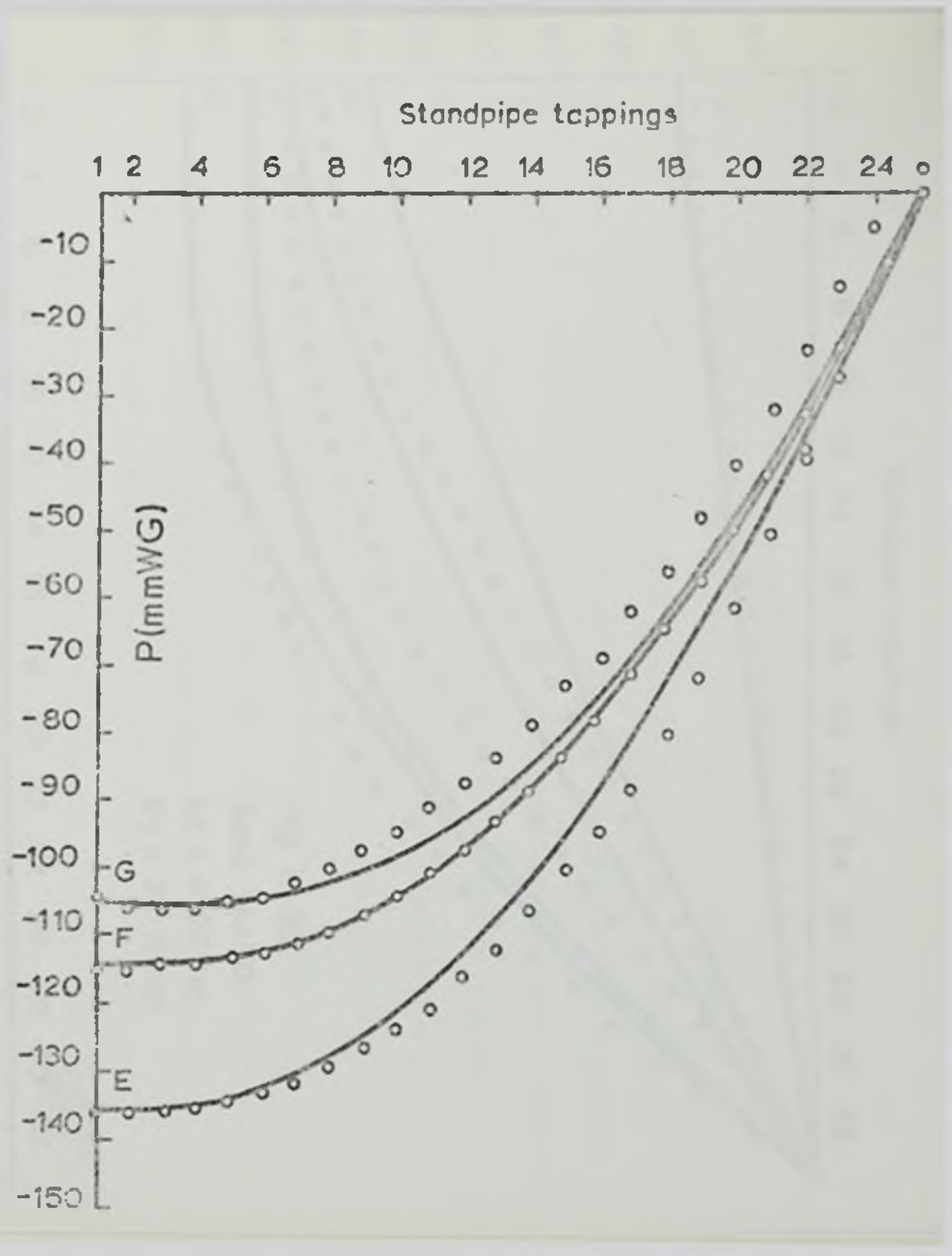
Standpipe tappings
1 2 4 6 8 10 12 14 16 18 20 22 24 0
-10
-20
-30
-40
-50
-60
-70
-80
-90
-100
-110
-120
-130
-140
-150
P(mmWG)
G
F
E

Standpipe tappings

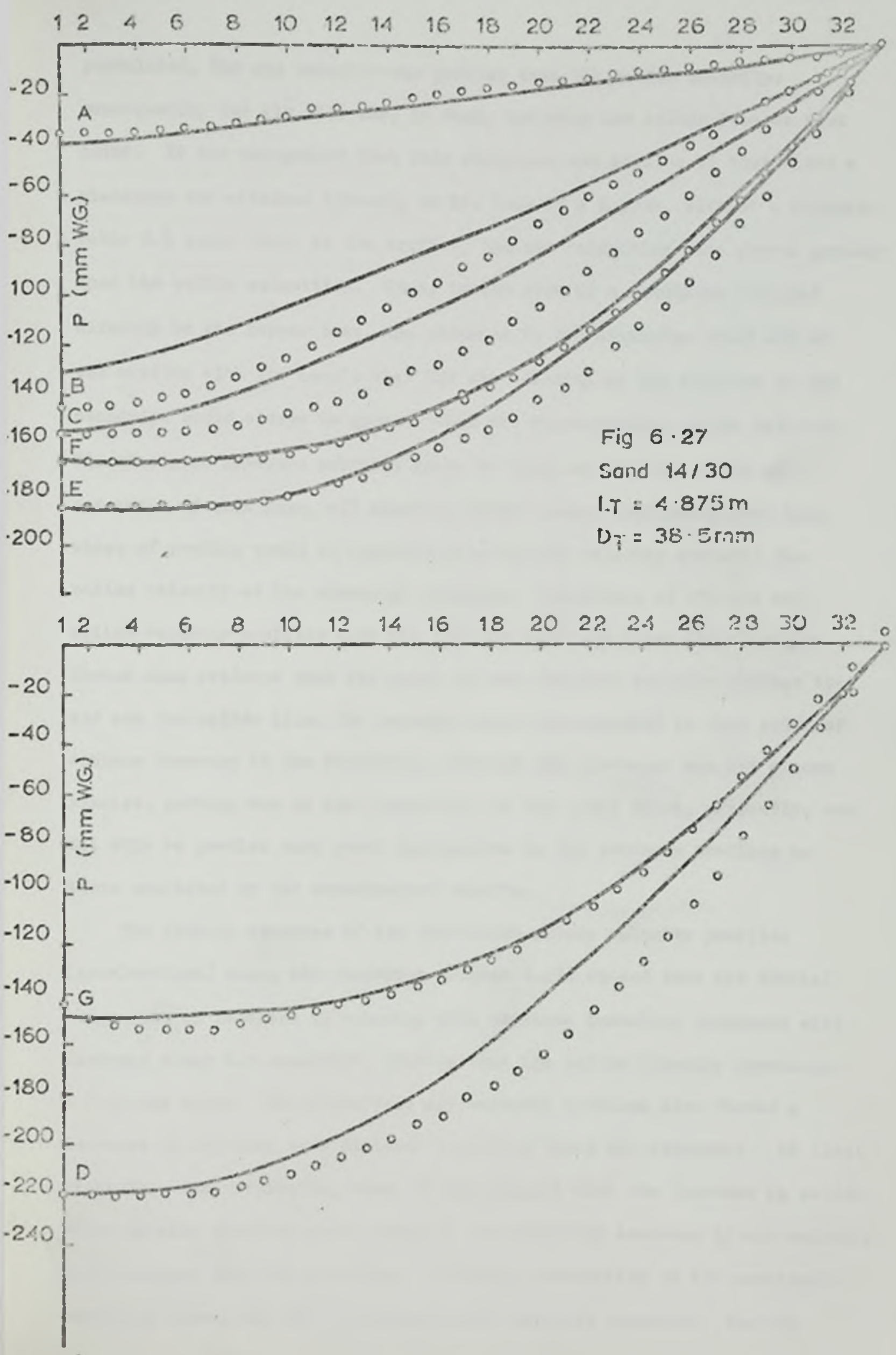

postulated, the air velocity was greater than the solids velocity: consequently the air flow was, in fact, inducing the solids flow at that point. It was recognised that this situation was similar to that where a standpipe was attached directly to the base of a hopper, without a chamber. Table 6.9 shows that, at the orifice, the air velocities were always greater than the solids velocities. Thus, in the case of a standpipe attached directly to the hopper base, the entrance to the standpipe would act as the orifice with the result that the air velocity at the entrance to the standpipe would always be greater than the corresponding solids velocity. The standpipe pressure profiles found by Yuasa et al (74), using an apparatus of this form, all showed a 'hook' shape, confirming that this shape of profile would be produced when the air velocity exceeded the solids velocity at the standpipe entrance. Comparison of the air and solids velocity profiles with the pressure profiles along the standpipe showed some evidence that the point of zero relative velocity between the air and the solids (i.e. the turning point) corresponded to that point of minimum pressure in the standpipe, although the agreement was not always precise, perhaps due to the limitations of the model which, generally, was not able to predict such great depressions in the pressure profiles as those exhibited by the experimental results.

The typical examples of the calculated solids velocity profiles (acceleration) along the standpipe (Figure 6.28) showed that the initial large rate of increase in velocity with distance travelled decreased with distance along the standpipe, showing that the solids velocity approached a limiting value. The calculated air velocity profiles also showed a decrease in velocity with distance travelled along the standpipe. At first sight this was surprising, since it was thought that the increase in solids velocity with distance would induce a corresponding increase in air velocity with distance down the standpipe. However, examination of the continuity equations showed why this decrease in air velocity occurred. For the

solids

$$(1 - e) = \frac{M_s}{U_s \varphi_s A_t} \qquad (3.49)$$

Thus, as the solids velocity increased down the standpipe due to gravitational effects, the solids volume fraction at any point decreased with a consequent increase in voidage (e) at that point. For the air

$$U_a = \frac{Q_{at}}{eA_t} \qquad (3.49a)$$

so, as the voidage increased with distance along the standpipe, the air velocity had to suffer a decrease if the volume flow rate were to remain constant, as assumed.

Calculations of the solids and air velocities showed that limiting velocity conditions for both the air and solids velocities could be attained within standpipes, most notably with the smaller particles of sand 60 in the larger diameter standpipes. The terminal situation in the standpipe was felt to be complicated by the presence of the standpipe wall and moving fluid. Firstly, the usual definition of a terminal solids velocity did not seem relevant to the present situation, since it applies to a single particle in an infinite fluid, with no particle-particle interference, no particle-wall reaction, no bulk movement of the fluid, and with a drag coefficient based only on particle properties and particle-fluid relative velocity. The presence of other particles was taken into account in the model by a modification of the particle-air drag coefficient based on the position down the standpipe (taken as an indication of the solids volume fraction at that point). Thus, the velocities of the particles and air were not just dependent on their mutual single particle drag coefficient, but also on the particle-particle interaction, the particle-wall friction, the air-wall friction, and the position in the standpipe; also the presence of a mass of particles could be expected to have an effect on the nature of the air flow in the standpipe, e.g. the

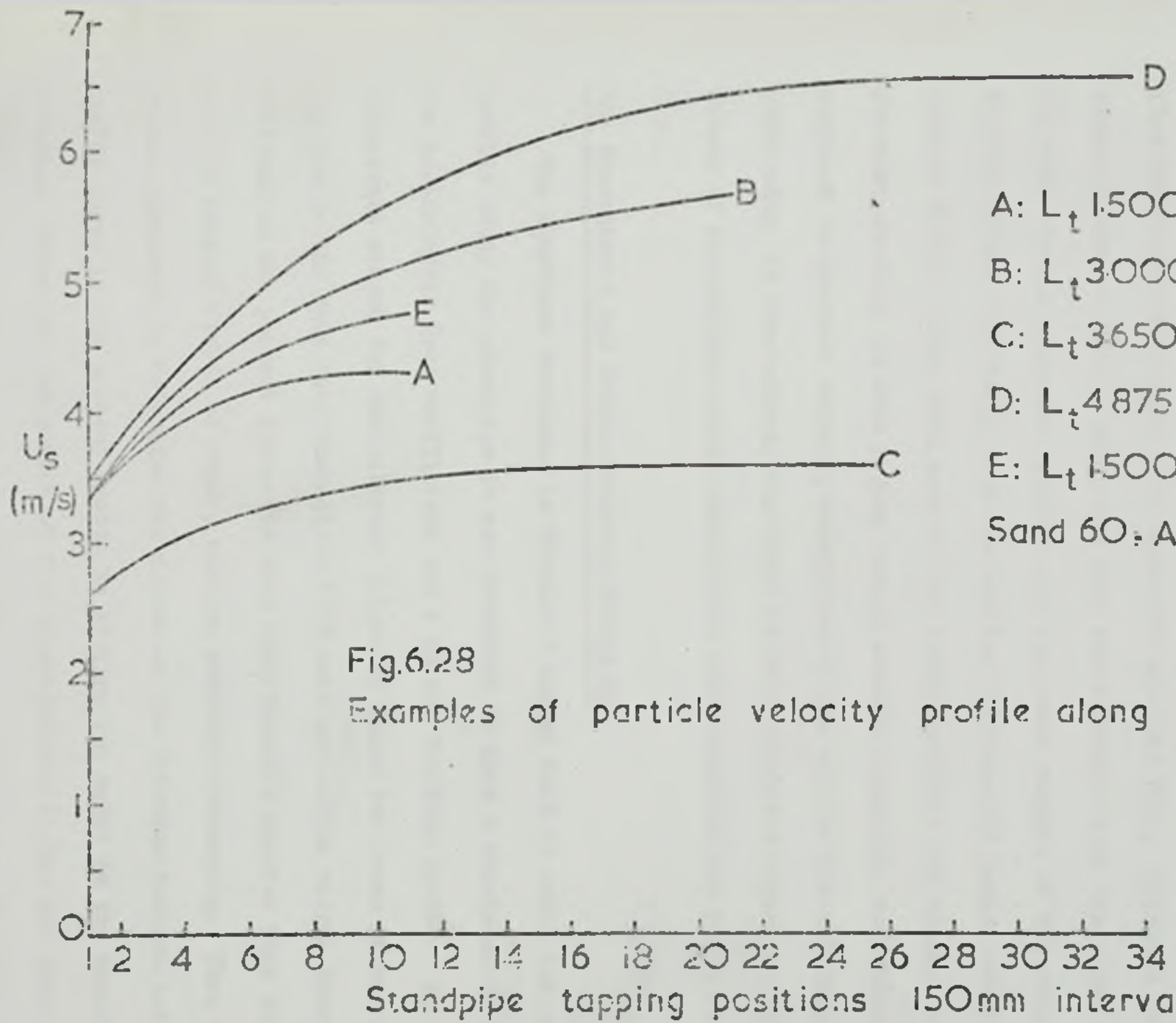

A: L_t 1.500m. D_t 25.5mm. D_o 25.4mm.

B: L_t 3.000m. D_t 38.1mm. D_o 19.01mm.

C: L_t 3.650m. D_t 50.5mm. D_o 12.7mm.

D: L_t 4.875m. D_t 38.5mm. D_o 38.1mm.

E: L_t 1.500m. D_t 50.5mm. D_o 25.4mm.

Sand 60 : A,C,D,E Sand 14/30 : B

Fig.6.28

Examples of particle velocity profile along the standpipes

production of turbulence within the air stream. Consequently, the calculated values of the free-field solids terminal velocity relative to the air were not thought to be particularly meaningful, except as indicating that some type of limiting condition was likely to occur within the standpipe or that, given a long enough standpipe, constant velocity conditions could be achieved by both particles and air. Consideration of limiting flow conditions in a tube, i.e. constant velocity flow, indicated that a linear pressure profile along the tube would result: this was clear from the experimental pressure profiles for the lower regions of the standpipes in some cases, especially with the smaller orifices and longer standpipes (Figure 6.27). Also, with some of the larger orifices and standpipes, the pressure profiles in this region tended towards linearity, indicating an approach to constant velocity conditions at the exit to the standpipe and confirming, to some extent, the shape of the calculated velocity profiles. Values of the maximum solids velocity in each standpipe are given in Table 6.11.

The Parameter w and Solids Friction Factor f_s

The equations developed in Chapter 3 showed that to model the pressure profile along the standpipe it was necessary to have a knowledge of both the particle/air drag coefficient and a solids friction factor. A literature search for the relevant values of these two terms proved unrewarding due to the fact that the solids flow rate and solids volume fraction obtained in the present apparatus were significantly greater than those used in related fields of study, such as pneumatic conveying. Thus it became necessary to determine the values of the friction factors and drag coefficients in the present system by fitting the model to the experimental results. Since, at the outset of the investigation it had not been recognised that this development would be necessary, some simplification had to be introduced into the determination of these terms. This was mainly due to certain limitations of the apparatus, particularly in the experimental

TABLE 6.11

Maximum Calculated Velocities attained in the Standpipes

Sand 60

D_t = 25.5 mm	D_o (mm)	L_t (m)	1.500	3.000	3.650	4.875
	12.7		3.73	4.68	4.83	5.40
	19.01		5.29	5.40	5.68	6.73*
	25.4		4.32	6.48	6.54	7.58
	31.75		5.09	6.24	6.29	-
	38.1		5.95	6.28	-	-

D_t = 38.5 mm	D_o (mm)	L_t (m)	1.500	2.000	3.000	3.650	4.250	4.875
	12.7		3.44	3.54	3.68*	3.74*	3.81*	4.00*
	19.01		4.47	4.14*	4.66*	4.78*	4.83*	5.03*
	25.4		5.00	4.33	5.03*	5.27*	5.69*	6.07*
	31.75		4.93	4.29	5.18	5.42*	6.03*	6.89*
	38.1		5.27	5.05	5.90	5.82	6.23	6.58
	44.45		5.37	4.85	6.07	6.13	6.52	6.93
	50.8		5.52	5.34	5.95	6.23	6.67	-

D_t = 50.8 mm	D_o (mm)	L_t (m)	1.500	3.000	3.650	4.875
	12.7		-	3.59*	3.62*	3.67*
	19.01		4.81	4.87*	4.49*	4.76*
	25.4		4.77	5.82	5.10*	5.43*
	31.75		5.50	5.70	5.62*	6.53*
	38.1		5.99	6.78	6.33	6.87
	44.45		5.71	6.45	6.50	7.58
	50.8		5.79	6.54	6.65	-

* The solids velocity profile had reached a maximum value before the exit from the standpipe.

TABLE 6.11 (contd.)

Maximum Calculated Velocities attained in the Standpipes

Sand 14/30

D_t = 38.5 mm D_o (mm)	L_t (m)	1.500	3.000	3.650	4.875
12.7		4.71	5.43	5.63	6.00
19.01		5.24	5.70	6.11	6.64
25.4		4.29	6.16	6.52	7.25
31.75		5.29	6.44	7.38	8.08
38.1		5.77	7.08	7.63	8.27
44.45		5.52	7.15	7.31	8.41
50.8		5.53	7.55	8.07	8.79

TABLE 6.12

Calculated Values of Parameter w, Solids Friction Factor f_s and Average Standpipe Solids Velocity $\bar{U}_s$

Sand 60 D_t = 25.5

D_o \ L_t		1.500	3.000	3.650	4.875
12.7	w	∞	∞	∞	∞
	f_s	0.0	0.0	0.0	0.0
	$\bar{U}_s$	4.00	4.07	4.21	4.64
19.01	w	0.9	5.2	5.0	3.6
	f_s	0.00017	0.00082	0.00077	0.00025
	$\bar{U}_s$	4.69	5.04	5.26	6.17
25.4	w	1.2	1.6	4.2	4.2
	f_s	0.00354	0.00050	0.00077	0.00042
	$\bar{U}_s$	4.14	5.52	5.58	6.42
31.75	w	0.90	1.3	3.0	-
	f_s	0.00200	0.00143	0.00166	-
	$\bar{U}_s$	4.51	5.25	5.39	-
38.1	w	1.3	1.3	-	-
	f_s	0.00268	0.00161	-	-
	$\bar{U}_s$	4.28	5.31	-	-

TABLE 6.12 (contd.)

Calculated Values of Parameter w, Solids Friction Factor f_s and Average Standpipe Solids Velocity $\bar{U}_s$

Sand 60 D_t = 38.5

D_o \ L_t		1.500	2.000	3.000	3.650	4.250	4.875
12.7	w	∞	∞	∞	∞	∞	∞
	f_s	0.0	0.0	0.0	0.0	0.0	0.0
	$\bar{U}_s$	4.12	3.38	3.85	3.40	3.58	3.86
19.01	w	0.57	1.3	2.3	3.2	2.9	3.6
	f_s	0.00407	0.00476	0.00173	0.00135	0.00204	0.00109
	$\bar{U}_s$	4.07	3.95	4.51	4.44	4.60	4.87
25.4	w	0.4	0.8	1.3	1.9	1.8	1.8
	f_s	0.00256	0.00536	0.00242	0.00192	0.00135	0.00088
	$\bar{U}_s$	4.43	4.06	4.70	5.04	5.41	5.65
31.75	w	0.36	0.65	1.1	1.4	1.3	0.9
	f_s	0.00329	0.00639	0.00298	0.00256	0.00172	0.00104
	$\bar{U}_s$	4.36	4.13	4.86	5.02	5.57	6.10
38.1	w	0.34	0.55	0.9	1.0	1.0	0.8
	f_s	0.00214	0.00351	0.00184	0.00246	0.00218	0.00210
	$\bar{U}_s$	4.56	4.51	5.19	5.27	5.72	5.99
44.45	w	0.35	0.55	0.9	0.8	0.8	0.6
	f_s	0.00200	0.00483	0.00211	0.00264	0.00229	0.00210
	$\bar{U}_s$	4.55	4.51	5.38	5.41	5.67	6.04
50.8	w	0.5	0.8	0.8	0.7	0.7	-
	f_s	0.00141	0.00319	0.00285	0.00279	0.00240	-
	$\bar{U}_s$	4.77	4.73	5.29	5.50	5.79	-

TABLE 6.12 (contd.)

Calculated Values of Parameter w, Solids Friction Factor f_s and Average Standpipe Solids Velocity $\bar{U}_s$

Sand 60 D_t = 50.5

D_o \ L_t		1.500	3.000	3.650	4.875
12.7	w	-	∞	∞	∞
	f_s	-	0.0	0.0	0.0
	$\bar{U}_s$	-	4.42	3.98	3.63
19.01	w	0.38	1.90	3.80	4.09
	f_s	0.00440	0.00041	0.00043	0.00053
	$\bar{U}_s$	4.35	4.74	4.50	4.57
25.4	w	0.30	0.79	1.51	1.74
	f_s	0.00543	0.00469	0.00200	0.00174
	$\bar{U}_s$	4.34	5.33	4.89	5.36
31.75	w	0.20	0.42	0.89	0.66
	f_s	0.00213	0.00299	0.00207	0.00132
	$\bar{U}_s$	4.74	5.03	5.27	5.88
38.1	w	0.15	0.39	0.50	0.68
	f_s	0.00029	0.00050	0.00176	0.00113
	$\bar{U}_s$	4.81	5.68	5.68	6.03
44.45	w	0.12	0.31	0.45	0.43
	f_s	0.00189	0.00196	0.00187	0.00093
	$\bar{U}_s$	4.92	5.48	5.60	6.47
50.8	w	-	0.35	0.45	-
	f_s	-	0.00175	0.00192	-
	$\bar{U}_s$	-	5.44	5.69	

TABLE 6.12 (contd.)

Calculated Values of Parameter w, Solids Friction Factor f_s and Average Standpipe Solids Velocity $\overline{U}_s$

Sand 14/30 D_t = 38.5

D_o \ L_t		1.500	3.000	3.650	4.875
12.7	w	∞	∞	∞	∞
	f_s	0.0	0.0	0.0	0.0
	$\overline{U}_s$	3.44	4.45	4.61	4.64
19.01	w	0.8	8.5	∞	∞
	f_s	0.00200	0.000567	0.0	0.0
	$\overline{U}_s$	4.50	4.89	4.83	5.22
25.4	w	0.78	3.5	7.5	
	f_s	0.00693	0.000739	0.00053	0.00050
	$\overline{U}_s$	4.08	5.30	5.47	5.00
31.75	w	0.6	1.5	2.10	2.50
	f_s	0.00248	0.00139	0.000258	0.000300
	$\overline{U}_s$	4.49	5.53	5.59	6.60
38.1	w	0.5	1.0	1.20	1.30
	f_s	0.00099	0.000765	0.00058	0.00071
	$\overline{U}_s$	4.69	5.83	6.20	6.76
44.45	w	0.6	0.8	0.9	0.9
	f_s	0.00200	0.00102	0.00138	0.000881
	$\overline{U}_s$	6.76	5.83	6.00	6.67
50.8	w	0.7	0.65	0.55	0.6
	f_s	0.00209	0.00059	0.00065	0.00075
	$\overline{U}_s$	4.65	5.93	6.29	6.90

determination of the solids velocity profile along the standpipe, and in the detailed observations of the nature of the solids stream throughout the standpipe. It is felt that further work in this context is needed to determine more fully the exact conditions of the solids flow through vertical standpipes.

As mentioned above and in Chapter 3, the solids/air drag coefficient throughout the standpipe was considered to be dependent on the expansion of the solids stream as well as the particle/air relative velocity. Since observations of this expansion along the standpipes was not possible, it was necessary to impose on the variation of the drag coefficient a form related to position down the standpipe, i.e.

$$C_D' = C_D(1 - e^{-\frac{wx}{L_t}}) \qquad (3.51)$$

As explained in Chapter 3, this seemed the simplest form consistent with the initial condition of zero drag coefficient at the entrance to the standpipe ($x = 0$) and with the contention that the effective particle drag coefficient at the exit of the standpipe ($x = L_t$) was not necessarily equal to the single particle value. The parameter w was introduced to account for the different flow conditions associated with each orifice-standpipe combination. Table 6.12 shows the value of w, the friction factor f_s obtained by the integration of equations 3.46 and 3.47, and the average experimental particle velocity obtained for each orifice/standpipe combination tested in the experimental work.

In the case of the smallest orifice, the single particle drag coefficient was used throughout the chamber and standpipe, since the low solids flow rate and the relatively large scatter showed by the solids stream with this orifice indicated little particle interaction; thus $w = \infty$ for $D_o = 12.7$ mm (and also for some other orifices for sand 14/30). Examination of the values of w obtained for different orifices for any one standpipe showed that, in general, w decreased with increasing orifice

diameter, or, since the solids mass flow rate was dependent on orifice diameter, the value of w decreased with increasing solids mass flow rate. This fitted the derivation of the drag coefficient relationship in Chapter 3, where it was indicated that w was expected to be dependent on the proximity of other particles. Analysis of the change of w with standpipe length for any particular orifice diameter was obscured by the presence of the standpipe length term in the exponential in equation 3.51. Thus it was necessary to look at the term $\frac{w}{L_t}$. In general, this term decreased with increase in standpipe length, which again seemed consistent with the increase in solids mass flow rate associated with increase in standpipe length. In the cases where solids mass flow rate showed a maximum value with increase in standpipe length, the values of $\frac{w}{L_t}$ and w decreased with increased standpipe length. This seemed to indicate that the effective drag coefficient for the solids stream at any point in the standpipe decreased with an increase in standpipe length for the same solids mass flow rate in such cases. The fact that a continued increase in standpipe length did not increase the mass flow rate indefinitely gave, in itself, some confirmation of these values of $\frac{w}{L_t}$. For, if the total effect of the solids stream drag in the standpipe could be regarded in terms of an 'average induction effect per unit length of standpipe', then for a further increase in standpipe length where there was no increase in solids mass flow rate or orifice pressure drop the 'induction effect per unit length of standpipe' must decrease.

Thus, the value of the parameter w behaved essentially as expected in Chapter 3 although attempts at correlation of w (or $\frac{w}{L_t}$) against solids average volume fraction or voidage in the standpipe did not yield any direct method of determining the parameter. It was felt that this was due both to the errors in the experimental values of average voidage, and to the uncertainties in the values of w due to the large approximations necessary in the model to describe the conditions within the standpipe.

Figure 6.29 shows the predicted variation of the effective drag

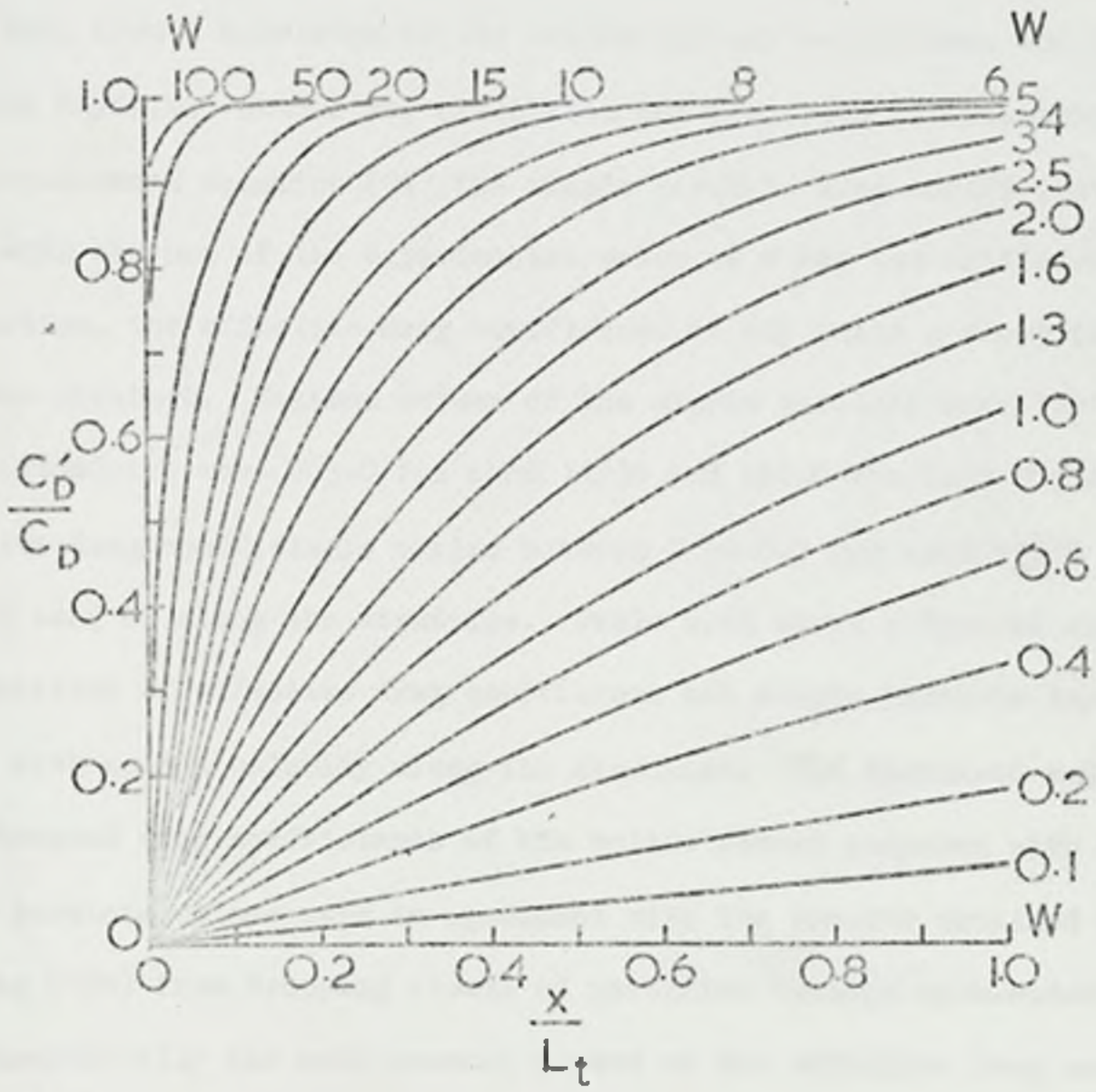

Fig.6.29 The effect of the parameter W on the variation of effective particle drag coeficient with position down the standpipe

coefficient with position down the standpipe, imposed by the equation 3.51 for various values of w. From the graph, it was seen that as w increased towards infinity the effective solids drag coefficient should become identical to the single particle value over the whole length of the standpipe; which, as shown above, was consistent with the variation of w, calculated from the standpipe equations, with the solids mass flow rates encountered in the experimental runs.

Thus, from a knowledge of the solids and air velocities, the single particle Reynolds' number was calculated and from such relationships as the Schiller-Naumann equation (96) the single particle drag coefficient found. Then, with the use of the experimental value of w for the orifice/standpipe combination, the effective drag coefficient at any point x along the standpipe was obtained. Maximum values of the single particle Reynolds' numbers in the standpipe were 263.0 for sand 14/30 and 190.0 for sand 60; and the effective drag coefficients varied between 0 to 0.7 for sand 14/30 and 0 to 1.2 for sand 60 along the standpipe. Table 6.13 shows a typical example of the variation of effective drag coefficient and single particle Reynolds' number with solids velocity along the standpipe. The increased velocities and decreased drag coefficients of the solids stream compared with the single particle values were in agreement with the results obtained by Stinzing (104) from dropping clouds of particles through open-ended tubes.

Superficially the most unusual aspect of the effective drag coefficient for the particles in the solids stream was that it increased as solids progressed down the standpipe and the solids velocity increased. This, of course, was a necessary consequence of the expansion of the solids stream and the model relating this to the particle drag coefficient.

As already mentioned, Table 6.13 shows the values of the solids friction factor (f_s) obtained for each orifice and standpipe combination. Attempts at correlating these friction factors against average solids velocity in the standpipe proved disappointing, and although in general a decrease in solids

TABLE 6.13

Example of Solids Effective Drag Coefficient

Sand 14/30 L_t = 3.000 m D_t = 38.5 mm D_o = 44.45 mm w = 0.8

Tapping position	Solids velocity	S.P. Reynolds' No.	Effective drag coefficient
1	3.38	19.3	0.000
2	3.76	45.0	0.064
3	4.10	65.9	0.103
4	4.41	84.5	0.134
5	4.68	101.2	0.161
6	4.95	116.4	0.185
7	5.18	130.3	0.207
8	5.40	143.1	0.227
9	5.61	155.8	0.246
10	5.79	165.7	0.264
11	5.97	175.8	0.280
12	6.13	185.1	0.296
13	6.28	193.7	0.311
14	6.42	201.7	0.326
15	6.55	209.1	0.339
16	6.67	215.9	0.352
17	6.78	222.2	0.365
18	6.88	228.1	0.377
19	6.98	233.4	0.388
20	7.06	238.4	0.399
21	7.15	243.0	0.410

friction factor was observed with increase in average solids velocity, there was sufficient scatter to make any relationship doubtful (Figure 6.30). Further, there was some evidence in the tabulated data (Table 6.13) to indicate that the solids friction factor increased with an increase in solids mass flow rate. Both these findings were consistent with published results of pneumatic conveying of solids in tubes (107, 108). In such cases, however, independent control of the solids and air flow rates was usually possible, enabling study of the variation of solids friction factors with each variable in turn, while keeping other conditions constant. In the present apparatus, it was, of course, not possible to impose any direct control on the solids or air flow rates since these were necessarily determined by the apparatus dimensions. Not surprisingly, it was found that virtually every orifice and standpipe combination produced different air and solids flow rates, making direct correlation of friction factors under constant conditions impossible. Moreover, the systems under investigation in pneumatic conveying used constant velocity conditions in constrast to the present apparatus where the velocities were subject to continual change through the standpipe.

Comparison of the friction factors obtained in the present investigation with those obtained in the pneumatic conveying of solids was thus hindered by the differences inherent in the two systems, especially in the ranges of solids mass flow and air flow rates. Examination of the literature on pneumatic conveying showed that the maximum solids/gas loadings $\frac{W_s}{W_a}$ obtained were about 30, whereas in the present system values up to 100 were obtained. Significant differences in particle and air velocities for the two systems were also apparent. In the present system solids velocities obtained were between 2.5 and 9.0 m/s and air velocities between 0.4 and 6.5 m/s, while the pneumatic conveying literature showed solids velocities up to 25 m/s and air velocities up to 35 m/s. Nevertheless, published values of solids friction factor - defined in the same manner as in the present work - found

Fig.6.30 Solids friction factor vs. average solids velocity

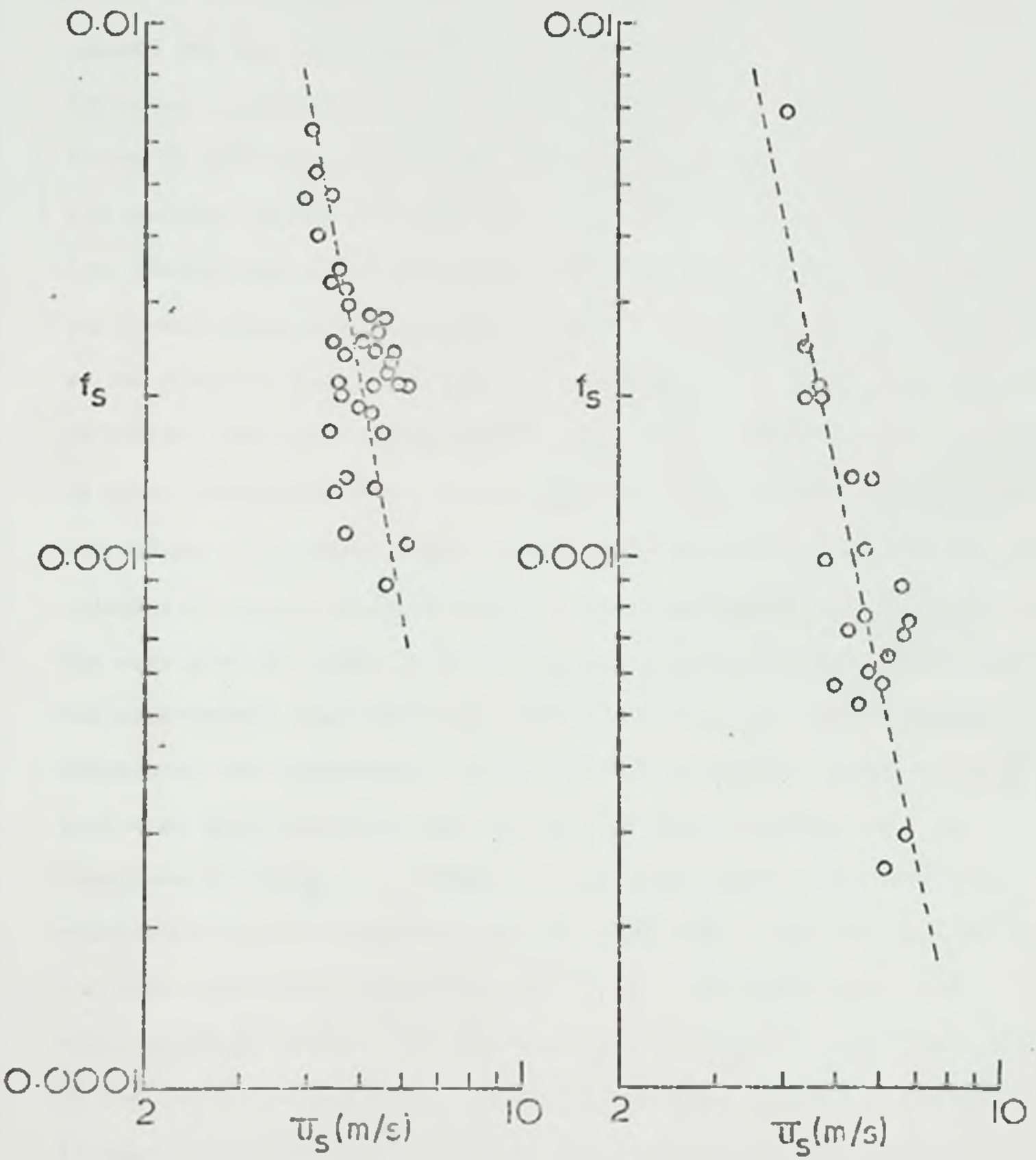

from such investigations were generally within the range 0.0005 - 0.01, which corresponded with the range of values found in the present apparatus.

The Standpipe Pressure Profiles and the Effects of the Parameter w and the Solids Friction Factor f_s

Overall, the calculated pressure profiles in the standpipe agreed extremely well with those obtained from the experimental work. As shown above, it was necessary to modify the single particle drag coefficients to account for the 'lee' effect of other particles in the solids stream, and to introduce a solids friction term to account for losses in particle kinetic energy by particle-particle and particle-wall collisions. In the case of the smallest orifice (12.7 mm) where the solids mass flow rates were very low, observations of the solids stream in the chamber and the standpipe, and measurements of the standpipe solids hold-up, showed that the solids volume fraction in the standpipe was extremely small (approximately 0.02), indicating that these modifications were not necessary in such conditions. In these particular cases, the calculated profiles were not fitted to the end values of the experimental profiles, nor was it necessary to fit the calculated average solids velocity to the experimental value. Consequently, the very good fit shown by the calculated pressure profiles with those from the experimental runs (curves A, Figure 6.27) and the good agreement of the calculated and experimental average solids velocities (generally within 5%) gave some confirmation to the structure of the theoretical equations developed in Chapter 3. Although the pressure profile fits were good, examination of the calculated profiles showed that they did not curve to the same extent at the upper regions of the standpipes, as did the experimental profiles. This was attributed to possible over-simplification by the use of the unmodified single particle drag coefficient in this case to describe the progress of the particles through the chamber and the standpipe, with a consequent reduction in the estimates of the values of the solids velocities at the standpipe entrance, compared to those which were calculated assuming no fluid drag in the chamber. Nevertheless, these

values of velocity were likely to be closer estimates of actual entrance particle velocities than those calculated with the assumption of no fluid drag in the chamber and, since it did not seem possible to calculate convincing intermediate estimates of solids velocity, it was decided to use them. As a consequence, it was also necessary to use the single particle drag coefficient unmodified throughout the standpipe in the case of the smallest orifices. The unmodified single particle drag coefficient was also used in the calculation of the pressure profile for the 19.01 mm and 25.4 mm orifices with the longer standpipes for sand 14/30. In these cases, although the average solids velocities showed good agreement, the pressure profiles did not fit so well.

The remaining pressure profiles in the standpipe were all calculated using the modified drag coefficient and a friction term in the equations. The fit of all these profiles to the experimental data followed, in general, the same trend when examined in terms of increasing orifice diameter with each standpipe. A comparison of the calculated and experimental pressure profiles in Figure 6.27 showed varying degrees of deviation at the centre of the profiles, which could be summarised by noting that the curvature of the calculated pressure profiles increased with orifice diameter: and that the calculated profiles exhibited by the smaller orifices were shallower than the experimental curves, indicating lower calculated pressures in the stand-pipe. In the case of the largest orifices, the calculated standpipe pressure profiles sometimes became steeper than those found during the experimental runs, indicating greater calculated pressures in the standpipe. Thus it could be seen that while the theoretical equations for the system did not completely fit the experimental picture in every case, the results straddled the physical data satisfactorily confirming the applicability of the equations. Moreover, closer examination of the calculated profiles showed that while the possible reasons for the lack of exact fit were fairly clear, the method of remedy was not so straightforward. Further analysis of the

causes of the deviations from the experimental values followed from a consideration of the three main assumptions:

(i) the method of estimation of the initial values of solids velocity,

(ii) the forms of modification of drag coefficient with position down the standpipe,

(iii) the assumption of a constant friction factor over the whole length of standpipe.

As mentioned above, only two methods of calculation of the solids inlet velocities to the standpipe could be justified, i.e. with the use of the single particle drag coefficient, or with the assumption of no drag at all on the particles in the chamber. The use of the 'no drag' assumption was believed to be closer to the real situation in the case of the larger orifices but to give rather high estimates of solids inlet velocity for the smaller orifices. This was confirmed by the good agreement between experimental and calculated pressure profiles obtained in the cases of the smallest orifice with the use of the single particle drag coefficient throughout both the chamber and the standpipe.

In the case of some larger orifices, the air velocity at the standpipe entrance was calculated to be greater than the solids velocity. There also, the assumption of zero fluid drag may have been incorrect due to the possible accelerating drag effect of the air on the solids at the standpipe entrance.

Since the modification of the drag coefficient was based on the inlet conditions to the standpipe (i.e. zero drag coefficient), and since it was only possible to adjust the parameter w by one experimental average solids velocity in the standpipe, the form of the drag coefficient modification was open to error from any inaccuracies in the calculated inlet solids velocities. The effect of high inlet solids velocities in the case of the smaller orifices seemed to be to produce low estimates of solids velocities in the standpipe, and thus high values of the parameter w, so giving high effective

drag coefficients. Examination of the effect of w on the pressure profile shape showed that high values of w produced shallower profiles, thus indicating a possible reason for the shallow profiles calculated for the smaller orifices. Conversely, in the case of some larger orifices, the low values of inlet solids velocity could produce low values of the parameter w, giving too great a curvature to the calculated pressure profiles.

Attempts were made to analyse the effect of a variation in the solids friction factor over the standpipe. Various modifications were made along the lines of those made to the drag coefficient but these showed a marked deterioration in the agreement of the pressure profiles, and thus it was concluded that the assumption of the constant friction factor over the whole length of the standpipe was the best available in the light of present knowledge.

Thus, although the calculated profiles did not exactly match the experimental values over the whole standpipe length, nevertheless the results as a whole were very promising, the explanation of the causes of such deviations as were shown being readily seen in terms of the above factors.

The values of the parameter w and friction factor produced from the pressure profile calculations followed the trends expected in the development of the standpipe equations, but rather unfortunately did not give sufficiently clear correlations to be of any direct value. Nevertheless, the results gave a good indication of the order of magnitude of the effective particle drag coefficients that could be expected to apply in the description of solids stream through vertical standpipes. Although these results gave a good insight into the situation, clearly further investigation will be needed, especially with regard to the shape of the solids stream in the standpipe and its effect on solids friction factor and particle drag coefficient.

Visual Observations and Description of the Solids Flow through the Chamber and Standpipe

In Chapter 3, in the development of the standpipe equations, certain

assumptions were made in order to model the flow system in the standpipe. Detailed consideration of the solids stream in the standpipe revealed a complex situation indicating great difficulties involved in modelling the system exactly, so showing the need for the simplifications made in the theoretical equations.

During the experimental runs for each orifice/standpipe combination, a descriptive record of the visual appearance and characteristics of the solids stream throughout the chamber and standpipe was kept. From these records, trends in the behaviour of the solids stream with the various orifices and standpipes were found.

Invariably, the solids stream flowing from the orifice appeared as a compact core with some particle scatter at the edges. The degree of scatter seemed to decrease with increase in orifice diameter, although an increase in the standpipe length seemed to increase the scatter somewhat in the case of the smaller orifices. Those scattered particles which at the start of the run did not fall directly into the standpipe collected to form a funnel about the entrance to the standpipe in the 'well' in the floor of the chamber (Figure 4.3): subsequent scattered particles falling on these were seen to disrupt this solids 'funnel' and slide towards the standpipe entrance. In most cases, except for the smallest orifice, the solids core in the chamber was seen to decrease in diameter as it fell towards the standpipe entrance. This was particularly noticeable in cases where the orifice diameters were greater than the standpipe diameter. This has been discussed earlier in this chapter and also in Chapter 5 with regard to the possible causes of the changeover from free flow to restricted flow conditions. In the case of the smallest orifice diameter, the solids core was less apparent due to the significant amount of solids scatter.

In all cases (i.e. all orifices with all standpipe lengths and diameters) an annulus, in which there was a significantly lower solids concentration, was noticed around a solids core immediately below the entrance to the

standpipe. This type of empty annulus has also been noted very recently in connection with vertical pneumatic conveying investigations and, moreover, the calculated slip velocities of the particles were consistently lower than those obtained experimentally (109, 110). This annulus and solids core situation was seen to extend throughout the standpipe in most cases, the solids concentration in the annulus being dependent on the amount of scatter of the solids core. As the solids progressed down the standpipe, scatter from the edges of the solids core became more pronounced until, in some cases (notably with the smaller orifices and longer standpipes), the core appeared to dissipate completely in the lower regions of the standpipe, the flow then appearing homogeneous across the diameter. Some lateral oscillation of the solids core in the standpipe was noticed with many orifices and, although this effect was much less marked for the larger orifices, it was much less marked for the larger orifices and it was felt that such non-axial velocities may have affected considerably the dissipation of the solids core for the smaller orifices. A possible cause for this oscillation of the solids stream was the short instabilities in solids flow often associated with smaller orifices. Instabilities in the solids stream have also been noted in the case of air-induced solids flow, the magnitude and growth rate of the instabilities appearing to increase with increasing air flow rate (55). As was seen in the chamber, the scatter from the solids core decreased with increase in orifice diameter, and although as the solids progressed towards the exit of the standpipe the solids core was still seen to dissipate into the empty annulus to some extent, the size of the annulus itself appeared to decrease with increase in orifice diameter. Since the solids scatter increased with distance down the standpipe, the effect of increasing the standpipe length from this point of view was to increase the particle scatter towards the exit, and to facilitate a more complete dissipation of the solids core before discharge from the standpipe.

When the air control valve on the chamber was open, giving rise to

simple gravity flow of solids, a marked decrease in the diameter of the solids core and particle scatter was observed, the solids stream continuing through the standpipe with virtually no wavering and very little particle scatter at any position. It was thought that much of the particle scatter in the chamber in the case of air-induced solids flow could be attributed to the expansion of the extra co-current air from the solids/air stream below the orifice, whereas in the case of gravity flow the only air present was the interstitial air normally associated with a solids bed. In the latter situation, the lack of scatter from the solids core in the standpipe was believed to be due partly to the influence of the large co-current flow of air (entering the system through the chamber valve) and partly due to the lack of initial particle scatter and solids stream oscillations.

Observations of the flow in the case of restricted flow also showed the presence of an annulus around the solids core in the standpipe. The solids core narrowed rapidly from covering the whole of the standpipe diameter at the entrance, thus producing an annulus, whereupon the solids appeared to fall through the standpipe in the same manner as in the case of the free flow conditions. This flow configuration was felt to be consistent with the form of 'vena contracta' in the solids stream below an orifice, frequently mentioned in the literature (3, 40, 72).

When viewed from above (through the chamber) the annulus at the entrance to the standpipe under free flow conditions was often obscured in the case of the largest orifices, apparently due to the particle scatter from the solids core in the chamber. For such orifices, the scattered particles in the chamber were less likely to fall directly into the standpipe since the solids 'core diameter' was approaching that of the standpipe, leaving the bulk of the scattered particles to fall on to the solids 'funnel' at the entrance to the standpipe. As the standpipe was comparatively small when this occurred, the scattered particles passing into the standpipe from the solids funnel increased the solids concentration immediately around the

solids core at the entrance to the standpipe, obscuring the annulus from view. The presence of these aberrant solids may have created some congestion at the standpipe entrance in these cases, and may have been the cause of the discontinuities shown by the chamber pressure in some of the experimental standpipe pressure profiles for large orifice/small standpipe diameter combinations (Figure 6.27).

The visual observations of the solids flow through the standpipe showed that the assumption of homogeneous solids distribution throughout the standpipe was not factually accurate. Thus, the values of voidage or solids volume fraction produced in the calculations were the average values at any level in the standpipe and did not describe the situation in the solids core, due to the presence of the empty annulus. Moreover, the solids core 'diameter' varied over the length of the standpipe, indicating that average values of voidage over the standpipe were not suitable to describe the conditions within the solids core. Hence it was not reasonable to use these values of voidage in any correlation against the parameter w or friction factor f_s.

The complete flow mechanism in the standpipe was not fully understood, but the observations in the present work suggested that in many cases the air was carried down the standpipe in two regions:

(i) air entrained in the central core of the solids stream

(ii) air flowing in the annulus between the pipe wall and the central core.

This picture was, of course, complicated by the dissipation of the central core as the solids progressed down the standpipe and, as in some cases the solids core was seen to dissipate almost completely towards the exit from the longer standpipes, the concept of two separate flow regions could not apply at those levels. It was not considered realistic to attempt to quantify this picture, since it was not possible to measure the solids core at any point in the standpipe, and the degree of particle scatter at

the edges of the core (different for each orifice/standpipe combination) made it hard to define a valid core diameter. Further, this model might imply a drag coefficient to relate the drag of the solids core on the surrounding annulus. No such relationships were available and it was difficult to imagine any general drag coefficient which would adequately describe the situation as the solids core dissipated towards the lower regions of the standpipe.

The gradual transitions between the two extremes in the mechanisms of solids flow, i.e. the two region flow and the homogeneous flow models, implied a solids velocity and concentration profile across the standpipe at any level which varied continuously with distance along the standpipe, but again it was not possible to use this model due to inability to measure such solids and air velocity profiles or solids concentration profiles in the standpipe with present apparatus.

However, although the lack of knowledge of the system within the standpipe prevented a detailed model being formulated, the overall assumption of an even solids concentration across the standpipe cross-sectional area was not considered to be unreasonable. It was seen that in the case of the smaller orifice diameters, the solids core dissipated substantially throughout the standpipe so that, for this case, the assumptions of constant solids concentration over the standpipe cross-section at any level was realistic. Moreover, for the largest orifice diameters, where $D_c \geqslant D_t$, the solids cores were comparable to the standpipe diameter and, although the annulus was still evident, the assumption was still regarded as justifiable. For the cases with orifice diameters between these extremes, the apparent solids core diameter increased and scatter at the edges decreased with increasing orifice diameter, showing the transition between the two extreme systems. In such cases the assumption might be thought of as encompassing the combination of the two factors (core diameter and solids scatter) in appropriate proportions; here the assumption was clearly at its weakest.

The discovery of the core flow of solids in the standpipe indicated a similarity to the flow of solids immediately after discharge from a hopper orifice. As reported in the literature (44, 87), the fluid drag on the solids in such a situation is usually considered to be negligible, due to the high solids concentration in the stream. It was, therefore, considered that the reduction in the solids-fluid drag in the standpipe, evident from the low effective drag coefficient, was due to the presence of this tight solids core, the increase in the effective drag coefficient towards the exit from the standpipe being due to the particle scatter and consequent expansion of the core. This situation was inherent in the model used in Chapter 3 to describe the effective drag coefficients within the standpipe.

The author considered that, of all the topics dealt with in the present investigation, the downward flow of solids through vertical standpipes especially warranted further study under conditions where the air and solids flow rates could be individually controlled; in particular, into the nature of the solids core, and its effect on the solids-fluid drag coefficients and solids friction factor.

6.9 Accuracy and Reproducibility of the Results

In a project such as this, the problem of accuracy was difficult to resolve. There were a large number of parameters which were known to have some influence on the flow of the particulate solids, and there were likely to be others which were at the time undefined - not least the condition of the solids in the bed. A few of these parameters have been controlled in the present work and this thesis constitutes a study of their influence on the solids flow. The significance (if any) of the rest remains largely unknown, so that they could be uncontrolled variables, inevitably causing the results to show some scatter and reducing reproducibility.

Briefly, the work amounted to an investigation into the effects of a co-current air flow on the discharge of solids through an orifice, the influence of a standpipe on such a system, and the way in which that influence

was produced by the co-current solids and air flow through the standpipe. In such systems the accuracy of controlled variable values depended on the accuracy of the instruments and observational error. More particularly, in the case of orifice flow, if the theoretical considerations were correct, the effects of the uncontrolled variables were likely to be small and should have become important only if comparison was attempted between the present results and the results from other workers and different systems.

In this work, the controlled variables were all material parts of the apparatus, i.e. orifice diameter, standpipe length and standpipe diameter, and the dependent variables were solids mass flow rate, constituent air flow rates, standpipe solids hold-up and air pressures within the apparatus.

The orifice plates were made to BS 1042 (1964) in brass plates, and thus were completely reproducible for successive runs: the errors in machining were well below 0.5% on all orifice diameters. The standpipe lengths were found to be within 2 mm of the specified values in all cases, thus giving a maximum error of $\pm$ 0.1% for the shortest length, and although the errors were less for the longer standpipes on this basis, it was not possible to check errors in measurement of the longest standpipes - up to 4.875 m. The glass manufacturer's specifications of the standpipe diameters were given in terms of outside diameter and wall thickness ranges. These showed on average a maximum possible error of $\pm$ 9% and a minimum of $\pm$ 1.5% in the internal standpipe diameters. For example, for the standpipe with 38.5 mm nominal internal diameter:

Manufacturer's specifications: O.D.: 45 - 48 mm

2 x wall thickness: 6 - 10 mm

Thus, Minimum range of I.D.: 39 - 38 mm, 38.5 $\pm$ 0.5 mm, 1.3%

Maximum range of I.D.: 35 - 42 mm, 38.5 $\pm$ 3.5 mm, 9%

Although it was not possible to measure the internal diameters throughout the whole length of the standpipe, test measurements at the ends of each standpipe showed that the minimum range of internal diameter figures were

the more likely.

With regard to the experimental results, the measuring instruments were a large capacity weighing machine for the flowing solids sample, standard gas meters, a manual stop-clock and an electronic stop-clock, a multi-revolution dial scale and single-leg water manometers. In general, the accuracy of these instruments (detailed below) was better than the observational error involved, so that the latter was the controlling factor.

The smallest scale division of the standard test gas meters used was 0.1 cu.ft (2.83×10^{-3} m^3) and the reading was estimated to 0.01 cu.ft (0.283×10^{-3} m^3). The air flows were the difference between two readings from the gas meters so that the maximum error was $\pm$ 0.02 cu.ft (0.566×10^{-3} m^3). The percentage error clearly depended on the total volume of air flow; in the great majority of cases, the total air flows through any one gas meter were well above 1 cu.ft (28.3×10^{-3} m^3) ranging up to 10 cu.ft (283.0×10^{-3} m^3), so the maximum percentage error in the readings should not have exceeded $\pm$ 2% and should have been less than this for most readings. The manufacturer's specifications for the gas meters stated that they were accurate to $\pm$ 1% for flow rates down to 1/20 capacity. The capacity of gas meter 1 (Figure 4.1) attached to the feed bed hopper was 200 cu.ft/h (1.57×10^{-3} m^3/s) and of gas meter 2 attached to the constant level bed section was 400 cu.ft/h (3.15×10^{-3} m^3/s), giving the lower limit of 1% accuracy as 0.079×10^{-3} m^3/s and 0.157×10^{-3} m^3/s respectively. Only in the case of the smallest orifice diameter (12.7 mm) were the air flow rates below these accuracy figures. The effects of the inaccuracies of the gas meters at such low air flow rates showed up in Figures 6.3, 6.4 and 6.5 and were recognised in the subsequent discussion.

The manual stop-clock was read to the nearest 1 sec, since it was felt that this was the limit of accuracy of the manual operation of the solids control valve. The length of each run was dependent on the orifice diameter and the weigh hopper capacity, the larger the orifice the shorter

the run time. The minimum run time was 40 sec for the 50.8 mm orifice with the 4.875 mm standpipes. In this case, the maximum error in the manual stop-clock readings was 0.5 sec in 40 sec or 1.2%, whereas the run time for the smaller orifices were up to 300 sec, giving a maximum error of 0.17%. Thus, the maximum observational error in the air flow rate readings was likely to be of the order of ± 2% for the whole range; including the error inherent in the gas meters, the maximum error in the air flow rate values should not have exceeded ± 3% over the whole range, except for the low air flow rates associated with the smallest orifices. It was not, of course, possible to include the effects of starting and stopping of the runs on the air flow readings. These, together with the indeterminable condition (e.g. aeration) of the solids bed during each run, were taken to be the cause of much of the scatter shown by the air flow readings.

The solids flow rate was determined by the weight of the solids collected in the weigh hopper over a given time. The solids were diverted into the weigh hopper by a swinging flap operated by a fast-acting pneumatic ram. The electric timer-clock was simultaneously triggered by the activation of this ram. There was a slight time lag between the starting of the timer-clock and the movement of the flap and, although this was not measured, it was felt that it was cancelled out by a similar lag between the stopping of the clock and the actual reverse movement of the flap. The weighing machine scale was 0.76 m diameter and was calibrated to 150 lb (68 kg) in 4 oz (0.113 kg) divisions. It was possible to estimate to the nearest 2 oz (0.057 kg) and, since it was only possible to set the scale to 0 ± 2 oz, the maximum observational error was ± 4 oz (0.113 kg), giving:

± 2.5% for a scale reading of 4.53 kg

± 0.25% for a scale reading of 45.3 kg

The weighing machine was tested at various times during the experimental period with known weights and the accuracy was found to be well within the

observational error.

The electric timer-clock was calibrated in 0.01 sec but readings were taken to 0.05 sec. The duration of the solids sampling was varied with the solids mass flow rate and associated orifice diameters, and was normally arranged to be approximately half the total run time. The range of solids sampling times was, therefore, 20 sec to 150 sec, giving a range of maximum errors of ± 0.25% to ± 0.033%. Thus, the solids mass flow rate values were considered to be within ± 2.5% over the whole range and generally below ± 1.5%.

The water manometers were read to the nearest 1 mm from the photographic negatives and, although the meniscus created some lack of definition in the liquid level (of the order of 3 mm), checks against direct visual observations taken during the runs showed that this did not seriously affect the reading of the pressures. The films suffered from some lack of definition, especially towards the edges of the frame and, therefore, could only be read with certainty to within ± 1mm water and probably less than this at the edges (the pressure readings towards the exit of the standpipe). The datum liquid level in the manometers (at zero pressure) was set before each run, and any error was felt to be contained within the film reading error. The percentage errors were, of course, dependent on the magnitude of the readings, so that the observational error for a 25 mm H_2O static pressure was ± 4%, while that for 500 mm H_2O was ± 0.2%. It was noted, however, that each of the pressures comprising the standpipe pressure profiles was measured separately, so that each reading was independent and did not affect the neighbouring pressure value; further, the use of percentage error lost its meaning for those pressure readings at the lower end of the standpipe where the values tended towards zero. The maximum observational errors for the differential pressures across the orifice and solids bed were ± 2 mm H_2O. Thus, in the case of the lowest pressure drops, the maximum possible errors were of about the same magnitude as the readings themselves. The effects of this were shown up in the graphs.

and have been discussed in the relevant sections of this thesis.

The mass of the pipe solids hold-up was determined by a multi-revolution dial scale with a capacity of 10 kg in 5 revolutions of a scale calibrated in 5 g divisions. The manufacturer's specifications stated an accuracy of ± 5 g over the whole range, although tests for low readings (100 g) showed that in fact the accuracy in this region was nearer ± 2 g, giving:

± 2% for a reading of 0.1 kg

± 0.5% for a reading of 1 kg

Inevitably, with all these instruments, the error was less when the readings were large. Thus, although it was difficult to determine the overall value of the observational error in the system, it was concluded that it was likely to be less than ± 7.5% for the majority of orifice and pipe diameter combinations.

As stated earlier, each run was repeated three times, and the order of the runs was randomised as much as possible so that any operator preference error should have been minimised. The results for each set of replications were, in general, averaged arithmetically except in the case of standpipe solids hold-up values where the large scatter in some of the results made this inadvisable. The purpose of the replications was to give an indication of the reproducibility of the apparatus by studying the spread of the three points resulting from the runs under the same set of conditions, and to increase the accuracy of the results by taking an average; this reduced the random and observational errors by a factor of 1.732, i.e. the square root of the number of observations.

In the case of the solids mass flow rate, the actual variation about the mean value of the replications was of the same level as the observational error in the great majority of cases, i.e. $\leq \pm$ 1.5%, the reproducibility being better for the lower solids mass flow rates.

The reproducibility of the air flow rates, defined on the same basis, was also within the observational error values: in the majority of cases $\leq \pm$ 3%.

In the case of the pressure throughout the apparatus, the reproducibility was considered to be very good, generally less than ± 2% in spite of the oscillations observed in the pressures during the runs. The reproducibility of the pipe solids hold-up was not so reliable since, although in most cases the results lay within ± 3% of their mean value, some sets of results contained a rogue figure well outside this range.

The overall picture of the accuracy of the experimental results was indicated by the Figures 6.3, 6.4, 6.5, 6.6, 6.7, 6.12, 6.13, 6.14 and 6.18 which were produced using the data from individual runs. Close inspection of the graphs, especially in Figures 6.3, 6.6, 6.7, 6.13 and 6.14 showed the grouping of the results from the replications, although in many cases only one point was shown because the scatter was so small.

The errors in the calculation of the parameter w and solids friction factor f_s were mainly caused by the limits of accuracy imposed on the convergence of the integration, and to a lesser extent by the fundamental errors inherent in numerical integration, although a change of step length was not seen to have any effect on the results. The limit of accuracy placed on the pressure profile was ± 1 mm H_2O, well within the experimental accuracy, and giving residuals of the friction factor of the order of $f_s \times 10^{-2}$. The accuracy of the parameter w seemed to depend not only on the limit of accuracy placed on the average solids velocity in the standpipe, i.e. ± 0.1 m/s or approximately ± 2.5% on average, but also on the rate of convergence of the iteration to the solution. Although this was not investigated in depth, it seemed from checks on the solutions of some of the runs that the estimates of w were likely to be within ± 10% of the optimum value. It was, of course, recognised that both these figures were also dependent on the accuracy of the experimental data, especially the values of pipe solids hold-up and air pressures which could cause significant variation in the calculated values of both w and f_s.

In general then, it was concluded that the experimental data showed a

high degree of reproducibility due mainly, it was believed, to the large scale of the apparatus, and should compare favourably with any future work directed at investigation of the flow of air and solids through systems of hopper/orifice/standpipe combinations.

CHAPTER 7

Conclusions and Suggestions for Further Work

7.1 Comments and Conclusions

A large-scale apparatus was built, tested and used successfully to investigate the flow of granular solids through vertical standpipes, and the influence of the standpipes on the discharge of the solids from an orifice set in the base of a hopper. The construction of the upper section of the apparatus (designed primarily to maintain a constant solids bed depth above the orifice) also offered facilities for subsidiary investigations into the flow of solids and air through the hoppers (which were fully exploited in the experimental programme).

As a general summary of the conclusions from this thesis, it appeared that:

(a) The bulk density and the voidage of a moving solids bed could be taken as the minimum static bed values.

(b) The total air flow rate through a moving solids bed could be considered as two components, the interstitial air and the percolating air, and that, under streamline conditions, the Kozeny-Carman equation could be used to relate the air flow rate to the pressure drop across the bed.

(c) The solids mass flow rate under the influence of a co-current air flow could be considered in two parts, the air-induced flow and the gravity flow, related to the two pressure components, the fluid pressure drop across the orifice and a pseudo-pressure due to the solids, respectively.

(d) The voidage of the solids stream at the orifice was greater than that in the bulk of the moving solids bed.

(e) The solids mass flow rate was increased if a standpipe was attached to the exit from the hopper, and that this increase tended to a maximum value with increase in standpipe length; the effect of the standpipe was to reduce the pressure below the orifice and create a co-current air flow with the solids.

(f) The interposition of a chamber between the hopper exit and the standpipe entrance aided the flow from the hopper by facilitating the positioning of the solids control valve above the entrance to the standpipe and allowed a wider range of orifice openings to be used in conjunction with the standpipe.

(g) The maximum likely solids flow rate was given by an orifice diameter and standpipe diameter of equal size.

(h) The solids stream in the standpipe flowed as a compact central core with a surrounding 'empty' annulus into which the solids from the edges of the core dispersed as they progressed down the standpipe.

(i) The particle drag coefficient could be considered as being dependent on the solids concentration as well as particle and fluid parameters, and that the effective drag coefficients in the core were substantially lower than the corresponding free-field particle drag coefficients.

7.2 Suggestions for Future Work

As with any field of study where the basic relationships had not been fully explained, an investigation of the present nature was likely to pose as many questions as it attempted to answer. Thus the present study, although elucidating many points, was not able to supply a complete answer to the problems associated with the flow of bulk solids through a standpipe attached to the outlet of a hopper.

Bed Voidage

It was not possible to directly investigate experimentally the change of voidage in the solids bed as it approached the orifice. It was thought that for a fuller understanding of the effects of air flow on the solids flow, direct measurement of this variation of voidage should be attempted, perhaps by the use of gamma-ray or X-ray techniques.

Pressure Difference through Flowing Beds

Previous work (34) and, to some extent, the present study had indicated

that the bed pressure drop was not so important as the orifice pressure drop in determining the solids mass flow rate. Nevertheless, it was felt that this should be fully investigated by using a range of orifices and bed heights in conjunction with an independently controlled air supply because, in the practical situation, the solids bed height above the orifice would be unlikely to remain constant. In addition, it has been suggested that the value of the chamber pressure in the present situation was the result of a balance between the solids drag forces in the standpipe and the resistance of the solids bed (and orifice solids). A further investigation into the effect of bed height in this context was considered a priority.

A 'pseudo-pressure' term to describe the gravity flow contribution to the total solids flow rate arose from the analysis of the equations concerning pressurised solids flow. The implications of this concept were not fully explored, and it was considered that further theoretical and experimental study was needed, perhaps particularly on its relation to 'step-flow' orifice pressure drop.

Standpipe Flow

The author considered that of all the topics dealt with in this study, the flow of the solids through the standpipes most warranted further investigation, preferably under conditions where the air and solids flow rates could be individually controlled. In particular, the nature of the solids core, the effective solids/fluid drag coefficients, and the nature of the solids friction should be studied. On the present apparatus it was not possible to study experimentally the change of solids velocity and voidage along the standpipe. A knowledge of these was considered essential for a complete modelling of the system. It would clearly be preferable if the method of determination of either of these factors did not significantly interrupt the continuity of the surface of the standpipe. Suitable arrangements from outside the standpipes might be X-ray analysis or gamma-ray

absorption techniques if a number of these units were available; otherwise some type of piezo electric needle probe in the solids stream might give an indication of the moving solids momentum or force, and thus a measure of the velocity.

Other Solids

Finally, it would be most useful if the present study could be continued using a wide range of solids to test, more completely, the generality of the present conclusions.

The mechanism of particulate solids flow is still a long way from being as exact a science as the flow of fluids, but it is hoped that the results of this work will help to clarify the situation, to assist in the design of solids handling systems, and to suggest suitable topics for subsequent investigation.

APPENDIX 1

Orifice Details

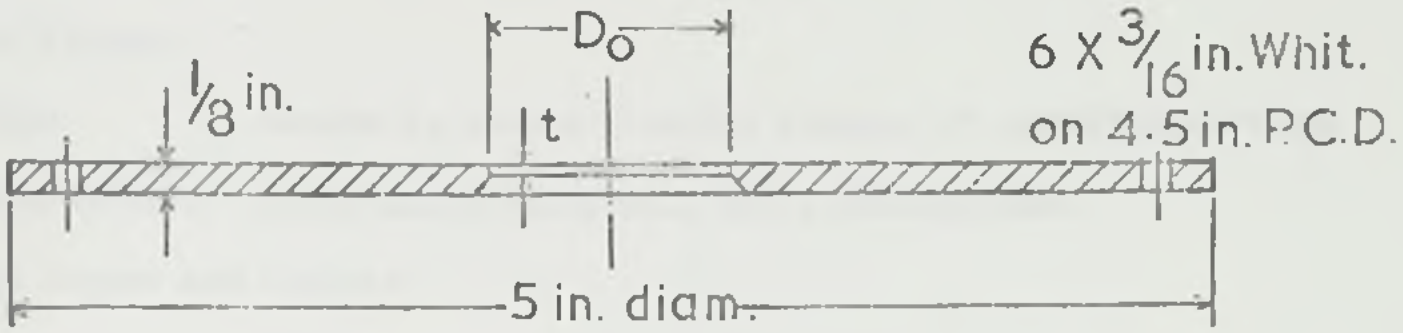

Orifice plates to BS 1042 (1964)

Orifice diameters D_o	(inches)	0.5	0.75	1.0	1.25	1.5	1.75	2.0
	(mm)	12.7	19.01	25.4	31.75	38.1	44.45	50.8
t, not greater than		0.05"	0.075"	0.1"	No bevelling needed.			

Standpipe Details

Lengths	(m)	1.500	2.000	3.000	3.650	4.250	4.875
Outside diameters	(mm)	32 - 34	45 - 48	57 - 60			
Wall thickness	(mm)	3 - 4.5	3 - 5	3 - 5			
Nominal inside diameters	(mm)	25.5	38.5	50.5			

APPENDIX 2

Commercial Apparatus: Manufacturers and Specifications

Mucon Valves:

Type: Series A, double flexible sleeve, 4" and 6" diameters.

Manufacturer: Mucon Engineering Co., Ltd., Basingstoke.

Weigh Hopper and Scales:

Type: 8091, capacity 0 - 150 lb.

Manufacturer: S. Parsons & Co., Ltd., Bradford.

Pneumatic Rams:

Type: S9125/3 (3 off).

Pneumatic Valves:

Type: M1702/122 (2 off).

Manufacturer: Martonair, Ltd., Twickenham.

Electric Clock:

Type: L15-365.

Supplier: Griffin and George, Ltd., Wembley.

Scales:

Type: 0213 multi-revolution scale.

Manufacturer: W. & T. Avery, Ltd., Warley.

Camera:

Type: Auto-camera Mk. 3, time-lapse camera.

Manufacturer: D. Shackman & Sons, Ltd., Chesham.

Lens:

Type: f3.5, focal length 36 mm.

Manufacturer: Wray (Optical Works), Ltd., Bromley.

Film:

Type: Pan F, 50 A.S.A.

Manufacturer: Ilford, Ltd., Ilford.

Silicon Rubber:

Type:	Silastomer 70 + Catalyst BC
Manufacturer:	A.M. Lock & Co., Ltd., Oldham.

Gas Meters:

Types:	D1 test meter, 200 cu.ft/h
	D4 test meter, 400 cu.ft/h
	Commercial meters, 700 cu.ft/h
Manufacturer:	Parkinson Cowan, Ltd., Manchester.

Film Reader:

Type:	Integral projector.
Manufacturer:	Hilger & Watts, Ltd., London, N.W. 1.

APPENDIX 3

Size Distribution of the Solids

Sand 60

Undersize Sieve

Mesh No.	Aperture Size (μm)	% retained	In Figure 6.2, taken as
18	850		0.10
22	710	0.40	0.30
25	600	11.74	
30	500	24.06	
36	425	35.86	
44	355	22.80	
52	300		2.36
60	250	3.54	1.18
72	212		0.98
pan	180	1.46	0.49

Sand 14/30

Undersize Sieve

Mesh No.	Aperture Size (μm)	% retained
12	1400	0.25
14	1180	9.63
16	1000	35.46
18	850	34.23
22	710	15.58
25	600	2.96
30	500	1.88

APPENDIX 4

Particle Shape Factors - Sphericity ϕ_s

Leva (43)	Korse (92)	Fair and Hatch (94)	Particle Nature
-	0.95	0.98	Rounded
0.86	0.83	0.94	Worn
0.67	0.75 - 0.65	0.85	Sharp

Leva defined shape factors as $\lambda = \frac{1}{\phi_s}$

Fair and Hatch defined shape factors as $\frac{\alpha_s}{\alpha_v} = \frac{6}{\phi_s}$

APPENDIX 5

Ancillary Physical Data

Air Density φ_a:	1.218 kg/m^3 at 15°C, 50% humidity.
Air Viscosity μ:	17.8 x 10^{-6} Ns/m^2 at 15 - 20°C.
Gravitational Acceleration g:	9.8067 m/s.
Area of Constant Depth Solids Bed:	0.164 m^2 (= area of cylindrical hopper cross-section).

APPENDIX 6

Averaged Data from Experimental Runs

Sand 60

D_t(m)	L_t(m)	D_o(m)	M_s(kg/s)	Q_{fb}(m^3/s)	Q_B(m^3/s)	ΔP_o(mm H_2O)	ΔP_B(mm H_2O)	m_p(kg)
$x10^{-3}$	-	$x10^{-3}$	-	$x10^{-3}$	$x10^{-3}$	-	-	-
25.4	1.500	12.7	0.072	0.029	0.199	26	13	0.027
"	3.000	"	0.103	0.056	0.607	80	35	0.076
"	3.650	"	0.136	0.075	0.652	145	34	0.119
"	4.875	"	0.147	0.085	0.900	178	39	0.154
"	1.500	19.01	0.235	0.144	0.419	38	28	0.095
"	3.000	"	0.348	0.223	1.058	167	48	0.207
"	3.650	"	0.421	0.267	1.158	247	52	0.292
"	4.875	"	0.507	0.334	1.456	359	68	0.426
"	1.500	25.4	0.414	0.258	0.606	57	30	0.140
"	3.000	"	0.651	0.420	1.294	159	62	0.354
"	3.650	"	0.742	0.499	1.558	227	69	0.485
"	4.875	"	0.857	0.565	1.938	305	89	0.651
"	1.500	31.75	0.798	0.509	0.855	65	32	0.271
"	3.000	"	0.962	0.615	1.384	132	51	0.516
"	3.650	"	1.033	0.666	1.622	144	81	0.618
"	4.875	"	1.190	1.779	2.143	209	95	0.845
"	1.500	38.1	1.187	0.754	0.926	62	46	0.381
"	3.000	"	1.372	0.861	1.363	113	47	0.724
"	3.650	"	1.504	0.951	1.741	151	53	0.952
"	4.875	"	1.607	1.026	1.986	173	68	1.248
38.5	1.500	12.7	0.050	0.018	0.031	6	3	0.018
"	2.000	"	0.057	0.019	0.080	14	4	0.035
"	3.000	"	0.077	0.035	0.149	37	6	0.057
"	3.650	"	0.101	0.045	0.223	61	11	0.108
"	4.250	"	0.116	0.065	0.281	93	12	0.139
"	4.875	"	0.094	0.049	0.516	71	23	0.117

APPENDIX 6 (contd.)

D_t(m)	L_t(m)	D_o(m)	M_s(kg/s)	Q_{fo}(m^3/s)	Q_B(m^3/s)	ΔP_o(mm H_2O)	ΔP_B(mm H_2O)	m_p(kg)
$x10^{-3}$	-	$x10^{-3}$	-	$x10^{-3}$	$x10^{-3}$	-	-	-
38.5	1.500	19.01	0.144	0.085	0.058	8	3	0.054
"	2.000	"	0.180	0.109	0.174	30	7	0.090
"	3.000	"	0.308	0.191	0.569	105	22	0.190
"	3.650	"	0.377	0.240	0.859	145	51	0.314
"	4.250	"	0.406	0.261	0.956	189	39	0.375
"	4.875	"	0.430	0.266	1.050	261	42	0.427
"	1.500	25.4	0.325	0.204	0.141	15	4	0.107
"	2.000	"	0.390	0.217	0.455	37	17	0.173
"	3.000	"	0.642	0.390	0.952	130	42	0.430
"	3.650	"	0.856	0.557	1.438	228	70	0.622
"	4.250	"	0.923	0.577	1.682	292	67	0.750
"	4.875	"	0.857	0.540	1.925	306	77	0.757
"	1.500	31.75	0.611	0.391	0.278	23	11	0.209
"	2.000	"	0.743	0.470	0.595	55	24	0.350
"	3.000	"	1.069	0.695	1.367	164	46	0.662
"	3.650	"	1.211	0.757	1.735	204	79	0.894
"	4.250	"	1.363	0.857	2.084	294	80	1.025
"	4.875	"	1.300	0.849	2.345	258	86	1.030
"	1.500	38.1	1.018	0.651	0.467	35	18	0.370
"	2.000	"	1.194	0.746	0.897	68	37	0.505
"	3.000	"	1.695	0.976	1.838	191	69	0.982
"	3.650	"	1.914	1.097	2.019	254	84	1.316
"	4.250	"	1.952	1.245	2.392	264	96	1.447
"	4.875	"	1.927	1.252	2.564	269	86	1.437
"	1.500	44.45	1.546	0.979	0.771	42	28	0.547
"	2.000	"	1.780	1.078	1.119	81	38	0.791
"	3.000	"	2.351	1.531	2.131	189	73	1.141
"	3.650	"	2.429	1.540	2.349	175	106	1.507

APPENDIX 6 (contd.)

D_t(m)	L_t(m)	D_o(m)	M_s(kg/s)	Q_{fb}(m^3/s)	Q_B(m^3/s)	ΔP_o(mm H_2O)	ΔP_B(mm H_2O)	m_p(kg)
x10^{-3}	-	x10^{-3}	-	x10^{-3}	x10^{-3}	-	-	-
38.5	4.250	44.45	2.426	1.534	2.723	203	101	1.755
"	4.875	"	2.479	1.556	2.831	211	100	1.931
"	1.500	50.8	2.320	1.409	1.251	65	44	0.748
"	2.000	"	2.649	1.644	1.695	109	56	1.122
"	3.000	"	3.070	1.778	2.322	162	78	1.723
"	3.650	"	3.166	1.957	2.374	154	113	1.961
"	4.250	"	3.177	1.964	2.795	180	105	2.375
"	4.875	"	3.652	2.179	3.606	256	139	-
50.5	1.500	12.7	0.045	0.002	0.023	1	1	0.012
"	3.000	"	0.057	0.019	0.099	8	7	0.039
"	3.650	"	0.060	0.026	0.159	18	8	0.054
"	4.875	"	0.075	0.029	0.257	27	14	0.099
"	1.500	19.01	0.133	0.075	0.024	3	2	0.046
"	3.000	"	0.189	0.115	0.285	34	11	0.120
"	3.650	"	0.238	0.145	0.374	69	15	0.193
"	4.875	"	0.272	0.169	0.640	92	38	0.290
"	1.500	25.4	0.295	0.172	0.061	4	4	0.102
"	3.000	"	0.409	0.251	0.483	44	18	0.231
"	3.650	"	0.529	0.336	0.789	100	30	0.395
"	4.875	"	0.608	0.376	1.487	139	64	0.553
"	1.500	31.75	0.543	0.322	0.117	5	5	0.172
"	3.000	"	0.671	0.423	0.580	36	22	0.382
"	3.650	"	0.909	0.583	1.189	110	46	0.631
"	4.875	"	1.002	0.632	1.486	140	61	0.831
"	1.500	38.1	0.878	0.548	0.180	9	8	0.274
"	3.000	"	0.158	0.730	0.980	60	37	0.612
"	3.650	"	1.408	0.892	1.365	112	47	0.906
"	4.875	"	1.787	1.123	2.541	214	92	1.444

APPENDIX 6 (contd.)

D_t(m)	L_t(m)	D_o(m)	M_s(kg/s)	Q_{fb}(m^3/s)	Q_B(m^3/s)	ΔP_o(mm H_2O)	ΔP_B(mm H_2O)	m_p(kg)
x10^{-3}	-	x10^{-3}	-	x10^{-3}	x10^{-3}	-	-	-
50.5	1.500	44.45	1.300	0.807	0.285	20	8	0.397
"	3.000	"	1.652	1.210	1.010	62	38	0.376
"	3.650	"	2.046	1.220	1.789	129	66	1.334
"	4.875	"	2.409	1.500	2.517	201	93	1.815
"	1.500	50.8	1.924	1.192	0.456	19	16	0.632
"	3.000	"	2.501	1.573	1.653	90	62	1.388
"	3.650	"	3.044	1.868	2.277	165	86	1.955
"	4.875	"	4.343	2.570	4.532	489	181	-

Sand 14/30

D_t(m)	L_t(m)	D_o(m)	M_s(kg/s)	Q_{fb}(m^3/s)	Q_B(m^3/s)	ΔP_o(mm H_2O)	ΔP_B(mm H_2O)	m_p(kg)
x10^{-3}	-	x10^{-3}	-	x10^{-3}	x10^{-3}	-	-	-
38.5	1.500	12.7	0.039	0.002	0.050	3	2	0.017
"	3.000	"	0.049	0.008	0.190	14	3	0.033
"	3.650	"	0.053	0.010	0.261	21	3	0.042
"	4.875	"	0.059	0.016	0.499	25	9	0.062
"	1.500	19.01	0.123	0.038	0.146	4	3	0.041
"	3.000	"	0.186	0.100	0.784	42	12	0.114
"	3.650	"	0.225	0.130	0.954	74	12	0.170
"	4.875	"	0.275	0.184	1.326	124	19	0.257
"	1.500	25.4	0.275	0.138	0.255	8	4	0.101
"	3.000	"	0.424	0.300	1.362	67	17	0.240
"	3.650	"	0.502	0.339	1.825	106	23	0.316
"	4.875	"	0.513	0.433	2.660	102	44	0.415
"	1.500	31.75	0.524	0.293	0.568	13	6	0.182
"	3.000	"	0.700	0.480	1.835	50	30	0.367
"	3.650	"	0.860	0.632	2.278	107	31	0.528
"	4.875	"	1.035	0.779	2.977	172	38	0.764

APPENDIX 6 (contd.)

D_t(m)	L_t(m)	D_o(m)	M_a(kg/s)	Q_{fb}(m^3/s)	Q_B(m^3/s)	ΔP_o(mm H_2O)	ΔP_B(mm H_2O)	m_p(kg)
$x10^{-3}$	-	$x10^{-3}$	-	$x10^{-3}$	$x10^{-3}$	-	-	-
38.5	1.500	38.1	0.876	0.546	0.885	17	10	0.284
"	3.000	"	1.157	0.783	2.112	65	29	0.580
"	3.650	"	1.285	0.901	2.590	94	34	0.756
"	4.875	"	1.448	1.058	3.280	140	36	1.035
"	1.500	44.45	1.328	0.840	1.216	21	5	0.463
"	3.000	"	1.555	1.064	2.489	47	35	0.800
"	3.650	"	1.643	1.144	2.792	61	43	0.957
"	4.875	"	1.869	1.326	3.438	105	47	1.365
"	1.500	50.8	1.923	1.189	1.543	24	20	0.622
"	3.000	"	2.145	1.434	2.703	46	38	1.092
"	3.650	"	2.247	1.501	2.934	52	43	1.303
"	4.875	"	2.440	1.662	3.524	83	46	1.708

APPENDIX 7

References

1. Furman, T.
   'Gravity flow of granular materials: a review of published information'
   N.C.B. Technical Memorandum No. 59, 1960.
2. Rudd, J.K.
   'How does material flow in bins?'
   Mod. Mat. Handl., 2, 1959, p. 94.
3. Hagen, E.
   Berliner Monatsberichte der Akademie der Wissenschaften, No. 35, 1852.
4. Ketchum, M.S.
   'Walls, bins and grain elevators'
   New York, 1911.
5. Phillips, C.E.S.
   'Electrical and other properties of sand'
   Proc. Roy. Instn., 19, 1910, p. 742.
6. Rose, H.E. and Tanaka, T.
   'Rate of discharge of granular materials from bins and hoppers'
   The Engineer, 208, 1959, p. 465.
7. Hinchley, J.W.
   'Chemical engineering'
   Encyclopaedia Brittanica, 1926.
8. Newton, R.H., Durham, G.S. and Simpson, T.P.
   'The T.C.C. catalytic cracking process'
   Trans. Am. Inst. Chem. Engrs., 41, 1945, p. 219.
9. Deming, W.E. and Mehring, A.L.
   'The gravitational flow of fertilisers and other comminuted solids'
   Ind. Enging. Chem., 21, 1929, p. 661.

10. Mehring, A.L.

'Measurement of the drillibility of fertilisers'

Ind. Engng. Chem. Anal. Ed., 3 (1), 1931, p. 34.

11. Kelley, A.E.

'Measurement of solids flow in T.C.C. process'

Petrol. Engng., 16, 1945, p. 136.

12. Gregory, S.A.

'Problems of plant design for fluidised processes'

J. Appl. Chem., 2, 1952, (Suppl. 1) p. S1.

13. Oyama, Y. and Nagano, K.

'Discharge rate of solid particles from a nozzle steeped in liquid'

Repts. Sci. Res. Inst., 29, 1953, p. 349.

14. Takahasi, K.

'Experimental investigation of the efflux of a granular mass'

Bull. Inst. Phys. Chem. Res. (Tokyo), 12, 1933, p. 984.

15. Grigoriyan, K.

Azerb. Neft. Teserufaty, Azerb. Neft., kh-vo, 6, 1960, p. 35.

16. Tsiborovskii, Ya. and Bondzyn'ski, M.

'The free flow of a granular material through an opening in the conical bottom of a vessel'

Inzh-Fiz. Zh., 7, 1963, p. 26.

17. Tanaka, T.

Kagaku-Kogaku (Chem. Eng. Tokyo), 20, 1956, p. 144.

18. Fowler, R.T. and Glastonbury, J.R.

'The flow of granular solids through orifices'

Chem. Eng. Sci., 10. 1959, p. 150.

19. Beverloo, W.A., Janiger, H.A. and van de Velde, J.

'The flow of granular solids through orifices'

Chem. Eng. Sci., 15, 1961, p. 260.

20. Zenkov, R.L.

Mekhanika nazypnykj gruzov Knshgiz, 1952.

21. Janssen, H.A.

'Versuche uber Getneidodruck in Silozellen'

Zeitschrift Verein Deutecher Ingenieure, 39, 1895, p. 1045.

22. Terzaghi, K. and Peck, R.B.

'Soil mechanics in engineering practice'

New York, Wiley, 1949.

23. Janiesen, J.A.

'Grain pressures in deep bins'

Trans. Can. Soc. Civ. Engrs., 17, 1903, p. 554, p. 603.

24. Luft, E.

'Tests of grain pressures in deep bins at Bounos Aires, Argentina'

Engineering News, 52, 1904, (15th Dec.).

25. Airy, W.

'The pressure of grain'

Mins. Proc. Inst. Civ. Engrs., 131, 1897.

26. Shaxby, J.H. and Evans, J.C.

'The variation of pressure with depth in columns of powders'

Trans. Faraday Soc., 19, 1923, p. 60.

27. Brown, R.L. and Richards, J.C.

'Principles of powder mechanics'

Pergamon Press, London, 1970.

28. Jenike, A.W.

'Flow of solids in bulk handling systems'

Bull. Univ. Utah, No. 64, Utah Engng. Exptl. Statn., 45, No. 9, 1954.

29. Bell, B.

'The lateral pressure resistance and supporting powder of clay foundations'

Proc. Inst. Civ. Engrs., 199, 1915.

30. Jeniko, A.W.

'Gravity flow of bulk solids'

Bull. Univ. Utah, No. 8, Utah Engng. Exptl. Statn., 52, 1961.

31. Jenike, A.W.

Bull. Univ. Utah, No. 123, Utah Engng. Exptl. Statn., 53, 1964.

32. Jenike, A.W. and Johanson, J.R.

J. Struct. Div. Proc.: Amer. Soc. Civ. Engrs., 94, 1968, p. 1011.

33. Delaplaine, J.W.

'Forces acting in flowing beds of solids'

J. Amer. Inst. Chem. Engrs., 2, 1956, p. 127.

34. Rausch, J.M.

'Gravity flow of solids beds in vertical towers'

Ph.D. Thesis, Princetown University, 1948.

35. Shirai, T.

'A powder-orifice nomograph'

Kagaku-Kikai (Chem. Eng. Tokyo), 16, 1952, p. 86.

36. Evans, A.C.

'A study of the gravity discharge of granular solids from a hopper followed by flow down a standpipe'

Ph.D. Thesis, University of Leeds, 1964.

37. Zenz, F.A.

'Use of fluid data for solids flow rates'

Petr. Ref., 41, 1962, p. 159.

38. Brown, R.L. and Richards, J.C.

'Exploratory study of the flow of granules through apertures'

Trans. Instn. Chem. Engrs., 37, 1959, p. 108.

39. Wieghardt, K.

'Some experiments on the flow of sand'

Ingen.-Arch., 20, 1952, p. 109.

40. Brown, R.L. and Richards, J.C.
'Profile of flow of granules through apertures'
Trans. Instn. Chem. Engrs., 38, 1960, p. 243.

41. Brown, R.L.
'Minimum energy theory for flow of dry granules through apertures'
Nature, 191, 1961, p. 458.

42. Harmens, A.
'Flow of granular material through horizontal apertures'
Chem. Eng. Sci., 18, 1963, p. 297.

43. Leva, M.
'Fluidisation'
McGray Hill, New York, 1959.

44. Shinohara, K., Idemitsu, Y., Gotoh, K. and Tanaka, T.
'Mechanism of gravity flow of particles from a hopper'
Ind. Eng. Chem. Proc. Des. Dev., 7, 1968, p. 378.

45. Bosley, J., Schofield, C. and Shook, C.A.
'An experimental study of granule discharge from model hoppers'
Trans. Instn. Chem. Engrs., 47, 1969, p. T147.

46. Holland, J., Miles, J.E.P., Schofield, C. and Shook, C.A.
'Fluid drag effects in the discharge of granules from hoppers'
Trans. Instn. Chem. Engrs., 47, 1969, p. T154.

47. Shook, C.A., Carlton, A.J. and Flain, R.J.
'Effect of fluid drag on the flow rate of granular solids from hoppers'
Trans. Instn. Chem. Engrs., 48, 1970, p. T154.

48. Wlodarsky, A. and Pfeffer A.
'Air pressure in the bulk of granular solids discharges from a bin'
Trans. A.S.M.E. (B) J. Eng. Ind., 91, 1969, p. 382.

49. Kuwai, G.
'Flow of powders through an orifice: flow rate under low air pressures'
Kagaku Kogaku, (Chem. Eng. Tokyo), 17, 1963, p. 453

50. Bulsara, P.U., Zenz, F.A. and Eckert, R.A.

'Pressure and additive effects on flow of bulk solids'

Ind. Eng. Chem. Proc. Des. Dev., 3, 1964, p. 348.

51. Resnick, W., Heled, Y., Klein, A. and Palm, E.

'Effect of differential pressure on flow of granular solids through orifices'

Ind. Eng. Chem. Fund., 5, 1966, p. 392.

52. McDougall, I.R. and Knowles, G.H.

'Flow of particles through orifices'

Trans. Instn. Chem. Engrs., 47, 1969, p.T173.

53. Engh, T.A.

'Effect of injected air on the rate of flow of solids'

Trans. A.S.M.E. (B) J. Eng. Ind., 91, 1969, p. 335.

54. Shinohara, K., Suzuki, E. and Tanaka, T.

'Effects of air pressures on flow criterion of cohesive powders from a hopper'

J. Chem. Engng., Japan, 6, 1973, p. 84.

55. Papazoglou, C.S. and Pulo, D.L.

'Air-assisted flow from a bed of particles'

Powder Technol., 4, 1970/71, p. 9.

56. Makishima, S., Ohtaka, S. and Shirai, T.

'Discharge rate of solid particles through an orifice with co-current stream of gas'

J. Chem. Engng., Japan, 3, 1970, p. 112.

57. de Jong, J.A.H.

'Vertical air-controlled particle flow from a bunker through circular orifices'

Powder Technol, 3, 1969/70, p. 279.

58. Massimilla, L., Betta, V. and Della Rocca C.

'A study of streams of solids flowing from solids gas fluidised beds'

J. A.I.Ch.E., 7, 1967, p. 502.

59. Massimilla, L. and Volpicelli, G.

'Note on efflux from solids gas fluidised beds'

J. A.I.Ch.E., 9, 1963, p. 139.

60. Stemerding, S. de Groot, J.H. and Kuypers, N.G.M.J.

'Engineering aspects of fluidisation'

Fluidisation, Symposium of the Society of Chemical Industry, 1963(1964), p. 35.

61. Jones, D.R.M. and Davidson, J.F.

'Flow of particles from a fluidised bed through an orifice'

Rheol. Acta., 4, 1965, p. 180.

62. Zenz, F.A. and Othmer, D.F.

'Fluidisation and fluid-particle systems'

Reinhold, New York, 1960.

63. Shanahan, C.E. and Schwarz, J.

'Characteristics of solid flow in a standpipe'

M.S. Thesis, Mass. Inst. Tech., 1954.

64. Kojabashian, C.

'The properties of fluidised solids in vertical downflow'

D.S./M.S. Thesis, Mass. Inst. Tech., 1954.

65. Matsen, J.M.

'Flow of fluidised solids and bubbles in standpipes and riser'

Powder Technol, 7, 1973, p. 93.

66. Leung, L.S. and Wilson, L.A.

'Downflow of solids in standpipes'

Powder Technol, 7, 1973, p. 343.

67. Bingham. E.C. and Wikoff, R.W.

'The flow of dry sand through capillary tubes'

J. Rheol., 2, 1931, p. 395.

68. Shipley, D.G.

(36) Tripos Report, Emmanuel College, Cambridge, 1962.

69. Whiteway, R.M.C.

(36) Tripos Report, Emmanuel College, Cambridge, 1962.

70. Train, J.

'A practical investigation of the flow of particulate solids through sloping pipes'

'The handling of solids', Symposium, Instn. Chem. Engrs., London, 1962, p. 52.

71. Manchanda, K.D. and Gopal Krishna, N.

'Gravity flow of granular solids through vertical and inclined tubes'

'Fluidisation and related processes', Symposium, Kharagpur, India, 1964

(Indian Inst. Technol, New Delhi 16), 1966, p. 35.

72. Miles, J.E.P., Schofield, C. and Valentin, F.H.H.

'The rate of discharge of powders from hoppers'

'The behaviour of granular materials', Symposium, Tripartite Chem. Engng. Conf., Montreal, 1968.

Instn. Chem. Engrs., London, 1968, Symposium Series No. 29, p. 25.

73. McDougall, I.R.

'Gravity flow of solids down vertical pipes'

Proc. Inst. Mech. Engrs., 184, (Pt. 3A), 1969/70, p. 1.

74. Yuasa, Y. and Kuno, H.

'Effects of an efflux tube on the rate of flow of glass beads from a hopper'

Powder Technol., 6, 1972, p. 97.

75. Langmaid, R.H. and Rose, H.E.

'Arch formation in a non-cohesive granular material'

J. Inst. Fuel, 30, 1957, p. 166.

76. Kvapil, R.

'The theory of the flow of granular and lump materials in hoppers'

S.N.T.L., 1955 (Czech. text).

77. Wolf, E.F. and von Hohenleiten, H.L.

'Experimental study of the flow of coal in chutes at Riverside Generating Station'

Trans. A.S.M.E., 67, 1945, p. 585.

78. Jenike, A.W.

'Better design for bulk handling'

Chem. Engng., 61, 1954, p. 175.

79. Brown, R.L. and Hawksley, P.G.W.

'The internal flow of granular masses'

Fuel, 26, 1947, p. 159.

80. McDougall, I.R.

'The ambient fluid influence on solids discharge from hoppers'

Brit. Chem. Engng., 14, 1969, p. 1079 (428).

81. Martin, J.B. and Richards, J.C.

'The determination of the dynamic zone within a free flowing granular mass'

J. Sci.-Technol., 11, 1965, p. 31.

82. Chatlynne, C.J. and Rosnick, W.

'Determination of flow patterns for unsteady state flow of granular materials'

Powder Technol, 8, 1973, p. 177.

83. Brown, R.L. and Richards, J.C.

'Kinematics of the flow of dry powders and bulk solids'

Rheol. Acta, 4, 1965, p. 153.

84. Novosad, J. and Surapatt, K.

'Flow of granular materials: determination and interpretation of flow patterns'

Powder Technol, 2, 1968/69, p. 82.

85. Richards, J.C. (ed.)

'The storage and recovery of particulate solids'

Instn. Chem. Engrs., London, 1966.

86. Soo, S.L.

'Fluid dynamics of multiphase systems'

Blaisdell, Waltham, Mass., U.S.A., 1967.

87. Boothroyd, R.G.

'Flowing gas-solids suspensions'

Chapman and Hall, London, 1971.

88. Davidson, J.F. and Harrison, D.

'Fluidised particles'

University Press, Cambridge, 1963.

89. Dallavalle, J.M.

'Micromenitics: the technology of fine particles'

Pitman, New York, 1948.

90. Mullin, J.W.

'Test sieve data'

Endecotts (Fitters), Ltd., London, 1972.

91. Carman, P.C.

'Fluid flow through granular beds'

Trans. Instn. Chem. Engrs., 15, 1937, p. 150.

92. Morse, R.D.

'Fluidisation of granular solids'

Ind. Eng. Chem., 41, 1949, p. 1117.

93. Happel, J.

'Pressure drop due to vapour flow through moving beds'

Ind. Eng. Chem., 41, 1949, p. 1161.

94. Fair, G.M. and Hatch, L.P.

'Fundamental factors governing the streamline flow of water through sand'

J. Amer. Water Works Assoc., 25, 1933, p. 1551.

95. Bird, R.B., Stewart, W.E. and Lightfoot, E.N.

'Transport phenomena'

Wiley, New York, 1962.

96. Coulson, J.M. and Richardson, J.F.

'Chemical engineering', Vol. 2

Pergamon Press, London, 1968 (2nd Edition)

97. Knowles, G.H.

Unpublished work, Chemical Engng. Dept., University of Leeds.

98. Weisbach, J.

'Principles of mechanics of machinery and engineering', Vol. 2

H. Balliere, London, 1848.

99. McDougall, I.R. and Pullen, R.J.F.

'The effect on solids mass flow rate of an expansion chamber between a hopper and a vertical standpipe'

Powder Technol., 8, 1973, p. 231.

100. Richardson, J.F. and McCleman, M.

'Pneumatic conveying - part 2: solids velocities and pressure gradients in a one-inch horizontal pipe'

Trans. Inst. Chem. Engrs., 38, 1960, p. 257.

101. Ridgeway, K. and Rupp, R.

J. Pharm. Pharmac., 21, 1969, p. 305.

102. Carleton, A.J.

'The effects of fluid-drag forces on the discharge of free flowing solids from hoppers'

Powder Technol., 6, 1972, p. 91.

103. Ergun, S.

'Fluid flow through packed columns'

Chem. Eng. Prog., 48, 1952, p. 89.

104. Stinzing, H.D.

'Drag on clouds consisting of solids particles enclosed in a pipe'

Proceedings of Pneumotransport (1), Cambridge, England, 1971, B.H.R.A. Fluid Engineering (1972), Paper C6, pages C6, 69-80.

105. Rowe, P.N. and Henwood, G.A.

'Drag forces in a hydraulic model of a fluidised bed - part 1'

Trans. Instn. Chem. Engrs., 39, 1961, p. 43.

106. Rowe, P.N.

'Drag forces in a hydraulic model of a fluidised bed - part 2'

Trans. Instn. Chem. Engrs., 39, 1961, p. 175.

107. Jotaki, T. and Tomita, Y.

'Solids velocities and pressure drops in a horizontal pneumatic conveying system'

Proceedings of Pneumotransport (1), Cambridge, England, 1971, B.H.R.A. Fluid Engineering (1972). Paper B3, pages B3, 33-34.

108. Rose, H.E. and Duckworth, R.A.

'Fluid transport of powdered materials in pipelines'

Instn. Chem. Engrs., Symposium Series No. 27, Brighton, 1968, p. 53-64.

109. Nakamura, K. and Capes, C.E.

'Vertical pneumatic conveying: a theoretical study of uniform and annular flow models'

Can. J. Chem. Engng., 51, 1973, p. 39.

110. Capes, C.E. and Nakamara, C.E.

'Vertical pneumatic conveying: an experimental study with particles in the intermediate and turbulent flow regimes'

Can. J. Chem. Engng., 51, 1973, p. 31.

111. Beck, M.S. and Mendies, P.J.

'Total volume and component flow in two-phase systems using cross-correlation techniques'

Symposium. 'The flow measurement of difficult fluids', Bradford, 15-16th April, 1971.